# Modeling anti-NMDAR encephalitis

**Dissertation**

for the award of the degree

*Doctor rerum naturalium*

of the Georg-August-Universität Göttingen


within the Center for System Neuroscience (CSN) doctoral program

of the Göttingen Graduate School for Neurosciences,

Biophysics and Molecular Biosciences (GGNB)

of the Georg-August University School of Science (GAUSS)


submitted by

Justus Benedikt Horst Wilke

born in Hamm, Germany


Göttingen, 2022

**Thesis Committee**

**Prof. Dr. Dr. Hannelore Ehrenreich (Supervisor, 1st referee)**

Clinical Neuroscience

Max Planck Institute for Multidisciplinary Sciences, Göttingen, Germany


**Prof. Dr. Jürgen Wienands (2nd referee)**

Institute for Cellular and Molecular Immunology

University Medical Center Göttingen, Germany


**Prof. Dr. Klaus-Armin Nave**

Department of Neurogenetics

Max Planck Institute for Multidisciplinary Sciences, Göttingen, Germany


**External Thesis Committee Member**

**Prof. Dr. Michael Hollmann**

Department of Receptor Biochemistry

Ruhr-University Bochum, Germany


**Members of the Examination Board**

**Prof. Dr. Susann Boretius**

Functional Imaging Laboratory

German Primate Center, Göttingen, Germany


**Prof. Dr. Alexander Flügel**

Institute for Neuroimmunology and Multiple Sclerosis Research

University Medical Center, Göttingen, Germany


**Ph.D. Brett Carter**

Synaptic Physiology and Plasticity

European Neuroscience Institute, Göttingen, Germany


**Prof. Walter Paulus**

Department of Neurology

Ludwig Maximilians University, Munich, Germany


Date of oral examination: 19.07.2022

# Acknowledgements

# Table of Contents

# Abbreviations

**AB**, autoantibody

**AE**, autoimmune encephalitis

**ASC**, antibody secreting cell

**BBB**, blood-brain barrier

**CNP**, 2'-3'-cylcic nucleotide 3'-phosphodiesterase

**CNS**, central nervous system

**CSF**, cerebrospinal fluid

**DTA**, diphtheria toxin fragment A

**EEG**, electroencephalography

**GABA$_A$R**, GABA$_A$ receptor

**GABA$_B$R**, GABA$_B$ receptor

**HSE**, herpes simplex encephalitis

**HSV**, herpes simplex virus

**IgA**, immunoglobulin A

**IgG**, immunoglobulin G

**IgM**, immunoglobulin M

**JE**, Japanese encephalitis

**JEV**, Japanese encephalitis virus

**KO**, knockout

**LTP**, long-term potentiation

**MRI**, magnetic resonance imaging

**mRS**, modified Rankin scale

**NMDA**, N-methyl-D-aspartate

**NMDAR**, NMDA receptor

**NMDARE**, anti-NMDAR encephalitis

**OCB**, oligoclonal bands

**PET**, positron emission tomography

**rs-fMRI**, resting state functional MRI

**WBC**, white blood cell count

# Abstract

The anti-NMDAR encephalitis (NMDARE) is an autoimmune condition with so far unclear etiology and pathogenesis. It manifests with a heterogeneous clinical disease course and is diagnosed based on the presence of NMDAR1-autoantibodies (NMDAR1-AB) of the IgG class in patients' cerebrospinal fluid. The associated NMDAR1-AB bind and cross-link surface N-methyl-D-aspartate receptors (NMDAR), resulting in NMDAR internalization and hypofunction. On a theoretical basis, the presence of NMDAR1-AB could contribute to the psychopathological phenotype of NMDARE patients and explain why psychoses and behavioral alterations are more frequent in NMDARE as compared to other encephalitides. However, the pathophysiological role of NMDAR1-AB in neuroinflammatory contexts has, so far, not been formally differentiated from the underlying pathomechanism(s) and previously established NMDARE-related animal models lack the neuroinflammatory component of the disease. To systematically disentangle the relative contribution of NMDAR1-AB from neuroinflammatory and neurodegenerative processes of encephalitides, core features of the anti-NMDAR encephalitis were modeled in mice. This was achieved by combining a standardized spatiotemporally defined gray matter inflammation mouse model ('DTA' mice), which was deeper characterized as part of this thesis, with a previously established immunization against a cocktail of extracellular GluN1-specific peptides that induces functional NMDAR1-AB expression. In addition, effects of NMDAR1-AB on white matter inflammation were investigated in *Cnp* knockout mice. Lastly, a replication study of a previously published immunization protocol was conducted with the aim to investigate the pathogenesis of anti-NMDAR encephalitis in wildtype mice.

In summary, DTA mice, independent of NMDAR1-AB, displayed key aspects of the anti-NMDAR encephalitis, namely (1) acute onset, (2) neuroinflammation in gray matter regions, prominently but not exclusively affecting the hippocampus, (3) blood-brain barrier impairment, and (4) pronounced learning/memory deficits. Consistent with NMDAR antagonism, the presence of NMDAR1-AB exacerbated hyperlocomotion, a psychosis-like readout, in DTA mice without add-on effects on neuroinflammation. Similarly, NMDAR1-AB did not alter white matter inflammation in *Cnp* knockout mice but exacerbated the behavioral pathology. Noteworthy, NMDAR1-AB affected distinct behavioral domains in gray and white matter inflammation, suggesting that the pathophysiological role of NMDAR1-AB depends on the underlying pathology, potentially due to distinct NMDAR1-AB distribution across the central nervous system which is largely related to blood-brain barrier (dys)function. Consistent with previous reports, extensive behavioral phenotyping did not reveal any effects of NMDAR1-AB in healthy control mice with an intact blood-brain barrier. Importantly, neither immunization against a cocktail of GluN1-specific peptides nor against $GluN1_{359-378}$ alone induced neuroinflammation in mice. In conclusion, NMDAR1-AB can modulate the behavioral phenotypes of underlying encephalitides but are not sufficient for the induction or exacerbation of neuroinflammation.

# 1  The anti-NMDAR encephalitis

Encephalitides are rapidly progressing neurological disorders caused by brain inflammation. Etiologies are often unclear but include various infectious agents as well as autoimmune causes (Venkatesan et al. 2013, Abboud et al. 2021). Fifteen years ago, Dalmau and colleagues identified an encephalitis sub-type associated with autoantibodies (AB) directed against N-methyl-D-aspartate receptors (NMDAR) and termed it 'anti-NMDAR encephalitis' (NMDARE). In their original publication, Dalmau et al. described the clinical course of twelve female patients of which eleven had ovarian teratoma. Most patients suffered from a viral-like prodrome before presenting with acute psychiatric syndromes, short-term memory loss followed by psychiatric symptoms or other cognitive impairments including decreased level of consciousness. Psychiatric symptoms included personality and behavioral alterations, agitation, or paranoia. During the disease course, seizures and movement abnormalities were common and patients' conditions rapidly deteriorated towards autonomic dysfunction, coma and/or death. A paraneoplastic cause was inferred upon analysis of five ovarian tumors that contained neuronal tissues ectopically expressing NMDAR subunits. Furthermore, pleocytosis and presence of autoantibodies in the cerebrospinal fluid (CSF) of patients indicated an immune-mediated neurological process. Concomitantly, six of seven patients treated with tumor resection and immunotherapy recovered, corroborating an autoimmune origin of the described disorder (Dalmau et al. 2007). Subsequently, a substantial number of studies, summarized hereafter, corroborated clinical features, examined diagnostic and prognostic factors, and investigated the pathophysiological role of associated autoantibodies (NMDAR1-AB, NR1-AB, or GluN1-AB are frequently used synonyms). Yet, despite intensive research in recent years, many aspects concerning the pathogenesis of NMDARE and relevance of NMDAR1-AB remain poorly understood and controversial.

## 1.1  Clinical manifestation and neuropsychiatry

After the first description of an autoimmune encephalitis associated with NMDAR1-AB, the so called anti-NMDAR encephalitis was frequently diagnosed across the world and various retrospective and prospective single- and multi-center studies in adult as well as pediatric patients were performed, focusing on the clinical manifestation, tumor association, diagnostic and prognostic factors, treatment success and long-term outcome (Dalmau et al. 2008, Florance et al. 2009, Irani et al. 2010, Titulaer et al. 2013, de Montmollin et al. 2017, Xu et al. 2020, Wang et al. 2021, Yang et al. 2021, Bastiaansen et al. 2022, Nissen et al. 2022). Systematic reviews were conducted to examine the acute psychopathology of NMDARE patients (Al-Diwani et al. 2019), the long-term neuropsychiatric outcome (McKeon et al. 2018), efficacy and safety of immunotherapy (Nosadini et al. 2021), or to compare clinical features of different antibody-associated autoimmune encephalitides (Broadley et al. 2019, Yeshokumar et al. 2021).

Although originally discovered in young female patients with ovarian teratoma, NMDARE is now frequently recognized in patients without neoplasms, males, children, and patients above 45 years old, sometimes referred to as late-onset NMDARE (Bastiaansen et al. 2022, Nissen et al. 2022). NMDARE is still most frequently diagnosed in young females (Dalmau et al. 2019, Nosadini et al. 2021,

Bastiaansen et al. 2022, Nissen et al. 2022), but, according to recent systematic reviews, a tumor association is only found in a quarter of NMDARE cases (Broadley et al. 2019, Nosadini et al. 2021). Two nation-wide observational cohort studies from Denmark and the Netherlands calculated a mean annual incidence of NMDARE of one case per one million inhabitants (Bastiaansen et al. 2022, Nissen et al. 2022).

Prior to admission, approximately half of NMDARE patients experience a 'flu-like' prodrome (Dalmau et al. 2019, Gibson et al. 2020, Yang et al. 2021). Subsequently, patients mostly present with prominent psychiatric or behavioral symptoms, in particular agitation and psychosis, and sometimes seizures (Florance et al. 2009, Irani et al. 2010, Titulaer et al. 2013, de Montmollin et al. 2017, Dalmau et al. 2019, Sarkis et al. 2019, Wang et al. 2020, Xu et al. 2020). Former cases can be particularly challenging to differentiate from primary psychiatric diseases, whereas seizures, CSF or MRI abnormalities commonly occur in other neurological diseases and in particular infectious encephalitides, resulting in a strong dependency on NMDAR1-AB assays for differential diagnosis (Kayser et al. 2013, Graus et al. 2016, Dalmau et al. 2019). After admission with mostly neuropsychiatric symptoms, patients' conditions typically deteriorate rapidly (within around 6 weeks) towards neurological dysfunction including seizures, cognitive dysfunction, decreased level of consciousness, movement disorders and autonomic dysfunction often resulting in admission to intensive care units, necessity for respiratory support, coma, and, in severe cases, death (Dalmau et al. 2008, Florance et al. 2009, Irani et al. 2010, Mohammad et al. 2016, de Montmollin et al. 2017, Dalmau et al. 2019, Gibson et al. 2020, Wang et al. 2020, Nosadini et al. 2021, Yang et al. 2021, Bastiaansen et al. 2022, Nissen et al. 2022). At disease nadir, symptoms frequently overlap, and most patients experience severe disabilities, which is typically ranked according to the modified Rankin Scale (mRS) score. Approximately half of the patients reach a mRS score of 5, another quarter reaches a score of 4, and about 50% of patients are admitted to an intensive care unit (van Swieten et al. 1988, Irani et al. 2010, Titulaer et al. 2013, de Montmollin et al. 2017, Nosadini et al. 2021, Bastiaansen et al. 2022).

Due to the severity of NMDARE symptoms, extensive cognitive testing and neuropsychological characterizations are challenging and mostly qualitative (Gibson et al. 2020). Despite these challenges, a recent systematic review examined the psychopathology of 464 adult NMDARE patients for which the psychopathology was individually reported (Al-Diwani et al. 2019). The authors identified 50 'lower-level' features that were categorized into behavior (including, amongst others, agitation, aggression, incoherent speech or violence), psychosis (including, amongst others, visual and auditory hallucinations, delusions/overvalued ideas), mood (including anxiety/panic, mood instability/lability/irritability, mania, depressed mood, hypomania), catatonia (including mutism, stupor, posturing/catalepsy, verbigeration, echolalia, waxy flexibility) and sleep disturbance (including insomnia, hypersomnia, sleep-wake reversal, bad dreams/night terrors, less need for sleep). Patients mostly displayed symptoms belonging to behavior (68%) and psychosis (67%), followed by mood (47%), catatonia (30%) and sleep disturbance (21%). Agitation was the most frequent 'lower-level' feature followed closely by hallucinations (both >40%) and a median of three lower-level features were identified per patient. A combination of seven lower-level features, namely agitation and aggression (behavior), hallucinations and delusions (psychosis), depressed mood and irritability or mood instability (mood), as well as mutism (catatonia), explained

77% of the variance in data. Because core aspects of various classical neuropsychological domains consistently overlapped in patients, the authors concluded that NMDARE psychopathology is distinct with respect to its complexity (Al-Diwani et al. 2019). However, a disease-specific psychiatric phenotype has neither emerged in this nor in similar studies (Warren et al. 2018, Al-Diwani et al. 2019, Dalmau et al. 2019, Gibson et al. 2019, Sarkis et al. 2019).

Equally complex are the movement disorders observed in NMDARE patients (Varley et al. 2019). Common movement disorders include facial dyskinesia as well as abnormal movements affecting the limbs and trunk of patients (Dalmau et al. 2008, Baizabal-Carvallo et al. 2013, Varley et al. 2019). Movement disorders occur in approximately ¾ of adult and almost all (95%) pediatric patients (Titulaer et al. 2013, Varley et al. 2019). These movement disorders are not disease specific (Dalmau et al. 2019) but show remarkable complexity in terms of overlap of distinct movement disorders and intra-individual variability within short-time spans (Varley et al. 2019).

The frequency of seizures and EEG abnormalities in patients suffering from antibody-associated auto-immune encephalitides (AE) including NMDARE was recently examined in a systematic review (Yeshokumar et al. 2021). Importantly, more than half of reported cases (1985/3722, 53.3%) were diagnosed with NMDARE indicating a high incidence of NMDARE among antibody-associated AE. Out of 3722 antibody-associated AE patients approximately 70% suffered from clinical seizures during the disease course and EEG data was abnormal in 84% of 2025 patients with available EEG data. Similar rates of seizures (72%) and EEG abnormalities (90%) were observed in a subgroup of NMDARE patients with available data. Amongst distinct AE subtypes, seizures were particularly frequent in $GABA_BR$-AB, LGI1-AB, and NMDAR1-AB associated AE. However, a statistical comparison of different AE subtypes dependent on associated autoantibodies was not performed and seizures commonly occurred in all AE subtypes associated with extracellular autoantibodies. Similarly, EEG abnormalities were frequently (>75%) observed in almost all antibody-associated AE subtypes (Yeshokumar et al. 2021). Another systematic review on clinical features in antibody-associated AE identified 1566 cases with NMDARE in which seizures were the most common symptom during the disease curse (81%), followed by psychosis and cognitive impairments (71% and 47%, respectively). However, these symptoms are not specific to NMDARE and frequently occur in other AE, although with different frequencies. Amongst anti-VGKC encephalitis patients with LGI1- and CASPR2-AB (430 cases) seizures occurred in 90%, cognitive impairments in 79% and psychosis in 22%. Similarly, in anti-$GABA_BR$-AB encephalitis patients (38 cases) seizures were present in 94%, cognitive impairments in 64% and psychosis in 51% (Broadley et al. 2019).

These observations were recently confirmed in a prospective multicenter study by Seifert-Held and colleagues comparing NMDARE with anti-LGI1/CASPR2-AB associated encephalitis as well as a group comprising various central nervous system (CNS) directed autoantibody associated encephalitides with respect to clinical and paraclinical presentation. At baseline, patient groups differed regarding frequency of prodromal symptoms (highest in NMDARE), psychosis (highest in NMDARE), seizures (highest in LGI1/CASPR2 encephalitis), CSF white blood cell counts (highest in NMDARE) and MRI T2 mesial temporal hyperintensities (highest in LGI1/CASPR2, lowest in NMDARE). Whereas memory impairments (42-51%), autonomic dysfunction (8-33%), altered behavior (11-25%), and movement disorder

(11-25%) were frequently observed and comparable between groups. Functional outcome at three months was worst in NMDARE patients despite the higher proportion of second-line immunosuppressive treatment at baseline. In all three encephalitis groups, approximately 50-70% of patients had a good functional outcome (mRS below 2, median mRS of 1) within 12 months (Seifert-Held et al. 2021).

Similar observations were obtained in two retrospective studies comparing encephalitis cases with and without NMDAR1-AB. First, Gable et al. compared clinical features of NMDAR1-AB positive encephalitis patients (n=10) to NMDAR1-AB negative herpes simplex encephalitis (HSE, n=52), enterovirus-associated encephalitis (n=85) and rabies cases (n=6). Compared to encephalitides of viral origin, NMDARE patients more frequently displayed psychiatric symptoms such as hallucinations, psychosis, personality change or irritability. With respect to neurological features, rates of altered consciousness were similar across encephalitis groups, whereas ataxia and focal neurological signs were most frequently observed in NMDARE patients. CSF white blood cell counts were highest in HSE and enterovirus encephalitis, followed by NMDARE and mostly normal in rabies cases (Gable et al. 2009). Second, Chen et al. compared NMDAR1-AB positive and negative encephalitis cases of heterogeneous etiology (11 HSE, five tuberculous meningoencephalitis, two $GABA_BR$-E, one LGI1-E, 37 unclear etiology) admitted to a neurological intensive care unit. CSF of 16/72 encephalitis patients contained NMDAR1-AB and positive patients more frequently display psychiatric or behavioral symptoms, dyskinesia and autonomic dysfunction. These clinical features were, however, not exclusive to NMDARE and commonly occurred in NMDAR1-AB negative encephalitides. Other common clinical features observed at similar frequency in NMDAR1-AB positive and negative encephalitis patients included prodromal symptoms, seizures, and cognitive dysfunctions (Chen et al. 2016).

To summarize, there is no neuropsychiatric or neurological feature exclusive to NMDARE and neurological symptoms such as seizures, cognitive dysfunction, and altered level of consciousness are prominent features of both infectious and autoimmune encephalitides. At disease onset, psychiatric and behavioral alterations are strikingly frequent in NMDARE patients and early differentiation of NMDARE from primary psychiatric diseases can be challenging. Based on the remarkably heterogeneous clinical manifestation, NMDARE is best described as a complex neuropsychiatric syndrome. However, new onset of psychiatric symptoms in combination with a rapid progression towards neurological dysfunction should raise suspicion of the so-called anti-NMDAR encephalitis and prompt further neurological examination, including neuroimaging and examination of cerebrospinal fluid.

## 1.2 Cerebrospinal fluid parameters

Analysis of cerebrospinal fluid is the most important test in the clinical workup of patients with suspected NMDARE and other encephalitides. CSF samples are routinely used to assess neuroinflammation, i.e. through white blood cell counts (WBC), presence of CSF-specific oligoclonal bands (OCB), and protein concentration. Furthermore, CSF is crucial for differential diagnosis of infectious and autoimmune encephalitides via assays for specific pathogens and autoantibodies (Abboud et al. 2021). For these reasons, routine CSF parameters are frequently reported in NMDARE patients (Dalmau et al. 2008, Irani et al. 2010, Titulaer et al. 2013, de Montmollin et al. 2017, Blinder and Lewerenz 2019, Xu et al. 2020, Broadley et al. 2021, Durr et al. 2021, Bastiaansen et al. 2022, Nissen et al. 2022).

Although the frequency of abnormal CSF findings differs between studies, abnormal CSF parameters, mostly consisting of increased WBC and/or presence of OCB, are commonly observed in 79-96% of NMDARE patients (Titulaer et al. 2013, Durr et al. 2021, Bastiaansen et al. 2022, Nissen et al. 2022). White blood cells are elevated in 68-81% (Irani et al. 2010, Xu et al. 2020, Bastiaansen et al. 2022) and OCBs are present in 72-84% of NMDARE patients (Durr et al. 2021, Bastiaansen et al. 2022, Nissen et al. 2022). Interestingly, WBC and OCB parameters seem to change with disease progression, showing higher WBC at onset and a time-dependent increase of OCB, indicating that intrathecal immunoglobulin synthesis is secondary to immune invasion and encephalitis onset (Irani et al. 2010, Durr et al. 2021).

These routine CSF parameters of NMDARE patients were recently reviewed and compared to other antibody-associated AE in a meta-analysis by Blinder and colleagues, including autoantibodies against NMDAR, AMPA receptors (AMPAR), glycine receptors, $GABA_A$ receptors ($GABA_AR$), $GABA_B$ receptors ($GABA_BR$), DPPX, CASPR2, LGI1, IgLON5, and GAD (Blinder and Lewerenz 2019). The comparison of different AE revealed that routine CSF parameters of NMDARE are similar to those of AMPAR-AB and $GABA_BR$-AB associated AE patients with frequent CSF pleocytosis (>50%) and median WBC >20 cells/µL. On the other hand, CSF was mostly normal in autoimmune encephalitides associated with CASPR2-AB, LGI1-AB, $GABA_AR$-AB or glycine receptor autoantibodies (Blinder and Lewerenz 2019). Presence of CSF-specific oligoclonal bands was reported in more than 50% of patients with GAD-, $GABA_BR$- and NMDAR1-autoantibodies, followed by 37% of patients with AMPAR- and 23-32% with glycine receptor-, $GABA_AR$-, CASPR2-, and DPPX-antibodies. OCBs were rare (5-7%) in patients with LGI1- and IgLON5-antibodies (Blinder and Lewerenz 2019). The study is, however, limited by its retrospective cross-sectional nature, and lack of individually reported patient data such as time of CSF sampling, medication, or comorbidities. To conclude, while routine CSF parameters are frequently abnormal in NMDARE patients and can be useful for establishing the diagnosis of encephalitis, they are neither disease-specific nor particularly helpful for the differentiation of AE subtypes. Furthermore, normal CSF findings do not exclude ongoing neuroinflammation.

In addition to routine CSF parameters, a number of studies explored potential diagnostic or prognostic CSF markers, such as cytokines and chemokines, typically comparing CSF of treatment-naïve NMDARE patients during the acute phase to CSF of non-inflammatory controls (Byun et al. 2016, Kothur et al. 2016b, Liba et al. 2016, Deng et al. 2017, Ai et al. 2018, Chen et al. 2018, Liu et al. 2018a, Liu et al. 2018b, Peng et al. 2019, Liu et al. 2020, Zou et al. 2020, Li et al. 2021). In summary, the broad-

spectrum pro-inflammatory cytokines IL-6, TNFα, IFNγ, the anti-inflammatory cytokine IL-10, as well as the chemokines CXCL10 and CXCL13 were consistently elevated in the CSF of acute NMDARE patients compared to non-inflammatory controls, whereas levels of IL-2, IL-4, IL-5, IL-15, IL-21, G-CSF, GM-CSF, CCL2, CCL4, CCL5, CCL11, CCL21, and CXCL8 were either normal or below detection limits (Byun et al. 2016, Kothur et al. 2016b, Liba et al. 2016, Chen et al. 2018, Liu et al. 2020, Zou et al. 2020, Li et al. 2021). Interestingly, Liba et al. noted a time-dependent decrease of CXCL10 and CXCL13 levels, which is in line with observations of decreased CSF pleocytosis with disease progression (Irani et al. 2010, Durr et al. 2021). In contrast, conflicting results were reported for IL-1RA, IL-1b, IL-13, IL-17A, IL-23, IFNα, CCL1, and CCL3 (Byun et al. 2016, Kothur et al. 2016b, Liba et al. 2016, Peng et al. 2019, Liu et al. 2020). Despite the strong B cell focus of NMDARE related research, few studies examined CSF levels of two major determinants of B cell and plasma cell survival, namely B cell activating factor (BAFF) and a proliferation-inducing ligand (APRIL) (Avery et al. 2003, Magliozzi et al. 2004, Krumbholz et al. 2005, Schneider 2005, Belnoue et al. 2008, Benson et al. 2008, Meinl et al. 2008, Peperzak et al. 2013, Nutt et al. 2015, Sabatino et al. 2019). Whilst one report observed increased BAFF and APRIL concentrations in CSF of NMDARE patients using ELISA (Deng et al. 2017), BAFF and APRIL were comparable to controls in two reports using multiplexed CSF analyses (Kothur et al. 2016b, Liba et al. 2016). Other proteins including osteopontin (Zou et al. 2020), CD146 (Li et al. 2021), HMGB1 (Ai et al. 2018), NSE and S100b (Liu et al. 2018b), PTX3 and sCD40L (Liu et al. 2018a), and NLRP3 (Peng et al. 2019) have been shown to be elevated in CSF of NMDARE patients compared to non-inflammatory controls, but remain unconfirmed so far.

A particular focus in some of the reports (Leypoldt et al. 2015, Byun et al. 2016, Kothur et al. 2016b, Liba et al. 2016, Liu et al. 2020) was placed on CXCL13, a major determinant for B cell recruitment into the CNS that correlates with intrathecal IgG, IgA, and IgM synthesis (Kowarik et al. 2012). Although consistently elevated amongst NMDARE patients, which is in line with the presence of B cells in patient CSF (Dale et al. 2013, Kreye et al. 2016, Malviya et al. 2017), CXCL13 has a low discriminatory value as it is frequently elevated in the CSF of patients with other inflammatory CNS conditions, including amongst others multiple sclerosis and Lyme neuroborreliosis (Kowarik et al. 2012, Huber and Irani 2015). Similarly, other cytokines or chemokines elevated in NMDARE are not disease-specific, although potentially useful for the diagnosis of ongoing neuroinflammation (Kothur et al. 2016a, Lepennetier et al. 2019). This is reflected by three studies directly comparing CSF of NMDARE patients to CSF of viral encephalitides (Kothur et al. 2016b, Zou et al. 2020) or autoimmune encephalitides, including LGI1-AE (Byun et al. 2016) and acute disseminated encephalomyelitis (Kothur et al. 2016b) that did not reveal differences in cytokine/chemokine concentrations except increased Th17- and Th2-related cytokines in CSF of acute disseminated encephalomyelitis patients. Similarly, a recent study investing biomarkers of neuronal and neuroaxonal damage, synaptic function, and neuroinflammation did not reveal differences in total tau, NfL, YKL-40, neurogranin, and SNAP-25 concentrations between CSF samples of 34 NMDARE and 11 LGI1/CASPR2-AE patients. However, compared to cognitively normal controls, NfL and YKL-40 were elevated in AE patients, indicating neuroaxonal damage and astroglial activation, respectively (Day et al. 2021). The study confirms previous findings of elevated YKL-40 concentrations in CSF of NMDARE patients (Chen et al. 2018) and is in line with another report showing increased serum NfL concentrations in NMDARE patients compared to healthy controls (Ma et al. 2022). Neurogranin

and SNAP-25 were decreased in CSF of AE patients suggesting synaptic dysfunction. Unexpectedly, VILIP-1, a proposed marker for neuronal injury, was significantly decreased in both AE subtypes compared to cognitively normal controls and lower in NMDARE compared to LGI1/CASPR2-AE patients (Day et al. 2021). AE patients were best discriminated from controls by a log-transformed YKL-40/SNAP25 ratio (Day et al. 2021).

In contrast to routine CSF parameters and biomarker studies, analysis of CSF cytology is relatively scarce. Crude immunophenotyping of two pediatric NMDARE patients sampled in the acute phase and upon relapse, respectively, revealed B cell expansion (10.2-10.7%) compared to non-inflammatory neurological disorders (<1%) and predominance of CD4+ (61-62%) and CD8+ (27-30%) T cells in the CSF of these patients (Dale et al. 2013, Kowarik et al. 2014). Later studies focusing on B cells and antibody secreting cells (ASC) confirmed the presence and expansion of B cells and ASC in CSF of 4 and 8 NMDARE patients (Kreye et al. 2016, Malviya et al. 2017). Importantly, the number of B cells and ASC in patient CSF showed a time-dependent decrease and was responsive to immunotherapy (Malviya et al. 2017). Sequence analysis of immunoglobulin heavy and light chain genes of CD27+/CD38+ ASC, CD20+/IgD-/CD27+ memory B cells, or CD138+ ASC revealed a polyclonal antibody response, presence of clonally expanded ASC, frequent somatic hypermutations, and predominant class switch recombination to IgG (Kreye et al. 2016, Malviya et al. 2017). However, neither B cell expansion nor the presence of ASC in CSF are specific to antibody associated autoimmune encephalitides. Two cross-sectional studies of immune cell subtypes in patients with various inflammatory and non-inflammatory CNS diseases observed increased CSF WBC, intrathecal immunoglobulin synthesis, and increased total numbers as well as percentages of B cells and plasmablasts in infectious (i.e. Lyme neuroborreliosis, bacterial and viral meningitis) and autoimmune neuroinflammatory diseases (i.e. multiple sclerosis) compared to non-inflammatory CNS conditions (Kowarik et al. 2014, Lepennetier et al. 2019).

To conclude, several CSF components support the diagnosis of a neuroinflammatory disorder. However, except for NMDAR1-AB, which are by definition a disease defining factor (see 1.5), no factor analyzed so far is pathognomonic for the anti-NMDAR encephalitis. Although various CSF components differentiate NMDARE patients from non-inflammatory controls on a population level, it is important to highlight that individual parameters often fall within the control range. For this reason, CSF analysis should include a variety of neuroinflammatory markers to enhance sensitivity. Furthermore, future research should focus on the clustering of several inflammatory mediators to decipher whether distinct disease mechanisms are at play within individuals with NMDARE.

## 1.3 Neuroimaging

Direct pathological examination of brain tissue, i.e. upon biopsy, has major disadvantages as diagnostic test for encephalitides due to the invasiveness and potential morbidity associated with neurosurgeries. For this reason, brain inflammation is typically diagnosed through surrogate markers such as CSF white blood cell counts or parenchymal abnormalities on neuroimaging. However, normal neuroimaging findings do not exclude encephalitis (Venkatesan et al. 2013, Abboud et al. 2021). Neuroimaging modalities include magnetic resonance imaging (MRI), computed tomography, and positron emission tomography (PET). Among these modalities, MRI is the most frequently used for diagnosis of NMDARE. Routine MRI typically includes T2-weighted, and/or fluid attenuated inversion recovery sequences. However, MRI findings are abnormal in only 25-50% of NMDARE patients, show diverse severity, heterogeneous anatomical distributions, and can normalize during the recovery phase of NMDARE (Irani et al. 2010, Titulaer et al. 2013, Heine et al. 2015, de Montmollin et al. 2017, Peer et al. 2017, Xu et al. 2020, Zhang et al. 2020, Wang et al. 2021, Bastiaansen et al. 2022, Nissen et al. 2022).

In contrast to MRI, PET is rarely employed in the diagnosis of NMDARE and studies are mostly limited to fluorodeoxyglucose-PET in a small number of cases. In these cases, metabolic alterations (both hypo- and hypermetabolism) were noted in various brain regions (Heine et al. 2015). A recent study found that abnormal brain fluorodeoxyglucose-PET was present in 15 out of 17 NMDARE patients, half of which had normal brain MRI, suggesting a higher sensitivity of PET compared to routine MRI (Nissen et al. 2022). However, both routine MRI and fluorodeoxyglucose-PET abnormalities are not disease-specific and more importantly can return normal results (Heine et al. 2015, Abboud et al. 2021). Recently, a PET tracer for activated NMDAR, namely 18F-GE179, was used in five NMDARE patients upon remission to quantify open NMDAR in various brain regions. Compared to healthy controls and one seroconverted NMDARE patient (NMDAR1-AB negative at PET), 18F-GE179 PET revealed a reduced density of open NMDAR in the anterior temporal and superior parietal cortices of NMDAR1-AB positive cases (Galovic et al. 2021). PET tracers developed to detect activated glia cells in other inflammatory CNS diseases, such as ligands targeting the translocator protein TSPO, i.e. 11C-PK11195, 11C-PBR28, 11C-DAA1106, 11C-DPA713 or 18F-PBR06 (Leng and Edison 2021), have not yet been tested in NMDARE patients.

In addition to routine clinical MRI, some studies performed multimodal MRI measurements in NMDARE patients after the acute phase and compared findings to healthy controls (Finke et al. 2013, Finke et al. 2016, Peer et al. 2017, Phillips et al. 2018, Guo et al. 2021, Wu et al. 2022). Advanced MRI techniques, including resting state functional MRI (rs-fMRI), diffusion tensor imaging, or arterial spin labeling, were used to derive parameters such as regional homogeneity, functional connectivity, cerebral blood flow, neurovascular coupling (correlation coefficients of regional homogeneity and cerebral blood flow), functional connectivity, fractional anisotropy, and mean diffusivity. An early multimodal MRI examination of structural and functional brain changes by Finke et al. found reduced functional connectivity between the anterior hippocampus and the anterior default mode network in 24 NMDARE patients, which correlated with memory performance (Finke et al. 2013). T1-weighted and T2-weigthed structural imaging did not reveal clinically relevant brain changes, and gray matter examined by voxel-based morphometry was not significantly reduced compared to healthy controls. Diffusion tensor imaging, however, revealed

reduced fractional anisotropy and increased mean diffusivity, in particular in the cingulum, indicating white matter changes (Finke et al. 2013). In contrast to this early study, a follow-up study by the same research group with extended patient number (n=40) and improved methodology found significant reductions in hippocampal volumes, bilateral atrophy of hippocampal input and output regions, as well as a bilateral increase of mean diffusivity in the hippocampus indicating impaired microstructural integrity. Importantly, these MRI findings were significantly correlated with memory performance, disease severity and duration (Finke et al. 2016). The significantly reduced hippocampal connectivity was replicated by the same research group in another observational study including 43 NMDARE patients, of which 24 were previously reported (Finke et al. 2013, Peer et al. 2017). Expectedly, hippocampal connectivity measurements in patients correlated with verbal memory performance assessed via the Rey auditory verbal learning test. Furthermore, the authors observed alterations of frontotemporal connections and a decoupling of medial temporal and default mode networks (Peer et al. 2017). The research group then analyzed superficial white matter via diffusion tensor imaging in a cohort of 46 NMDARE patients (Phillips et al. 2018). The authors observed significantly increased mean diffusivity, a measure of microstructural integrity, in the superficial white matter of non-recovered NMDARE patients, whereas recovered NMDARE patients were comparable to healthy controls. This white matter damage was not restricted to a single brain area and present within the frontal, temporal, and parietal lobes (Phillips et al. 2018). Similar to the initial report by Finke and colleagues, a recent longitudinal MRI investigation of brain morphology in 25 NMDARE patients did not reveal atrophy of hippocampal volumes despite a significant atrophy of total brain volume, the cerebellum and brain stem after a mean follow-up of 2 years (Gomez-Figueroa et al. 2021), which might be attributed to limitations of automated segmentation.

More recent MRI examinations of NMDARE patients focused on analyzing regional homogeneity, a proxy for neuronal activity synchronization, to assess resting state brain activity (Wu et al. 2022) and neurovascular coupling, a phenomenon that adjusts cerebral blood flow depending on neuronal activity and can be evaluated by correlating cerebral blood flow and regional homogeneity (Guo et al. 2021). Wang et al. observed lower regional homogeneity values in the cerebellum, basal ganglia, as well as the cerebral cortex, including the frontal, parietal and temporal lobes, indicating lower resting state brain activity in 40 NMDARE patients. Importantly, patients displayed worse executive function assessed via executive control scores in the attention network test, and executive control scores in patients were negatively correlated with regional homogeneity values of the bilateral inferior parietal lobule (Wu et al. 2022). Another recent cross-sectional study in 23 convalescent NMDARE patients by Guo et al. found decreased neurovascular coupling in several gray matter regions in NMDARE patients, which correlated with several cognitive function scores (Guo et al. 2021).

Although various MRI abnormalities have been identified in NMDARE patients and might be useful to monitor disease progression or treatment efficacy, it remains unclear whether these findings are disease-specific as NMDARE patients were compared to healthy controls, not to patients with other inflammatory CNS conditions (Oliveira and Ehrenreich 2018). In addition, none of the studies reported NMDAR1-AB titers at the time of magnetic resonance imaging. Hence it remains unclear if NMDAR1-AB directly contribute to these alterations.

## 1.4 Neuropathology

Examination of neuropathology in NMDARE patients are relatively scarce. Presently, autopsy results are reported for only eleven NMDARE patients (Tuzun et al. 2009, Martinez-Hernandez et al. 2011, Filatenkov et al. 2017, Nauen 2017, Hirano et al. 2019, Mariotto et al. 2019, Zrzavy et al. 2021a) and in some cases overlap with other pathologies, such as probable B cell lymphoma (Mariotto et al. 2019), post-transplant lymphoproliferative disease, small cell lung carcinoma, or demyelination (Zrzavy et al. 2021a). Brain biopsies, mostly from frontal lobe, were analyzed and reported in at least eight cases (Kruer et al. 2010, Camdessanche et al. 2011, Martinez-Hernandez et al. 2011, Bien et al. 2012, Takeda et al. 2014). Importantly, these cases represent a heterogeneous subgroup of severe NMDARE cases, differing in clinical manifestation, clinical course (mono- or polyphasic), time after presentation (31-1460 days), immunotherapy and treatment response, NMDAR1-AB titers, age, sex, and underlying pathologies. Furthermore, methodologies differ substantially between reports and are mostly limited to qualitative examination of gliosis and presence of general lymphocytic cell populations, including CD3+ T cells, sometimes differentiating CD4+ and CD8+ T cells, CD20+ or CD79a+ B cells as well as CD138+ ASC. Importantly, these reports repeatedly claim the presence of plasma cells. However, a detailed characterization of CD138+ ASC, i.e. by Ki-67 or BLIMP1 expression (Nutt et al. 2015), has not yet been performed. Hence, it remains unclear whether the CD138+ cell population constitute long-lived plasma cells or rather short-lived plasmablasts. Considering, the normal concentrations of CXCL12 in CSF of NMDARE patients (Kothur et al. 2016b, Liu et al. 2020), which is a major determinant of ASC recruitment and retention in the bone marrow (Nutt et al. 2015), direct recruitment and retention of plasma cells seems unlikely. However, elevated CXCL10 and CXCL13 concentrations in patient CSF (Leypoldt et al. 2015, Byun et al. 2016, Kothur et al. 2016b, Liba et al. 2016, Liu et al. 2020) may promote lymphocyte infiltration, including B cells and plasmablasts (Meinl et al. 2008, Nutt et al. 2015). Within the frequently observed perivascular cuffs, maintenance of ASC is likely supported by local synthesis of IL-6, TNFα, and APRIL, which were, except for APRIL that remains controversial (Kothur et al. 2016b, Deng et al. 2017), found to be elevated in CSF of NMDARE patients (Byun et al. 2016, Kothur et al. 2016b, Liba et al. 2016, Chen et al. 2018, Liu et al. 2020, Zou et al. 2020).

Consistent with the predominantly lymphocytic composition of white blood cells in CSF of NMDARE patients (Dalmau et al. 2008, de Montmollin et al. 2017, Xu et al. 2020), lymphocytic perivascular cuffs are frequently observed in various brain regions in autopsies as well as biopsies of NMDARE patients (Tuzun et al. 2009, Kruer et al. 2010, Camdessanche et al. 2011, Martinez-Hernandez et al. 2011, Bien et al. 2012, Takeda et al. 2014, Filatenkov et al. 2017, Nauen 2017, Hirano et al. 2019, Mariotto et al. 2019, Zrzavy et al. 2021a). Concomitantly, strong microgliosis indicating ongoing neuroinflammation is present in affected brain regions and particularly prominent in the hippocampus (Tuzun et al. 2009, Filatenkov et al. 2017, Nauen 2017, Hirano et al. 2019, Zrzavy et al. 2021a) and basal ganglia (Tuzun et al. 2009, Filatenkov et al. 2017, Zrzavy et al. 2021a). Often, other gray matter regions, such as the neocortex (Tuzun et al. 2009, Bien et al. 2012), superior temporal gyrus, basal fore brain (Tuzun et al. 2009), amygdala, medial temporal gyrus (Zrzavy et al. 2021a), fusiform gyrus (Hirano et al. 2019), medial temporal lobe (Nauen 2017), or the frontal lobe (Kruer et al. 2010, Camdessanche et al. 2011, Martinez-Hernandez et al. 2011, Bien et al. 2012, Takeda et al. 2014, Filatenkov et al. 2017) are affected

in some NMDARE patients, however with striking variability. Interestingly, white matter abnormalities and demyelination with and without axonal degeneration were observed in some patients (Takeda et al. 2014, Hirano et al. 2019, Zrzavy et al. 2021a).

Concomitant with reports of intrathecal IgG synthesis, perivascular infiltration of CD20+ or CD79a+ B cells or CD138+ ASC, along with CD4+ T cells, and CD8+ T cells was found in all autopsy cases. In contrast to infiltrating T cells, which were abundant in perivascular cuffs and scattered throughout the parenchyma of affected brain regions, infiltrating B cells and ASC were restricted to perivascular cuffs and rarely found in the parenchyma (Tuzun et al. 2009, Martinez-Hernandez et al. 2011, Bien et al. 2012, Filatenkov et al. 2017, Nauen 2017, Zrzavy et al. 2021a). Although most studies are limited to qualitative examinations, few studies have investigated the proportions of T and B cells showing that T cells out-numbered B cells and ASC (Bien et al. 2012, Filatenkov et al. 2017, Zrzavy et al. 2021a). Interestingly, the predominance of T cells, the perivascular enrichment of B cells, and sparse B cell infiltration into the brain parenchyma is similar to histopathological findings in multiple sclerosis lesions (Serafini et al. 2004, Machado-Santos et al. 2018, Sabatino et al. 2019).

Despite the abundance of CD8+ T cells in the CNS of NMDARE patients, cytotoxic (FasL+, granzymeB+, or perforin+) T cells are rare or absent (Tuzun et al. 2009, Bien et al. 2012, Zrzavy et al. 2021a). Similarly rare are Fas+ or TIA-1+ cells (Tuzun et al. 2009), pointing against a major role of T-cell mediated cyto-toxicity or antibody-dependent cellular cytotoxicity. Also, deposition of the complement component C9 was absent (Tuzun et al. 2009, Bien et al. 2012, Zrzavy et al. 2021a), indicating that complement-de-pendent cytotoxicity does not play a major role in NMDARE pathogenesis. A single report found CD4d deposition in small vessels of the frontal lobe and basal ganglia (Filatenkov et al. 2017). Deposition of earlier complement components, the role of glial complement receptors or Fc-receptors have not yet been investigated.

Neuronal loss was found in an early report and involved loss of pyramidal neurons in the hippocampus of one autopsied patient and mild neuronal loss in the basal ganglia of another patient (Tuzun et al. 2009). Another autopsy case showed scattered lesions and neuronal loss in the limbic system (Hirano et al. 2019). In contrast, five other autopsies did not reveal obvious neuronal loss (Nauen 2017, Zrzavy et al. 2021a). Interestingly, one autopsy case of a NMDARE patient with a probable B cell lymphoma showed severe tissue destruction with neuronal loss and massive lymphomatous infiltrates, predomi-nantly consisting of CD20+ B cells, in the cerebral white matter, thalamus and basal ganglia. Whereas neuronal loss was absent in tumor free frontal regions and the hippocampus despite the presence of perivascular CD79a+ B cells (Mariotto et al. 2019) suggesting that the presence of neuronal damage may depend on underlying or concomitant pathologies. Indirect evidence for CNS injury, neuronal and neuroaxonal damage was obtained in three studies that found elevated serum concentrations of neuro-filament light chain, neuron specific enolase, and S100b in NMDARE patients (Liu et al. 2018b, Guasp et al. 2022, Ma et al. 2022). Hence, neuronal damage can be assumed in some NMDARE cases but does not seem to be a major determinant of NMDARE pathogenesis.

In conclusion, histopathological studies revealed neuroinflammation, characterized by microgliosis, T cell, B cell, and ASC infiltration, in several brain regions, often prominently affecting the hippocampus. The findings furthermore underscore the heterogeneity of NMDARE and point against a uniform pathomechanism. It should, however, be noted that post mortem tissues were limited to a subgroup of severely affected NMDARE cases in a progressed disease stage that often underwent multiple rounds of immunotherapy. In contrast, brain biopsies were limited to single brain regions, such as the frontal lobe, that may not be the focal point of neuroinflammation. Therefore, to study the etiology and pathomechanism(s) of NMDARE, construct valid animal models are of utmost importance.

## 1.5 Diagnosis, treatment and outcome

The current consensus guidelines for diagnosing NMDARE were proposed by Graus et al. in 2016. The diagnostic criteria for probable NMDARE include a rapid onset (<3 months) of symptoms (at least 4 of 6) such as (I) abnormal behavior or cognitive dysfunction, (II) speech dysfunction, (III) seizures, (IV) movement disorder, dyskinesia, or rigidity, (V) decreased level of consciousness, (VI) autonomic dysfunction or central hypoventilation. Secondly, abnormal EEG, CSF pleocytosis or presence of oligoclonal bands are indicative of a neuroinflammatory disease and NMDARE. Lastly, other disorders must be reasonably excluded. If all these three criteria are met, a diagnosis of 'probable NMDARE' can be made without the testing for NMDAR1-AB. However, according to Graus and colleagues, a definite diagnosis of NMDARE requires the detection of NMDAR1-AB in CSF of patients. Furthermore, the authors proposed that, if NMDAR1-AB are detected in CSF and other disorders are reasonably excluded, the presence of one of the above mentioned symptoms is sufficient for a definite diagnosis of NMDARE (Graus et al. 2016). Importantly, using these criteria to retrospectively classify NMDARE cases reported in a large observational cohort study (Titulaer et al. 2013), Graus et al. identified a 'probable NMDARE diagnosis' in only 80% of 532 patients (Graus et al. 2016) reflecting the heterogeneous and complex clinical manifestation in many NMDARE patients. For this reason and because the proposed diagnostic criteria are not pathognomonic to NMDARE, the diagnosis still heavily relies on NMDAR1-AB testing.

The current best practice guidelines for treatment of NMDARE, established by the Autoimmune Encephalitis Alliance Clinicians Network, recommend initiation of first line immunotherapy, in patients with suspected autoimmune encephalitis, once infectious etiologies have been ruled out (Abboud et al. 2021). First line immunotherapies typically include corticosteroids (i.e. intravenous methylprednisolone, 1g/day for 3-7 days) alone or in combination with intravenous immunoglobulin (2g/kg for 2-5 days), and/or plasma exchange/ therapeutic apheresis (typically 5-10 sessions every other day) depending on disease severity (Abboud et al. 2021). If patients do not improve upon completion of first line immunotherapy, B cell depletion with rituximab (commonly dosed at 375mg/m$^2$ weekly for 4 weeks or two times 1000mg in two week intervals) is recommended for NMDARE cases (Abboud et al. 2021, Thaler et al. 2021). However, a recent meta-analysis of 1550 NMDARE cases found a 7.3-fold increased risk for poor functional outcome if second-line immunotherapy was initiated within 60 days of disease onset, which was not confounded by the disease severity at nadir (Nosadini et al. 2021). In NMDARE patients unresponsive to second-line therapeutics, the protease inhibitor bortezomib and the IL-6 receptor antagonist tocilizumab have been tested as third-line immunotherapy with limited success (Dalmau et al. 2019, Abboud et al. 2021, Dinoto et al. 2021). Fortunately, classical immunotherapy is usually well tolerated and severe adverse events are relatively rare and reported in only 3% of NMDARE patients according to a recent systematic review (Nosadini et al. 2021). Furthermore, immunotherapy with corticosteroids may even benefit viral encephalitis patients if used adjunctive to antivirals (Thompson et al. 2000, Meyding-Lamade et al. 2003, Kamei et al. 2005) enabling early polypragmatic treatment approaches with combined antiviral, antibiotic, and immunosuppressive therapy.

In addition to immunotherapy, early tumor resection is pivotal in paraneoplastic NMDARE cases (Dalmau et al. 2008, Titulaer et al. 2013, Dalmau et al. 2019). Less efficient are symptomatic treatment

approaches such as standard anti-seizure medication that, if considered, should be complementary to immunotherapy (Mohammad et al. 2016, de Bruijn et al. 2019, Wright et al. 2021). Noteworthy, NMDARE patients may be prone to antipsychotic-related adverse effects (Mohammad et al. 2016, Sarkis et al. 2019). Surprisingly, the administration of ketamine, an NMDAR antagonist, effectively suppressed agitation in six out of six pediatric NMDARE patients without causing a worsening of other symptoms (Mohammad et al. 2016).

Recently, novel treatment approaches have been experimentally tested in animal models with the aim to reverse NMDAR1-AB mediated NMDAR hypofunction. Promising candidates include the neurosteroid pregnenolone sulfate, which potentially counteracts NMDAR internalization by increasing the trafficking of functional NMDAR to the cell surface (Kostakis et al. 2013, Wright et al. 2021). However, the inhibitory effects of pregnenolone sulfate on other ionotropic receptors and its dualistic allosteric modulation of NMDA receptors depending on their subunit composition (Geoffroy et al. 2022) may limit its clinical use. In contrast to pregnenolone sulfate, the structurally-related neurosteroid 24(S)-hydroxycholesterol and its derivative SGE-301 potentiate NMDAR function without distinct subunit selectivity (Paul et al. 2013, Geoffroy et al. 2022) and can reverse NMDAR1-AB mediated effects in vitro (Warikoo et al. 2018) and in rodent passive transfer models (Mannara et al. 2020, Radosevic et al. 2022). However, the exact mechanism by which NMDAR surface expression was rescued in SGE-301 treated animals is unclear and probably goes beyond simple positive allosteric modulation.

Fortunately, the functional outcome one year after NMDARE onset is considered favorable (mRS≤2; independent living) in the majority (about 70%) of patients (McKeon et al. 2018, Broadley et al. 2019, Nosadini et al. 2021, Bastiaansen et al. 2022, Nissen et al. 2022) in particular when immunotherapy and, if applicable, tumor resection are initiated early on (Irani et al. 2010, Titulaer et al. 2013, de Montmollin et al. 2017, McKeon et al. 2018, Balu et al. 2019, Peng et al. 2020, Abboud et al. 2021, Heine et al. 2021, Nosadini et al. 2021). Compared to anti-LGI1/CASPR2 encephalitis, as well as a group comprising various autoantibody-associated AE, NMDARE was associated with the worst functional outcome at three months follow up in a recent prospective multicenter observational study. However, after 12 months, functional outcome was comparable between groups and favorable (mRS≤2) in 50-70% of AE patients (Seifert-Held et al. 2021). Lasting disabilities (mRS≥3 at ≥1 year follow up) were noted in 22-27% of NMDARE patients despite immunotherapy (Nosadini et al. 2021, Bastiaansen et al. 2022, Nissen et al. 2022) and are more frequent in late-onset (>45 years old) NMDARE (Peng et al. 2020, Bastiaansen et al. 2022, Nissen et al. 2022) as well as in adult compared to pediatric patients (Nosadini et al. 2021). Expectedly, lack of immunotherapy is also associated with a poor prognosis (Broadley et al. 2019). Clinical relapses of NMDARE occur in approx. 12-17% of cases (Titulaer et al. 2013, Thaler et al. 2021, Bastiaansen et al. 2022, Feng et al. 2022, Nissen et al. 2022). The mortality rate of NMDARE is about 6-10% (Nosadini et al. 2021, Bastiaansen et al. 2022, Nissen et al. 2022, Zhong et al. 2022).

To improve prognosis of NMDARE cases, Balu et al. retrospectively analyzed the association between early clinical features and poor functional outcome (mRS≥3) one year after initial symptoms in a cohort of 382 NMDARE patients. The authors identified five statistically independent variables that were associated with a poor functional outcome, namely delayed immunotherapy (>4 weeks after onset), lack of clinical improvement within 4 weeks, abnormal MRI, increased WBC in CSF (>20 cells/μL), and ICU

admission. The authors used these parameters to construct the 'anti-NMDAR Encephalitis One Year Functional Status (NEOS)' score - a 5-point prediction score, in which each parameter contributes 1 point (Balu et al. 2019). In addition to the original report, the NEOS score was retrospectively validated in a pediatric cohort and prospectively in Chinese patients (Peng et al. 2020, Loerinc et al. 2021, Ma et al. 2022).

In contrast to crude outcome measures of physical impairment, such as the mRS, detailed neuropsychological evaluations of convalescent NMDARE patients are relatively scarce. Nevertheless, various case series and cohort studies investigated the neuropsychological outcome of NMDARE, typically focusing on cognitive domains such as verbal memory, visuospatial memory, working memory, executive function, verbal fluency/language, overall intellectual function, attention, and processing speed. Although all studies found a substantial frequency of long-lasting cognitive dysfunction in convalescent NMDARE patients, including patients considered functionally recovered (mRS=0), the affected cognitive domains were remarkably diverse (Finke et al. 2012, Finke et al. 2013, Finke et al. 2016, Matricardi et al. 2016, McKeon et al. 2016, de Bruijn et al. 2018, McKeon et al. 2018, Phillips et al. 2018, Guo et al. 2021), which is likely a result of the relatively small cohort sizes in combination with the heterogeneous clinical manifestation of NMDARE. Later, McKeon and colleagues extracted the clinical features of 109 treated NMDARE patients in a systematic review of 44 small scale studies and evaluated neuropsychological dysfunction at three time points during disease progression (acute, subacute, and chronic). Overall, diverse cognitive deficits were identified in three quarters of patients across all time points. While some individual cognitive domains, i.e. working memory, visuospatial memory, language and attention, significantly improved upon recovery from NMDARE, impairments in processing speed, episodic memory, and some executive functions persisted (McKeon et al. 2018). Complementing these earlier observations, a prospective longitudinal study examined the neuropsychological long-term outcome of NMDARE in 43 adult convalescent patients, focusing on executive function, verbal and visuospatial memory, working memory, and attention (Heine et al. 2021). Importantly, Heine et al. identified cognitive deficits in all patients more than two years after disease onset and moderate/severe impairments were persistent in two thirds of patients, despite significant improvements and absence of lasting physical disability (median mRS=1, range 0-1) at the follow up around 5 years (Heine et al. 2021). Although patients improved in some cognitive domains upon the second study visit, the overall rate of executive dysfunction (60% of patients) and memory impairments (20-55% depending on domain) remained high at the follow up around 5 years (Heine et al. 2021). In contrast to previous reports, Heine et al. did not observe speech/language disorder, which might be explained by the long follow-up period.

To summarize, despite its severity at disease nadir, NMDARE has a relatively good functional outcome if treated appropriately. However, cognitive deficits persist in the majority of patients and long-term recovery can be slow, prompting the development of new adjunctive therapies.

## 1.6  Pathogenesis

Currently, the pathogenesis and in particular the pathomechanism(s) initiating neuroinflammation remain the least investigated aspects of NMDARE. Although, autoantibodies against NMDAR1 have been extensively studied and their potential to cause NMDAR hypofunction has been proven beyond reasonable doubt, they have never been shown to initiate neuroinflammation (see 1.7-1.9). Yet, the pathogenesis and sometimes etiology of NMDARE is often incorrectly attributed to NMDAR1-AB (Chen et al. 2018, Makuch et al. 2018, Rosch et al. 2018, Gibson et al. 2020, Liu et al. 2020, Guo et al. 2021, Yue et al. 2021). The extensive focus on NMDAR1-AB provided a number of observations that may help to understand at least some aspects of NMDARE pathogenesis. In addition, two potential triggers of NMDARE have been identified, namely tumors, in particular ovarian teratomas, and virus encephalitis such as HSV or JEV encephalitis (Dalmau et al. 2019). Noteworthy, these triggers only amount to a fraction of NMDARE cases and a cause remains unrecognized in the majority of patients, suggesting complex and potentially diverse pathomechanisms. Two recent systematic reviews account a quarter of NMDARE cases to tumors (Broadley et al. 2019, Nosadini et al. 2021) and two nation-wide observational cohort studies from Denmark and the Netherlands found prior HSE in 10-16% of NMDARE patients (Bastiaansen et al. 2022, Nissen et al. 2022) and an antedated autoimmune disease in 7% (Nissen et al. 2022).

**NMDAR1 autoantibodies**

A frequently neglected observation is that NMDAR1-AB titers are at least one order of magnitude higher in serum compared to CSF of NMDARE patients (Irani et al. 2010, Gresa-Arribas et al. 2014, Makuch et al. 2018, Bastiaansen et al. 2022), indicating that the autoimmune processes initiate in the periphery and 'spill-over' into the CNS compartment. The persistence of peripheral autoimmune processes and continuous generation of NMDAR1-specific B cells in NMDARE patients may explain the efficacy of rituximab, a B cell depleting anti-CD20 antibody, in NMDARE (Nosadini et al. 2021, Zografou et al. 2021). The hypothesis of ongoing autoimmune reactions in the periphery, of at least a fraction of NMDARE patients, was further substantiated by Makuch and colleagues in a cross-sectional analysis of peripheral blood mononuclear cells, serum, and CSF isolated from ten NMDARE patients. Makuch et al. observed circulating NMDAR1-specific peripheral B cells as well as NMDAR1-AB of the IgM and IgG isotype that persisted for several months or years after disease onset, suggesting continuous germinal center reactions instead of a primary immunization that generates long-lived plasma cells (Makuch et al. 2018). In addition to germinal center reactions, NMDAR1-AB may be produced upon activation of naïve B cells. Cloning of heavy and light chain genes from NMDARE-associated intrathecal B cells revealed a lack of somatic hypermutations in some NMDAR1-AB clones, indicating that NMDAR1-specific B cells are part of the naïve B cell repertoire (Kreye et al. 2016, Wenke et al. 2019). However, it remains unknown where and how these cells are activated, and whether NMDAR1-specific B cells migrate into the CNS prior to or in response to neuroinflammation.

In contrast to the migration of B cells into the CNS, more is known about potential entry routes of NMDAR1-AB during NMDARE. Under physiological conditions, continuous 'spill-over' of peripheral

NMDAR1-AB into the CNS is limited by the blood-brain barrier (BBB) to about 0.2% of the serum anti-body pool (Reiber and Peter 2001). However, in 27-39% of NMDARE cases, the entry of peripheral NMDAR1-AB into the CNS is facilitated by a dysfunctional blood-brain or blood-CSF barrier, which is typically assessed via an albumin quotient of paired serum and CSF samples (Reiber and Peter 2001, Malter et al. 2013, Durr et al. 2021, Yu et al. 2021). In addition to continuous 'spill-over' of NMDAR1-AB from the periphery into the CNS, intrathecal immunoglobulin synthesis is frequently observed in NMDARE patients and may be an additional source of NMDAR1-AB. Qualitative evidence of intrathecal IgG synthesis, namely CSF specific oligoclonal bands, is observed in approximately 72-84% of NMDARE patients (Durr et al. 2021, Bastiaansen et al. 2022, Nissen et al. 2022). Noteworthy, some reports observed a change of WBC and OCB with disease progression, showing higher WBC at onset and a time-dependent increase of OCB, suggesting that intrathecal immunoglobulin synthesis is secondary to immune invasion and encephalitis onset (Irani et al. 2010, Durr et al. 2021). Importantly, CSF specific OCBs are likely not explained by NMDAR1-AB as these antibodies are present at higher concentrations in serum. Quantitative evidence for intrathecal immunoglobulin synthesis, via determination of immunoglobulin and albumin concentrations in paired serum and CSF samples, was observed in 21-44% NMDARE patients for IgG (Durr et al. 2021, Yu et al. 2021, Bastiaansen et al. 2022), in 35% for IgM and 15% for IgA (Durr et al. 2021). Notably, neither OCBs nor immunoglobulin quotients confirm intrathecal synthesis of NMDAR1-AB. To assess intrathecal synthesis of NMDAR1-AB, a specific antibody index based on NMDAR1-AB titers and total IgG quotients in paired serum and CSF samples can be evaluated. Although intrathecal NMDAR1-AB synthesis can be assumed if CSF titers are higher or within a hundred-fold lower than serum titers, formal evidence either by NMDAR1-AB specific antibody indices or by cloning of NMDAR1-specific B cells from patients CSF is limited to a few exemplary NMDARE and HSE cases (Pruss et al. 2012, Hansen et al. 2013, Kreye et al. 2016, Malviya et al. 2017). In fact, Kreye and colleagues observed that only nine out of 170 antibodies cloned from CSF derived ASC from three out of eight NMDARE patients are directed against NMDAR1, whereas the vast majority of cloned antibodies recognized other neuronal or astrocytic antigens (Kreye et al. 2016). Due to the small number of patients in which NMDAR1-AB antibody indices were determined the proportion of NMDARE patients with intrathecal NMDAR1-AB synthesis remains unknown. It should, however, be noted that intrathecal NMDAR1-AB are likely immunoprecipitated by binding to the GluN1 subunit of NMDAR (Castillo-Gomez et al. 2016), which is abundantly expressed throughout the CNS (Moriyoshi et al. 1991, Kutsuwada et al. 1992, Meguro et al. 1992, Monyer et al. 1992, Monyer et al. 1994, Paoletti et al. 2013) resulting in 'artificially' lowered NMDAR1-AB titers in CSF compared to serum samples, which may result in false-negative antibody indices.

Although NMDAR1-AB are frequently implicated in the pathogenesis of NMDARE, correlations between NMDAR1-AB titers and clinical outcome or cognitive function remain relatively poor and highly controversial. Contributing to this are underreported NMDAR1-AB titers, in particular in CSF, at follow-up time points in longitudinal studies. Considering the reversible mode of action of NMDAR1-AB, correlations between NMDAR1-AB titers at disease onset and long-term outcome, although frequently reported, suffer from a rather questionable relevance. Furthermore, NMDAR1-AB and disease severity might be confounded by the underlying autoimmune processes, whereas NMDAR1-AB titers at follow-up are

likely biased by the timing of and response to immunotherapy. This might explain why correlations between outcome and NMDAR1-AB titers remain controversial with some studies reporting a significant association (Irani et al. 2010, Gresa-Arribas et al. 2014) whereas others do not (Finke et al. 2016, Finke et al. 2017). Furthermore, no correlation was found between NMDAR1-AB titers and cognitive function or structural hippocampal measures (Finke et al. 2016, Phillips et al. 2018), and NMDAR1-AB CSF titers of fully recovered (mRS=0) NMDARE patients did not differ from non-recovered patients (Phillips et al. 2018). Also, clinical improvements and recovery of NMDARE patients frequently occurs despite the persistence of NMDAR1-AB in patient CSF (Hansen et al. 2013, Gresa-Arribas et al. 2014, Liba et al. 2016, Liu et al. 2020), suggesting a major contribution of the underlying neuroinflammatory processes to the clinical phenotype and disease severity.

**Ovarian teratomas**

Originally, the anti-NMDAR encephalitis was described as a paraneoplastic disease associated with ovarian teratomas, as patients recovered upon tumor resection and immunotherapy. This hypothesis was corroborated by histological analysis of resected teratomas containing neuronal tissues that ectopically express NMDAR subunits (Dalmau et al. 2007). However, after substantial research and implementation of diagnostic consensus guidelines (Graus et al. 2016) NMDARE is now mostly diagnosed in tumor-free patients. Overall, a tumor association is found in about one quarter of NMDARE patients (Broadley et al. 2019, Nosadini et al. 2021) and ovarian teratomas are the most frequent tumor type, in particular amongst young patients (Dalmau et al. 2011, Titulaer et al. 2013, Bost et al. 2018, Bastiaansen et al. 2022). Importantly, in paraneoplastic NMDARE cases, tumors are likely involved in the pathogenesis of NMDARE as tumor resection is pivotal for recovery (Dalmau et al. 2008, Titulaer et al. 2013, Dalmau et al. 2019).

Until recently, histopathological analyses of NMDARE-associated ovarian teratomas were limited to controlled case series with a limited amount of NMDARE cases (Tuzun et al. 2009, Dabner et al. 2012, Day et al. 2014, Tabata et al. 2014, Iemura et al. 2018, Makuch et al. 2018). These studies were recently supplemented by Chefdeville and colleagues, who compared the histopathology of 27 ovarian teratomas from NMDARE patients to 40 'sporadic' ovarian teratomas without associated autoimmune disease (Chefdeville et al. 2019). Both mature as well as immature ovarian teratomas have been associated with NMDARE, with mature teratomas being more common (Tuzun et al. 2009, Dabner et al. 2012, Day et al. 2014, Bost et al. 2018, Iemura et al. 2018, Chefdeville et al. 2019). Importantly, nervous tissue is not exclusively expressed in NMDARE-associated teratomas and found in the majority of ovarian teratomas (Tuzun et al. 2009, Dabner et al. 2012, Day et al. 2014, Tabata et al. 2014, Iemura et al. 2018, Chefdeville et al. 2019). The frequency with which nervous tissue elements were identified in control teratomas, however, differs between reports. While Chefdeville et al. found nervous tissue in all but one NMDARE-associated teratoma, in contrast to only 40% of control teratomas, earlier reports observed nervous tissues in almost all teratomas, independent of disease status (Tuzun et al. 2009, Dabner et al. 2012, Day et al. 2014, Tabata et al. 2014, Iemura et al. 2018) If nervous tissue was present, GluN1 and GluN2 subunits were, independent of disease status, commonly expressed in neuroglial elements, indicating that ectopic expression of GluN1/NMDAR does not inevitably result in autoimmune encephalitis (Tuzun et al. 2009, Tabata et al. 2014, Iemura et al. 2018, Chefdeville et al. 2019). Interestingly, close

to the nervous tissue/neuroglial elements, intratumoral lymphoid infiltrates consisting of CD3+ T cells and CD20+ B cells were present in the majority of NMDARE-associated teratomas and strikingly rare in other sporadic teratomas (Tuzun et al. 2009, Dabner et al. 2012, Day et al. 2014, Tabata et al. 2014, Iemura et al. 2018, Chefdeville et al. 2019). This suggests that the initiation of NMDARE-associated autoimmune processes may require ectopic expression of NMDAR coinciding with a prominent immune activation or a particular type of antigen presentation. In support of this hypothesis are findings of tertiary lymphoid structures, reactive germinal centers, lymphoid follicles, and B cell aggregates in close proximity to neuroglial elements in a fraction of NMDARE-associated teratomas (Tuzun et al. 2009, Dabner et al. 2012, Day et al. 2014, Iemura et al. 2018, Makuch et al. 2018, Chefdeville et al. 2019). Furthermore, diffuse IgG and IgA deposition were observed in the majority of NMDARE-associated teratomas (Chefdeville et al. 2019), indicating ongoing autoimmune/antitumor processes in paraneoplastic NMDARE cases. Importantly, direct evidence of autoreactive B cells directed against the GluN1 subunit and intratumoral NMDAR1-AB synthesis was obtained by Makuch and colleagues who cultured teratoma explants as well as B cells and ASC aspirated from ovarian teratomas. In conditions favoring either maintenance of ASC or B cell proliferation, NMDAR1-AB of the IgG class were detected in cell culture supernatants (Makuch et al. 2018).

**Viral encephalitides**

Some years after the first description of NMDARE, a retrospective analysis of CSF and serum samples from herpes simplex virus encephalitis patients reported NMDAR1-AB in 30% of HSV encephalitis (HSE) patients. HSE-associated NMDAR1-AB were of either IgM, IgA, or IgG isotypes and intrathecal synthesis of IgG NMDAR1-AB was identified in three out of 44 cases (Pruss et al. 2012). Concomitantly, a retrospective analysis of CSF samples that were PCR positive for family members of Herpesviridae, including HSV-1, HSV-2, HHV-6, VZV, EBV, or CMV, showed that 27% contained autoantibodies against either NMDAR1, AMPAR or other unclassified neuronal or non-neuronal antigens (Linnoila et al. 2016). These findings led to the hypothesis, that NMDAR1-AB are associated with HSE relapses in patients with HSV-negative CSF. Indeed, a variety of case series and a prospective study observed NMDAR1-AB and other anti-neuronal autoantibodies in the CSF of patients relapsing from HSE ('post-HSE AE') as well as beneficial effects of immunotherapy in these patients (Armangue et al. 2014, Hacohen et al. 2014, Mohammad et al. 2014, Armangue et al. 2015, Sutcu et al. 2016, Westman et al. 2016, Pruss 2017, Armangue et al. 2018). These findings were further substantiated by a systematic review and a prospective study, showing that post-HSE autoimmune encephalitis occurs on average within one month in about one quarter of HSE patients, of which more than half had NMDAR1-AB positive CSF (Nosadini et al. 2017, Armangue et al. 2018). Noteworthy, autoantibodies against other anti-neuronal antibodies, including GABA$_A$R, AMPAR, D2R-AB, were frequent in CSF of AE as well as non-AE patients post-HSE (Armangue et al. 2014, Mohammad et al. 2014, Armangue et al. 2015, Graus et al. 2016, Linnoila et al. 2016, Pruss 2017, Armangue et al. 2018). Importantly, some patients develop NMDAR1-AB after HSE without clinical signs of relapse (Linnoila et al. 2016, Armangue et al. 2018), indicating that NMDAR1-AB and AE are not directly linked by causality but instead are generated in response to a shared underlying autoimmune response. Furthermore, the clinical manifestation and cognitive performance of NMDAR1-AB positive HSE cases did not differ from NMDAR1-AB negative

HSE cases (Pruss et al. 2012, Westman et al. 2016). In contrast, Armangue and colleagues observed that psychosis and choreoathetosis were more frequent in NMDAR1-AB positive post-HSE AE cases compared to NMDAR1-AB negative post-HSE cases (Armangue et al. 2018). However, the interpretation of this observation is difficult as the results were potentially confounded by a substantially younger age of NMDAR1-AB positive patients (approx. 2 vs. 56 years).

In addition to HSE, Japanese encephalitis (JE), which is caused by the Japanese encephalitis virus (JEV), has been associated with NMDARE and NMDAR1-AB (Ma et al. 2017, Ma et al. 2020, Liu et al. 2021). After an initial description NMDAR1-AB in the CSF of three patients and NMDARE-associated clinical symptoms during a relapse from the usually monophasic JE (Ma et al. 2017, Ashraf et al. 2021), two prospective studies have further substantiated post-JE NMDARE (Ma et al. 2020, Liu et al. 2021). Similar to post-HSE NMDARE, NMDARE can occur within one month after JE onset (Ma et al. 2017, Ma et al. 2020) and other anti-neuronal autoantibodies, including $GABA_BR$-AB and unclassified neuronal autoantibodies were found in the CSF of a fraction of post-JE AE cases (Liu et al. 2021). The absence of anti-neuronal autoantibodies during the acute phase of JE (Liu et al. 2021) indicates de novo autoantibody formation, further supporting the hypothesis that neuronal autoantigen shedding in response neuronal destruction, which is common in both HSE and JE (Kennedy and Chaudhuri 2002, Whitley 2006, Ashraf et al. 2021), in combination with sufficient immune stimulation may initiate autoimmune processes. Importantly, the use and safety of approved inactivated and live attenuated JEV vaccines (Ashraf et al. 2021) points against a major role of molecular mimicry.

Considering the rarity of AE, JE, and HSE, their chronological connection, and absence of anti-neuronal autoantibodies in CSF at HSE and JE onset (Westman et al. 2016, Liu et al. 2021), a causal relationship is likely. Furthermore, post-HSE and post-JE autoimmune mechanisms are not limited to NMDAR1-AB and also induce other anti-neuronal autoantibodies, suggesting that HSV- and JEV-associated nervous tissue destruction and immune stimulation via damage associated molecular patterns (DAMPs) and/or pathogen associated molecular patterns (PAMPs) are more likely involved than molecular mimicry. The shedding of neuronal autoantigens in response to encephalitides was demonstrated by analyses of exosomes derived from sera of HSV1-infected rodents or CSF of antibody-associated AE, including NMDARE, which contained neuronal autoantigens such as NMDAR, $GABA_BR$, and AMPAR (Gu et al. 2021, Li et al. 2022). Importantly, the presence of NMDAR1-AB in CSF of some patients without clinical relapse after HSE (Linnoila et al. 2016, Armangue et al. 2018), suggests a complex encephalitogenesis that goes beyond simple presence of intrathecal NMDAR1-AB. Furthermore, serum NMDAR1-AB have been associated with prior influenza A/B infections (Hammer et al. 2014a) indicating that NMDAR1-AB may also be expressed antigen-independently after general immune activation. In conclusion, the pathomechanism(s) by which neuroinflammation is initiated in NMDARE remain understudied and unknown.

## 1.7 NMDAR1 autoantibodies

**Prevalence**

Although, originally implicated in NMDARE, NMDAR1-AB are frequently present in healthy humans and other mammals (Dahm et al. 2014, Hammer et al. 2014a, Hammer et al. 2014b, Pan et al. 2018, Pan et al. 2021) and these so-called 'naturally occurring' NMDAR1-AB have been extensively reviewed elsewhere (Ehrenreich 2017, 2018, Wilke et al. 2019, Ehrenreich et al. 2021). In brief, naturally occurring NMDAR1-AB are of either IgM, IgA, or IgG subclasses, are highly prevalent in serum, and their seroprevalence increases with age. In comparison to NMDARE, titers of naturally occurring NMDAR1-AB are relatively low and typically range from 1:10 to 1:320 in the current 'gold-standard' cell-based assay (Euroimmun) (Dahm et al. 2014). Importantly, NMDAR1-AB have not yet been convincingly associated with the development of neuropsychiatric diseases but have been associated with prior influenza infection and might be related to neuropsychiatric symptoms in individuals with an impaired blood-brain barrier (Dahm et al. 2014, Hammer et al. 2014a, Hammer et al. 2014b, Ehrenreich 2018). Furthermore, the high seroprevalence of NMDAR1-AB in healthy individuals, their presence in different mammals, and relative frequency in comparison to other anti-neuronal autoantibodies (Dahm et al. 2014) point against a purely pathogenic relevance (Ehrenreich et al. 2021).

**Isotypes**

While NMDARE has originally been associated with NMDAR1-AB of the IgG subclass, a retrospective analysis of 94 CSF samples from NMDARE patients revealed the presence of NMDAR1-AB of both IgA and IgG isotypes in 41%, which was significantly associated with the presence of ovarian teratomas. However, the authors did not observe differences in the clinical manifestation of NMDAR1-AB IgG+/IgA+ patients compared to IgG+/IgA- NDMARE patients despite higher IgG NMDAR1-AB titers in IgA positive CSF samples. Interestingly, a linear correlation between IgA and IgG NMDAR1-AB titers was observed in double positive CSF samples, potentially reflecting a stronger autoimmune response in patients with ovarian teratoma (Desestret et al. 2015). Furthermore, a longitudinal analysis of serum samples revealed continuous production of NMDAR1-AB of the IgM subclass, in addition to NMDAR1-AB IgG, that was highest at disease onset but persisted for months and sometimes years in some NMDARE patients (Makuch et al. 2018). Further characterization of patients NMDAR1-IgG repertoire revealed a predominance of IgG1 as well as the presence of IgG2 and IgG3 isotypes, whereas IgG4 NMDAR1-AB were absent (Dalmau et al. 2008, Tuzun et al. 2009, Hughes et al. 2010, Irani et al. 2010, Kreye et al. 2016).

**Epitopes**

As NMDAR1-AB are frequently found in healthy individuals, a variety of studies investigated whether NMDARE-associated NMDAR1-AB recognize a distinct epitope on the GluN1 subunit. First evidence for a binding of patient NMDAR1-AB to the amino-terminal domain of GluN1 was obtained by Dalmau et al. who showed that antibody binding is abrogated in truncated GluN1 constructs lacking amino acids 25-380 (Dalmau et al. 2008). Furthermore, NMDAR1-AB binding to GluN1 is independent of exon five and does not require expression of other NMDAR subunits such as GluN2A or GluN2B (Dalmau et al. 2008, Gleichman et al. 2012). Epitope mapping revealed that binding of patient CSF derived NMDAR1-

AB depends on amino acids within the seventh N-glycosylation site of GluN1 (Asn368, Gly369, Thr370, hereafter referred to as G7 epitope). However, it remained inconclusive if post-translational modification of the G7 epitope is required for NMDAR1-AB binding. While treatment of GluN1-transfected cells with tunicamycin, or mutations of the N-X-T/S consensus motif of N-glycosylation sites (Kornfeld and Kornfeld 1985, Mellquist et al. 1998), including N368Q, N368D, and T370A, all prevented N368 glycosylation, only tunicamycin treatment and N368Q mutation fully abolished NMDAR1-AB staining. In contrast, N368D and T370A mutation only partially blocked antibody binding (Gleichman et al. 2012). Furthermore, mutations of G369, which did not affect glycosylation of N368, similarly interfered with NMDAR1-AB binding. While G369 mutation to nonpolar amino acids (G369A, G369I, or G369L) fully prevented antibody binding, G369 mutation to polar amino acids (G369S, G369T) only partially reduced the NMDAR1-AB staining (Gleichman et al. 2012, Gresa-Arribas et al. 2014). The authors also confirmed that N368 glycosylation itself does not interfere with NMDAR1-AB binding, by immunoprecipitation of N368 glycosylated GluN1, extracted from rodent brains, with patient CSF (Gleichman et al. 2012).

Importantly, the main function of NMDAR1-AB, which involves binding and cross-linking of NMDAR resulting in NMDAR internalization and reduced surface expression, does not depend on binding to the G7 epitope (Castillo-Gomez et al. 2017) and G7-epitope binding NMDAR1-AB have not yet been associated with distinct functional properties. Although the G7 epitope is frequently recognized by NMDAR1-AB, the NMDAR1-AB repertoire is often polyclonal (Kreye et al. 2016, Castillo-Gomez et al. 2017) and not every NMDARE CSF sample contains G7-epitope binding NMDAR1-AB (Castillo-Gomez et al. 2017). Furthermore, a recent immunohistochemical analysis of binding patterns of NMDARE CSF samples as well as monoclonal NMDAR1-AB revealed two distinct binding patterns (Wagner et al. 2020), which point against a limitation of NMDAR1-AB binding to a single epitope. Pattern one includes strong binding to pyramidal cell bodies in CA1 pyramidal layer, occurs in a fraction of NMDARE patient samples, and is common to commercial polyclonal anti-NMDAR1 antibodies. In contrast, pattern two is often referred to as 'neuropil' staining in NMDARE related publications and shows prominent staining of the hippocampal neuropil without staining of pyramidal cell bodies, indicating binding to postsynaptic NMDAR (Wagner et al. 2020).

**Patient derived monoclonal NMDAR1-AB**

By now, a variety of NMDAR1-AB have been cloned from NMDARE patient derived intrathecal B cells, including, amongst others, clone SSM5 (Malviya et al. 2017), clones 5F5 and 2G6 (Sharma et al. 2018), the somatically hypermutated clone #003-102 (Kreye 2016) as well as the 'germline configured' clone #003-109 (Kreye et al. 2016, Wenke et al. 2019). Clone SSM5 has been shown to compete with patient CSF for binding to hippocampal NMDAR, requires an intact G7-epitope, and reduces NMDAR-dependent functions in cultured oligodendrocytes (Matute 2006, Malviya et al. 2017). Clones 5F5 and 2G6 were derived from peripheral blood of a single patient and sequence analysis revealed that these clones likely originated from independent B cell lineages confirming that NMDARE patients can have a polyclonal repertoire of functional NMDAR1-AB. Furthermore, both clones recognized epitopes in the amino terminal domain of NMDAR. Importantly, both 5F5 and 2G6 were functional in vitro and in vivo, but did not compete for NMDAR binding (Sharma et al. 2018), further supporting an epitope independent pathogenic potential of NMDAR1-AB and diversity of NMDAR1-AB epitopes. The 'germline configured'

NMDAR1-AB clone #003-109 binds to native, fixed, as well as ectopically expressed GluN1, albeit with lower affinity compared to the matured #003-102 (Wenke et al. 2019). Both #003-109 and #003-102 recognize epitopes that depend on N368 of GluN1 as they do not bind to N368Q mutants (Kreye et al. 2016, Wenke et al. 2019). Typical NMDAR1-AB functionality (NMDAR internalization) has been confirmed in vitro for the somatically hypermutated #003-102 as well as germline configured antibody clone #003-109, indicating that functionality does not require affinity maturation (Kreye et al. 2016, Wenke et al. 2019)

**Molecular mode of action**

As the name suggests, anti-NMDAR1 autoantibodies bind to the GluN1 subunit of NMDAR. N-methyl-D-aspartate receptors are $Ca^{2+}$ permeable cation channels, key players in excitatory neurotransmission (Figure 1A), and activated by glutamate in combination with glycine or D-serine (Traynelis et al. 2010, Paoletti et al. 2013). NMDA receptors consist of two GluN1 subunits that alternatingly assemble with two GluN2A, GluN2B, GluN2C, GluN2D, GluN3A, and/or GluN3B subunits (1-2-1-2 or 1-2-1-3) to diheterotetrameric or triheterotetrameric receptors (Lee et al. 2014, Tajima et al. 2016, Zhu et al. 2016, Lu et al. 2017, Zhang et al. 2021). While GluN1 is obligatory for functional NMDAR (Monyer et al. 1992, Forrest et al. 1994, Cui et al. 2004, Paoletti et al. 2013) and ubiquitously expressed throughout the CNS, the composition of GluN2 and GluN3 subunits differs between brain regions and is highly plastic (Monaghan and Cotman 1985, Moriyoshi et al. 1991, Kutsuwada et al. 1992, Meguro et al. 1992, Monyer et al. 1992, Monyer et al. 1994, Traynelis et al. 2010, Paoletti et al. 2013). Importantly, as NMDAR1-AB binding to GluN1 is unaffected by the subunit composition and independent of alternative GluN1-splicing (Dalmau et al. 2008, Gleichman et al. 2012), NMDAR1-AB theoretically have the potential to act on NMDAR throughout the brain as long as they are expressed on the cell surface and not sterically hindered by NMDAR-associated proteins (Wilke et al. 2019). Topologically, NMDAR are transmembrane proteins consisting of four domains, the amino-terminal domain, the ligand-binding domain, a transmembrane domain, and the intracellular C-terminal domain (Traynelis et al. 2010). Both the amino terminal and the ligand binding domain are located on the extracellular site and hence are the main targets of functionally relevant NMDAR1-AB (Wilke et al. 2019).

On a theoretical basis, NMDAR1-AB binding could affect single receptor properties and agonize, antagonize, or allosterically modulate NMDA receptors. In addition, NMDAR1-AB could affect NMDAR function by altering NMDAR trafficking, including receptor cross-linking and internalization, or indirectly alter cellular functions through interactions with molecular or cellular immune system components, such as complement proteins or Fc-receptors (Diamond et al. 2009, Wilke et al. 2019). Based on histopathological findings in NMDARE brains, complement dependent cytotoxicity and antibody-dependent cellular cytotoxicity are unlikely associated with NMDAR1-AB binding (see 1.4). In contrast, antibody-dependent cellular phagocytosis, i.e. via deposition of early complement components and recognition by microglial complement receptors (Brown and Neher 2014), have not yet been investigated and cannot be ruled out by the present state literature. As most patient-derived NMDAR1-AB bind to the amino-terminal domain and not the agonist-binding domain (Dalmau et al. 2008, Gleichman et al. 2012, Gresa-Arribas et al. 2014, Kreye et al. 2016, Castillo-Gomez et al. 2017) allosteric modulation seems more likely than direct receptor activation or inactivation. Furthermore, the arrangement of NMDAR subunits (two GluN1

subunits on opposing sites) favors bivalent inter-NMDAR binding (crosslinking) instead of bivalent intra-NMDAR binding.
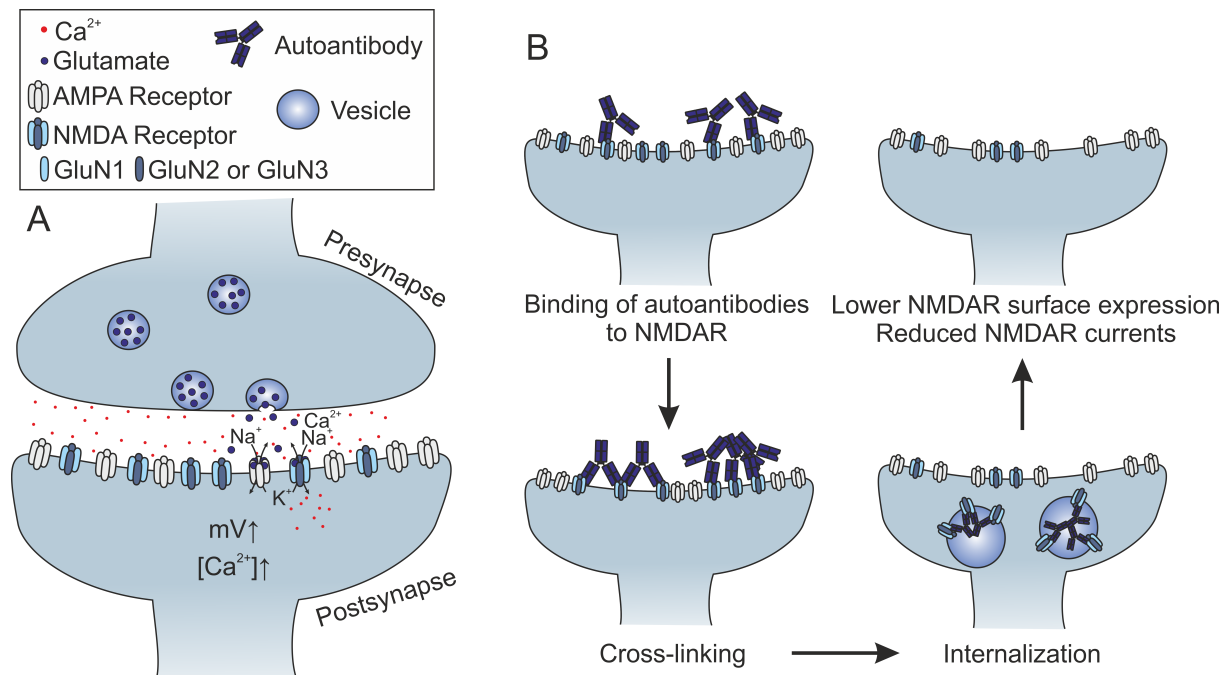


**Figure 1:** Function of NMDAR and NMDAR1-autoantibodies, published in (Wilke et al. 2019). **A**, Postsynaptic NMDA receptors are key players of excitatory neurotransmission. In response to presynaptic glutamate release, postsynaptic AMPA receptors are activated resulting in a depolarization of the membrane potential (mV). This depolarization releases a $Mg^{2+}$ block from NMDAR resulting enabling glutamate-evoked channel opening and influx of $Ca^{2+}$, and $Na^+$ ions and outflow of $K^+$. While AMPAR contribute mainly to the fast component of excitatory postsynaptic potentials (EPSCs), the slow EPSC component is dominated by NMDAR-mediated currents, due to their delayed activation and slower inactivation kinetics. Furthermore, the influx of $Ca^{2+}$ initiates a variety of intracellular signaling pathways involved in long-term potentiation (Paoletti et al. 2013). **B**, Effect of NMDAR1-AB. NMDAR1-AB bind both synaptic and extrasynaptic NMDAR resulting in NMDAR cross-linking and subsequent internalization. The lower NMDAR surface expression reduces NMDAR-mediated currents, thereby inducing a state of NMDAR hypofunction.

By now, a substantial number of in vitro studies have investigated effects of NMDAR1-AB on various NMDAR-expressing cells and collectively shown that NMDAR1-AB mediate a reduction of surface NMDAR expression (Hughes et al. 2010, Mikasova et al. 2012, Hammer et al. 2014a, Moscato et al. 2014, Kreye et al. 2016, Malviya et al. 2017, Ladepeche et al. 2018, Pan et al. 2018, Sharma et al. 2018, Warikoo et al. 2018, Jones et al. 2019, Mannara et al. 2020, Ding et al. 2021), reduce NMDAR-mediated currents or $Ca^{2+}$ response (Hughes et al. 2010, Mikasova et al. 2012, Moscato et al. 2014, Kreye et al. 2016, Castillo-Gomez et al. 2017, Malviya et al. 2017, Warikoo et al. 2018, Jones et al. 2019, Wenke et al. 2019, Matute et al. 2020, Ding et al. 2021), and impair NMDAR-dependent long-term potentiation (LTP) (Zhang et al. 2012, Ding et al. 2021). The underlying mode of action, involves bivalent binding of NMDAR1-AB to synaptic and extrasynaptic NMDA receptors (Hughes et al. 2010), which affects NMDAR surface dynamics depending on NMDAR subunit composition and causes a clustering of GluN2B-containing NMDAR (Mikasova et al. 2012, Ladepeche et al. 2018). Independent of subunit composition or NMDAR activation, NMDAR1-AB binding causes a dose-dependent and reversible NMDAR internalization (Hughes et al. 2010, Mikasova et al. 2012, Moscato et al. 2014, Ladepeche et al. 2018, Warikoo et al. 2018, Wenke et al. 2019), thereby explaining the observed reduction in surface NMDAR expression and NMDAR-mediated currents, as well as the impaired hippocampal long-term potentiation (Figure 1B).

This NMDAR1-AB-dependent NMDAR internalization has been shown multiple times in different in vitro systems, including murine hippocampal or cortical neuron cultures (Hughes et al. 2010, Mikasova et al. 2012, Hammer et al. 2014a, Moscato et al. 2014, Kreye et al. 2016, Malviya et al. 2017, Ladepeche et al. 2018, Sharma et al. 2018, Warikoo et al. 2018, Jones et al. 2019, Mannara et al. 2020), acute brain slices (Zhang et al. 2012, Ding et al. 2021), primary oligodendrocyte cultures (Matute et al. 2020), human neuron cultures derived from induced pluripotent stem cells (Castillo-Gomez et al. 2017, Pan et al. 2018), and heterologous expression systems such as oocytes (Castillo-Gomez et al. 2017, Malviya et al. 2017), indicating that NMDAR internalization is neither species specific nor exclusive to neurons. Analyzed NMDAR1-AB containing samples include commercial NMDAR1-AB (Castillo-Gomez et al. 2017, Pan et al. 2018), purified immunoglobulins (Hughes et al. 2010, Mikasova et al. 2012, Hammer et al. 2014a, Jones et al. 2019, Ding et al. 2021), patient derived monoclonal NMDAR1-AB (Kreye et al. 2016, Malviya et al. 2017, Wenke et al. 2019, Matute et al. 2020), patient CSF (Hughes et al. 2010, Mikasova et al. 2012, Zhang et al. 2012, Moscato et al. 2014, Ladepeche et al. 2018, Warikoo et al. 2018, Mannara et al. 2020), or diluted and/or dialyzed serum/plasma samples (Castillo-Gomez et al. 2017, Pan et al. 2018, Wagnon et al. 2020, Ding et al. 2021). Importantly, NMDAR1-AB mediated NMDAR internalization did neither depend on binding to the G7 epitope nor on the immunoglobulin class (IgG, IgA, IgM) (Hammer et al. 2014a, Castillo-Gomez et al. 2017, Pan et al. 2018). NMDAR internalization has been observed after several minutes (Zhang et al. 2012, Hammer et al. 2014a, Castillo-Gomez et al. 2017, Pan et al. 2018, Sharma et al. 2018, Ding et al. 2021) hours (Mikasova et al. 2012, Kreye et al. 2016, Malviya et al. 2017, Ladepeche et al. 2018, Wenke et al. 2019, Mannara et al. 2020, Matute et al. 2020, Ding et al. 2021) and days (Hughes et al. 2010, Moscato et al. 2014, Warikoo et al. 2018) of NMDAR1-AB application. Although internalization typically occurs within minutes (Schneider et al. 2008, de Juan-Sanz et al. 2011, Hammer et al. 2014b), some studies did not find an effect of NMDAR1-AB within 30 min (Mikasova et al. 2012, Moscato et al. 2014, Ladepeche et al. 2018, Wenke et al. 2019) potentially due to different assay sensitivities or recycling of internalized NMDAR after prolonged incubation (Hammer et al. 2014b). Indeed, most internalized NMDAR accumulate in recycling endosomes (Moscato et al. 2014), which usually form within 30 min after internalization (Schneider et al. 2008, de Juan-Sanz et al. 2011, Hammer et al. 2014b). In addition to receptor recycling, a fraction of the internalized NMDAR is degraded in lysosomes (Moscato et al. 2014) resulting in a time-dependent decrease of surface NMDAR that plateaus after 12 h (Moscato et al. 2014). Importantly, NMDAR1-AB had no major effects on neuronal viability or morphology, including dendritic branching and number of synapses (Hughes et al. 2010, Mikasova et al. 2012), and did not affected AMPA receptor expression or currents (Hughes et al. 2010, Wenke et al. 2019), inhibitory postsynaptic currents (Moscato et al. 2014), kainate- or GABA-evoked currents (Wenke et al. 2019) or residual surface NMDAR function (Warikoo et al. 2018, Wenke et al. 2019).

In contrast to NMDAR internalization, which is measurable on a bulk receptor level and usually measured after preincubation with NMDAR1-AB, electrophysiological studies about acute effects (time scale of seconds) on NMDA receptor function in the presence of NMDAR1-AB are scarce. One study observed that acute local perfusion of hippocampal neurons with NMDAR1-AB did not alter NMDA-evoked current amplitudes, whereas NMDAR currents were reduced after 24h preincubation with NMDAR1-AB (Jones

et al. 2019), suggesting that NMDAR1-AB mainly act via NMDAR internalization but do not directly antagonize NMDAR function.

**NMDAR hypofunction**

Already prior to the discovery of NMDARE and NMDAR1-AB function, NMDA receptor hypofunction has been intensively researched as it is associated with schizophrenia-like symptoms in both humans and rodents (Willetts et al. 1990, Jentsch and Roth 1999, Newcomer et al. 1999, Olney et al. 1999, Newcomer and Krystal 2001, Coyle et al. 2003, van den Buuse 2010, Moghaddam and Javitt 2012, Paoletti et al. 2013, Balu 2016, Geoffroy et al. 2022).

In humans, acute exposure to sub anesthetic doses of NMDAR antagonists, such as the use-dependent open-channel blockers ketamine and phencyclidine (PCP) (Traynelis et al. 2010), induces a dose-dependent and reversible state of NMDAR hypofunction that is accompanied by reduced cognitive function. Particularly affected domains include working memory, declarative memory, attention, verbal fluency, and reaction time. Furthermore, positive symptoms of schizophrenia, such as agitation, hallucinations, delusions, or disorganized thinking, and negative symptoms like motor retardation, blunted affect, or emotional withdrawal are frequently induced by NMDAR antagonists (Krystal et al. 1994, Jentsch and Roth 1999, Newcomer et al. 1999, Newcomer and Krystal 2001, Coyle et al. 2003, Balu 2016). In addition, acute administration of ketamine transiently reduces symptoms of major depressive disorder and treatment resistant depression (Aan Het Rot et al. 2012, Krystal et al. 2019, Carboni et al. 2021). At higher doses the NMDAR antagonist ketamine acts as dissociative anesthetic and has been associated with anterograde amnesia (Newcomer and Krystal 2001). Importantly, subtle memory impairments are measurable at lower doses than those required to induce schizophrenia like symptoms (Newcomer et al. 1999, Newcomer and Krystal 2001).

In rodents, administration of PCP, MK-801, ketamine, and other NMDAR antagonists results in spatial memory impairments, reduces some non-spatial memory functions, and induces psychosis-like symptoms characterized by hyperlocomotion, altered pre-pulse inhibition, and stereotypic behavior, such as circling and head weaving (Morris et al. 1986, Morris 1989, Willetts et al. 1990, Jentsch and Roth 1999, Newcomer and Krystal 2001, van den Buuse 2010). At higher doses, hyperlocomotion is replaced by hypolocomotion due to an increase in stereotypic behavior, emergence of ataxia, and, at even higher doses, anesthetic effects (van den Buuse 2010).

In addition to pharmacological studies, chronic NMDAR hypofunction has been genetically modeled in mice. Importantly, a complete knockout of the GluN1 subunit (Grin1$^{-/-}$ mice) is lethal and results in postnatal death within 8-15 h (Forrest et al. 1994), highlighting the physiological importance of NMDAR. To study less severe NMDAR hypofunction, a variety of GluN1 mutant mouse models, including Grin1$^{Neo}$ (Mohn et al. 1999, Fradley et al. 2005, Bickel et al. 2008), Grin1$^{K483Q}$ (Kew et al. 2000), Grin1$^{D481N}$ (Kew et al. 2000), Grin1$^{D481N/K483Q}$ (Ballard et al. 2002), as well as conditional Grin1 knockout mice (Cui et al. 2004, Dang et al. 2006) have been developed. While some models investigate consequences of a global NMDAR hypofunction caused by either a reduction of GluN1/NMDAR expression (Grin1$^{Neo}$) or NMDAR glycine affinities (Grin1$^{K483Q}$, Grin1$^{D481N}$, or Grin1$^{D481N/K483Q}$) (Mohn et al. 1999, Kew et al. 2000, Ballard et al. 2002, Fradley et al. 2005, Bickel et al. 2008), other models have focused on the role of NMDAR

hypofunction in specific brain regions by conditional knockouts of GluN1 in regions such as the striatum (Dang et al. 2006), forebrain (Cui et al. 2004) or hippocampal CA1 (Tsien et al. 1996). Mice carrying a homozygous Grin1$^{Neo}$ mutation expressed only about 5-10% of normal GluN1/NMDAR amounts and were characterized by hyperlocomotion, increased stereotypic behavior, deficits in social and sexual interaction, increased startle response, and an altered pre-pulse inhibition (Mohn et al. 1999, Fradley et al. 2005, Bickel et al. 2008). In contrast, mice carrying homozygous Grin1$^{D481N}$ mutations, which reduces glycine affinity by 5-fold, display altered NMDAR expression accompanied by deficits in hippocampal LTP and spatial learning, reduced sensitivity to NMDA-induced seizures, increased startle response, but normal pre-pulse inhibition, normal anxiety-related behavior, no difference in locomotor activity or stereotypic behavior (Kew et al. 2000). A more severe reduction in glycine affinity (i.e. by 86-fold) in mice carrying homozygous Grin1$^{K483Q}$ mutations results in early postnatal death (Kew et al. 2000), similar to Grin1$^{-/-}$ mice (Forrest et al. 1994). Grin1$^{D481N/K483Q}$ hybrid mice are viable but display persistent hyperactivity and increased stereotypic behavior, disrupted nest building ability, and impaired spatial learning and memory (Ballard et al. 2002). In summary, these findings indicate that NMDAR hypofunction induces symptoms in a dose/severity-dependent manner with subtle memory deficits preceding, hyperlocomotion, increased stereotypic behavior, and impaired pre-pulse inhibition.

Collectively, these findings from human and rodent studies suggests that NMDAR antagonism/hypofunction induces cognitive deficits as well as negative and positive symptoms of schizophrenia in a dose dependent manner, starting with subtle deficits in NMDAR-dependent memory function (i.e. spatial learning/memory in rodents, and working and declarative memory in humans), followed by psychiatric symptoms, such as hyperlocomotion and stereotypic behavior in rodents, or agitation and hallucinations in humans. At higher doses, NMDAR antagonism/hypofunction causes dissociation and loss of consciousness. As these symptoms are common in NMDARE patients and because NMDAR1-AB can cause NMDAR hypofunction, NMDAR1-AB are often considered as a major pathogenic driving force underlying the anti-NMDAR encephalitis.

## 1.8 Passive transfer models

By now, a variety of rodent passive transfer models have been established to investigate effects of NMDAR1-AB in vivo. Table 1 summarizes main findings of these studies as well as critical parameters, that must be considered when different passive transfer models are compared, including the time period (acute versus continuous), administration routes (peripheral, intracerebroventricular, intrahippocampal), as well as the transferred sample type (crude CSF, dialyzed CSF, purified AB, or recombinant/mono-clonal AB). Despite these differences between studies, some molecular, electrophysiological, electro-encephalographic, and behavioral observations have been repeatedly reported in different models.

Molecularly, NMDAR1-AB infused rodents typically display IgG deposition (Hughes et al. 2010, Malviya et al. 2017, Sharma et al. 2018), decreased GluN1 immunoreactivity (Hughes et al. 2010, Mikasova et al. 2012, Malviya et al. 2017), and decreased synaptic NMDAR density (Planaguma et al. 2015, Malviya et al. 2017, Mannara et al. 2020, Radosevic et al. 2022) in the hippocampus, confirming the NMDAR1-AB mediated NMDAR internalization observed in vitro. Importantly, passive transfer of patient CSF, purified patient IgG, purified commercial NMDAR1-AB, or patient-derived monoclonal NMDAR1-AB did not result in neuroinflammation or neuronal loss (Li et al. 2015, Planaguma et al. 2015, Malviya et al. 2017, Taraschenko et al. 2019) pointing against an encephalitogenic potential of NMDAR1-AB in healthy brains.

A NMDAR1-AB dose-dependent increase of extracellular glutamate, nitric oxide and concomitant dysregulation of AMPA receptors was found in an early acute passive transfer model (Manto et al. 2010). However, this study is in stark contrast to various passive transfer models showing normal hippocampal AMPA receptor density (Planaguma et al. 2015) and function (Wang et al. 2019), normal presynaptic release probability measured by paired pulse ratios or mEPSC frequency (Planaguma et al. 2016, Wurdemann et al. 2016, Blome et al. 2018, Wang et al. 2019, Mannara et al. 2020, Radosevic et al. 2022), and normal NMDAR-independent mossy fiber LTP (Blome et al. 2018). In line with NMDAR1-AB mediated NMDAR internalization, electrophysiology in brain slices obtained from NMDAR1-AB infused rodents consistently shows reduced NMDAR-dependent LTP in various hippocampal regions (Planaguma et al. 2016, Wurdemann et al. 2016, Blome et al. 2018, Kersten et al. 2019, Mannara et al. 2020, Radosevic et al. 2022). Furthermore, reduced NMDAR-mediated excitatory postsynaptic poten-tials in dentate granule cells (Wurdemann et al. 2016), reduced amplitudes and increased interevent intervals of spontaneous excitatory postsynaptic currents in CA3 pyramidal neurons (Wright et al. 2021), as well as reduced amplitudes but normal frequencies of NMDAR-mediated miniature excitatory postsynaptic currents in hippocampal neurons (Wang et al. 2019) were observed upon passive transfer of NMDAR1-AB, indicating decreased excitatory neurotransmission in the hippocampus. In contrast, hippocampal inhibitory neurotransmission seems to be unaffected, as NMDAR1-AB infusion did not alter the amplitude or frequency of inhibitory postsynaptic currents (Wright et al. 2021). Also, a depolarized resting membrane potential and increased excitability was observed in CA3 pyramidal neurons upon NMDAR1-AB infusion (Wright et al. 2021). Although, NMDAR1-AB infused rodents do not display spon-taneous seizures and show variable drug-induced seizure susceptibility (Wright et al. 2015, Wurdemann et al. 2016), electroencephalographic analyses revealed increased seizure burden (Taraschenko et al.

2019, Wright et al. 2021).

Behavioral abnormalities upon infusion of NMDAR1-AB into the CNS of rodents include reversibly impaired novel object recognition (Planaguma et al. 2015, Planaguma et al. 2016, Malviya et al. 2017, Kersten et al. 2019, Mannara et al. 2020, Radosevic et al. 2022), impaired working memory (Wang et al. 2019), depressive-like behavior (Planaguma et al. 2015, Planaguma et al. 2016), as well as impaired spatial learning/memory performance in the Morris water maze (Li et al. 2015). Normal locomotor activity (Li et al. 2015, Planaguma et al. 2015, Kersten et al. 2019, Taraschenko et al. 2019, Mannara et al. 2020, Radosevic et al. 2022) and normal anxiety-like behavior (Planaguma et al. 2015, Kersten et al. 2019, Taraschenko et al. 2019) were observed in rodents upon intracerebroventricular or intrahippocampal NMDAR1-AB infusion. In contrast, NMDAR1-AB dependent increased voluntary wheel running and exacerbation of MK-801 induced hyperlocomotion were observed in peripheral passive transfer models upon blood-brain barrier dysfunction (Hammer et al. 2014a, Sharma et al. 2018).

While impaired novel object recognition, working memory, and spatial learning/memory can be explained by NMDAR-hypofunction, depressive-like behavior and normal locomotor activity are not easily explained by classical effects of NMDAR-antagonists, such as ketamine and MK-801, in rodents (Morris et al. 1986, Morris 1989, Willetts et al. 1990, Jentsch and Roth 1999, Newcomer and Krystal 2001, van den Buuse 2010). Furthermore, some researchers observed effects of NMDAR1-AB directed against intracellular epitopes (Wurdemann et al. 2016), which conflict with the proposed mechanism of reversible NMDAR internalization as intracellular epitopes are not regularly accessible in live cells.

In addition to direct passive transfer models, two reports established placental transfer models in which pregnant mice were injected with NMDAR1-AB between embryonic/gestational day 13-17 (Jurek et al. 2019, Garcia-Serra et al. 2021). Fetuses exposed to NMDAR1-AB displayed decreased NMDAR expression and cortical thinning (Garcia-Serra et al. 2021). NMDAR1-AB exposed neonates displayed reduced NMDAR density, impaired hippocampal LTP, decreased sEPSC amplitudes, normal sEPSC frequency, as well as impaired neurodevelopmental reflexes and deficits in novel object recognition (Jurek et al. 2019, Garcia-Serra et al. 2021). Young adult offspring of NMDAR1-AB treated dams transiently displayed lasting hyperlocomotion, lower anxiety, as well reduced volumes of several brain regions, including the hippocampus, which mostly normalized upon aging (Jurek et al. 2019). Importantly, the effects of an in utero exposure to NMDAR1-AB can be ameliorated by blocking the neonatal Fc-receptor (Garcia-Serra et al. 2021).

Other treatment approaches targeting NMDAR1-AB mediated effects in direct continuous passive transfer models include intracerebroventricular infusion of ephrin B2, a ligand of the EphB2 receptor (Planaguma et al. 2016), subcutaneous delivery of the CNS accessible IL1-receptor antagonist anakinra (Taraschenko et al. 2021), as well as subcutaneous administration of SGE-301 - a CNS accessible 24(S)-hydroxycholesterol derivative (Mannara et al. 2020, Radosevic et al. 2022). While Taraschenko et al. show that anakinra treatment reduced the seizure burden and expression of Iba1 and GFAP, two glial markers upregulated upon inflammation, in mice infused with NMDAR1-AB, the study lacks proper controls (anakinra versus vehicle treatment of control IgG infused mice) necessary to attribute the observed effects to NMDAR1-AB. In the first place, prior work of this group has shown, that Iba1 and GFAP expression was not elevated upon NMDAR1-AB infusion (Taraschenko et al. 2019) questioning the

relevance of the observed reduction upon anakinra treatment. In contrast, continuous intracerebroventricular infusion of ephrin B2 ameliorated most NMDAR1-AB mediated effects in mice (Planaguma et al. 2016). However, continuous intracerebroventricular treatment with ephrin B2 would be technically challenging in humans and has not been followed-up. Furthermore, the exact mechanism by which ephrin B2 reverses NMDAR1-AB mediated effects is still poorly understood. While ephrin B2 administration antagonized NMDAR internalization without affecting the binding of NMDAR1-AB to NMDAR, it activated EphB2 and increased EphB2/NMDAR interaction (Planaguma et al. 2016) indicating that the effects are mediated indirectly via EphB2. The effects of a direct modulation of NMDA receptors via SGE-301, a NMDAR-specific positive allosteric modulator (Geoffroy et al. 2022), were recently studied in similar continuous passive transfer mouse models (Mannara et al. 2020, Radosevic et al. 2022). Both studies observed partial recovery of most NMDAR1-AB mediated impairments upon SGE-301 treatment. However, the mechanism by which SGE-301 restored NMDAR surface expression in NMDAR1-AB infused mice is unclear and not easily explained by an interference with NMDAR1-AB mediated receptor internalization. Binding of NMDAR1-AB to NMDAR was not affected by SGE-301 and treatment of SGE-301 had opposing effects on synaptic NMDAR in mice infused with patient or control CSF (Mannara et al. 2020). In contrast, SGE-301 effects on synaptic NMDAR in control CSF infused mice was not observed if the treatment was delayed (Radosevic et al. 2022). In general, effects of allosteric modulators such as SGE-301 are limited to surface NMDAR and might show limited therapeutic potential, if too many NMDAR have been internalized by NMDAR1-AB.

**Table 1:** Overview of NMDAR1-AB related passive transfer models. BBB, blood-brain barrier; EPSC, excitatory postsynaptic currents; EPSP, excitatory postsynaptic potential; LPS, lipopolysaccharide; LTP, long-term potentiation; MWCO, molecular weight cut off.

| Study | Passive transfer type (acute/chronic, sample) | Cellular and molecular changes in NMDAR1-AB infused animals | Behavioral alterations in NMDAR1-AB infused animals |
|---|---|---|---|
| Hughes et al. 2010, J Neurosci | Continuous (2 weeks) transfer of undiluted patient and control CSF into hippocampus of rats | • IgG deposition and decreased GluN1 immunoreactivity in the hippocampus | not assessed |
| Manto et al. 2010, Orphanet J Rare Dis | Acute transfer of dialyzed patient, control CSF, or purified IgG into CA1 and cortex of rats | • dose-dependent increase of glutamate, increased NO, and dysregulation of AMPAR. | not assessed |
| Manto et al. 2011, J Neurol | Acute transfer of dialyzed patient or purified patient IgG into motor area in cerebral cortex of rats | • enhanced excitability of motor cortex upon high-frequency stimulation on the premotor area | not assessed |
| Mikasova et al. 2012, Brain | Acute (4-7h) transfer of purified patient or control IgG bilaterally into hippocampus of mice | • reduced GluN1 immunoreactivity in the hippocampus | not assessed |
| Hammer et al. 2014, Mol Psychiatry | Acute transfer of purified immunoglobulins containing NMDAR1-AB (IgG, IgA, IgM) into peritoneum of mice with BBB dysfunction, | not assessed | • NMDAR1-AB exacerbated MK-801 induced hyperlocomotion in mice with open BBB |
| Planaguma et al. 2015, Brain | Continuous (2 weeks) bilateral transfer of dialyzed (7kD MWCO) patient or control CSF into lateral ventricles of mice | • decrease of hippocampal NMDAR<br>• no T cell or B cell infiltration, complement deposition or neuronal apoptosis | • reversible deficits in novel object recognition and depressive-like behavior<br>• normal anxiety-like behavior, normal aggression, and normal locomotor activity. |
| Li et al. 2015, Tohoku J Exp Med | Continuous (18 days) transfer of patient or control CSF into lateral ventricles of mice | • no immune cell infiltration, neuronal loss, or gliosis | • normal locomotor activity and novel object recognition<br>• impaired spatial learning/memory in Morris water maze |
| Wright et al. 2015, Brain | Acute transfer of purified patient or control IgG into left hippocampus of mice | • increased seizure susceptibility to pentylenetetrazole | • no spontaneous seizures |
| Planaguma et al. 2016, Ann Neurol | Continuous (2weeks) of dialyzed (30kD MWCO) patient or control CSF with and without ephrin-B2 into lateral ventricles of mice | • altered long-term plasticity and normal short-term plasticity | • deficits in novel object recognition, and increased depressive-like behavior |

| Study | Passive transfer type (acute/chronic, sample) | Cellular and molecular changes in NMDAR1-AB infused animals | Behavioral alterations in NMDAR1-AB infused animals |
|---|---|---|---|
| Würdemann et al. 2016, Brain Res | Acute bilateral transfer of patient or control CSF, or commercial intracellular anti-GluN1 IgG into dentate gyrus of rats | <ul><li>reduced NMDAR-mediated EPSPs in dentate gyrus granule cells</li><li>reduced LTP in the perforant path</li><li>normal epileptogenicity</li><li>normal paired-pulse ratio</li></ul> | <ul><li>impaired performance in the hidden platform training days of the Morris water maze</li><li>increased thigmotaxis</li></ul> |
| Malviya et al. 2017, Ann Clin Transl Neurol | Continuous (2weeks) bilateral transfer of patient derived monoclonal NMDAR1-AB or control IgG into lateral ventricles of mice | <ul><li>progressive IgG deposition and loss of NMDAR immunoreactivity in hippocampus</li><li>reduced NMDAR cluster density</li><li>no neuronal death</li></ul> | <ul><li>reversible impairment in novel object recognition</li></ul> |
| Blome et al. 2018, Front Synaptic Neurosci | Acute transfer of patient or control CSF into hippocampus of rats | <ul><li>decreased LTP at A/C fiber-CA3 synapses</li><li>normal paired-pulse ratio</li><li>NMDAR-independent mossy fiber LTP was unaffected</li></ul> | not assessed |
| Sharma et al. 2018, Ann Clin Transl Neurol | Acute transfer of patient derived monoclonal NMDAR1-IgG into peritoneum or blood of LPS injected mice | <ul><li>IgG deposition in hippocampus</li></ul> | <ul><li>increased voluntary wheel running similar to mice injected with MK-801</li></ul> |
| Kersten et al. 2019, Front Neurol | Acute transfer of patient or control CSF into hippocampus or rats | <ul><li>impaired NMDAR-dependent LTP in CA1</li></ul> | <ul><li>normal locomotor activity</li><li>normal anxiety-like behavior</li><li>impaired novel object recognition</li></ul> |
| Taraschenko et al. 2019, Epilepsia | Continuous (2weeks) transfer of patient CSF, purified patient derived IgG, commercial polyclonal NMDAR1-AB or respective controls into lateral ventricles of mice | <ul><li>no gliosis or neurodegeneration in hippocampus</li><li>increased spontaneous electrographic seizure burden</li><li>reduced excitability of CA1 neurons and membrane resistance</li></ul> | <ul><li>comparable novel object recognition between groups</li><li>normal locomotion and anxiety-like behavior in the open field</li></ul> |
| Wang et al. 2019, Front Neurol | Acute transfer of commercial NMDAR1-AB or vehicle control into dentate gyrus of rats followed, in some cases, by continuous ventricular infusion of vehicle, TNFa, or IL-6 | <ul><li>chronic intraventricular infusion of TNFa or IL.6 exacerbated NMDAR1-AB induced electrophysiological alteration, namely decrease of NMDAR-mediated mEPSC amplitudes.</li><li>NMDAR1-AB did not affect the frequency of hippocampal NMDAR-mediated mEPSC, indicating that presynaptic release probability is unaffected.</li></ul> | <ul><li>TNFa or IL.6 exacerbated NMDAR1-AB induced working memory impairments (spontaneous alternations), worsened performance in MWM hidden platform training days (already from d1)</li></ul> |

**Table 1:** continued.

| Study | Passive transfer type (acute/chronic, sample) | Cellular and molecular changes in NMDAR1-AB infused animals | Behavioral alterations in NMDAR1-AB infused animals |
|---|---|---|---|
| Jurek et al. 2019, Ann Neurol | Placental transfer model. Pregnant mice received intravenous patient derived monoclonal NMDAR1-AB or control IgG at d14-16 of gestation | • reduced sEPSC amplitudes and normal sEPSC frequency in NMDAR1-AB exposed neonates<br>• increased postnatal mortality<br>• impaired neonatal reflexes<br>• lasting alterations in brain morphology | • lasting hyperlocomotion, lower anxiety-related behavior in adult offspring |
| Mannara et al. 2020, Brain | Continuous (2weeks) transfer of patient or control CSF into ventricles of mice with and without SGE-301 treatment | • reduced hippocampal NMDAR density<br>• impaired hippocampal LTP<br>• normal paired-pulse facilitation | • impaired novel object recognition<br>• normal locomotor activity |
| Taraschenko et al. 2021, Epilepsia | Continuous (2weeks) transfer of patient derived purified IgG or monoclonal NMDAR1-AB (no controls) into ventricles of mice with or without anakinra (IL1R antagonist) | • anakinra treatment reduced seizure burden and expression of Iba1 and GFAP in the hippocampus | • no difference in novel object recognition between treatment groups<br>• anakinra treatment did not alter locomotor activity or anxiety-like behavior in the open field |
| Garcia-Serra et al. 2021, Neurol Neuroimmunol Neuroinflamm | Placental transfer model. Pregnant mice received intravenous purified patient or control IgG at d14-16 of gestation with or without neonatal Fc receptor inhibitors | • Fetuses exposed to NMDAR1-AB displayed decreased NMDAR expression and thinning of the cortical plate.<br>• NMDAR1-AB exposed newborns suffered from hippocampal LTP impairments | • NMDAR1-AB exposed newborns showed deficits in novel object recognition. |
| Wright et al. 2021, Commun Biol | Acute and continuous (1week) transfer of purified or control IgG into lateral ventricle of juvenile rats | • in vivo and ex vivo electrophysiological recordings showed effective reduction of hippocampal excitatory neurotransmission which contributed to epileptogenicity | not assessed |
| Radosevic et al. 2022, Neurol Neuroimmunol Neuroinflamm | Continuous (2weeks) transfer of patient or control CSF into ventricles of mice with and without SGE-301 treatment | • decrease of synaptic NMDAR<br>• impaired hippocampal LTP<br>• normal paired-pulse facilitation | • deficits in novel object recognition<br>• normal locomotor activity |
| Kuchling et al. 2022, bioRxiv | Continuous (2weeks) transfer of patient derived monoclonal NMDAR1-AB or isotype control into lateral ventricles of mice | • impaired functional connectivity (rs-fMRI) in dentate gyrus only | not assessed |

## 1.9 Active immunization models

In the past years, a variety of active immunization rodent models have been developed to either study the impact of NMDAR1-AB or to establish models of the anti-NMDAR encephalitis. Most of these immunization strategies are based on GluN1-peptides emulsified in complete Freund's adjuvant (Pan et al. 2018, Wagnon et al. 2020, Ding et al. 2021, Yue et al. 2021). One immunization protocol used recombinant proteins specific to distinct parts of the GluN1 subunit mixed with alum (Lin et al. 2014). Two immunization strategies utilized full-length post-translationally modified GluN1 subunits either ectopically expressed in lamina propria cells of the gut upon adeno associated virus transduction (During et al. 2000) or packaged as natively folded GluN1/GluN2A- or GluN1/GluN2B- containing heterotetrameric holoreceptors reconstituted into proteoliposomes (Jones et al. 2019). Figure 2 illustrates the peptide locations within a natively folded triheterotetrameric (Glun1/GluN2A/GluN1/GluN2B) NMDAR (PDB ID 5UP2; (Lu et al. 2017)). Noteworthy, all immunization strategies target extracellular regions of GluN1 and most contain the G7 epitope.
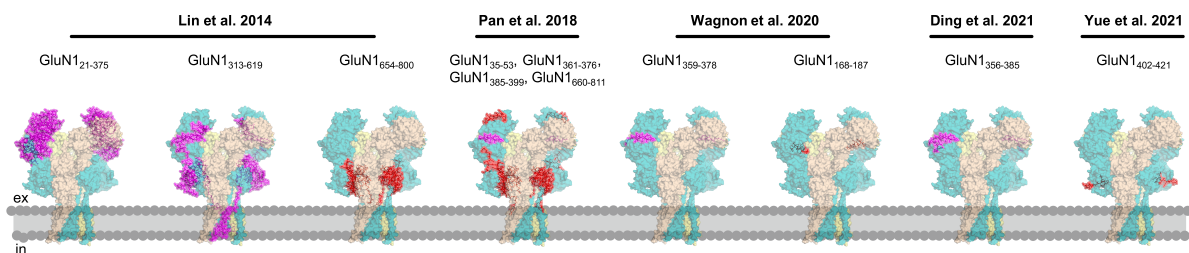


**Figure 2:** Localization of GluN1 peptides used in active immunization models. Published amino acid sequences of GluN1 peptides used for active immunization models are visualized as licorices in a triheterotetrameric NMDAR structure (PDB ID 5UP2; (Lu et al. 2017)) containing two GluN1 subunits (pale cyan), GluN2A (pale yellow), and GluN2B (wheat). Peptides containing the G7 epitope are displayed in magenta, others in red. Note that the structure lacks the intracellular carboxyl-terminal domain and that all peptides are localized in extracellular domains of GluN1.

Importantly, neither immunization against a cocktail of four extracellular GluN1-peptides (GluN1$_{35-53}$, GluN1$_{361-376}$, GluN1$_{385-399}$, GluN1$_{660-811}$), or three different recombinant GluN1 protein fragments (GluN1$_{21-375}$, GluN1$_{313-619}$, or GluN1$_{654-800}$), nor ectopic expression of GluN1 in lamina propria cells resulted in neuroinflammation despite the induction of functional NMDAR1-AB (During et al. 2000, Lin et al. 2014, Pan et al. 2018). Furthermore, these studies highlight the importance of the blood-brain barrier as a regulator of peripheral NMDAR1-AB function and show effects, consistent with NMDAR hypofunction, upon access of NMDAR1-AB to the CNS. While Pan et al. used APOE knockout mice, which display an impaired blood-brain barrier, to show that NMDAR1-AB exacerbate hyperlocomotion induced by the NMDAR-antagonist MK-801 (Pan et al. 2018), During et al. observed neuroprotective effects of NMDAR1-AB, potentially by reducing NMDAR-dependent excitotoxicity, in a kainate induced seizure model as well as upon middle cerebral artery occlusion, a model of ischemic stroke (During et al. 2000). A later follow-up study by Lin and colleagues attributed the neuroprotective effect of NMDAR1-AB to epitopes located within GluN1$_{654-800}$ (Lin et al. 2014). Another study that investigated effects of NMDAR1-AB on mice with an intact blood-brain barrier observed no major behavioral abnormalities except for a reproducible reduction of spontaneous alternation in the T-maze, indicating impairments in novelty detection or spatial working memory. Importantly, also these GluN1$_{402-421}$ immunized mice were free of neuroinflammation (Yue et al. 2021).

In contrast, active immunization of mice with natively folded GluN1/GluN2B- or GluN1/GluN2A-containing NMDAR reconstituted into liposomes developed typical encephalitis symptoms within one month after initial immunization (Ehrenreich et al. 2019, Jones et al. 2019). Crude behavioral monitoring identified hyperlocomotion in >80% of NMDAR-proteoliposome immunized mice, whereas seizures were present in 20%. Behavioral testing confirmed the hyperlocomotor phenotype and demonstrated impaired nest building ability and anxiolytic behavior of NMDAR-proteoliposome immunized mice. Histological examination revealed karyolysis and pyknosis in the dentate gyrus granular layer and neocortex as well as perivascular cuffing. Pronounced microgliosis was present in the CA subregions of the hippocampus, whereas the dentate gyrus appeared relatively unaffected. Astrogliosis was prominent throughout the hippocampus. Three weeks after initial immunization, neuroinflammation and immune cell infiltration was already present in the hippocampus. Interestingly, the immune cell composition in the hippocampus changed with disease progression. While CD4+ T cell numbers were more than twice as high as B cell or ASC numbers after three weeks, CD138+ antibody secreting cells outnumbered T cells after six weeks. Importantly, three weeks after immunization NMDAR1-AB were below the detection limit in a Western Blot assay, whereas all assays detected NMDAR1-AB after 6 weeks, potentially indicating that neuroinflammation preceded the development of high NMDAR1-AB titers. CD8+ T cells were relatively scarce at both time points. Characterization of the NMDAR1-AB repertoire revealed NMDAR1-AB that were functionally similar to patient derived NMDAR1-AB and recognized various GluN1 isoforms as well as a deletion construct lacking the amino-terminal domain, indicating a polyclonal immune response. Furthermore, immunization of transgenic T cell or B cell deficient mice (Tcra-, MuMt-, respectively) revealed that both mature T cells and B cells are required for the induction of neuroinflammation and NMDAR1-AB (Jones et al. 2018, Jones et al. 2019). Although this study may provide a construct valid mouse model of NMDARE, it cannot be used to disentangle the relative effects of NMDAR1-AB and neuroinflammation as both are inherently linked by the underlying autoimmune response. Furthermore, the authors' suggestion that encephalitis induction may depend on conformationally restricted epitopes, is not supported by the reported data that showed NMDAR1-AB binding to fully-denatured GluN1 in Western blot assays and binding to cells transfected with GluN1 in the absence of other NMDAR subunits.

In addition, to the NMDARE model developed by Jones and colleagues, two recent studies claimed the induction of an NMDARE-like encephalitis upon peptide-based immunization of mice (Wagnon et al. 2020, Ding et al. 2021). However, in contrast to Jones and colleagues, these reports fail to prove neuroinflammation in their mouse models. According to Wagnon and colleagues, immunization against GluN1$_{359-378}$, in contrast to sham or GluN1$_{168-187}$ immunizations, induced a B cell dependent encephalopathy. GluN1$_{359-378}$ immunized mice displayed behavioral alterations, increased seizure susceptibility, blood-brain barrier dysfunction, B cell and ASC infiltration into meningeal vessels, ventricles, and the choroid plexus without overt T cell recruitment. However, neither T cells nor B cells were recruited into the hippocampus of GluN1$_{359-387}$ immunized mice, pointing against NMDARE-like pathology (see 1.4). Of note, classical neuroinflammatory read-outs such as reactive astrogliosis and microgliosis were not investigated. Furthermore, the observed behavioral alterations, including impaired spatial memory/novelty detection, normal locomotion, increased anxiety, and depressive-like behavior phenotype (Wagnon et al. 2020), oppose those of other reports (Jones et al. 2019, Ding et al. 2021) and partially conflict with

NMDAR antagonism (see 1.7). Overall, the observed behavioral alterations resemble typical 'sickness behavior' of mice (Wilson et al. 2002, Dantzer et al. 2008, Terrando et al. 2010, Pape et al. 2019, Salvador et al. 2021) rather than NMDAR antagonism. Similar to Wagnon and colleagues, Ding et al. claim encephalitis induction after triple immunization against a GluN1-specific peptide but fail to investigate neuroinflammation. Importantly, the authors tested immunizations against a total of ten overlapping GluN1-peptides between amino acids 356-386, containing the G7-epitope. Out of these peptides, $GluN1_{356-385}$ was the only one capable of inducing NMDAR1-AB spillover into the CNS, whereas the peptide most similar to that of Wagnon et al. ($GluN1_{359-377}$ and $GluN1_{359-378}$ respectively) did not induce measurable NMDAR1-AB in CSF of immunized mice. After triple immunization, $GluN1_{356-385}$-immunized mice developed functional NMDAR1-AB, displayed behavioral alterations, and impaired LTP. Behavioral alterations of $GluN1_{356-385}$-immunized mice were characterized by decreased novel object and social recognition in the novel object recognition and three chamber tests, whereas locomotion and anxiety-like behavior were comparable to control mice. Overall, the phenotype of $GluN1_{356-385}$-immunized mice resembles passive transfer models and is likely mediated by NMDAR1-AB (Ding et al. 2021).

# 2  Scope of the thesis

The anti-NMDAR encephalitis is an autoimmune encephalitis with so far unclear pathogenesis, manifests with a heterogeneous clinical disease course, and is diagnosed based on the presence of NMDAR1-AB in patients' CSF. NMDAR1-AB have been shown to bind and cross-link surface NMDAR resulting in their internalization thereby inducing NMDAR hypofunction. On a theoretical basis, the presence of NMDAR1-AB could contribute to the psychopathological phenotype of NMDARE patients and explain why psychoses and behavioral alterations are more frequent in NMDARE as compared to other autoimmune encephalitides. However, the relative contribution of NMDAR1-AB to the neuropsychological phenotype of encephalitides has, so far, not been formally disentangled from the underlying neuroinflammatory processes. For this purpose, the effects and pathophysiological relevance of NMDAR1-AB was studied in healthy mice, in mice with gray matter inflammation, and in mice with progressive white matter inflammation.

## 2.1  Aims of Project I

Project I was designed to characterize an inducible gray matter inflammation mouse model ('DTA' mice) in vivo by state-of-the-art behavioral and magnetic resonance imaging tools and to assess, ex vivo, the neuroinflammatory and neurodegenerative consequences of spatiotemporally defined pyramidal cell death.

## 2.2  Aims of Project II

Project II investigated if and how NMDAR1-AB shape the clinical phenotype of gray matter inflammation. To experimentally address this hypothesis, the gray matter mouse model characterized in Project I was utilized. Following immunization of control and DTA mice against a cocktail of four GluN1-specific peptides located in extracellular regions or against ovalbumin (OVA) as comparator, pyramidal cell death was induced in DTA mice via tamoxifen administration. DTA as well as healthy control mice carrying either NMDAR1-AB or OVA-AB were behaviorally phenotyped and the degree of neuroinflammation was examined histologically. In addition, the encephalitogenic potential of another recently published peptide-based immunization was assessed through behavioral phenotyping, histology, and flow cytometry.

## 2.3  Aims of Project III

Project III was designed to unravel the role of NMDAR1-AB in a mouse model of progressive white matter inflammation. For this purpose, *Cnp* knockout mice were immunized similar to DTA mice and phenotyped in relevant behavioral tests. In addition, potential effects of NMDAR1-AB on gray and white matter pathology were assessed histologically.

# 3 Project I: Inducing sterile pyramidal neuronal death in mice to model distinct aspects of gray matter encephalitis

## 3.1 Overview of Project I

The clinical manifestation of encephalitides involving the limbic system show remarkable similarities and the differential diagnosis of autoantibody-associated autoimmune encephalitides strongly relies on the detection of respective autoantibodies in the CSF of patients. However, disentangling cause and consequences of autoantibodies and neuroinflammation is challenging in a clinical setting. To provide means to experimentally unravel the pathophysiological relevance of autoantibodies and their contribution in a neuroinflammatory context, an inducible mouse model for gray matter inflammation was thoroughly characterized. By cross-breeding mice expressing a tamoxifen-inducible Cre recombinase under transcriptional control of the Nex1 (Neurod6) promoter ('NexCreERT2' mice) to mice carrying a diphtheria toxin fragment A (DTA) gene downstream of a transcriptional STOP-cassette in the ubiquitously expressed Rosa26 genetic locus (Rosa26-eGFP-DTA), cell death in Nex1 expressing pyramidal neurons can be dose-dependently induced by tamoxifen administration, subsequently initiating an inflammatory response in affected brain regions (Agarwal et al. 2012). Here, double heterozygous adult male NexCreERT2xRosa26-eGFP-DTA (='DTA') mice were used and compared to heterozygous NexCreERT2 littermates lacking the DTA allele. Multifaceted behavioral testing revealed a pathology typical for hippocampal dysfunction, which was in line with a strong hippocampal atrophy observed by high-resolution in vivo magnetic resonance imaging as well as ex-vivo histological examinations. Although most pronounced in the hippocampus, several other gray matter brain regions displayed atrophy and total brain mass was expectedly reduced. Long-lasting neuroinflammation was confirmed ex-vivo by histology and brain flow cytometry, two months after encephalitis induction. Similarly, the blood-brain barrier dysfunction measured by in vivo fluorescent tracer extravasation was long lasting. Interestingly, magnetic resonance imaging revealed altered perfusion of affected brain regions. In summary, DTA mice display key features of encephalitides involving the limbic system and represent a useful and standardizable experimental tool that can be used to study how the presence of additional factors such as brain-directed autoantibodies affect the encephalitic phenotype.

## 3.2 Original Publication

**Wilke JBH\***, Hindermann M\*, Moussavi A, Butt UJ., Dadarwal R, Berghoff SA, Sarcheshmeh AK, Ronnenberg A, Zihsler S, Arinrad S, Hardeland R, Seidel J, Lühder F, Nave KA, Boretius S and Ehrenreich H (2021). "Inducing sterile pyramidal neuronal death in mice to model distinct aspects of gray matter encephalitis." Acta Neuropathol Commun 9(121): https://doi.org/10.1186/s40478-40021-01214-40476.

\*shared first authorship

## Personal Contribution

I substantially contributed (data acquisition, analysis, and interpretation) to all experiments involving animal treatments, complex wheel running, ELISA, blood flow cytometry, brain flow cytometry, histology and was involved in the data analysis (image segmentation) and interpretation of MRI datasets. Furthermore, I significantly contributed to drafting the manuscript and display items.

# Inducing sterile pyramidal neuronal death in mice to model distinct aspects of gray matter encephalitis

Justus B. H. Wilke[1] , Martin Hindermann[1], Amir Moussavi[2], Umer Javed Butt[1], Rakshit Dadarwal[2,3], Stefan A. Berghoff[4], Aref Kalantari Sarcheshmeh[2], Anja Ronnenberg[1], Svenja Zihsler[1], Sahab Arinrad[1], Rüdiger Hardeland[5], Jan Seidel[1], Fred Lühder[6], Klaus-Armin Nave[4], Susann Boretius[2,3]* and Hannelore Ehrenreich[1]*

## Abstract

Up to one person in a population of 10,000 is diagnosed once in lifetime with an encephalitis, in 50–70% of unknown origin. Recognized causes amount to 20–50% viral infections. Approximately one third of affected subjects develops moderate and severe subsequent damage. Several neurotropic viruses can directly infect pyramidal neurons and induce neuronal death in cortex and hippocampus. The resulting encephalitic syndromes are frequently associated with cognitive deterioration and dementia, but involve numerous parallel and downstream cellular and molecular events that make the interpretation of direct consequences of sudden pyramidal neuronal loss difficult. This, how-ever, would be pivotal for understanding how neuroinflammatory processes initiate the development of neurode-generation, and thus for targeted prophylactic and therapeutic interventions. Here we utilized adult male NexCre-ERT2xRosa26-eGFP-DTA (='DTA') mice for the induction of a sterile encephalitis by diphtheria toxin-mediated ablation of cortical and hippocampal pyramidal neurons which also recruits immune cells into gray matter. We report mul-tifaceted aftereffects of this defined process, including the expected pathology of classical hippocampal behaviors, evaluated in Morris water maze, but also of (pre)frontal circuit function, assessed by prepulse inhibition. Importantly, we modelled in encephalitis mice novel translationally relevant sequelae, namely altered social interaction/cognition, accompanied by compromised thermoreaction to social stimuli as convenient readout of parallel autonomic nervous system (dys)function. High resolution magnetic resonance imaging disclosed distinct abnormalities in brain dimen-sions, including cortical and hippocampal layering, as well as of cerebral blood flow and volume. Fluorescent tracer injection, immunohistochemistry and brain flow cytometry revealed persistent blood–brain-barrier perturbance and chronic brain inflammation. Surprisingly, blood flow cytometry showed no abnormalities in circulating major immune cell subsets and plasma high-mobility group box 1 (HMGB1) as proinflammatory marker remained unchanged. The present experimental work, analyzing multidimensional outcomes of direct pyramidal neuronal loss, will open new avenues for urgently needed encephalitis research.

*Correspondence: SBoretius@dpz.eu; ehrenreich@em.mpg.de
[1] Clinical Neuroscience, Max Planck Institute of Experimental Medicine, Hermann-Rein-Str.3, 37075 Göttingen, Germany
[2] Functional Imaging Laboratory, German Primate Center, Leibniz Institute for Primate Research, Kellnerweg 4, 37077 Göttingen, Germany
Full list of author information is available at the end of the article
Justus B. H. Wilke and Martin Hindermann have shared first authorship.

## Introduction

Encephalitis is best defined as inflammation of the brain parenchyma associated with variable neuropsychiatric dysfunction, ranging from mild to sometimes life-threatening severity. The underlying origins of encephalitis are multitude, and include infectious causes, comprising viral, bacterial, fungal, and parasitic agents, but also toxic, metabolic, (para)neoplastic and autoimmune or rarely post-immunization etiologies [29, 40, 42]. World travellers for example may be exposed to a variety of neurotropic pathogens leading to 'exotic' causes of central nervous system (CNS) infections [22]. Interestingly, increasing evidence points to genetic reasons of mild encephalitis which may often escape recognition until progressed age [17, 20, 37]. In about 50–70% of encephalitis cases, an etiologic agent is never identified, presumably due to the broad range of possible underlying origins and limitations in contemporary diagnostic testing, but likely also because of continuing pathogenetic dynamics in the absence of the formerly inducing agent [22, 29, 40, 42].

As recurrent common denominator in encephalitides and mediator of severe downstream sequelae, neuronal dysfunction or death are observed, associated with cognitive decline and dementia. Viral infections with neurotropism, particularly affecting neurons of cortex and hippocampus occur across many species. They include for instance human immunodeficiency, Theiler's murine encephalomyelitis, West Nile, human herpes simplex, Japanese encephalitis, and in immunocompromised humans or macaques, respectively, John Cunningham (JC) and Simian 40 (SV40) virus [10, 11, 21, 41, 47, 48]. Encephalitis is also a common neurological complication in patients with COVID-19, where we just begin to understand mechanisms of brain infection and post-infection sequelae [6, 18, 25, 28].

Comprehending the pathophysiological mechanisms of encephalitides is crucially important for developing more efficient treatment strategies, including neuroprotective interventions, particularly with regard to longterm damage. Although mortality markedly decreased and etiologies somewhat shifted, no clear long-term improvements in outcome were seen, as reported in a 40-year survey in Sweden [45]. Considering the prevailing neuropsychiatric disabilities following encephalitides, refining their outcome should be a highly prioritised research issue [45].

The present longitudinal study has been designed to analyze by innovative behavioral and magnetic resonance imaging tools in vivo, as well as by various ex vivo and *post mortem* tests, the downstream consequences of sudden pyramidal neuronal loss, including reactive neuroinflammatory and subsequent neurodegenerative processes. Experimentally eliminating in our model the numerous parallel cellular and molecular events characterizing infections, that make interpretation of causes and consequences often hard, will aid in better understanding mechanisms of neurodegeneration in general and thus in developing more targeted diagnostic instruments and therapeutic interventions.

## Materials and methods

### Mice

All animal experiments were approved by the local animal care and use committee (LAVES, Niedersächsisches Landesamt für Verbraucherschutz und Lebensmittelsicherheit, Oldenburg, Germany) in accordance with the German animal protection law. Mice were maintained in temperature- and humidity- controlled environment ($\sim 22$ °C, $\sim 50\%$), 12 h light/dark cycle (light on at 7am) with food and water ad libitum. Cages were enriched with wood-chip bedding and nesting material (Sizzle Nest, Datesand). All experiments were performed by investigators unaware of group assignment ('fully blinded'). Behavioral testing-order was balanced between groups prior to experiments and randomized within groups via random selection by the blinded investigator.

C57BL/6 mice bearing the tamoxifen-inducible diphtheria toxin chain A allele were generated by crossing homozygous Neurod6[tm2.1(cre/ERT2)Kan] ('NexCreERT2', [1]) with heterozygous Gt(ROSA)26Sor[tm1(DTA)Jpmb] ('Rosa26-eGFP-DTA', [19]) resulting in double heterozygous inducible ('DTA') mice and heterozygous NexCreERT2 littermate ('control') mice lacking the DTA allele. Detailed PCR-based genotyping protocols are available upon request. Male transgenic mice were weaned at postnatal day 21 and separated by genotype to avoid inclusion effects or aggressive behavior against potentially affected animals. Experiments were performed on adult male mice (starting age 6–8 months) over a period of approximately 2 months.

### Tamoxifen induction

Tamoxifen (CAS#10540-29-1 T5648, Sigma-Aldrich) was dissolved in corn oil (C8267, Sigma-Aldrich) on injection days at 10 mg/mL. Dependent on the experimental

cohort, mice received either 3 or 5 daily intraperitoneal injections of 100 mg tamoxifen/kg body weight.

### Blood sampling and high-mobility group box 1 (HMGB1) ELISA

Intermediate blood samples (100µL) were collected 2 weeks after the last tamoxifen injection from the retroorbital sinus. Terminal blood (500µL) was sampled by cardiac puncture before transcardial perfusion. EDTA plasma aliquots were stored at -80 °C. Plasma HMGB1 concentrations were determined using a commercial HMGB1 ELISA assay (USC-SEA399MU-96, Biozol) according to the manufacturer's instructions.

### Behavioral phenotyping

Experiments were performed during light phase in the following order: Open field, prepulse inhibition, Morris water maze, SocioBox and complex wheel running (the latter 2 only in 3 × tamoxifen mice).

#### Open field

To evaluate exploratory activity in a novel environment, mice were placed in the center of a gray circular Perspex arena (120 cm diameter, 25 cm height of outer wall). First, time to reach the outer wall (escape latency) was measured, followed by 7 min to freely explore the open field. When exceeding 180 s to reach the outer wall, mice were placed in the periphery zone to start 7 min exploration time. Behavior of the mice was recorded via tracking software (Viewer3, Biobserve). Analyzed parameters were covered distance and the time spent in the central, intermediate and peripheral zones of the open field. Animals were tested at the age of 27 (3 × tamoxifen) and 32 (5 × tamoxifen) weeks with light intensity of 120–140 lx in the center.

#### Prepulse inhibition (PPI) of the startle response

This paradigm has been described previously in detail [12]. In brief, to evaluate sensorimotor gating, animals were placed in small metal cages to prevent major movements. Cages were placed in sound attenuating cabinets (TSE Systems) on a sensor-attached platform to record movement. After habituation to 65 dB white noise, loudspeakers delivered acoustic stimuli to evoke startle reflexes. Stimuli of different intensity (70, 75, 80 and 120 dB) were used in a pseudo-randomized order. The amplitudes of the startle response were averaged within the various intensities for each mouse. PPI was calculated as percentage of the startle response using following formula: %PPI = 100–[(startle response after prepulse)/(startle amplitude after pulse only) × 100]. For analysis, data from non-performing mice (negative PPI) were excluded.

### Morris water maze (MWM)

This test has been described previously in detail [12, 31]. Briefly, to measure spatial learning and memory, mice were placed in a circular tank (120 cm diameter, 60 cm height) filled with opaque water at room temperature (~ 22 °C) with the escape platform (10 cm diameter) approximately 1 cm submerged. Animals' movement was recorded by video-tracking system (Viewer3, Biobserve). After 2 days of a visual platform task in which extra maze cues were covered by the tank walls, the visual cue (flag on platform) was removed, the platform was relocated and the water height was adjusted so that extra maze cues were visible. For 8 consecutive days, mice had to reach the "hidden" platform in 4 trials per day. Afterwards, the platform was removed and mice were observed during a single "probe trial". Analyzed parameters were escape latency to platform and covered distance. Additionally, during probe trial, the time spent in, visits and latency to the target quadrant (formerly containing platform) and covered distance were measured. If groups showed no significant differences, the platform was once again relocated for another 4 days of reversal learning, followed by another probe trial. Except for the probe trials, each day consisted of 4 test runs with a maximum of 90 s each and an intertrial interval of 5 min. In between trials, mice were placed in single cages containing paper towels and standing on a heating pad to prevent hypothermia and overexertion of the mice. In absence of a platform to reach, both probe trials consisted of a single test run of 90 s. Animals were tested at the age of 28–30 (3 × tamoxifen) and 33–35 (5 × tamoxifen) weeks with light intensity of 120–140 lx.

### SocioBox

A detailed description of this test has been published before [23]. Briefly, to evaluate social recognition and memory, 3 × tamoxifen mice were tested in the SocioBox at the age of 31–32 weeks with light intensity of 10–15 lx. They were placed in a circular apparatus (34 cm inner and 56 cm outer diameter) with 5 small boxes ("inserts") within the outer wall. For each mouse, the SocioBox experiment consisted of 3 habituation sessions on 3 consecutive days and 2 exposures and 1 recognition trial on day 4. Within each trial, for the first 5 min, mice stayed in a circular partition (19 cm diameter) to prevent immediate exploring of the SocioBox (initiation stage). After lifting of this partition, mice were allowed to freely explore the SocioBox for another 5 min (interaction stage). While the 5 inserts in the outer ring were empty during all 3 habituation trials, they contained a mouse each for interaction purposes ("stimulus mice" or "stimuli"). For both exposure trials, the same 5 stimulus mice in the same

position and order were used. For the final recognition test, one stimulus mouse was replaced by a new stimulus mouse ("stranger"), unknown to the test mouse. Perforated fronts of the inserts allowed limited interaction between test mouse and stimulus mice and front walls of each insert were exchanged after each trial. Age and sex matched C3H mice were used as stimuli, based on their reported robust social interaction in test situations [33]. Mouse movement was recorded via tracking software (Viewer3, Biobserve).

### *Thermography*
This technique and data extraction/processing have been published previously in detail [39] and were slightly modified for the present application. In short, for SocioBox experiments (performed with $3 \times$ tamoxifen mice), an A655sc infrared thermography camera (FLIR) was mounted 110 cm above the arena, recording images at $640 \times 480$ pixels and framerate of 2 Hz (habituation 3, exposure $1 + 2$) and 5 Hz (memory test), via ResearchIR (FLIR Systems, Oregon, USA) and connected to a computer located in a separate room. Extraction of thermal data was done using OpenCV 4 in Python 3.6. Images were loaded and normalized to values between 0 and 255, with higher values meaning higher temperatures. The SocioBox arena in which the test mouse was allowed to move was defined as the relevant ROI for extracting thermal data. To keep only thermal data from the test mouse, a binary mask for whole body (including tail) was created by applying intensity thresholding and processing steps to decrease image noise. By doing so, one large cluster of connected pixels within this ROI could be detected, constituting the contour of the mouse. Due to the shape and temperature differences, the whole-body area could then be segmented into a central body and a distinct tail area, and the mean temperature of each of those 2 areas could be extracted. Analyzed parameters were temperature changes over time of test mice, latency and duration of interaction with stimulus mice and "strangers"

and visits to interaction zones. The Centralization Index (ratio body/tail temperature = T ratio) was used as continuous temperature measure [39].

### *Complex wheel running*
To stimulate neuronal activation-induced cFos expression in the hippocampus, mice were subjected to a complex running wheel (CRW) set-up for 4 h [43]. Mice were single housed in type III cages ($42 \times 26 \times 18$ cm, Tecniplast), equipped with CRW (TSE-Systems) characterized by randomized omitted bars [26, 27]. Mice were habituated to the experimental room and CRW for 2 h prior to dark phase. After dark phase onset, voluntary running was automatically tracked for 4 h via Phenomaster software (TSE-Systems) and the total running distance per mouse calculated. Mice were perfused with Ringer and 4% formaldehyde/PBS, 30 min after removal from the CRW set-up.

### Magnetic resonance imaging (MRI)
Mice ($5 \times$ tamoxifen) were anesthetized with ketamine and medetomidine (60 mg/kg and 0.4 mg/kg body weight), intubated and kept under 1.5% isoflurane by active ventilation with constant ventilation frequency of 85 breaths/min (Animal-Respirator-AdvancedTM, TSE-Systems). Inside the MR-System, mice were placed in a prone position with head fixed to a teeth and palate holder [7]. All MR measurements were performed at magnetic field strength of 9.4 T (Biospec®, Bruker BioSpin MRI, Ettlingen, Germany) comprising the following methods and acquisition parameters: High-resolution T2-weighted images (2D Rapid Acquisition with Relaxation Enhancement (RARE), TE/TR = 55/6000 ms, 8 echoes, spatial resolution $40 \times 40 \times 300$ μm$^3$), magnetization-transfer (MT) weighted images for volumetric analyses (3D fast low angle shot (FLASH), TE/TR = 3.4/15.2 ms, flip angle 5°, Gaussian-shaped off resonance pulse (off-resonance frequency 7.5 ppm, RF power 6μT), spatial resolution 100 μm isotropic), measurements

---

(See figure on next page.)

**Fig. 1** Effects of sterile gray matter encephalitis, induced by pyramidal neuronal ablation, on diverse behavioral paradigms. **a** Schematic description of the diphtheria toxin chain A (DTA) allele. Tamoxifen-dependent Cre-mediated excision of a STOP-cassette leads to expression of DTA, subsequent inhibition of protein synthesis, and cell death. **b** Genotype of the DTA model targeting pyramidal neurons and tamoxifen dosing scheme. Cohorts induced with $3 \times$ tamoxifen included 16 DTA and 18 control mice. The $5 \times$ tamoxifen cohort comprised 16 DTA and 19 control animals. **c** Fluorojade staining of hippocampal sections at 1 week after $5 \times$ tamoxifen induction. Note the massive acute neurodegeneration and pyramidal neuronal loss. **d** Experimental outline illustrates groups, experiments and timeline of testing (DPI = days post induction, CRW = complex running wheel, MRI = magnetic resonance imaging). **e** Cognitive testing in Morris water maze (MWM), with hidden platform task showing significantly inferior learning curve (latency to reach the platform) of $3 \times$ DTA mice (light red) compared to control (black); repeated measures mixed-model ANOVA; mean ± SEM. **f** Spatial memory testing in the probe trial indicating significantly less time spent in target quadrant (TQ, formerly containing hidden platform), less visits to TQ and longer latency to reach TQ of $3 \times$ DTA mice. Total swimming distance of both groups did not differ. Data presented as mean ± SD. **g** Testing $5 \times$ tamoxifen groups for anxiety and exploratory behavior in the open field showed a tendency of increased escape latency from center towards periphery. DTA compared to control mice covered less distance, spent less time in the periphery and more time in "mid" (intermediate zone between center and periphery). Time in center showed no differences between both groups ($p = 0.9546$). Data presented as mean ± SD. **h** $5 \times$ DTA compared to control mice displayed a decreased prepulse inhibition; repeated measures mixed-model ANOVA; mean ± SEM
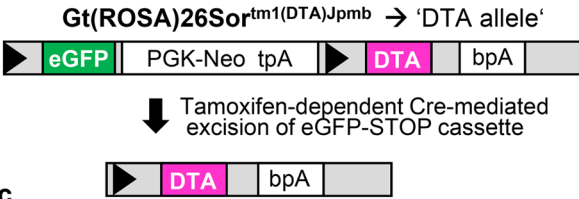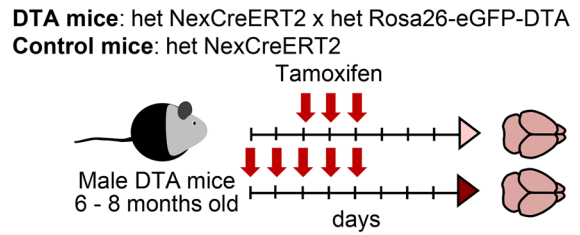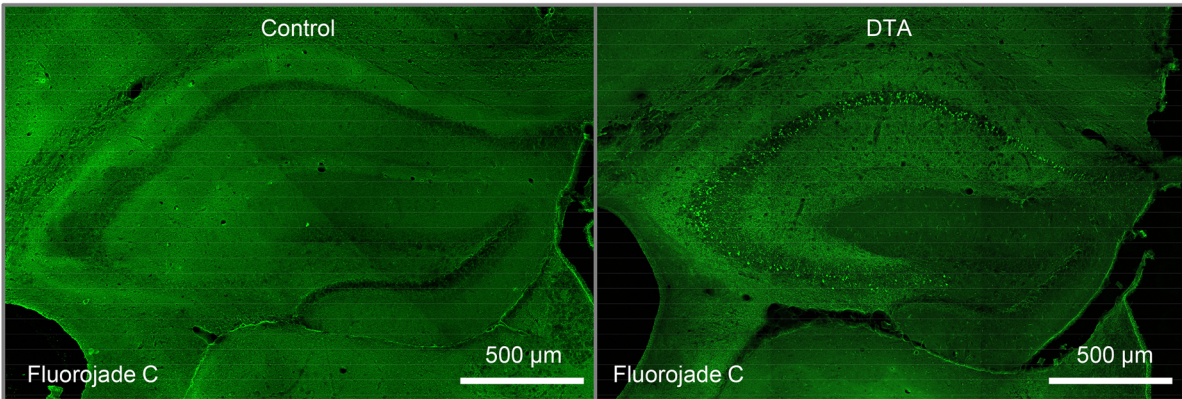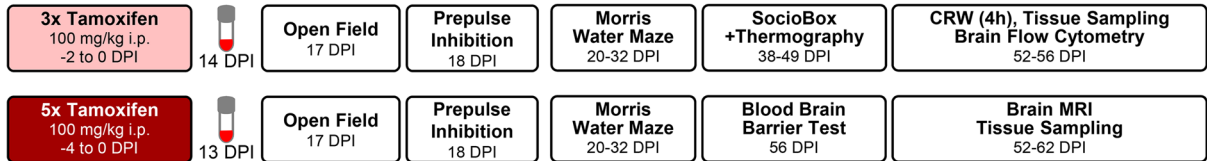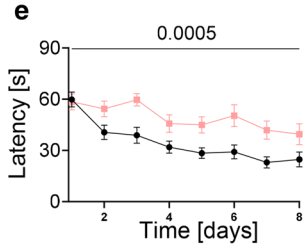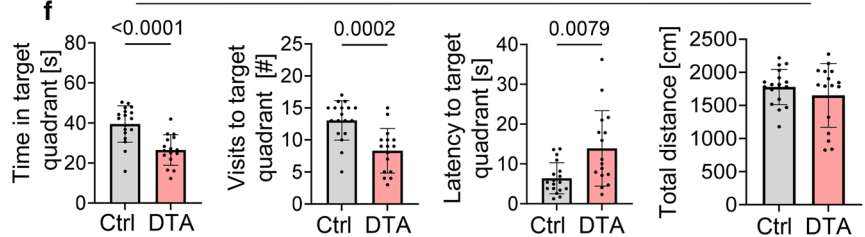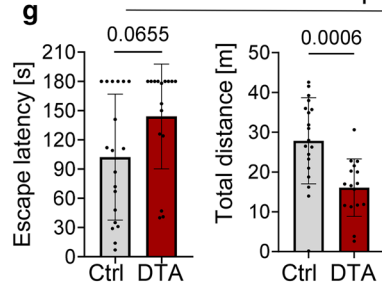
**Fig. 1** (See legend on previous page.)

**Table 1** Results of behavioral testing of the 3× tamoxifen induced encephalitis mice (t = 2-sided Welch's corrected *t*-test; U = 2-sided Mann–Whitney U-test. *TQ* target quadrant, *IZ* interaction zone, *CI* centralization index)

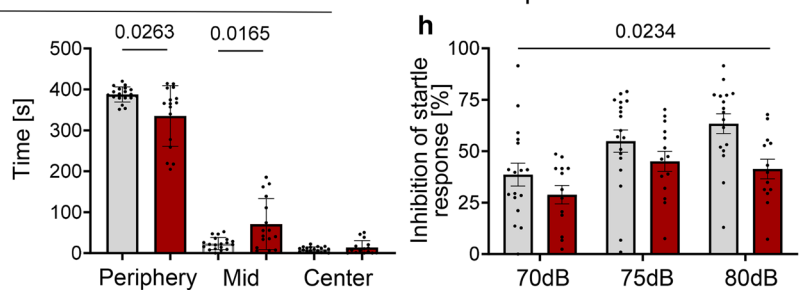| | Group 1 Control, 3x tamoxifen | | | Group 2 DTA, 3x tamoxifen | | | Comparison Group 1 vs 2 | |
|---|---|---|---|---|---|---|---|---|
| **Health Status** | mean | ± SD | n | mean | ± SD | n | test | p-value |
| Body weight [g] pre Tamoxifen | 33.8 | ± 1.9 | 18 | 32.8 | ± 2.7 | 16 | t | 0.2439 |
| Body weight [g] 3d post Tamoxifen | 33.8 | ± 1.6 | 18 | 33.0 | ± 2.3 | 16 | t | 0.2919 |
| Body weight [g] 10d post Tamoxifen | 34.2 | ± 2.0 | 18 | 32.5 | ± 2.4 | 16 | t | **0.0391** |
| Body weight [g] 35d post Tamoxifen | 34.4 | ± 1.6 | 18 | 34.1 | ± 2.3 | 16 | t | 0.6324 |
| **Open Field** | | | | Age: 27 weeks, 17 DPI | | | | |
| Escape latency [s] | 47.9 | ± 46.4 | 18 | 46.4 | ± 49.4 | 16 | U | 0.7558 |
| Total distance [m] | 27.4 | ± 6.5 | 18 | 22.4 | ± 9.9 | 16 | t | 0.0942 |
| Visits to periphery [#] | 10.6 | ± 5.4 | 18 | 8.5 | ± 4.5 | 16 | t | 0.2222 |
| Visits to intermediate [#] | 15.7 | ± 8.4 | 18 | 12.5 | ± 7.5 | 16 | t | 0.2536 |
| Visits to center [#] | 5.4 | ± 4.7 | 18 | 3.8 | ± 5.4 | 16 | U | 0.1342 |
| Time in periphery [s] | 368.8 | ± 36.3 | 18 | 364.4 | ± 63.2 | 16 | U | 0.5973 |
| Time in intermediate [s] | 38.3 | ± 26.0 | 18 | 42.8 | ± 46.3 | 16 | U | 0.6518 |
| Time in center [s] | 12.8 | ± 12.6 | 18 | 12.8 | ± 19.4 | 16 | U | 0.3291 |
| **Prepulse Inhibition** | | | | Age: 27 weeks, 18 DPI | | | | |
| Startle response to 65db [AU] | 0.9 | ± 0.4 | 18 | 0.7 | ± 0.2 | 16 | U | 0.1417 |
| Startle response to 120dB [AU] | 2.8 | ± 2.6 | 18 | 2.6 | ± 2.5 | 16 | U | 0.3256 |
| Prepulse Inhibition at 70db [%] | 37.8 | ± 19.2 | 18 | 42.8 | ± 16.8 | 16 | t | 0.4275 |
| Prepulse Inhibition at 75db [%] | 36.2 | ± 39.5 | 18 | 48.5 | ± 23.3 | 16 | t | 0.3653 |
| Prepulse Inhibition at 80db [%] | 51.1 | ± 15.2 | 18 | 52.0 | ± 17.8 | 16 | t | 0.8692 |
| ANOVA PPI 70-80dB | Genotype p=0.3393, Intensity p=**0.0336**, GxI p=0.4388 | | | | | | | |
| **Morris Water Maze** | | | | Age: 28-30 weeks, 20-32 DPI | | | | |
| Visible1 - escape latency [s] | 24.7 | ± 20.7 | 18 | 18.9 | ± 12.5 | 16 | U | 0.4844 |
| Visible2 - escape latency [s] | 9.1 | ± 4.8 | 18 | 6.8 | ± 3.3 | 16 | U | 0.0504 |
| Visible 1 vs 2 - escape latency [s] | U | **0.0008** | | U | **<0.0001** | | | |
| Hidden1 - escape latency [s] | 60.4 | ± 17.2 | 18 | 60.4 | ± 19.1 | 16 | U | 0.7522 |
| Hidden2 - escape latency [s] | 40.6 | ± 17.8 | 18 | 54.3 | ± 18.4 | 16 | t | **0.0350** |
| Hidden3 - escape latency [s] | 38.9 | ± 19.7 | 18 | 59.7 | ± 14.5 | 16 | t | **0.0013** |
| Hidden4 - escape latency [s] | 31.9 | ± 15.2 | 18 | 45.8 | ± 20.4 | 16 | t | **0.0347** |
| Hidden5 - escape latency [s] | 28.4 | ± 13.2 | 18 | 45.0 | ± 19.1 | 16 | t | **0.0073** |
| Hidden6 - escape latency [s] | 29.2 | ± 17.4 | 18 | 50.4 | ± 25.6 | 16 | U | **0.0087** |
| Hidden7 - escape latency [s] | 23.0 | ± 14.0 | 18 | 41.9 | ± 21.5 | 16 | U | **0.0056** |
| Hidden8 - escape latency [s] | 24.7 | ± 18.6 | 18 | 40.9 | ± 24.3 | 16 | U | **0.0425** |
| Hidden1-8 - ANOVA escape latency | Genotype p=**0.0005**, Days p<**0.0001**, GxD p=0.0929 | | | | | | | |
| Probe trial - average velocity [cm/s] | 19.8 | ± 3.0 | 18 | 18.4 | ± 5.3 | 16 | U | 0.8515 |
| Probe trial - time in TQ [s] | 39.5 | ± 9.1 | 18 | 26.5 | ± 7.7 | 16 | t | **<0.0001** |
| Probe trial - visits to TQ [#] | 13.1 | ± 3.1 | 18 | 8.3 | ± 3.5 | 16 | U | **0.0002** |
| Probe trial - latency to TQ [s] | 6.4 | ± 3.9 | 18 | 13.9 | ± 9.5 | 16 | t | **0.0079** |
| Probe trial - latency to former platform zone [s] | 27.9 | ± 26.7 | 18 | 57.5 | ± 38.6 | 16 | U | 0.0647 |
| **SocioBox – Activity** | | | | Age: 31-32 weeks, 38-49 DPI | | | | |
| Habituation - total distance [m] | 6.8 | ± 1.6 | 15 | 8.4 | ± 1.8 | 14 | U | **0.0088** |
| Exposure1 - total distance [m] | 7.4 | ± 1.9 | 18 | 9.9 | ± 2.5 | 16 | U | **0.0010** |
| Exposure2 - total distance [m] | 6.5 | ± 3.4 | 18 | 9.1 | ± 2.9 | 16 | U | **0.0039** |
| Memory test - total distance [m] | 5.8 | ± 1.8 | 18 | 8.8 | ± 2.8 | 16 | U | **0.0012** |
| Habituation - latency to 1st IZ [s] | 3.0 | ± 1.3 | 18 | 3.0 | ± 2.2 | 16 | U | 0.4755 |
| Exposure1 - latency to 1st IZ [s] | 2.9 | ± 1.7 | 18 | 2.3 | ± 1.0 | 16 | U | 0.4280 |
| Exposure2 - latency to 1st IZ [s] | 3.0 | ± 1.5 | 18 | 1.7 | ± 0.8 | 16 | t | **0.0035** |
| Exposure3 - latency to 1st IZ [s] | 3.0 | ± 2.7 | 18 | 2.1 | ± 1.5 | 16 | U | 0.3475 |
| Memory test - latency stranger [s] | 20.5 | ± 17.3 | 18 | 9.0 | ± 8.0 | 16 | U | **0.0241** |
| Habituation - total visits to IZ [#] | 22.3 | ± 4.6 | 18 | 31.2 | ± 9.3 | 16 | U | **0.0022** |
| Exposure1 - total visits to IZ [#] | 30.2 | ± 6.4 | 18 | 41.6 | ± 10.0 | 16 | t | **0.0006** |
| Exposure2 - total visits to IZ [#] | 25.0 | ± 8.7 | 18 | 38.9 | ± 10.3 | 16 | U | **<0.0001** |
| Memory test - total visits to IZ [#] | 24.6 | ± 7.3 | 18 | 37.0 | ± 12.5 | 16 | t | **0.0020** |
| **SocioBox – Social interaction** | | | | | | | | |
| Habituation - total time in IZ [s] | 138.0 | ± 52.1 | 18 | 148.5 | ± 30.1 | 16 | t | 0.4694 |
| Exposure1 - total time in IZ [s] | 172.9 | ± 30.9 | 18 | 187.5 | ± 15.4 | 16 | t | 0.0885 |
| Exposure2 - total time in IZ [s] | 148.1 | ± 36.2 | 18 | 172.2 | ± 30.1 | 16 | U | **0.0349** |
| Memory test - total time in IZ [s] | 135.4 | ± 43.6 | 18 | 167.0 | ± 41.8 | 16 | t | **0.0384** |
| E1 vs E2 - total time in IZ [s] | U | **0.0059** | | t | 0.0832 | | | |
| E2 vs Memory test - total time in IZ [s] | U | 0.3550 | | t | 0.6896 | | | |
| Memory test - visits to stimulus IZ [%] | 19.2 | ± 1.8 | 18 | 20.1 | ± 0.9 | 16 | t | 0.0771 |
| Memory test - visits to stranger IZ [%] | 23.4 | ± 7.1 | 18 | 19.8 | ± 3.8 | 16 | t | 0.0770 |
| Memory test - stimulus vs stranger [%] | t | **0.0253** | | t | 0.8127 | | | |
| Memory test - time with stimulus mice [%] | 17.1 | ± 4.2 | 18 | 19.0 | ± 3.3 | 16 | U | 0.1752 |
| Memory test - time with stranger [%] | 31.8 | ± 16.6 | 18 | 23.9 | ± 13.2 | 16 | U | 0.1752 |
| Memory test - stimulus vs stranger [%] | t | **0.0017** | | U | 0.2871 | | | |
| Habituation - time/visit [s/#] | 6.3 | ± 2.3 | 18 | 5.3 | ± 2.4 | 16 | U | 0.1324 |
| Exposure1 - time/visit [s/#] | 6.0 | ± 1.6 | 18 | 4.7 | ± 1.0 | 16 | t | **0.0107** |
| Exposure2 - time/visit [s/#] | 6.5 | ± 2.6 | 18 | 4.8 | ± 1.6 | 16 | U | **0.0184** |
| Memory test - time/visit [s/#] | 5.8 | ± 2.0 | 18 | 5.0 | ± 2.1 | 16 | U | 0.1616 |
| Memory test - time/visit to stimulus [s/#] | 5.0 | ± 1.6 | 18 | 4.9 | ± 2.8 | 16 | U | 0.2811 |
| Memory test - time/visit to stranger [s/#] | 8.2 | ± 5.6 | 18 | 5.6 | ± 3.3 | 16 | U | 0.1153 |
| Memory test - stimulus vs stranger [s/#] | U | 0.0723 | | U | 0.3414 | | | |
| **SocioBox - Thermoresponse** | | | | | | | | |
| Habituation - CI - mixed model ANOVA for genotype | 1-300s p=0.9482      301-600s p=0.1839 | | | | | | | |
| Exposure1 - CI - mixed model ANOVA for genotype | 1-300s p=**0.0272**      301-600s p=0.3960 | | | | | | | |
| Exposure2 - CI - mixed model ANOVA for genotype | 1-300s p=0.0979      301-600s p=**0.0407** | | | | | | | |
| Memory test - CI - mixed model ANOVA for genotype | 1-300s p=0.0732      301-600s p=0.0996 | | | | | | | |
| **Complex Running Wheel (4h)** | | | | Age: 34 weeks, 52-56 DPI | | | | |
| All mice - total distance [m] | 799.0 | ± 353.4 | 18 | 769.2 | ± 469.7 | 16 | t | 0.8378 |
| cFos cohort - total distance [m] | 658.9 | ± 238.2 | 8 | 945.8 | ± 523.5 | 8 | t | 0.1247 |

**Table 2** Results of behavioral testing of the 5 × tamoxifen induced encephalitis mice (t = 2-sided Welch's corrected *t*-test; U = 2-sided Mann–Whitney U-test)

| | Group 3 Control, 5x tamoxifen | | | Group 4 DTA, 5x tamoxifen | | | Comparison Group 3 vs 4 | |
|---|---|---|---|---|---|---|---|---|
| **Health Status** | mean | ± SD | n | mean | ± SD | n | test | p-value |
| Body weight [g] pre Tamoxifen | 35.9 ± 3.1 | | 19 | 33.6 ± 1.7 | | 16 | t | 0.0102 |
| Body weight [g] 3d post Tamoxifen | 36.9 ± 2.0 | | 19 | 33.8 ± 1.4 | | 16 | t | **<0.0001** |
| Body weight [g] 10d post Tamoxifen | 36.4 ± 1.8 | | 19 | 33.6 ± 1.5 | | 16 | t | **<0.0001** |
| Body weight [g] 38d post Tamoxifen | 35.0 ± 1.6 | | 19 | 33.3 ± 1.8 | | 14 | t | **0.0059** |
| **Open Field** | Age: 32 weeks, 17 DPI | | | | | | | |
| Escape latency [s] | 102.3 ± 64.6 | | 19 | 143.9 ± 53.7 | | 16 | U | 0.0655 |
| Total distance [m] | 27.8 ± 10.8 | | 19 | 16.1 ± 7.2 | | 16 | t | **0.0006** |
| Visits to periphery [#] | 8.3 ± 4.5 | | 19 | 10.2 ± 5.9 | | 16 | t | 0.3052 |
| Visits to intermediate [#] | 11.3 ± 5.8 | | 19 | 14.8 ± 10.6 | | 16 | t | 0.2521 |
| Visits to center [#] | 2.8 ± 1.6 | | 19 | 4.4 ± 5.8 | | 16 | U | 0.9537 |
| Time in periphery [s] | 387.6 ± 18.5 | | 19 | 335.2 ± 74.1 | | 16 | U | **0.0263** |
| Time in intermediate [s] | 23.3 ± 14.7 | | 19 | 70.9 ± 62.2 | | 16 | U | **0.0165** |
| Time in center [s] | 9.0 ± 6.2 | | 19 | 13.9 ± 16.8 | | 16 | U | 0.9546 |
| **Prepulse Inhibition** | Age: 32 weeks, 18 DPI | | | | | | | |
| Startle response to 65db [AU] | 1.4 ± 1.5 | | 19 | 1.3 ± 0.9 | | 16 | U | 0.6767 |
| Startle response to 120dB [AU] | 3.6 ± 2.8 | | 19 | 1.8 ± 0.8 | | 16 | U | **0.0146** |
| Prepulse Inhibition at 70db [%] | 38.6 ± 22.9 | | 17 | 28.9 ± 16.1 | | 13 | t | 0.1818 |
| Prepulse Inhibition at 75db [%] | 55.0 ± 22.9 | | 18 | 45.1 ± 18.2 | | 14 | t | 0.0771 |
| Prepulse Inhibition at 80db [%] | 63.4 ± 19.8 | | 17 | 41.4 ± 17.3 | | 13 | t | **0.0031** |
| ANOVA PPI 70-80dB | Genotype p=**0.0234**, Intensity p<**0.0001**, GxI p=0.2559 | | | | | | | |
| **Morris Water Maze** | Age: 33-35 weeks, 20-37 DPI | | | | | | | |
| Visible1 - escape latency [s] | 30.6 ± 13.0 | | 19 | 20.9 ± 13.2 | | 16 | U | **0.0165** |
| Visible2 - escape latency [s] | 8.5 ± 6.4 | | 19 | 8.4 ± 4.0 | | 16 | U | 0.5448 |
| Visible 1 vs 2 - escape latency [s] | U **<0.0001** | | | U **0.0002** | | | | |
| Hidden1 - escape latency [s] | 45.5 ± 20.1 | | 19 | 59.6 ± 13.1 | | 16 | t | **0.0182** |
| Hidden2 - escape latency [s] | 39.4 ± 19.8 | | 19 | 59.1 ± 14.7 | | 16 | U | **0.0052** |
| Hidden3 - escape latency [s] | 34.9 ± 20.9 | | 19 | 53.5 ± 18.2 | | 16 | U | **0.0018** |
| Hidden4 - escape latency [s] | 33.4 ± 16.6 | | 19 | 41.0 ± 16.5 | | 16 | U | 0.1166 |
| Hidden5 - escape latency [s] | 30.1 ± 16.7 | | 19 | 38.1 ± 17.5 | | 16 | U | 0.0821 |
| Hidden6 - escape latency [s] | 27.2 ± 19.1 | | 19 | 37.1 ± 21.2 | | 16 | U | 0.1310 |
| Hidden7 - escape latency [s] | 26.1 ± 18.7 | | 19 | 37.4 ± 16.7 | | 16 | U | **0.0288** |
| Hidden8 - escape latency [s] | 23.5 ± 15.4 | | 19 | 42.3 ± 19.7 | | 16 | U | **0.0018** |
| Hidden1-8 - ANOVA escape latency | Genotype p=**0.0020**, Days p<**0.0001**, GxD p=0.4023 | | | | | | | |
| Probe trial - average velocity [cm/s] | 18.4 ± 3.3 | | 19 | 19.3 ± 3.3 | | 16 | U | 0.5075 |
| Probe trial - time in TQ [s] | 37.7 ± 11.1 | | 19 | 33.1 ± 14.8 | | 16 | U | 0.3096 |
| Probe trial - visits to TQ [#] | 12.1 ± 3.8 | | 19 | 10.8 ± 3.3 | | 16 | t | 0.3093 |
| Probe trial - latency to TQ [s] | 9.7 ± 7.9 | | 19 | 12.2 ± 6.3 | | 16 | U | 0.0883 |
| Probe trial - latency to former platform [s] | 31.0 ± 23.1 | | 19 | 36.4 ± 23.5 | | 16 | U | 0.3717 |
| Reversal hidden1 - escape latency [s] | 34.8 ± 18.2 | | 19 | 47.6 ± 20.7 | | 16 | U | 0.0479 |
| Reversal hidden2 - escape latency [s] | 30.9 ± 19.7 | | 19 | 47.2 ± 17.1 | | 16 | U | **0.0042** |
| Reversal hidden3 - escape latency [s] | 26.1 ± 20.5 | | 19 | 47.4 ± 24.3 | | 16 | U | **0.0065** |
| Reversal hidden4 - escape latency [s] | 23.0 ± 17.1 | | 19 | 38.9 ± 22.1 | | 16 | U | **0.0150** |
| Probe trial 2 - average velocity [cm/s] | 19.4 ± 3.4 | | 19 | 19.0 ± 2.9 | | 16 | U | 0.5726 |
| Probe trial 2 - time in TQ [s] | 33.2 ± 8.8 | | 19 | 23.0 ± 8.4 | | 16 | t | **0.0013** |
| Probe trial 2 - visits to TQ [#] | 11.7 ± 3.2 | | 19 | 9.4 ± 4.7 | | 16 | U | **0.0285** |
| Probe trial 2 - latency to TQ [s] | 8.0 ± 6.8 | | 19 | 15.7 ± 8.0 | | 16 | U | **0.0036** |
| Probe trial 2 - latency to former platform [s] | 18.2 ± 20.5 | | 19 | 44.4 ± 35.4 | | 16 | U | **0.0124** |

(See figure on next page.)
**Fig. 2** Consequences of defined gray matter encephalitis on social recognition memory and thermoregulation in the SocioBox. **a** SocioBox experiments were performed using the 3 × tamoxifen cohort (DTA n = 16, control n = 18). Infrared thermography recordings show test mouse during habituation 3 in an otherwise empty SocioBox (left side) and during exposure to 5 stimulus mice (right side). Note the presence of the divider (partition) in the upper row that is lifted in the lower row. **b** Schematic outline of the 6 SocioBox trials. Habituations 1–3 were performed on 3 consecutive days, while exposure 1–2 and memory test were all performed on day 4. Each trial consisted of an initiation and interaction stage (5 min each; separated by divider lifting). During exposure, each test mouse (middle) was confronted with 5 stimulus mice (stimuli; S1-S5, light blue). For the memory test, 1 stimulus mouse was exchanged with a new mouse ("stranger", S, red) unknown to the test mouse. **c** General activity during memory test was increased in DTA compared to control mice (total distance, total interaction time, visits to interaction zone), whereas the latency to first interaction zone and time/visit were similar. **d** DTA mice were significantly faster to approach the stranger than control mice. **e** Evaluation of social recognition memory in the SocioBox memory test: Comparing the interaction of DTA and control mice with their conspecifics showed that control mice spent more time with the stranger than with the stimulus mice and undertook more visits to the stranger than to stimulus mice. DTA mice displayed no differences in these parameters, indicating a lack of distinction between stimulus mice and stranger; for clarity, parameters given in % total interaction time and average of time spent with all 4 stimulus mice shown. Time per visit to stranger over stimuli tended to be increased in controls but not DTA mice. **f** Centralization Index (CI) was calculated by mean body temperature divided by mean tail temperature for every frame of recording. **g–j** CI changes of the test mice during SocioBox trials. Dotted line indicates partition lifting after 300 s; repeated measure mixed-model ANOVA, mean ± SEM presented. **g** During habituation 3, there were no CI differences between both groups, neither before (*p* = 9482) nor after partition lifting (*p* = 0.1839). **h** During first half of exposure 1, DTA mice showed a higher CI than controls, but no difference after partition lifting (*p* = 0.3960). **i** First half of exposure 2 showed no significant differences between both groups (*p* = 0.0979), but revealed higher CI of control mice during second half (*p* = 0.0407). Interestingly, control mice presented increased CI values towards partition lifting (250-350 s, light blue field). **j** During the memory test, differences between groups in first (*p* = 0.0732) or second half (*p* = 0.0996) were not significant, but controls exhibited higher CI values in anticipation of partition lifting (210-290 s, *p* = 0.0395, light blue field)

**Fig. 2**  (See legend on previous page.)
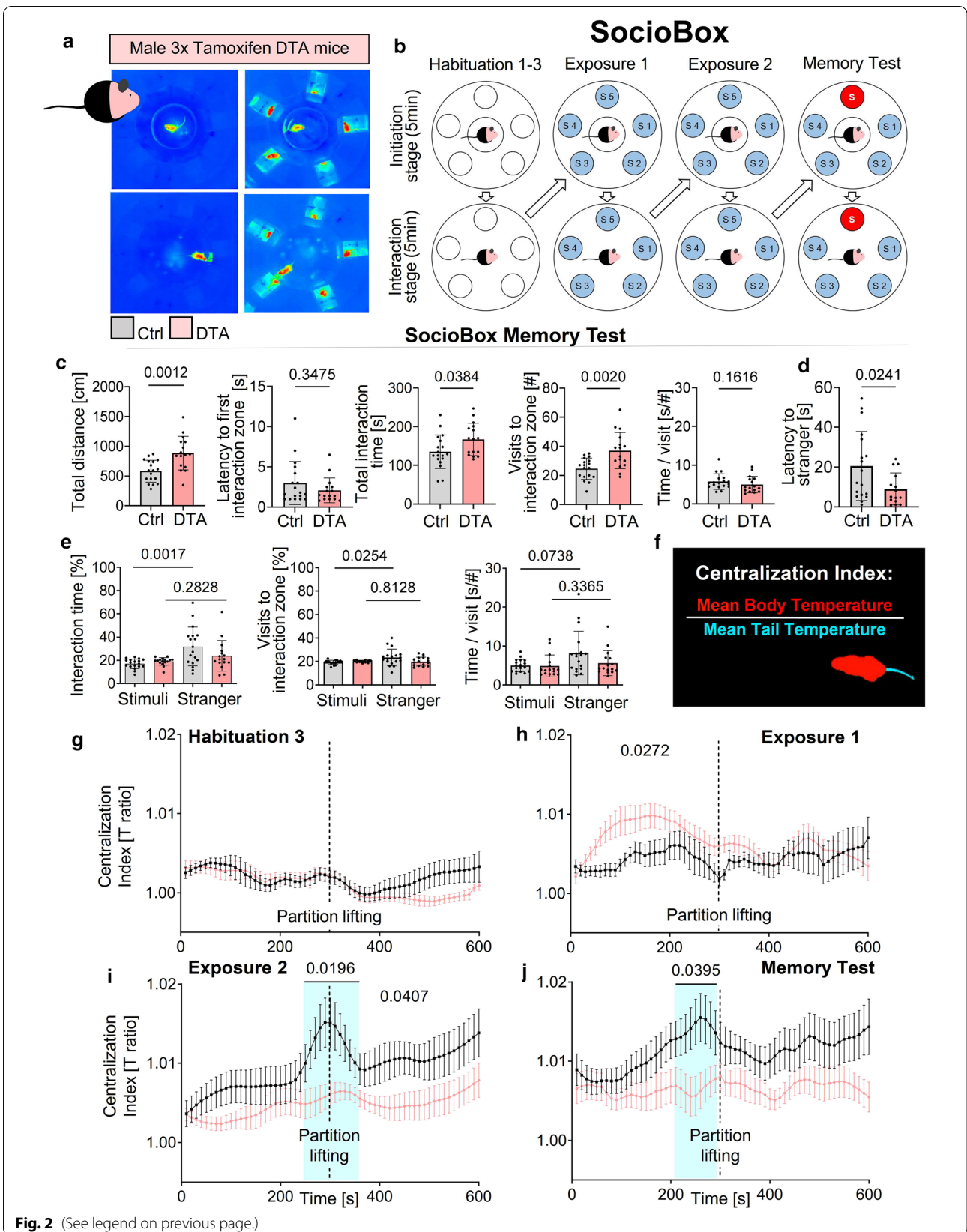
of blood perfusion by dynamic susceptibility contrast (DSC) MRI (2D RF-spoiled radial multi-echo FLASH [32]: TE1,2,3 = 1/2.15/3.3 ms, TR = 9 ms, flip angle = 11°, spatial resolution = $150 \times 150 \times 900$ $\mu m^3$, 2 slices, 201 spokes, temporal resolution = 0.55 frames per second, 800 repetitions) and intra-voxel incoherent motion (IVIM) MRI (Stejskal-Tanner pulsed gradient spin-echo sequence, TE/TR = 19/2000 ms, 4 segments, $\delta = 2.5$ ms, $\Delta = 10$ ms, 19 b-values (10, 20, 30, 40, 50, 60, 70, 80, 110, 140, 170, 200, 300, 400, 500, 600, 700, 800, 900 s/mm$^2$) applied in 3 orthogonal directions, spatial resolution $150 \times 150 \times 400$ $\mu m^3$).

## MRI data analyses
### Volumetry
MT-weighted images were first converted to NIfTI and preprocessed through denoising and bias field correction [3] in order to create an unbiased anatomical population template using the python pipeline twolevel_ants_dbm (https://github.com/CoBrALab/). Nonlinear deformation fields of the extracted brains were then used to estimate voxel-wise Jacobian determinants. Student's *t*-test was performed on the 3D Gaussian-smoothed maps of Jacobian determinants (FWHM 0.1 mm) for voxel-vise comparison of DTA and control mice. Q-values (false discovery rate (FDR) adjusted p-values) and the respective z-scores were calculated using the 3dFDR function of AFNI [9]. To visualize significant volume reductions in DTA mice z-scores smaller − 2.57 corresponding to a FDR of less than 1% were overlaid on the study template. In order to quantify the volume of selected brain regions, regions of interest (ROIs) including third and lateral ventricles, cerebrum (without hippocampus, ventricles and olfactory bulb), hippocampus, and cerebellum were determined on the study template by manual segmentation using the software package AMIRA (Visage Imaging GmbH, Berlin, Germany). ROIs were then retransformed into the subject space, individually inspected, and, if required, manually corrected. Finally, the respective volume information was extracted.

### IVIM
Diffusion weighted images were co-registered (translation only, imregister function, Matlab 2018b, Natock, MA) and the geometrical mean of the diffusion directions, the apparent diffusion coefficient (ADC) was calculated considering only those images obtained with b-values greater than 200 s/mm$^2$. The ADC was then used to estimate the perfusion fraction (f) and the pseudo-diffusion coefficient (D*) by utilizing all acquired b-value-images [13].

### DSC-MRI
Maps of R2*-relaxation rate (1/T2*) were estimated assuming a mono-exponential TE-dependent signal decay. A gamma variate function was fitted to the R2*-time curve of the contrast agent bolus-injection in order to estimate the cerebral blood volume (CBV) and the mean transit time (MTT) from which the cerebral blood flow (CBF) was calculated (CBF = CBV/MTT).
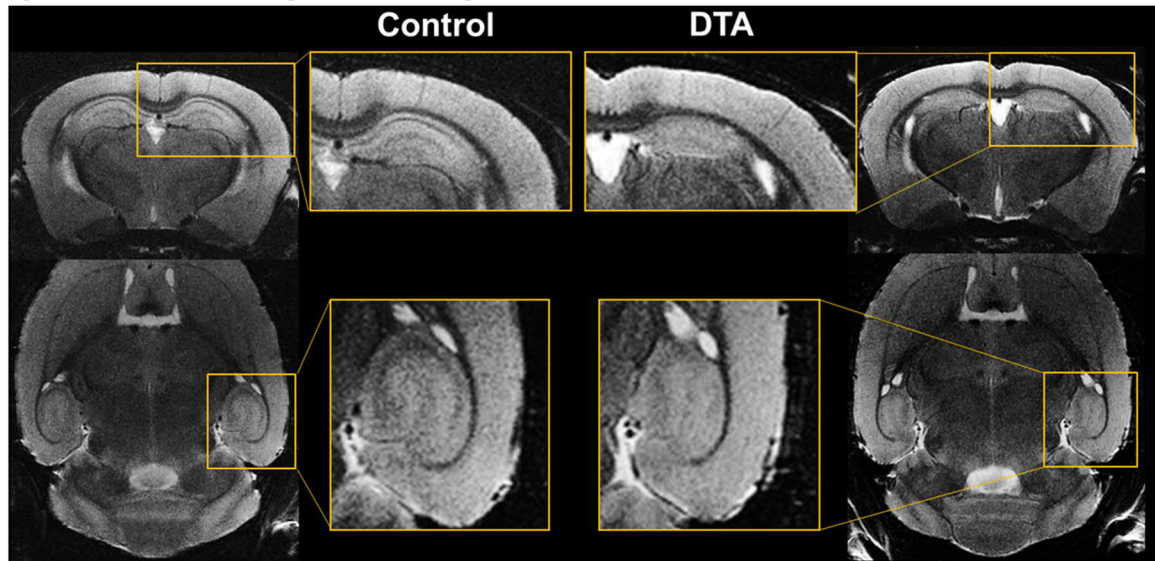
## Measurements assessing blood–brain-barrier integrity
Blood–brain barrier (BBB) integrity along with brain water content and dry brain mass was evaluated as previously described [5, 34]. Briefly, mice received intravenous injections of Evans blue (50 μg/g body weight, E2129, Sigma-Aldrich) and sodium fluorescein (200 μg/g body weight, F6377, Sigma-Aldrich). After 4 h, mice were anesthetized and transcardially perfused. Brains were collected, frozen on dry ice, weighted and lyophilized.
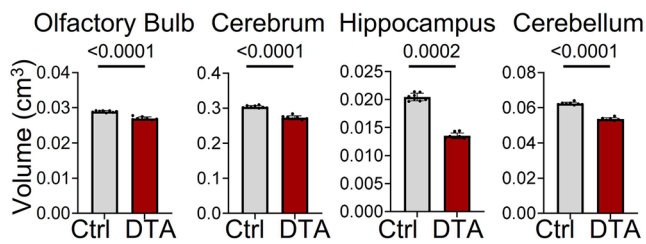
---

(See figure on next page.)

**Fig. 3** Magnetic resonance imaging 2 months after 5 × tamoxifen induction. **a** High-resolution T2-weighted MRI images of control and DTA mice. DTA mice displayed a reduction of the hippocampal dimensions in high-resolution T2-weighted MRI in vivo (top coronal view, bottom axial view). Dentate gyrus and CA region exhibited a clear rarefaction, making these regions in DTA mice almost undetectable. **b** Volumetric comparison of various brain regions. DTA mice showed atrophy of olfactory bulb, whole cerebrum (without hippocampus and ventricles), hippocampus, and cerebellum. **c** Comparison of Jacobian determinants. Maps of z-score derived from the comparison of Jacobian determinants, overlaid on the study template, revealed lower volume of the cortex (particularly in the region of layer V), the hippocampus and its projection regions in DTA mice compared to controls. A z-score lower than -2.57 corresponds to a false discovery rate lower than 1%. **d–f** Comparison of vasculature and perfusion by IVIM-MRI and DSC-MRI. DTA mice showed higher cerebral blood volume in the hippocampus as shown independently by IVIM-MRI **d** and DSC-MRI **e**. In addition, the vascular volume fraction was enhanced in the cortex of DTA mice. The cerebral blood flow **f** was increased in all analyzed brain regions. **g** Comparison of brain water content, determined by IVIM-MRI: Apparent diffusion coefficient (ADC) was increased in cortex and hippocampus of DTA mice, indicating higher water content in brain regions particularly affected by diphtheria toxin expression; MRI data from 6–8 mice/group, mean ± SD presented. **h** Molecular quantification of brain water, dry brain mass and blood brain barrier function in additional DTA and control mice at 2 months after encephalitis induction. Using this independent method, brains of DTA mice showed again higher water content and decreased brain mass. Increased extravasation of Evans blue and fluorescein indicate lasting blood–brain-barrier dysfunction; data from 5 mice/group, mean ± SD given; 2-tailed unpaired Welch's corrected *t*-tests or Mann–Whitney U-tests. All experiments in Fig. 3 were performed with 5 × tamoxifen DTA mice
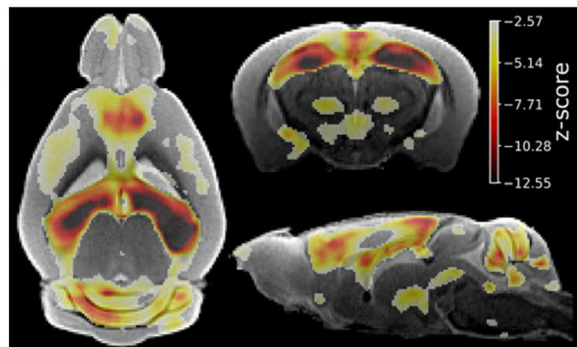
**Fig. 3** (See legend on previous page.)

After lyophilization, dehydrated brains were weighted to obtain dry brain mass and to calculate brain water content. Afterwards, tracers were extracted from hemispheres with formamide and quantified in triplicates on a fluorescent microscope (Observer Z2, Zeiss). The concentrations of tracers were calculated using a standard curve and normalized to controls.

### Blood flow cytometry
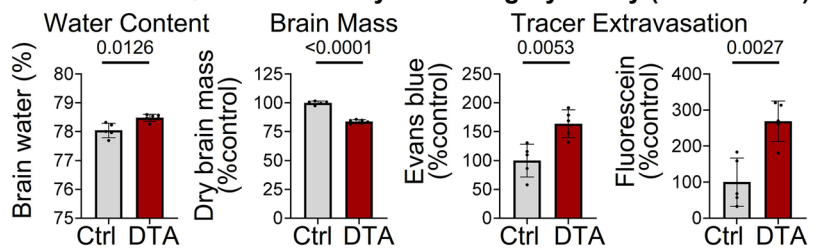EDTA-blood was collected from the orbital sinus 2 weeks after last tamoxifen injection. Per mouse, 50μL blood were diluted in 50μL PBS and overlaid on 100μL lymphocyte separation medium (1077, PromoCell). After centrifugation, peripheral blood mononuclear cells were isolated, washed and stained for 15 min at 4 °C with the following antibodies: PECy5 anti-CD4 (1:1000, clone H129.19, Biolegend), PECy7 anti-CD8 (1:500, clone 53–6.7, Biolegend), BV510 anti-B220 (1:500, clone RA3-6B2, Biolegend) and PerCpCy5.5 anti-CD11b (1:100, clone M1/70, Biolegend). After staining, cells were washed, suspended in 200μL PBS containing 2% bovine serum albumin (#8076.3, Roth), and filtered through 40 μm cell strainers. Samples were measured on a FACSAria Sorp (BD). Number of lymphocytes were determined using forward and side scatter. Frequency of T-helper cells (CD4$^+$,CD8$^-$), cytotoxic T-cells (CD8$^+$, CD4$^-$), B cells (B220$^+$, CD11b$^-$, CD8$^-$, CD4$^-$), and myeloid cells (CD11b$^+$, B220$^-$, CD8$^-$, CD4$^-$) were determined as percentage of total lymphocytes.

### Brain flow cytometry
Mice (3 × tamoxifen) were anesthetized with Avertin (1.36% 2,2,2,-tribromoethanol in ddH$_2$O; 24μL/g body weight) and transcardially perfused with 40 mL Ringer solution (B.Braun). Brains were stored on ice in 10% fetal bovine serum (FBS, #10500–064 Thermo)/DMEM (#41965 Thermo) until all brains were collected. Olfactory bulbs and brain stems were removed and brains

mashed through 70 μm cell strainers. To remove myelin, cells were suspended in isotonic Percoll (17-0891-01, GE Healthcare) to a final concentration of 30% and centrifuged. Cells were washed with FACS buffer (2% FBS, 10 mM EDTA in PBS) and filtered through 40 μm cell strainers. Fc-receptors were blocked for 10 min at 4 °C with anti-mouse CD16/32 antibodies (1:100, 14–0161, eBioscience). Cells were stained for 30 min at 4 °C with the following antibody mix: APC anti-CD45 (1:200, clone 104, BioLegend), PE anti-CD11b (1:200, clone M1/70, BioLegend), PECy5 anti-CD4 (1:1000, clone H129.19, BioLegend), PECy7 anti-CD8 (1:500, clone 53–6.7, Biolegend), APCCy7 anti-CD19 (1:200, clone 6D5, BioLegend), PerCP-Cy5.5 anti-CD138 (1:200, clone 281–2, BioLegend). After staining, cells were washed and suspended in 400μL FACS buffer. Per sample, 100μL APC quantification beads (#340487, BD) were added. Samples were measured on a FACSAria Sorp (BD). Cell numbers were corrected for the number of recorded APC beads. Leukocytes (CD45$^{high}$, CD11b$^-$), microglia (CD45$^{low}$, CD11b$^{high}$) and macrophages (CD45$^{high}$, CD11b$^{high}$) were quantified within single cell gate determined by forward and side scatter. CD4$^+$ T-cells and CD8$^+$ T-cells were quantified within leukocyte gate. CD19$^+$ B-cells and CD138$^+$ plasma cells were quantified in CD4$^-$ CD8$^-$ leukocyte gate.

### Histology
Mice were anesthetized with Avertin, transcardially perfused with Ringer (B.Braun) and subsequently 4% formaldehyde/PBS. Brains were collected, post-fixed in 4% formaldehyde/PBS for 12 h, dehydrated in 30% sucrose/PBS for 48 h, embedded in optimal cutting medium (Tissue-Tek, #4583, Sakura) and frozen on dry ice. Frozen brains were cut into 30 μm coronal sections on a cryostat (CM1950, Leica) and stored at -20 °C in anti-freeze medium (25% ethylene glycol/25% glycerol/PBS). Quantifications were performed using 4–6 hippocampi from 2–3 sections per mouse. Sections were

(See figure on next page.)

**Fig. 4** Histological analysis of neuroinflammatory readouts in the hippocampus 2 months after 3 × versus 5 × tamoxifen induction. **a** Representative coronal sections demonstrating persistent neuroinflammatory changes in DTA mice dependent on the tamoxifen dose. In the hippocampus of DTA mice, changes include increased microglia (Iba1$^+$ cells, white) and GFAP (red) density as well as apparent changes in morphology. High-resolution images of CA1, CA3 and dentate gyrus (DG) regions were acquired as 10 μm Z-stacks and are displayed as maximum-intensity projections. **b** To assess atrophy in hippocampal regions, 4–6 hippocampi per mouse (within Bregma -1.34 mm and -1.94 mm) were manually segmented and areas of respective regions normalized to the mean of control mice. DTA mice after both tamoxifen doses showed strong atrophy in whole hippocampus (HC) and particularly its CA regions, whereas the DG was only weakly affected. **c** Evaluation of astrogliosis in DTA compared to control mice. Prominent astrogliosis was observed in HC and CA regions of DTA mice in both tamoxifen dose groups, while the DG remained relatively unaffected. The GFAP$^+$ area fraction was determined densitometrically upon uniform thresholding, and fold changes were calculated based on the mean of control mice. **d** Quantification of Iba1$^+$ cells (microglia). DTA compared to control mice showed increased microglia numbers in all hippocampal regions. Data from 7–8 mice/group displayed as mean ± SD; 2-tailed unpaired Welch's corrected *t*-tests or Mann–Whitney U-tests

**Fig. 4** (See legend on previous page.)

**Fig. 5** Indicators of neuronal activity and circuitry in the hippocampus upon complex wheel running. **a** Schematic experimental outline. Approximately 2 months after 3 × tamoxifen induction mice were challenged for 4 h exposure to voluntary complex wheel running to induce neuronal activation. **b** Representative images of cFos (white) and PV (red) double staining in control and DTA mice. **c** Quantification of total number of cFos^{+} cells in hippocampal regions upon CRW. DTA mice showed significantly reduced numbers of cFos^{+} cells in HC and its CA regions, whereas the dentate gyrus (DG) remained unaffected. **d** PV[+] interneuron numbers 2 months after ablation of pyramidal neurons. DTA mice displayed increased PV[+] interneuron numbers in HC and its CA regions, but not in DG. **e** Evaluation of PV[+] interneuron activation upon CRW. PV[+] interneurons were less frequently activated (evaluated by cFos expression) in CA3 region of DTA mice, with similar tendency in CA1. DG was again similar between both groups. Data from 8 mice/group displayed as mean ± SD; 2-tailed unpaired Welch's corrected *t*-tests or Mann–Whitney U-tests
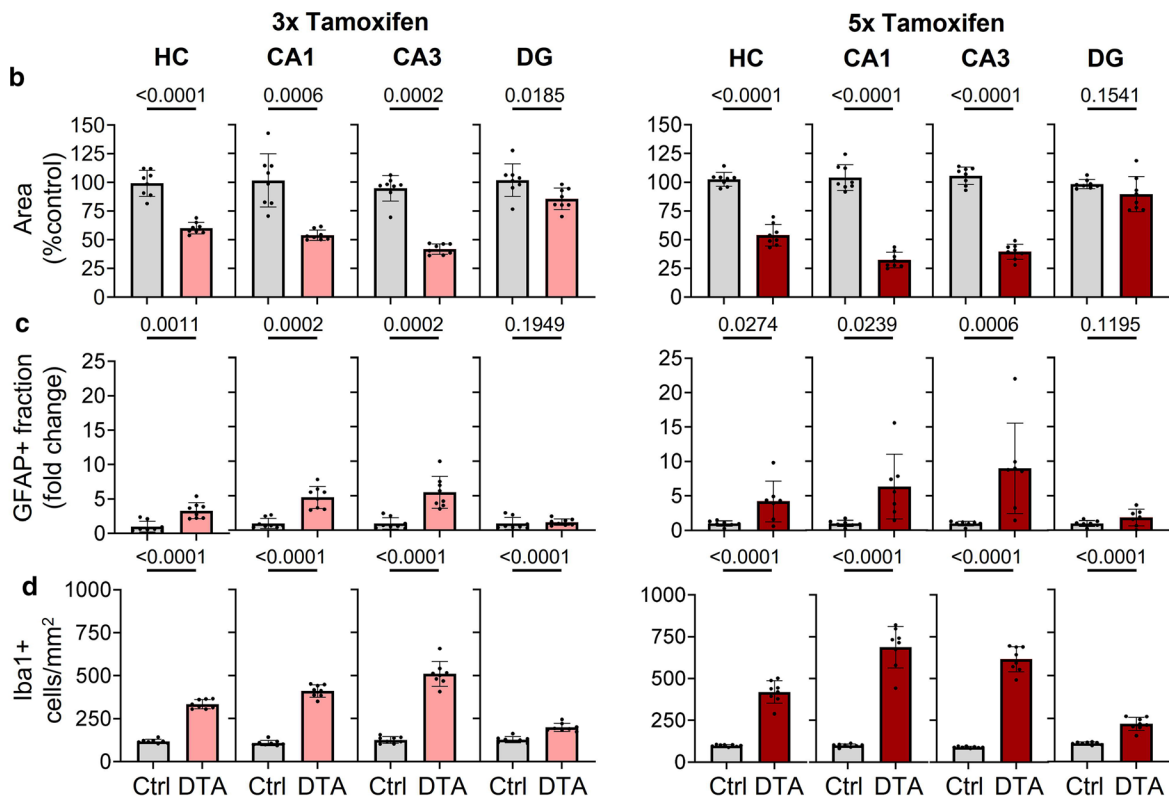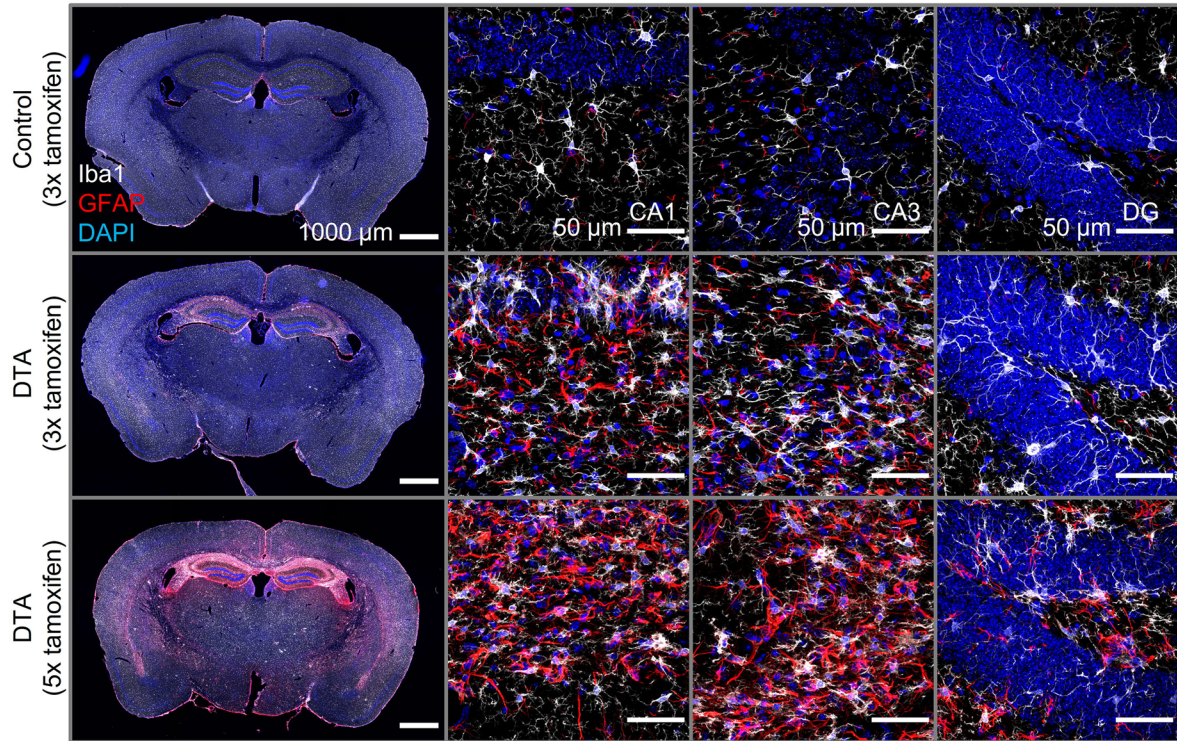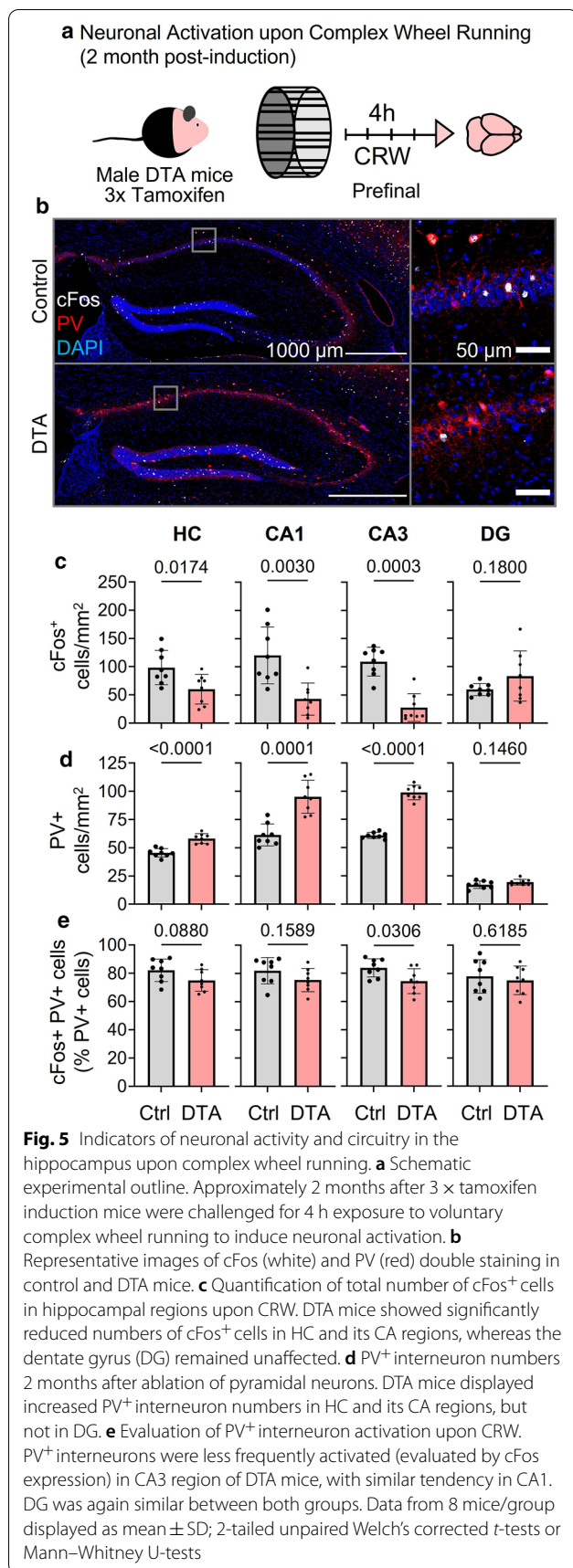
selected in regularly spaced intervals (every 300 μm) between Bregma coordinates -1.34 to -2.24 mm. Free-floating frozen sections were blocked and permeabilized for 1 h at RT with 5% normal horse serum (NHS, 26,050–088, Thermo) in 0.5% Triton X-100/PBS, incubated overnight at 4 °C with primary antibodies and subsequently stained with corresponding fluorescently-labeled secondary antibodies for 2 h at RT. Nuclei were stained for 10 min at RT with 0.2 μg/mL 4′,6-diamidino-2-phenylindole in PBS (DAPI, D9542, Sigma-Aldrich) and sections were mounted on SuperFrost®-Plus slides (J1800AMNZ, Thermo) with Aqua-Poly/Mount (#18606, Polysciences). The following primary antibodies were used: Mouse anti-GFAP (1:500, NCL-GFAP-GA5, NovoCastra), rabbit anti-Iba1 (1:1000, #019–19741, Wako), rabbit anti-cFos (1:1000, #226003, Synaptic Systems), guinea pig anti-parvalbumin (1:1000, #195004, Synaptic Systems). Corresponding secondary antibodies included: Alexa Fluor 555 anti-rabbit (1:1000, A21428, Thermo), Alexa Fluor 647 anti-mouse (1:1000, A31571, Thermo) Alexa Fluor 633 anti-guinea pig (1:1000, A21105, Thermo). For Fluorojade C staining (AG325, Sigma) of dying neurons, sections were incubated in 0.06% potassium permanganate solution for 10 min. Following a 1 min water rinse, tissue was transferred for 10 min to a 0.0001% solution of Fluorojade C, dissolved in 0.1% acetic acid. Slides were rinsed with ddH2O and dried at 60 °C. Overview images of whole brain sections were obtained on Eclipse-TI 2 epifluorescence microscope (Nikon), equipped with 4 × objective (4x/0.2 NA PLAN APO #MRD00045, Nikon). For quantification of Iba1^{+} cells and GFAP[+] area fraction by densitometry, 1 μm thick optical sections of hippocampi were acquired as tile scans on a confocal laser scanning microscope (LSM 880, Zeiss), furnished with a 40 × oil objective (40x/1.4 NA Plan-APOCHROMAT, #420762–9900, Zeiss). For quantification of parvalbumin[+] and cFos^{+} neurons, 2 μm thick optical sections of hippocampi were acquired as tile scans using the same microscope, equipped with a 20 × air objective (20x/0.8 Plan-APOCHROMAT, #420640–9903 Zeiss). Image acquisition parameters were kept constant within experiments. Quantifications and image processing were performed with FIJI-ImageJ software (Schindelin et al., 2012). Iba1^{+} cells (mostly microglia), parvalbumin^{+} cells (inhibitory neurons) and cFos^{+} neurons were manually counted. GFAP[+] area fraction (GFAP[+] area/total area of region of interest) was quantified densitometrically upon uniform thresholding and fold change to control animals was calculated. Atrophy in regions of interest (CA1, CA3, dentate gyrus) was determined through manual segmentation. Resulting

areas were normalized to the respective average of control animals. CA2/CA3 region is referred to as CA3 in text and figures. Cell counts were normalized to quantified areas. Data obtained from 4 to 6 hippocampi/mouse was averaged for analysis.

### Statistical analysis

Statistical analyses were performed using Prism9 software (GraphPad Software). Results are presented as mean ± standard deviations (SD), unless otherwise stated. Normal distribution of data was assessed using the Shapiro–Wilk test with an alpha error of 0.05. Dependent on data distribution, 2-tailed unpaired Welch's corrected *t*-tests or Mann–Whitney U-tests were used to compare groups. Repeated measure data was analyzed using mixed-model ANOVA. P values < 0.05 were considered statistically significant.

## Results and discussion

### Sudden pyramidal neuronal loss by induced *diphtheria* toxin expression for sterile modeling of viral-like gray matter encephalitis

To comprehensively study distinct features of moderate brain inflammation that affects primarily gray matter, we targeted pyramidal neurons. By inducible *diphtheria* toxin expression in these cells, we generated a sterile, spatially and temporally defined, moderate experimental encephalitis in 6–8 months old male Nex-CreERT2xRosa26-eGFP-DTA (='DTA') mice [1, 8, 19]. Tamoxifen dosing in this mouse line controls the amount of cell death. After a series of dose-titrating pilot experiments, we here selected a 3-day (3x) versus 5-day (5x) tamoxifen injection design (Fig. 1a, b). Acute hippocampus overview images, taken from trial mice at 1 week after 5 × tamoxifen induction, demonstrate by fluorojade staining the acute neurodegeneration/pyramidal neuronal loss (Fig. 1c). Using the 3 × versus 5 × tamoxifen design, we performed a longitudinal ~ 60 day analysis of these mice, which included behavioral experiments to target hippocampal and (pre)frontal cortex functions, with both established (MWM, PPI) and novel (SocioBox, thermography) paradigms, several sophisticated MRI readouts, BBB testing, flow cytometry analyses of brain and blood, plasma HMGB1 measurements as circulating inflammation marker, as well as histological quantifications, including a neuronal functionality readout (immediate early gene cFos induction after brief complex wheel running). In order to reduce the necessary number of animals (RRR principle), not all experiments were performed in mice of both induction schedules (Fig. 1d).

### Behavioral testing reveals manifold disturbance of brain functions in DTA mice
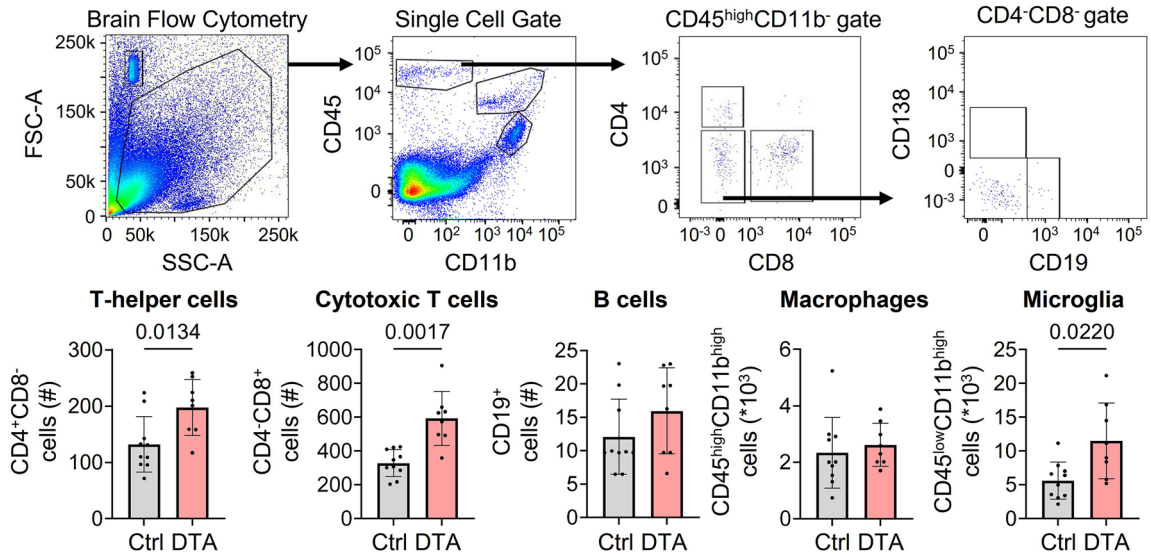
After destruction of substantial numbers of pyramidal neurons, hippocampal learning and memory, determined by the classical MWM, was highly significantly affected in encephalitis mice of both induction schemes (Fig. 1e-f and Tables 1,2). In the 5 ×, but not the 3 × tamoxifen group, the open field performance reflected behavioral pathology with reduced overall mobility and dampened natural drive to prefer the periphery (Fig. 1g; Tables 1,2). Both escape latency and enhanced time spent in the middle zone may additionally be related to the slower motion/reduced total distance. The PPI data in 5 × mice demonstrated also (pre)frontal network dysfunction (Fig. 1h; Table 2).

On top of these expected behavioral changes, we addressed novel readouts of social behavior, suspected to reflect CA2/CA3 destruction in our model, and known to play a role in human viral encephalitis [4, 35]. We tested in the 3 × tamoxifen mice social recognition memory, employing our recently developed SocioBox, and combined it with thermography (Fig. 2a-b; Table 1). The SocioBox test is superior to other presently available social recognition tests, successfully addressing multiple social contacts in parallel [23, 39]. We noted overall hyperactivity in the SocioBox memory test displayed by DTA mice, from total distance traveled to social interactions, including increased total interaction time and visits to the interaction zone, combined with a trend of shorter initial latency to interaction zone and time/visit (Fig. 2c). Surprisingly at first view, the latency to meet the stranger was reduced in DTA mice (Fig. 2d). The following readouts, however, clarified that this reduced latency was by
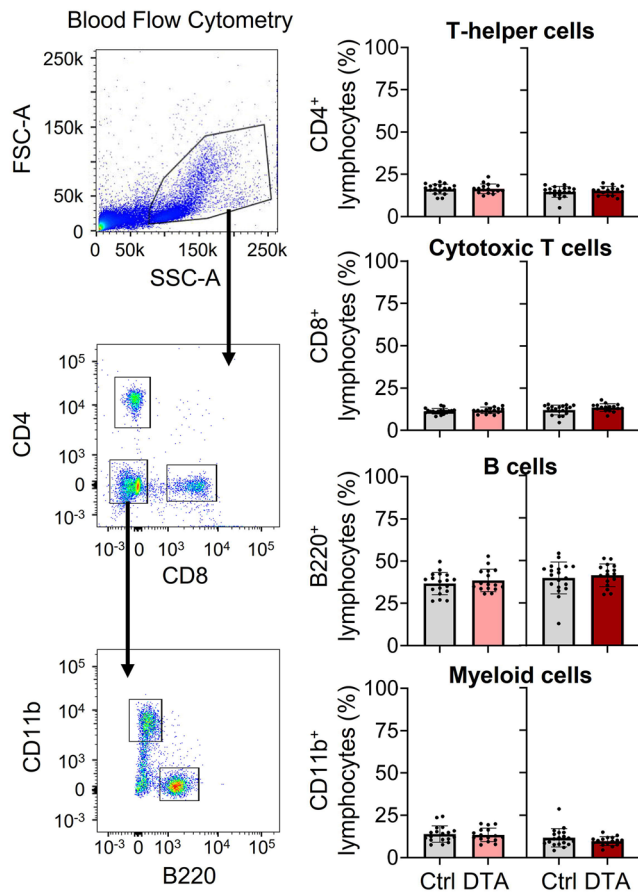
---

(See figure on next page.)

**Fig. 6** Evaluation of the brain and peripheral immune compartments. **a** Flow cytometry of brain tissue from DTA and control mice 2 months after 3 × tamoxifen induction. Gating strategy is depicted in the top row. DTA mice showed stronger infiltration of T-helper cells (CD11b⁻, CD45ʰⁱᵍʰ, CD8⁻, CD4⁺), cytotoxic T cells (CD11b⁻, CD45ʰⁱᵍʰ, CD4⁻, CD8⁺), and increased microglia numbers (CD11bʰⁱᵍʰ, CD45ˡᵒʷ). B cell numbers (CD11b⁻, CD45ʰⁱᵍʰ, CD8⁻, CD4⁻, CD19⁺) were low in brain tissue of both groups. Macrophage numbers (CD11bʰⁱᵍʰ, CD45ʰⁱᵍʰ) were not different. Data from 8–10 mice/group. **b** Flow cytometry of lymphocytes derived from peripheral blood 2 weeks after 3 × and 5 × tamoxifen induction. Gating strategy in left panel. DTA and control mice showed comparable and physiological numbers of major lymphocyte subsets (right panel). Data from 16–19 mice/group. **c** HMGB1 ELISA at 2 weeks and 2 months after 3 × or 5 × tamoxifen induction shows no difference in plasma concentrations between groups. Data from 10 mice/group. Data displayed as mean ± SD; 2-tailed unpaired Welch's corrected *t*-tests or Mann–Whitney U-tests
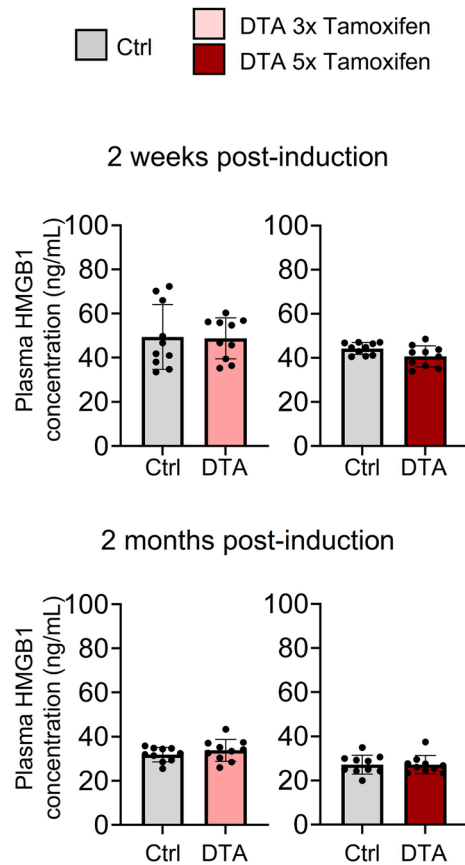
**Fig. 6** (See legend on previous page.)

no means a signal of better social memory. Comparing the behavior towards acquainted conspecifics (stimuli) versus the stranger confirmed that DTA mice were not able to distinguish between them, whereas control mice discriminated well (Fig. 2e), explicitly indicating social cognition deficits of encephalitis mice. For better comprehension of this novel test paradigm, we provide supplementary videos, showing a healthy control mouse. The video on the left illustrates the centralization index. The video on the right demonstrates the SocioBox with the test mouse in the middle, surrounded by 5 stimulus mice. The stranger mouse is encircled. Note the experimentator's arm in the middle of the video when partition lifting takes place.

### Thermography as convenient measure of autonomic dysfunction in DTA mice

We had reported previously that the SocioBox test with its forced and inescapable social interaction delivers substantial stress to healthy mice, even leading to the development of social avoidance, and thus constitutes a terminal test in behavioral batteries [39]. The distinct thermographic changes in this situation, resulting from stress-related blood flow alterations via reactive vasoconstriction and vasodilation, respectively, suggested the concomitant screening of body/tail temperature during SocioBox performance in our model. Interestingly, upon CNS inflammation, both on experimental autoimmune encephalitis in rats and human limbic encephalitis, evidence of thermoregulatory and autonomic dysfunction has been reported [2, 46].

In our thermography approach, the Centralization Index (ratio body/tail temperature = T ratio; see supplementary video) serves as whole body stress readout and convenient measure of potential autonomic dysfunction. Indeed, encephalitis mice (3 × tamoxifen) showed altered thermo-responses as compared to controls. Whereas during habituation 3, no appreciable dissociation in the thermo-curves appeared yet, DTA mice revealed higher centralization values in exposure 1 before partition lifting, perhaps pointing to an initially higher 'non-specific' agitation/stress. In both exposure 2 and memory test, the DTA mice thermo-responded in an overall blunted fashion compared to controls. In fact, a highly interesting thermo-pattern was observed in healthy mice that showed from exposure 1 over 2 to memory test a strong thermo-response, likely reflecting rising anticipation of partition lifting (Fig. 2f–j). The complete lack of this amazingly robust and fast experience-induced thermo-response in the sense of an 'autonomically expressed short-term memory', uncovered altered vasoactivity in peripheral and core body regions

as indication of autonomic dysfunction and/or compromised short-term memory in DTA mice.

### Brain dimensions and structural changes of DTA mice in high-resolution MRI

DTA mice (5 × tamoxifen) displayed a significant shrinkage of the hippocampal area shown by in vivo high-resolution T2-weighted MRI. Dentate gyrus and CA region exhibited a clear rarefaction, rendering these regions almost undetectable (Fig. 3a, top axial view, bottom transversal view). Volumetrical analysis of MT-weighted MRI demonstrated highly significant reductions in essentially all brain areas, including olfactory bulb, cerebrum, hippocampus and cerebellum (Fig. 3b). Maps of z-score derived from the comparison of Jacobian determinants and overlaid on the study template revealed significantly lower volume of the cortex (in particular in the region of layer V), the hippocampus and its projection areas in DTA mice compared to controls. A z-score lower than -2.57 corresponds to a false discovery rate of lower than 1% (Fig. 3c).

DTA mice had a higher vascular volume in the hippocampus as shown independently by both IVIM-MRI (vascular volume fraction) and DSC-MRI (cerebral blood volume). In addition, the vascular volume fraction was increased in the cortex of DTA mice. This phenomenon is highly interesting and will require deeper mechanistic search via experimental approaches in the future, as any clear insight from the literature [24] or from the present data is still lacking. Importantly, cerebral blood flow (DSC-MRI) was increased in all analyzed brain regions (Fig. 3d–f). Taking these findings together, we suggest a working model where the enhanced vascular volume, in parallel to neural tissue loss in this sterile encephalitis, reflects a 'relative' increase in vascular density rather than simple vessel dilatation. This would also reconcile with the observed increase in cerebral blood flow.

The apparent diffusion coefficient (ADC) was augmented in cortex and hippocampus but not thalamus of DTA mice, indicating higher water content in brain regions directly affected by the toxin (Fig. 3g). This finding was independently verified in the BBB integrity assay [5, 34], showing increased water content and reduced brain mass. At the same time, this assay yielded distinct tracer extravasation, both of Evans blue and fluorescein, proving BBB leakage (Fig. 3h).

### Lasting neuroinflammation following pyramidal neuronal death in DTA mice

Histological analysis demonstrated lasting prominent micro- and astrogliosis in hippocampus and cortex of DTA mice, more pronounced after 5 × compared to

$3 \times$ tamoxifen (Fig. 4a). Quantifications validated again a clear reduction in the areas of whole hippocampus as well as of CA1 and CA3 subfields. The dentate gyrus was less noticeably affected (Fig. 4b). Similarly, the highest density of GFAP$^+$ area and strongest increases in Iba1$^+$ cell numbers were seen in total hippocampus, CA1 and CA3, but less in dentate gyrus (Fig. 4 c-d).

The prolonged neuroinflammatory response upon DTA-induced neuronal death is consistent with a mouse model, in which DTA expression was coupled to regulatory elements of Camk2α in a tetracyclin-responsive fashion [49], although kinetics of DTA induction, severity and regional selectivity expectedly differ between the 2 models. Interestingly, in this earlier mouse model, some of the neuroinflammatory responses, including reactive microglia, have been dampened upon microglia depletion and repopulation via CSF1R inhibitor treatment and withdrawal [38], demonstrating the importance of such animal models for developing translationally relevant treatment strategies.

To evaluate neuronal activation and interneuron density after selective ablation of pyramidal neurons in DTA mice, cFos expression and parvalbumin$^+$ interneuron numbers were assessed. In fact, the toxin is tamoxifen-inducibly expressed by glutamatergic pyramidal neurons, which are preferentially destroyed. In contrast to the disease *Diphtheria*, however, only the catalytically active fragment A is expressed in our genetic model, while fragment B was purposely omitted to prevent receptor-mediated entry to neighboring cells [1, 8, 19]. Hence, cFos activity in inhibitory neurons should not have been directly affected by the toxin.

Indeed, determination of cFos expression after brief complex wheel running as neuronal activity readout confirmed the expected decrease of immediate early gene expression in whole hippocampus, CA1 and CA3 of DTA mice, due to the ablation of pyramidal neurons. In contrast, cFos$^+$ cells in dentate gyrus did not differ from controls, again underlining the widely intact situation of this region (Fig. 5a–c). We note that both DTA and control mice performed comparably in this short-term CRW exposure (running distance: $659 \pm 238$ m versus $946 \pm 523$ m, respectively, $p = 0.1893$). The number of parvalbumin$^+$ interneurons normalized to the respective hippocampal area showed highly significant 'relative' increases, consistent with circuit adjustments in the sense of altered inhibition. The cFos$^+$ interneurons among them, however, tended to be decreased in whole hippocampus and CA subfields, pointing perhaps to mildly compromised cellular activatability. Again, the dentate gyrus was spared in DTA mice and appeared comparable to controls (Fig. 5d, e).

## Flow cytometry shows clear alterations in the brain immune compartment following pyramidal neuronal death in absence of measurable effects in blood

Brain flow cytometry after 2 months of DTA induction ($3 \times$ tamoxifen) confirmed not only the histologically quantified microgliosis but also revealed persistent increases in T cells, in particular CD8$^+$ cytotoxic T cells, shown very recently to drive axon degeneration in the normal aging mouse CNS and contribute to age-related cognitive and motor decline [16]. B cell numbers were low and like macrophages unaltered (Fig. 6a).

In contrast, blood flow cytometry at 2 weeks after DTA induction (in $3 \times$ and $5 \times$ tamoxifen mice) and upon considerable acute brain inflammation did not show any immune cell alterations in the periphery (Fig. 6b). This complete lack of peripheral changes reflects in our mouse model the enormous and well-known clinical problems of diagnosing even substantial brain inflammation in vivo, often leading to wrong assumptions regarding suddenly occuring behavioral abnormalities in neuropsychiatric practice.

In an approach to identify a possible peripheral diagnostic marker, we came across an alarmin, namely high-mobility group box 1 (HMGB1), a key molecule of host defense systems that can be released under acute and chronic pathological conditions. HMGB1 is a non-histone nuclear protein with dual functions depending on localization. Within cells, it is confined primarily to the nucleus where it binds DNA and plays a role in transcriptional regulation. However, extracellular HMGB1 serves as proinflammatory cytokine. Elevated HMGB1 levels in serum and CSF have been reported in neurological infection, indicating that excessive host inflammation may be relevant to the pathogenesis of encephalitis. Beyond infections, HMGB1 has pathogenic roles during trauma and sterile inflammation, such as systemic inflammatory response syndrome [14, 15, 30, 36, 44]. Thus, we followed HMGB1 plasma levels at 14 days and 2 months after DTA induction in both $3 \times$ and $5 \times$ tamoxifen mice. Surprisingly, there were no differences between groups at any time point or induction scheme (Fig. 6c).

Again, it is fascinating, but certainly also alarming for clinicians, that extensive inflammatory degeneration in the brain, including BBB breakdown, can occur without indication in the blood. Since this clear result is of major relevance also for human neurodegenerative disease, it will hopefully stimulate the development of even more sophisticated brain imaging paradigms, sensitive enough for in vivo diagnosis of ongoing brain inflammation.

**Modeling aspects of viral gray matter encephalitis by sterile pyramidal neuronal death: Synopsis and outlook**
With the present longitudinal study, we aimed at defining downstream consequences of sudden pyramidal neuronal loss as it characterizes many viral infections, including reactive neuroinflammatory and subsequent neurodegenerative processes. Employing DTA mice, we present an animal model that allows sterile and targeted induction of cell death, thereby excluding the numerous parallel cellular and molecular events that characterize infections from the beginning and make delineation of causes and consequences often impossible. We provide not only the predictable histological evidence of a dose-dependent mild to moderate encephalitis together with the expected behavioral consequences of hippocampal and (pre)frontal damage. We also deliver clearcut and easily quantifiable novel results on disturbed social cognition with pathological thermoreaction/autonomic dysfunction as well as multifaceted sophisticated MRI readouts as future endpoints of targeted therapeutic approaches.

## Supplementary Information

The online version contains supplementary material available at https://doi.org/10.1186/s40478-021-01214-6.

---

**Additional file 1.**

---

## Availability of data and materials
All data are available upon request.

## Declarations

## Competing interests
The authors declare no competing financial or other interests.

## Author details
[1] Clinical Neuroscience, Max Planck Institute of Experimental Medicine, Hermann-Rein-Str.3, 37075 Göttingen, Germany. [2] Functional Imaging Laboratory, German Primate Center, Leibniz Institute for Primate Research, Kellnerweg 4, 37077 Göttingen, Germany. [3] Georg August University, Göttingen, Germany. [4] Department of Neurogenetics, Max Planck Institute of Experimental Medicine, Göttingen, Germany. [5] Johann Friedrich Blumenbach Institute of Zoology & Anthropology, University of Göttingen, Göttingen, Germany. [6] Institute for Neuroimmunology and Multiple Sclerosis Research, University Medical Center Göttingen, Göttingen, Germany.

## References
1. Agarwal A, Dibaj P, Kassmann CM, Goebbels S, Nave KA, Schwab MH (2012) In vivo imaging and noninvasive ablation of pyramidal neurons in adult NEX-CreERT2 mice. Cereb Cortex 22:1473–1486. https://doi.org/10.1093/cercor/bhr214
2. Asahina M, Fujinuma Y, Yamanaka Y, Fukushima T, Katagiri A, Ito S, Kuwabara S (2011) Diminished emotional sweating in patients with limbic encephalitis. J Neurol Sci 306:16–19. https://doi.org/10.1016/j.jns.2011.04.007
3. Avants BB, Tustison NJ, Song G, Cook PA, Klein A, Gee JC (2011) A reproducible evaluation of ANTs similarity metric performance in brain image registration. Neuroimage 54:2033–2044. https://doi.org/10.1016/j.neuroimage.2010.09.025
4. Belaunzaran-Zamudio PF, Ortega-Villa AM, Mimenza-Alvarado AJ, Guerra-De-Blas PDC, Aguilar-Navarro SG, Sepulveda-Delgado J, Hunsberger S, Salgado RV, Ramos-Castaneda J, Rincon Leon HA et al (2021) Comparison of the impact of Zika and Dengue virus infection, and other acute illnesses of unidentified origin on cognitive functions in a prospective cohort in chiapas Mexico. Front Neurol 12:631801. https://doi.org/10.3389/fneur.2021.631801
5. Berghoff SA, Gerndt N, Winchenbach J, Stumpf SK, Hosang L, Odoardi F, Ruhwedel T, Bohler C, Barrette B, Stassart R et al (2017) Dietary cholesterol promotes repair of demyelinated lesions in the adult brain. Nat Commun 8:14241. https://doi.org/10.1038/ncomms14241
6. Boldrini M, Canoll PD, Klein RS (2021) How COVID-19 Affects the Brain. JAMA Psychiat. https://doi.org/10.1001/jamapsychiatry.2021.0500
7. Boretius S, Kasper L, Tammer R, Michaelis T, Frahm J (2009) MRI of cellular layers in mouse brain in vivo. Neuroimage 47:1252–1260. https://doi.org/10.1016/j.neuroimage.2009.05.095
8. Brockschnieder D, Lappe-Siefke C, Goebbels S, Boesl MR, Nave KA, Riethmacher D (2004) Cell depletion due to diphtheria toxin fragment A after Cre-mediated recombination. Mol Cell Biol 24:7636–7642. https://doi.org/10.1128/MCB.24.17.7636-7642.2004
9. Cox RW, Hyde JS (1997) Software tools for analysis and visualization of fMRI data. NMR Biomed 10:171–178. https://doi.org/10.1002/(sici)1099-1492(199706/08)10:4/5%3c171::aid-nbm453%3e3.0.co;2-l
10. Crews L, Patrick C, Achim CL, Everall IP, Masliah E (2009) Molecular pathology of neuro-AIDS (CNS-HIV). Int J Mol Sci 10:1045–1063. https://doi.org/10.3390/ijms10031045
11. Deng X, Shi Z, Li S, Wang X, Qiu Y, Shao D, Wei J, Tong G, Ma Z (2011) Characterization of nonstructural protein 3 of a neurovirulent Japanese encephalitis virus strain isolated from a pig. Virol J 8:209. https://doi.org/10.1186/1743-422X-8-209
12. Dere E, Dahm L, Lu D, Hammerschmidt K, Ju A, Tantra M, Kastner A, Chowdhury K, Ehrenreich H (2014) Heterozygous ambra1 deficiency in mice: a genetic trait with autism-like behavior restricted to the female gender. Front Behav Neurosci 8:181. https://doi.org/10.3389/fnbeh.2014.00181
13. Federau C, O'Brien K, Meuli R, Hagmann P, Maeder P (2014) Measuring brain perfusion with intravoxel incoherent motion (IVIM): initial clinical experience. J Magn Reson Imaging 39:624–632. https://doi.org/10.1002/jmri.24195
14. Festoff BW, Sajja RK, van Dreden P, Cucullo L (2016) HMGB1 and thrombin mediate the blood-brain barrier dysfunction acting as biomarkers of neuroinflammation and progression to neurodegeneration in Alzheimer's disease. J Neuroinflammation 13:194. https://doi.org/10.1186/s12974-016-0670-z
15. Fonken LK, Frank MG, Kitt MM, D'Angelo HM, Norden DM, Weber MD, Barrientos RM, Godbout JP, Watkins LR, Maier SF (2016) The Alarmin HMGB1 mediates age-induced neuroinflammatory priming. J Neurosci 36:7946–7956. https://doi.org/10.1523/JNEUROSCI.1161-16.2016
16. Groh J, Knöpper K, Arampatzi P, Yuan X, Lößlein L, Saliba A-E, Kastenmüller W, Martini R (2021) Accumulation of cytotoxic T cells in the aged CNS leads to axon degeneration and contributes to cognitive

and motor decline. Nature Aging 1:357–367. https://doi.org/10.1038/s43587-021-00049-z

17. Hagemeyer N, Goebbels S, Papiol S, Kastner A, Hofer S, Begemann M, Gerwig UC, Boretius S, Wieser GL, Ronnenberg A et al (2012) A myelin gene causative of a catatonia-depression syndrome upon aging. EMBO Mol Med 4:528–539. https://doi.org/10.1002/emmm.201200230

18. Huo L, Xu KL, Wang H (2021) Clinical features of SARS-CoV-2-associated encephalitis and meningitis amid COVID-19 pandemic. World J Clin Cases 9:1058–1078. https://doi.org/10.12998/wjcc.v9.i5.1058

19. Ivanova A, Signore M, Caro N, Greene ND, Copp AJ, Martinez-Barbera JP (2005) In vivo genetic ablation by Cre-mediated expression of diphtheria toxin fragment A. Genesis 43:129–135. https://doi.org/10.1002/gene.20162

20. Janova H, Arinrad S, Balmuth E, Mitjans M, Hertel J, Habes M, Bittner RA, Pan H, Goebbels S, Begemann M et al (2018) Microglia ablation alleviates myelin-associated catatonic signs in mice. J Clin Invest 128:734–745. https://doi.org/10.1172/JCI97032

21. Kaliyaperumal S, Dang X, Wuethrich C, Knight HL, Pearson C, MacKey J, Mansfield KG, Koralnik IJ, Westmoreland SV (2013) Frequent infection of neurons by SV40 virus in SIV-infected macaque monkeys with progressive multifocal leukoencephalopathy and meningoencephalitis. Am J Pathol 183:1910–1917. https://doi.org/10.1016/j.ajpath.2013.08.007

22. Kenfak A, Eperon G, Schibler M, Lamoth F, Vargas MI, Stahl JP (2019) Diagnostic approach to encephalitis and meningoencephalitis in adult returning travellers. Clin Microbiol Infect 25:415–421. https://doi.org/10.1016/j.cmi.2019.01.008

23. Krueger-Burg D, Winkler D, Mitkovski M, Daher F, Ronnenberg A, Schluter OM, Dere E, Ehrenreich H (2016) The SocioBox: a novel paradigm to assess complex social recognition in male mice. Front Behav Neurosci 10:151. https://doi.org/10.3389/fnbeh.2016.00151

24. Lapointe E, Li DKB, Traboulsee AL, Rauscher A (2018) What have we learned from perfusion MRI in multiple sclerosis? Am J Neuroradiol 39:994–1000

25. LaRovere KL, Riggs BJ, Poussaint TY, Young CC, Newhams MM, Maamari M, Walker TC, Singh AR, Dapul H, Hobbs CV et al (2021) Neurologic involvement in children and adolescents hospitalized in the United States for COVID-19 or multisystem inflammatory syndrome. JAMA Neurol. https://doi.org/10.1001/jamaneurol.2021.0504

26. Liebetanz D, Baier PC, Paulus W, Meuer K, Bahr M, Weishaupt JH (2007) A highly sensitive automated complex running wheel test to detect latent motor deficits in the mouse MPTP model of Parkinson's disease. Exp Neurol 205:207–213. https://doi.org/10.1016/j.expneurol.2007.01.030

27. McKenzie IA, Ohayon D, Li H, de Faria JP, Emery B, Tohyama K, Richardson WD (2014) Motor skill learning requires active central myelination. Science 346:318–322. https://doi.org/10.1126/science.1254960

28. Meinhardt J, Radke J, Dittmayer C, Franz J, Thomas C, Mothes R, Laue M, Schneider J, Brunink S, Greuel S et al (2021) Olfactory transmucosal SARS-CoV-2 invasion as a port of central nervous system entry in individuals with COVID-19. Nat Neurosci 24:168–175. https://doi.org/10.1038/s41593-020-00758-5

29. Messacar K, Fischer M, Dominguez SR, Tyler KL, Abzug MJ (2018) Encephalitis in US Children. Infect Dis Clin North Am 32:145–162. https://doi.org/10.1016/j.idc.2017.10.007

30. Moniuszko-Malinowska A, Penza P, Czupryna P, Zajkowska O, Pancewicz S, Swierzbinska R, Dunaj J, Zajkowska J (2018) Assessment of HMGB-1 concentration in tick-borne encephalitis and neuroborreliosis. Int J Infect Dis 70:131–136. https://doi.org/10.1016/j.ijid.2018.03.013

31. Morris RGM (1981) Spatial localization does not require the presence of local cues. Learn Motiv 12:239–260. https://doi.org/10.1016/0023-9690(81)90020-5

32. Moussavi A, Boretius S (2019) Imperfect magnetic field gradients in radial k-space encoding-Quantification, correction, and parameter dependency. Magn Reson Med 81:962–975. https://doi.org/10.1002/mrm.27449

33. Moy SS, Nadler JJ, Young NB, Perez A, Holloway LP, Barbaro RP, Barbaro JR, Wilson LM, Threadgill DW, Lauder JM et al (2007) Mouse behavioral tasks relevant to autism: phenotypes of 10 inbred strains. Behav Brain Res 176:4–20. https://doi.org/10.1016/j.bbr.2006.07.030

34. Pan H, Oliveira B, Saher G, Dere E, Tapken D, Mitjans M, Seidel J, Wesolowski J, Wakhloo D, Klein-Schmidt C et al (2019) Uncoupling the widespread occurrence of anti-NMDAR1 autoantibodies from

35. Pang CC, Kiecker C, O'Brien JT, Noble W, Chang RC (2019) Ammon's Horn 2 (CA2) of the hippocampus: a long-known region with a new potential role in neurodegeneration. Neuroscientist 25:167–180. https://doi.org/10.1177/1073858418778747

36. Paudel YN, Angelopoulou E, C BK, Piperi C, Othman I, (2019) High mobility group box 1 (HMGB1) protein in Multiple Sclerosis (MS): Mechanisms and therapeutic potential. Life Sci 238:116924. https://doi.org/10.1016/j.lfs.2019.116924

37. Poggi G, Boretius S, Mobius W, Moschny N, Baudewig J, Ruhwedel T, Hassouna I, Wieser GL, Werner HB, Goebbels S et al (2016) Cortical network dysfunction caused by a subtle defect of myelination. Glia 64:2025–2040. https://doi.org/10.1002/glia.23039

38. Rice RA, Pham J, Lee RJ, Najafi AR, West BL, Green KN (2017) Microglial repopulation resolves inflammation and promotes brain recovery after injury. Glia 65:931–944. https://doi.org/10.1002/glia.23135

39. Seidel J, Bockhop F, Mitkovski M, Martin S, Ronnenberg A, Krueger-Burg D, Schneider K, Rohse H, Wustefeld L, Cosi F et al (2020) Vascular response to social cognitive performance measured by infrared thermography: a translational study from mouse to man. FASEB Bioadv 2:18–32. https://doi.org/10.1096/fba.2019-00085

40. Sejvar JJ, Kohl KS, Bilynsky R, Blumberg D, Cvetkovich T, Galama J, Gidudu J, Katikaneni L, Khuri-Bulos N, Oleske J et al (2007) Encephalitis, myelitis, and acute disseminated encephalomyelitis (ADEM): case definitions and guidelines for collection, analysis, and presentation of immunization safety data. Vaccine 25:5771–5792. https://doi.org/10.1016/j.vaccine.2007.04.060

41. Smeal RM, Stewart KA, Iacob E, Fujinami RS, White HS, Wilcox KS (2012) The activity within the CA3 excitatory network during Theiler's virus encephalitis is distinct from that observed during chronic epilepsy. J Neurovirol 18:30–44. https://doi.org/10.1007/s13365-012-0082-5

42. Venkatesan A, Tunkel AR, Bloch KC, Lauring AS, Sejvar J, Bitnun A, Stahl JP, Mailles A, Drebot M, Rupprecht CE et al (2013) Case definitions, diagnostic algorithms, and priorities in encephalitis: consensus statement of the international encephalitis consortium. Clin Infect Dis 57:1114–1128. https://doi.org/10.1093/cid/cit458

43. Wakhloo D, Scharkowski F, Curto Y, Javed Butt U, Bansal V, Steixner-Kumar AA, Wustefeld L, Rajput A, Arinrad S, Zillmann MR et al (2020) Functional hypoxia drives neuroplasticity and neurogenesis via brain erythropoietin. Nat Commun 11:1313. https://doi.org/10.1038/s41467-020-15041-1

44. Walker LE, Griffiths MJ, McGill F, Lewthwaite P, Sills GJ, Jorgensen A, Antoine DJ, Solomon T, Marson AG, Pirmohamed M (2017) A comparison of HMGB1 concentrations between cerebrospinal fluid and blood in patients with neurological disease. Biomarkers 22:635–642. https://doi.org/10.1080/1354750X.2016.1265003

45. Wickstrom R, Fowler A, Bogdanovic G, Bennet R, Eriksson M (2017) Review of the aetiology, diagnostics and outcomes of childhood encephalitis from 1970 to 2009. Acta Paediatr 106:463–469. https://doi.org/10.1111/apa.13682

46. Wrotek S, Nowakowska A, Caputa M, Kozak W (2020) Unbalanced thermoregulation in experimental autoimmune encephalitis induced in Lewis rats. J Therm Biol 89:102529. https://doi.org/10.1016/j.jtherbio.2020.102529

47. Wuthrich C, Dang X, Westmoreland S, McKay J, Maheshwari A, Anderson MP, Ropper AH, Viscidi RP, Koralnik IJ (2009) Fulminant JC virus encephalopathy with productive infection of cortical pyramidal neurons. Ann Neurol 65:742–748. https://doi.org/10.1002/ana.21619

48. Wuthrich C, Koralnik IJ (2012) Frequent infection of cortical neurons by JC virus in patients with progressive multifocal leukoencephalopathy. J Neuropathol Exp Neurol 71:54–65. https://doi.org/10.1097/NEN.0b013e31823ede59

49. Yamasaki TR, Blurton-Jones M, Morrissette DA, Kitazawa M, Oddo S, LaFerla FM (2007) Neural stem cells improve memory in an inducible mouse model of neuronal loss. J Neurosci 27:11925. https://doi.org/10.1523/JNEUROSCI.1627-07.2007

## Publisher's Note

# 4 Project II: Autoantibodies against NMDA receptor 1 modify rather than cause encephalitis

## 4.1 Overview of Project II

After the discovery of an encephalitis associated with autoantibodies directed against the NMDAR1 subunit of N-methyl-D-aspartate receptors (NMDAR), a vast number of studies investigated the pathogenicity of these autoantibodies, resulting in some understanding of their function and mode of action. Prior work has shown that NMDAR are internalized upon binding of NMDAR1-autoantibodies (NMDAR1-AB) resulting in NMDAR-hypofunction. This decrease in surface NMDAR expression potentially explains some psychiatric and neurological symptoms observed in patients with the so-called anti-NMDAR encephalitis. However, the actual pathomechanism(s) that induce encephalitis and drive neuroinflammation are understudied and few studies investigated the pathophysiological relevance of NMDAR1-AB in a neuroinflammatory context. To investigate the effects of NMDAR1-AB during gray matter inflammation, the previously characterized DTA mouse model was utilized (Wilke et al. 2021b).To better represent the demographics of NMDARE patients, young female mice were used and the tamoxifen dose was lowered to prevent excessive pyramidal cell death. Young female mice were immunized against ovalbumin (OVA) as 'non-sense' immunization control and against a previously described cocktail of four GluN1-specific peptides, which induces functional NMDAR1-AB within ten days after immunization (Pan et al. 2018). After NMDAR1-AB formation and prior to encephalitis induction, no behavioral abnormalities were observed in the LABORAS-based experimenter-independent tracking of home cage behavior. In DTA mice, tamoxifen administration resulted in an acute neuroinflammatory response within one week, which was particularly prominent in the hippocampus. Systematic behavioral phenotyping after encephalitis induction revealed normal exploratory and stereotypic behavior in several behavioral tests, lack of catalepsy in the bar test, normal executive function in the hurdle test and normal performance in IntelliCage based cognitive challenges. However, DTA mice in contrast to littermate controls lacking the DTA allele displayed typical hippocampal learning and memory deficits in the Morris water maze, prefrontal cortical network dysfunction as well as hyperlocomotion in three homecage based test settings. Compared to ovalbumin-immunized DTA mice, DTA mice carrying NMDAR1-AB displayed increased hyperlocomotion, reminiscent of mice treated with the NMDAR antagonist MK-801. Furthermore, DTA mice developed long-lasting blood-brain barrier dysfunction, gray matter inflammation and neurodegeneration, particularly in the hippocampus. Importantly, the neuroinflammation was not further aggravated by the presence of NMDAR1-AB and immunized non-DTA mice were free of any signs of neuroinflammation. In addition, the replication of a previously published immunization protocol, claiming encephalitis induction upon immunization against a GluN1$_{359-378}$ peptide (Wagnon et al. 2020), failed completely. Immunized mice, although carrying IgG autoantibodies against the GluN1$_{359-378}$ peptide, did not develop neuroinflammation. To conclude, while the encephalitogenic potential of NMDAR1-AB remains to be proven, NMDAR1-AB can modulate the behavioral phenotype of an underlying gray matter inflammation (Wilke et al. 2021a).

## 4.2 Original Publication

**Wilke JBH**, Hindermann M, Berghoff SA, Zihsler S, Arinrad S, Ronnenberg A, Barnkothe N, Steixner-Kumar AA, Röglin S, Stöcker W, Hollmann M, Nave KA, Lühder F and Ehrenreich H (2021). "Autoantibodies against NMDA receptor 1 modify rather than cause encephalitis." Mol Psychiatry 26(12): 7746-7759.

## Personal Contribution

I substantially contributed (data acquisition, analysis, and interpretation) to all experiments involving treatments, behavioral phenotyping, ELISA, cell-based assays, histology, and flow cytometry. Furthermore, I significantly contributed to drafting the manuscript and display items.

# ARTICLE     OPEN

Check for updates

# Autoantibodies against NMDA receptor 1 modify rather than cause encephalitis

Justus B. H. Wilke [ORCID][1], Martin Hindermann[1], Stefan A. Berghoff[2], Svenja Zihsler[1], Sahab Arinrad[1], Anja Ronnenberg[1], Nadine Barnkothe[1], Agnes A. Steixner-Kumar [ORCID][1], Stefan Röglin[1], Winfried Stöcker[3], Michael Hollmann[4], Klaus-Armin Nave [ORCID][2], Fred Lühder[5] and Hannelore Ehrenreich [ORCID][1 ✉]

The etiology and pathogenesis of "anti-N-methyl-D-aspartate-receptor (NMDAR) encephalitis" and the role of autoantibodies (AB) in this condition are still obscure. While NMDAR1-AB exert NMDAR-antagonistic properties by receptor internalization, no firm evidence exists to date that NMDAR1-AB by themselves induce brain inflammation/encephalitis. NMDAR1-AB of all immunoglobulin classes are highly frequent across mammals with multiple possible inducers and boosters. We hypothesized that "NMDAR encephalitis" results from any primary brain inflammation coinciding with the presence of NMDAR1-AB, which may shape the encephalitis phenotype. Thus, we tested whether following immunization with a "cocktail" of 4 NMDAR1 peptides, induction of a spatially and temporally defined sterile encephalitis by *diphtheria* toxin-mediated ablation of pyramidal neurons ("DTA" mice) would modify/ aggravate the ensuing phenotype. In addition, we tried to replicate a recent report claiming that immunizing just against the NMDAR1-N368/G369 region induced brain inflammation. Mice after DTA induction revealed a syndrome comprising hyperactivity, hippocampal learning/memory deficits, prefrontal cortical network dysfunction, lasting blood brain-barrier impairment, brain inflammation, mainly in hippocampal and cortical regions with pyramidal neuronal death, microgliosis, astrogliosis, modest immune cell infiltration, regional atrophy, and relative increases in parvalbumin-positive interneurons. The presence of NMDAR1-AB enhanced the hyperactivity (psychosis-like) phenotype, whereas all other readouts were identical to control-immunized DTA mice. Non-DTA mice with or without NMDAR1-AB were free of any encephalitic signs. Replication of the reported NMDAR1-N368/G369-immunizing protocol in two large independent cohorts of wild-type mice completely failed. To conclude, while NMDAR1-AB can contribute to the behavioral phenotype of an underlying encephalitis, induction of an encephalitis by NMDAR1-AB themselves remains to be proven.

*Molecular Psychiatry*; https://doi.org/10.1038/s41380-021-01238-3

## INTRODUCTION

Since, the first report on a novel paraneoplastic autoimmune disease with autoantibodies against the NMDA receptor subunit NR1 (NMDAR1-AB = GluN1-AB) appeared >12 years ago [1, 2], this condition attracted considerable attention both by clinicians and basic researchers worldwide, resulting in currently nearly 2000 entries in PubMed. Variably associated with psychosis, cognitive decline, extrapyramidal symptoms, or seizures, this "NMDAR encephalitis" was already early on described to be mediated by lower surface expression of neuronal NMDAR after exposure to NMDAR1-AB of the immunoglobulin G (IgG) class [3]. The resulting NMDAR antagonistic or "ketamine-like" effects, demonstrated also in various rodent models via passive transfer of NMDAR1-AB [4–13], were interpreted as potential mechanisms of action. Thus far, however, they have failed to explain the inflammatory or encephalitic component of this condition. Interestingly, comparison of NMDAR1-AB-positive and -negative human encephalitis cases did not reveal differences, except for few perhaps NMDAR-antagonistic (ketamine-like) symptoms [14].

Even sophisticated preclinical approaches raised further questions rather than providing answers. For example, immunization of

mice with liposome-embedded tetrameric NMDAR was stated to induce NMDAR-AB and fulminant encephalitis. Highly variable behavioral changes in this model included hyperactivity, immobility, circling, seizures, hunched back/lethargy, and increased mortality, including neuroinflammation, and immune cell infiltration [15], all nonspecific features of any severe encephalitis. Adequate "negative" controls like the use of other liposome-embedded holoreceptors or of control proteins of similar size would have been required to link NMDAR-AB causally with the occurrence of an encephalitis. To validate that "disease induction depends on conformationally restricted epitopes" [15], infusion of purified NMDAR-AB should have been used to clarify whether they act encephalitogenic on their own [16].

During performance of the present work, a report claimed that immunizing mice against the NMDAR1-N368/G369 region alone at high dose induced encephalitis-like behavioral and morphological impairments, including blood brain-barrier (BBB) breakdown [17]. We thus decided to follow this initially exciting report's protocol, hoping to answer several important questions related to our own research. However, using two large independent cohorts of wild-

type mice, we were unable to reproduce any of the described findings. This replication failure is now also included in the present paper.

To summarize, despite all efforts, etiology and pathogenesis of the "NMDAR encephalitis" are still as uncertain as the role of NMDAR1-AB in this condition. We note that multiple brain-directed AB apart from NMDAR1-AB have been reported in serum of healthy humans and of various other mammalian species, likely belonging to the normal pre-existing "autoimmune repertoire." These AB do have potential functionality and also potential pathogenicity [18–22]. In fact, functional serum NMDAR1-AB of all immunoglobulin classes are a highly frequent finding across mammals, with multiple possible inducers or boosters identified thus far, ranging from genetic predisposition, various viral infections (e.g., influenza, herpes), oncological conditions, and brain lesions to chronic life stress [1, 6, 23–26]. However, no solid proof exists to date that NMDAR1-AB by themselves can induce an encephalitic process.

The present study addresses the hypothesis that "NMDAR encephalitis" may result from a primary brain inflammation coinciding with the presence of NMDAR1-AB, which ultimately shape the encephalitis phenotype. Therefore, a spatially and temporally defined" sterile encephalitis was induced in young female NexCreERT2xRosa26-eGFP-DTA (= "DTA") mice after immunization with a cocktail of 4 NMDAR1 peptides, also including a peptide covering the NMDAR1-N368/G369 region. Females were chosen to account for the ~4:1 female/male ratio observed in human "NMDAR encephalitis" [27]. As shown in vivo earlier, this cocktail induces functionally highly active NMDAR1-AB, leading to psychosis-like symptoms in mice with compromised BBB but no brain inflammation [28]. Here, we report that NMDAR1-AB can contribute to the behavioral abnormalities of an underlying gray-matter encephalitis, but that the multifaceted encephalitic phenotype itself, involving pyramidal neurons and their NMDAR, is nearly identical between NMDAR1-AB carriers and noncarriers.

## MATERIALS AND METHODS
### Mice
Mouse experiments (all C57BL/6 background) were approved by the Local Animal Care and Use Committee (LAVES, Niedersächsisches Landesamt für Verbraucherschutz und Lebensmittelsicherheit, Oldenburg, Germany) in accordance with the German animal protection law. Sample sizes were based on previous experience under consideration of the RRR-principle and technical limitations (i.e., maximum of 16 animals per IntelliCage). All experiments were performed by investigators unaware of group assignment (fully-blinded). Mice were separated by genotype and treatment to avoid inclusion effects [29] or aggressive behavior against potentially affected animals. Unless otherwise stated, mice were maintained in temperature- and humidity-controlled environments in 12 h light/dark cycle (light on at 7am) with wood-chip bedding, nesting material (Sizzle Nest, Datesand, Bredbury, UK) and, ad libitum food and water.

**DTA cohort:** Mice with the tamoxifen-inducible gray-matter inflammation were generated by crossing homozygous Neurod6[tm2.1(cre/ERT2)Kan] (NexCreERT2) [30] with heterozygous Gt(ROSA)26Sor[tm1(DTA)Jpmb] (Rosa26-eGFP-DTA) [31], resulting in double-heterozygous (DTA) mice and heterozygous NexCreERT2 littermate (control) mice lacking the DTA allele. Detailed genotyping protocols are available upon request. Experiments involving DTA mice were performed on females to account for the ~4:1 female/male ratio observed in human "NMDAR encephalitis" patients [27]. Female transgenic mice were weaned at postnatal day 21 into type IV cages (55 × 38.5 × 20.5 cm, Tecniplast, Hohenpeißenberg, Germany) in groups of 16.

**Replication cohorts** comprised male C57BL/6 J wildtype mice immunized at 8–9 weeks of age [17]. Wildtype mice were obtained from Janvier (Le Genest-Saint-Isle, France), transported to our behavior unit at 3 weeks of age, and housed in type II cages (36.5 × 20.7 × 14 cm, Tecniplast) in groups of 3–5.

### Treatments
**Immunization of the DTA cohort** was conducted as previously described [28], except that immunizations were performed on postnatal day 30. Mice were immunized with a cocktail of 4 GluN1 extracellular peptides (GluN1$_{35-53}$, GluN1$_{361-376}$, GluN1$_{385-399}$, and GluN1$_{660-811}$ coupled to keyhole limpet hemocyanin; Synaptic Systems, Göttingen, Germany) and/or chicken ovalbumin ("OVA", A5503, Sigma-Aldrich, Darmstadt, Germany) emulsified in an equal volume of complete Freund's adjuvant (CFA) containing 1 mg/mL heat-killed Mycobacterium tuberculosis H37 Ra (#231141, Difco, BD, Heidelberg, Germany) in incomplete Freund's adjuvant. GluN1 peptide cocktail (50 µg) and/or ovalbumin (20 µg) were injected subcutaneously at the tail base.

**Immunization of the replication cohorts** followed the protocol of Wagnon et al. [17]. Male C57B/6 J mice were immunized at 8–9 weeks of age with either GluN1$_{168-187}$ (control peptide), GluN1$_{359-378}$ (active peptide) or for our additional comparison with ovalbumin, each emulsified in an equal volume of CFA (as described above). Antigens (200 µg) were equally distributed over 4 subcutaneous injections, 2 at shoulders and 2 at hind limbs. In addition, mice received 2 intraperitoneal injections of 200 ng of Bordetella pertussis toxin (#180, List Biological Laboratories) in PBS, immediately and 48 h after immunization.

**Tamoxifen induction:** Tamoxifen (CAS#10540-29-1, T5648, Sigma) was dissolved in corn oil (C8267, Sigma) on injection days at 10 mg/mL. Mice received 2 intraperitoneal injections of 100 mg of tamoxifen/kg body weight on 2 consecutive days.

**Transponder placement:** For the experimenter-independent phenotyping of mice in the IntelliCage® apparatus (TSE Systems, Bad Homburg, Germany) ISO standard transponders (8.5 mm length, 1.2 mm diameter, PM162-8) were implanted below the skin of the neck after intraperitoneal injection of 24 µL of 1.36% 2,2,2,-tribromoethanol (T48402, Sigma) in ddH$_2$O/g body weight (Avertin). One week after implantation, mice were placed into IntelliCages.

**Blood sampling:** Intermediate blood samples (100 µL) were collected from the retro-orbital sinus. Terminal blood (500 µL) was sampled by cardiac puncture before transcardial perfusion. EDTA-plasma aliquots were stored at −80 °C.

### Behavioral phenotyping
**Experiments of the DTA cohort** were performed in the following order: LABORAS (baseline–prior to tamoxifen induction), bar test, hurdle test, IntelliCage-based phenotyping including pheromone preference, LABORAS, Morris water maze, hole board, prepulse inhibition (PPI), marble-burying test, and complex wheel running.

**Behavioral testing of the replication cohort** followed the design of Wagnon et al. [17]. Behavioral analyses comprised open-field activity, Y-maze working memory, elevated plus maze (anxiety), and forced-swim test (depression-like behavior). For the second replication cohort, we rearranged the test schedule to assess anxiety-like behavior in behaviorally naive mice, followed by testing in open field and Y-maze.

Except for home cage-based tests, all tests ran during the light phase. Behavioral testing was performed as previously described in detail [17, 29, 32–38]. Only home cage-based tests are briefly summarized below.

### LABORAS
To characterize the spontaneous home cage behavior of mice prior to and after a tamoxifen-induced gray-matter inflammation, the LABORAS system (Metris B.V.) was employed [32–34, 37]. Briefly, mice habituated for 2 nights to the experimental room and single housing in clear polycarbonate cages (Makrolon type I, 22 cm × 16 cm × 14 cm, Tecniplast) with wood-chip bedding, food, and water ad libitum. After two nights, cages were placed on a sensor platform (Carbon Fiber Plate 1000 mm × 700 mm × 700 mm × 30 mm, Metris B.V., Hoofddorp, Netherland) and the resulting electrical signals recorded throughout the dark phase (12 h) and classified into behavioral categories, i.e., eating, drinking, scratching, circling, climbing, immobility, locomotion, and grooming.

### IntelliCage-based phenotyping
To assess a variety of cognitive measures with minimal experimenter intervention on a 24/7 basis in a social home cage-based setting, 16 mice per group were placed in standard laboratory rodent cages (55 × 38.5 × 20.5 cm, Tecniplast) equipped with the IntelliCage® apparatus (TSE-Systems) controlled by NewBehavior software (version 3.1.7), as we

described in great detail previously [29]. Water was accessible in four triangular conditioning chambers (15 × 15 × 21 cm), located in cage corners. The conditioning chambers were equipped with temperature sensors and RFID antennas to identify entering mice. If mice entered a correct corner during the allocated time window, doors blocking access to water or sucrose bottles (dependent on test setting) could be opened via nosepokes sensed by light barriers. Lickometers registered licks on bottles.

The experimental setup comprised measurement of place learning (day 1), reversal learning (day 2), sucrose preference (day 3), acquisition and recollection of a place time-reward/episodic-like memory (days 4 and 5), and behavioral extinction of operant responses (days 6 and 7). General activity and day/night pattern were assessed by recording number and timing of visits to operant chambers (corner visits). On days 1–2, each mouse had access to water at a single corner (4 mice/corner), during days 3–5 to a 2% sucrose solution on one corner and water at the opposite site (8 mice/corner). On days 6–7, mice had access to only water at previously rewarded corners. In-between test sessions, corners were re allocated. The efficiency of place and reversal learning was assessed for 24 h each by calculating the percentage of place errors (visits to blocked corner/total corner visits *100%). Sucrose preference means the percentage of licks at sucrose bottle/total licks within 24 h. To evaluate episodic-like memory, access to water and sucrose solution was restricted to the first 2 h after dark-phase onset. Within this 2 h period, preference to sucrose corner was calculated as percentage of visits to sucrose corner/total corner visits.

Two weeks after this IntelliCage testing, mice returned to IntelliCages to evaluate pheromone preference using two social boxes, supplemented with fresh wood-chip bedding, connected to the left and right side of the IntelliCage via two plastic tubes, equipped with two ring RFID antennas to track individual mouse. The time each mouse spent in the IntelliCage, the neutral or the target social box was recorded along with the number of social box visits. After habituation of 1 h, social boxes were replaced by novel cages filled with either fresh wood-chip bedding (neutral site) or bedding from male C3H mice (target site) and mice again had 1 h to explore the social boxes. In addition to time spent on the target site, the time spent exploring either social box was evaluated as the readout for exploratory behavior.

## Complex wheel running

To assess locomotor activity and motor-cognitive learning, a complex running-wheel-setup (CRW) was used. Mice were single-housed in type-III cages (42 × 26 × 18 cm, Tecniplast), equipped with CRW (TSE-Systems). CRW are characterized by randomized omitted bars [39–41]. Mice were habituated to the experimental room and CRW for 2 h prior to the dark phase. After dark-phase onset, voluntary running was automatically tracked for 4 h via Phenomaster software (TSE-Systems) and the total running distance per mouse calculated.

## Antibody determinations

**ELISA:** Immunizations were confirmed by antigen ELISA, at 21–27 days after immunization in the DTA cohort and at 17–18 days in replication cohorts. ELISA was performed as described [28]. ELISA plates (96-well F-bottom Immuno MediSorp, Nunc) were coated overnight at 4 °C with either 0.2 µg ovalbumin, 0.5 µg GluN1-antigen cocktail, 1 µg GluN1$_{168-187}$ or 1 µg GluN1$_{359-378}$ in 50 µL PBS per well. After blocking with 5% bovine serum albumin (BSA, #8076.3, Roth) in PBS, mouse plasma (1:1000 dilution with 5% BSA/PBS 50 µl/well) was added for 2 h at RT. Antigen-specific IgG antibodies were detected using HRP-coupled anti-mouse-IgG-specific antibodies (1:10,000, A9917, Sigma) and 3,3′,5,5′-tetramethylbenzidine substrate (#555214, BD OptEIA, BD). Absorbance at 450 nm was measured and corrected for values at 620 nm by microplate reader (Tecan-Trading AG, Männedorf, Switzerland). The threshold for a positive classification was set as three standard deviations above the mean of control samples.

**Cell-based assay (CBA) for NMDAR1-AB detection:** To determine NMDAR1-AB IgG titers against full-length GluN1, a commercially available cell-based assay comprising *Grin1*-transfected and control-transfected HEK293 cells (FB 112d-1010-51, EUROIMMUN, Lübeck, Germany) was used according to the manufacturer's instructions with minor modifications. The anti-human secondary antibody solution was replaced by Alexa Fluor 488-labeled anti-mouse IgG (1:1000, A21202, Thermo Fisher Scientific, Darmstadt, Germany) in 0.2% Tween20/PBS. Titers were determined starting at 1:100 dilutions with subsequent testing of positive samples at 1:1000 and 1:10,000 and independently evaluated by three investigators. For colocalization experiments, diluted plasma samples were spiked with a

non overlapping rabbit IgG anti-GluN1 antibody directed against the C-terminal domain (1:1000, G8913, Sigma) and an Alexa Fluor 647-labeled anti-rabbit IgG antibody (1:1000, A31573, Thermo) was added to the secondary antibody solution. Images were acquired on a confocal microscope (LSM880, Zeiss, Oberkochen, Germany).

## Measurements assessing blood–brain-barrier integrity

BBB integrity was evaluated as previously described [28, 42]. Briefly, mice received intravenous injections of Evans blue (50 µg/g body weight, E2129, Sigma) and sodium fluorescein (200 µg/g body weight, F6377, Sigma). After 4 h, mice were anesthetized and transcardially perfused. Brains were collected, frozen on dry ice, and lyophilized. Tracers were extracted from hemispheres with formamide and quantified in triplicates on a fluorescent microscope (Observer Z2, Zeiss). The concentrations of tracers were calculated using a standard curve and normalized to controls.
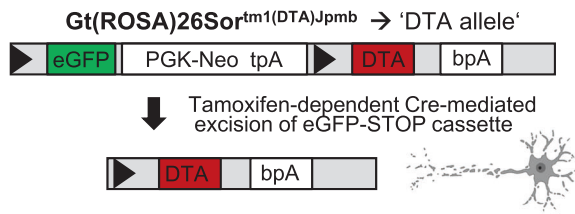
## Histology

Mice were anesthetized with Avertin, transcardially perfused with Ringer (B. Braun, Melsungen, Germany) and subsequently 4% formaldehyde/PBS solution. Brains were collected, post fixed in 4% formaldehyde/PBS for 12 h, dehydrated in 30% sucrose/PBS for 48 h, embedded in optimal cutting medium (Tissue-Tek, #4583, Sakura, Umkirch, Germany) and frozen on dry ice. Frozen brains were cut into 30 µm coronal sections on a cryostat (CM1950, Leica, Wetzlar, Germany), and stored at −20 °C in 25% ethylene glycol/25% glycerol/PBS. Quantifications were performed on regularly spaced sections (every 300 µm) between Bregma coordinates −1.34 to −2.24 mm and 4–6 hippocampi from 2 to 3 sections were used per mouse. CA2/CA3 region is referred to as CA3 in text and figures.

Free-floating frozen sections were blocked and permeabilized for 1 h at RT with 5% normal horse serum (NHS, 26050-088, Thermo) in 0.5% Triton X-100/PBS, incubated overnight at 4 °C with primary antibodies and subsequently stained with the corresponding fluorescently labeled secondary antibodies, for 2 h at RT. Nuclei were stained for 10 min at RT with 0.2 µg/mL 4′,6-diamidino-2-phenylindole in PBS (DAPI, D9542, Sigma) and sections mounted on SuperFrost®-Plus slides (J1800AMNZ, Thermo) with Aqua-Poly/Mount (#18606, Polysciences, Warrington, PA, USA). The following primary antibodies were used: Mouse anti-GFAP (1:500, NCL-GFAP-GA5, NovoCastra-Leica, Newcastle upon Tyne, UK), guinea pig anti-S100b (1:750, #287004, Synaptic Systems), rabbit anti-Iba1 (1:1000, #019-19,741, Wako, Neuss, Germany), rat anti-CD68 (1:500, MCA1957GA, BioRad, München, Germany), rat anti-CD45 (1:100, #103101, BioLegend, Koblenz, Germany), and guinea pig anti-parvalbumin (1:1000, #195004, Synaptic Systems). The corresponding secondary antibodies included Alexa Fluor 555 anti-rabbit (1:1000, A21428, Thermo), Alexa Fluor 555 anti-mouse (1:1000, A31570, Thermo), Alexa Fluor 647 anti-mouse (1:1000, A31571, Thermo), Alexa Fluor 633 anti-guinea pig (1:1000, A21105, Thermo), Alexa Fluor 647 anti-rat (1:1000, A21247, Thermo). For Fluorojade C-staining (AG325, Sigma) of dying neurons, sections were incubated in 0.06% potassium permanganate solution for 10 min. Following a 1 min water rinse, tissue was transferred for 10 min to a 0.0001% solution of Fluorojade C, dissolved in 0.1% acetic acid. Slides were rinsed with ddH2O and dried at 60 °C. Slides were mounted with Aqua-Poly/Mount (#18606, Polysciences). Overview images of whole-brain sections were obtained on Eclipse-TI 2 epifluorescence microscope (Nikon, Düsseldorf, Germany), equipped with 4× objective (4×/0.2 NA PLAN APO #MRD00045, Nikon). For quantification, 1 µm-thick optical sections of hippocampi were acquired as tile scans on a confocal laser scanning microscope (LSM 880, Zeiss), furnished with a 40× oil objective (40 × /1.4 NA Plan-APOCHROMAT, #420762-9900, Zeiss). Image-acquisition parameters were kept constant within experiments. Quantifications and image processing were performed with FIJI-ImageJ software [43]. Iba1+ cells (mostly microglia), parvalbumin+ cells (inhibitory neurons), and CD45+ Iba1− cells (leukocytes) were manually counted. GFAP+ area was quantified densitometrically upon uniform thresholding. Cell counts and GFAP + area were normalized to quantified areas. Data from 4 to 6 hippocampi/mouse was averaged.

## Flow cytometry

Mice were anesthetized with Avertin and transcardially perfused with 40 mL of Ringer solution (B. Braun). Brains were stored on ice in 10% fetal bovine serum (FBS, #10500-064, Thermo)/DMEM (#41965, Thermo). Olfactory bulbs and brain stems were removed and brains meshed

## A Schematic description of the construct

**Gt(ROSA)26Sor^tm1(DTA)Jpmb** → 'DTA allele'

▶ eGFP | PGK-Neo tpA | ▶ | DTA | bpA

Tamoxifen-dependent Cre-mediated
excision of eGFP-STOP cassette

▶ | DTA | bpA

## B Experimental validation of DTA model

NexCreERT2xRosa26-eGFP-DTA (='DTA')

Tamoxifen
(or corn oil control)
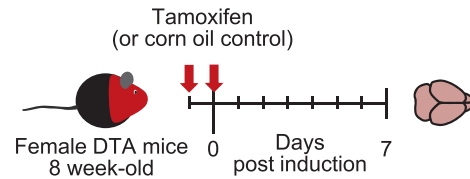
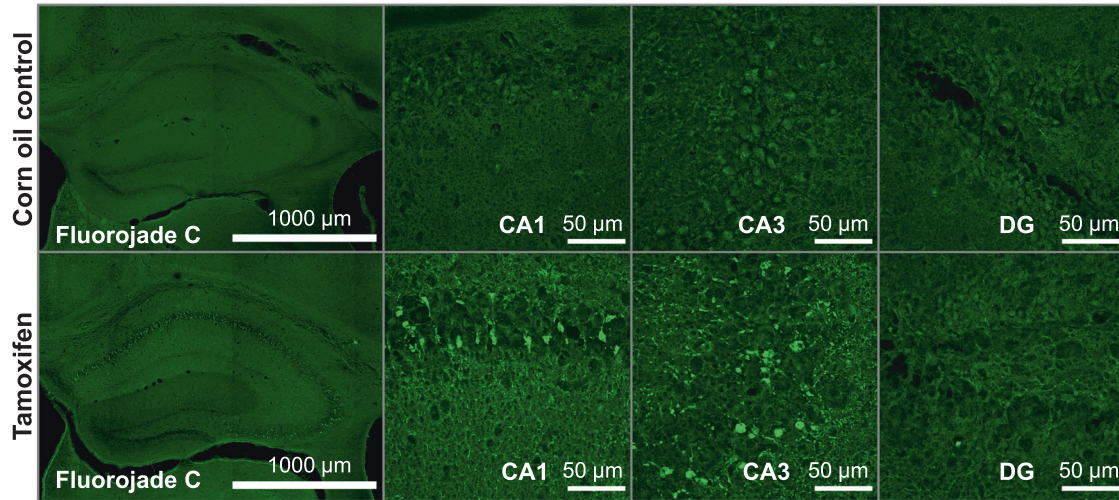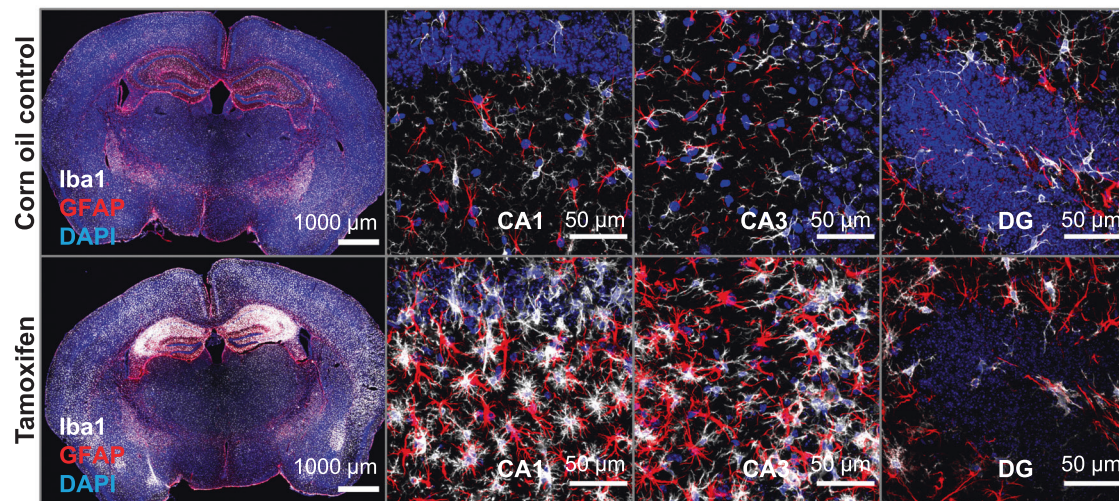Female DTA mice
8 week-old

Days
post induction
0        7

## C Fluorojade C staining demonstrating neurodegeneration in DTA mice



## D Acute inflammatory response after tamoxifen-induced neuronal death in DTA mice



**Fig. 1 Acute inflammatory response upon tamoxifen-induced Cre recombination in NexCreERT2xRosa26-eGFP-DTA (DTA) mice.**
**A** Schematic description of the Rosa26-eGFP-DTA allele. Upon tamoxifen-dependent Cre translocation, a loxP- (triangles) flanked eGFP-STOP cassette is excised, resulting in expression of *diphtheria* toxin chain A and ultimately cell death. **B** Experimental validation of the acute inflammatory response in DTA mice. Female DTA mice, 8-week old, received 2 intraperitoneal injections of either tamoxifen or solvent control (corn oil). **C, D** Brains were collected after 7 days and stained for neurodegeneration/cell death with Fluorojade C, as well as microglia (Iba1) and astrocytes (GFAP) as indicators of reactive gliosis. High-resolution images of CA1, CA3, and dentate gyrus (DG) regions were acquired as 10 µm Z-stacks and are displayed as maximum-intensity projections.

through 70 µm cell strainers. Cells were suspended in isotonic Percoll (17-0891-01, Sigma) to a final concentration of 30% and centrifuged to remove myelin. Cells were washed with FACS buffer (2% FBS, 10 mM EDTA in PBS) and filtered through 40 µm cell strainers. Fc receptors were blocked for 10 min at 4 °C with anti-mouse CD16/32 antibodies (1:100, 14-0161, Thermo). Cells were stained for 30 min at 4 °C with the following antibody mix: APC anti-CD45 (1:200, clone 104, BioLegend), PE anti-CD11b (1:200, clone M1/70, BioLegend), PECy5 anti-CD4 (1:1000, clone H129.19, BioLegend), PECy7 anti-CD8 (1:500, clone 53-6.7, Biolegend), APCCy7 anti-CD19 (1:200, clone 6D5, BioLegend), FITC anti-B220 (1:250, clone RA3-6B2, BioLegend), and PerCP-Cy5.5 anti-CD138 (1:200, clone 281-2, BioLegend). After staining, cells were washed and suspended in 400 µL of FACS buffer and 100 µL of APC quantification beads (#340487, BD). Samples were measured on a FACSAria Sorp (BD) and CytoFLEX S

**A** Experimental outline

Experimental groups:
CTRL-OVA
CTRL-GluN1
DTA-OVA
DTA-GluN1
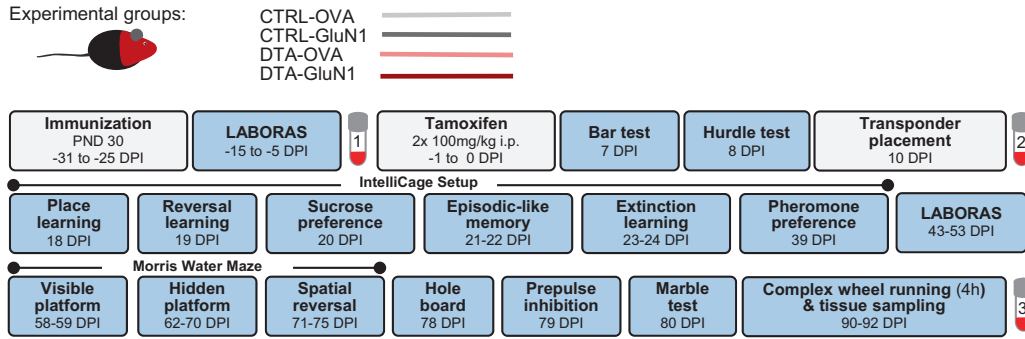
**B** GluN1 cocktail ELISA (Time point 1)
**C** GluN1 cell based assay
**D** Immunocytochemistry: GluN1 cell based assay
**E** LABORAS
**F** IntelliCage Activity
**G** Activity correlation
**H** Complex wheel running
**I** MWM visible – day 1
**J** MWM visible – day 2
**K** MWM visible platform – task learning
**L** MWM hidden platform
**M** MWM probe trial
**N** MWM reversal
**O** MWM reversal probe
**P** Prepulse Inhibition
**Q** IntelliCage Place learning (24h)
**R** IntelliCage Reversal learning (24h)
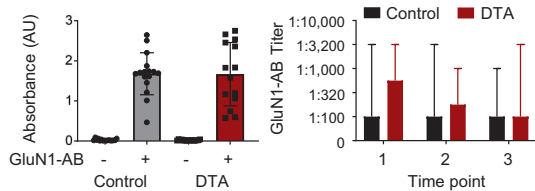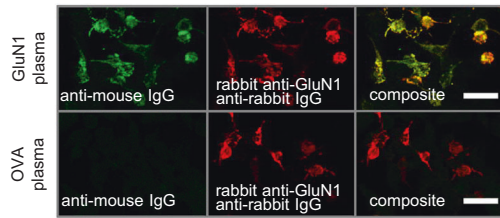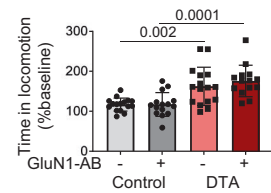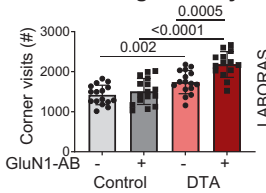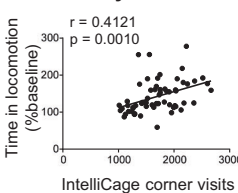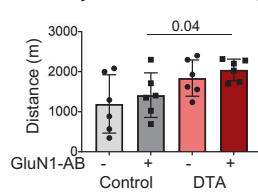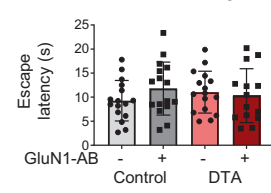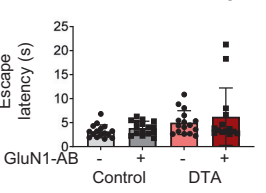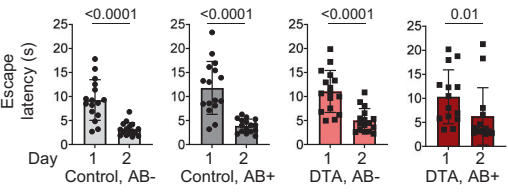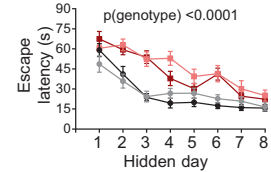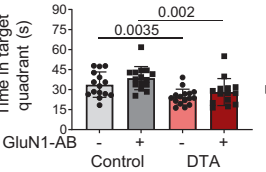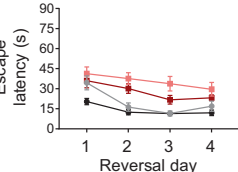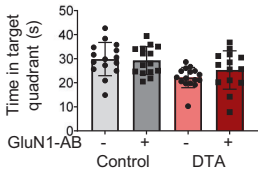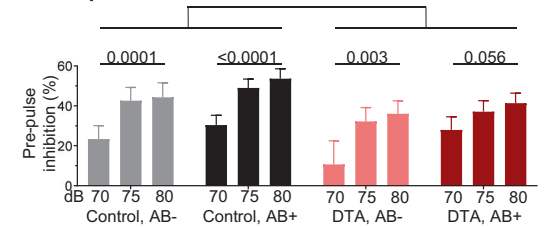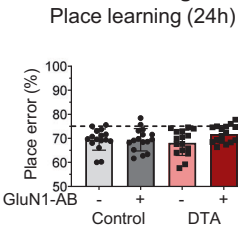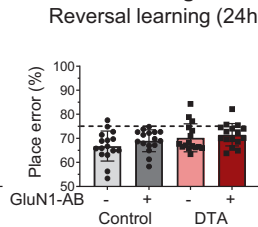
(Beckman Coulter, Krefeld, Germany). Cell numbers were corrected for the number of recorded APC beads. Leukocytes (CD45$^{high}$, CD11b$^{low}$) and microglia/macrophages (CD45$^{mid}$, CD11b$^{high}$) were quantified within single-cell gate determined by forward and side scatter. CD4$^+$ and CD8$^+$ T-cells were quantified within leukocyte gate. CD19$^+$ B cells and CD138$^+$ plasma cells were quantified in CD4$^-$ CD8$^-$ leukocyte gate.

## Statistical analysis

Statistical analyses were performed using Prism software (GraphPad Software) with the exception of the mixed ANOVA that was conducted on PPI data with R4.0.3 [44] using the rstatix package [45]. The results are presented as mean ± standard deviations (SD), with few exceptions as indicated in the figure legends. Data normality was assessed using the

6

**Fig. 2 Pathophysiological relevance of NMDAR1-AB (=GluN1-AB) in the context of gray-matter inflammation. A** Experimental outline indicating experimental groups, as well as order and time of behavioral tests (DPI = days post induction, i.e., after the last tamoxifen injection). **B** NMDAR1-AB validation by ELISA. **C** Cell-based (HEK293T) clinical standard assay for NMDAR1-AB (Euroimmun). **D** Immunocytochemical colocalization (CBA, Euroimmun) with a commercial rabbit GluN1-AB directed against the C-terminal domain. **E** Intra individual change of locomotor activity assessed in LABORAS at baseline and after tamoxifen induction. For each mouse, time in locomotion after tamoxifen induction was normalized to time in locomotion prior to tamoxifen application (baseline). **F** Activity (number of corner visits) over a 7-day IntelliCage session. **G** Pearson correlation between IntelliCage activity and intra individual changes of LABORAS locomotor activity. **H** Locomotor activity assessed by 4 h voluntary complex wheel running. **I–O** Cognitive testing in Morris water maze (MWM). **I–K** Visible platform task comprising 2 training days, demonstrating the ability for fast escape and simple task learning using within-maze cues. **L** Training of hidden platform task using extra-maze cues. DTA mice performed significantly worse than control mice (repeated-measures ANOVA, $p < 0.0001$), whereas no effect of NMDAR1-AB was observed in either DTA ($p = 0.3273$) or control mice ($p = 0.5972$). **M** Evaluation of spatial memory in the probe trial. **N** Spatial reversal of the hidden platform. **O** Evaluation of cognitive flexibility and reversal learning in a second probe trial after spatial reversal training. **P** Prepulse inhibition of acoustic startle. Intra group comparisons performed using repeated-measure one-way ANOVA; inter group comparison between genotypes for 75 and 80 dB prepulses performed using mixed ANOVA. **Q** IntelliCage-based evaluation of place learning and **R** reversal learning within 24 h sessions shows similar performance across groups. Dashed lines indicate performance at chance level (75%). Experiments were performed with 14–16 mice/group, except for CRW (**H**, $n = 6$ mice/group). Data presented as mean ± SD, except for repeated measure data (**L, N, P**; mean ± SEM) and AB titers (**C**, median, range).

◄

Shapiro–Wilk test with an alpha error of 0.05. Dependent on data distribution, two-tailed unpaired Welch's-corrected *t*-tests or Mann–Whitney *U*-tests were used to compare groups of 2. Similarly, repeated-measure ANOVA, one-way ANOVA or Kruskal-Wallis test were used to compare multiple groups. *P* values < 0.05 were considered statistically significant.

## RESULTS AND DISCUSSION
### *Diphtheria* toxin-mediated ablation of pyramidal neurons to mimic encephalitis affecting primarily gray matter
To mimic features of a viral encephalitis in a spatially and temporally defined sterile experimental approach, we employed young female NexCreERT2xRosa26-eGFP-DTA ( = "DTA") mice with an inducible transgene for *diphtheria* toxin-mediated ablation of pyramidal neurons, generating gray-matter inflammation [30, 31, 46]. Cell death can be controlled by dosing tamoxifen. Thus, in a series of dose-titrating pilot experiments, we selected a 2-day tamoxifen-injection design (Fig. 1A, B). After 7 days, we histologically confirmed acute neurodegeneration, pyramidal neuron loss, and a distinct inflammatory response comprising micro- and astrogliosis (Fig. 1C, D).

### Generation of primary brain inflammation coinciding with the controlled presence of NMDAR1-AB following immunization
We next addressed our hypothesis that "NMDAR encephalitis" may result from a primary brain inflammation concurring with the presence of NMDAR1-AB, which ultimately shape the encephalitis phenotype. Therefore, the above-described, defined sterile encephalitis was induced in young female DTA mice after active immunization with a cocktail of four peptides of extracellular NMDAR1/GluN1 domains, including a peptide covering the NMDAR1-N368/G369 region, versus ovalbumin as control immunization. This cocktail induces sufficient titers of highly functional NMDAR1-AB of the IgG class [28]. Active-immunization was performed at postnatal day 30, followed by an experimental scheme as detailed in Fig. 2A, comprising induction of encephalitis, extensive behavioral testing, blood sampling, and finally perfusion.

Immunization of mice against the 4 NMDAR1 peptides led to high circulating levels (even though somewhat variable between subjects) of specific AB, as shown by ELISA and cell-based assay, which persisted throughout the experiment, i.e., over 4 months. Titers did not differ between DTA mice and controls (Fig. 2B–D).

### Comparison of multidimensional behavioral readouts among DTA and control groups with or without NMDAR1-AB
Testing mice in a multifaceted battery should reveal behavioral domains affected by the induced gray-matter encephalitis and shaped by NMDAR1-AB (Fig. 2E–R; Table 1). Indeed, spontaneous home cage behavior, measured by LABORAS, and corner visits as activity readout in the IntelliCage setup, revealed considerable hyperactivity of the DTA mice, interpretable as psychosis-like behavior or "loss of inhibition" [47]. The hyperactivity measures substantially inter correlated and were more pronounced upon the presence of NMDAR1-AB (Fig. 2E–G). Additional evidence of pathological hyperactivity is presented in Table 1. In fact, this psychosis-like feature seemed to persevere, since also the final test performed before perfusion, complex wheel running, similarly indicated hyperactivity (Fig. 2H).

For hippocampal learning and memory, the classical Morris water maze (MWM) test was employed [48]. Whereas the visible platform days showed comparable ability of task learning among groups (Fig. 2I–K), substantial deficits arose regarding the hidden platform learning curves (Fig. 2L) and the probe trial results (Fig. 2M). Here, DTA mice, independent of the presence of NMDAR1-AB, demonstrated inferior performance consistent with hippocampal damage. This was also seen as a clear tendency in MWM reversal testing as hippocampus-dependent cognitive flexibility measure, again without an appreciable NMDAR1-AB effect (Fig. 2N–O).

Prepulse inhibition of the startle response (PPI) was employed as a surrogate marker for gating defects in the prefrontal cortex–known also as a highly relevant translational test in human patients with psychosis. PPI deficit is among the most reliable objective features of severe neuropsychiatric phenotypes, likely affecting the ability to adequately filter and interpret environmental stimuli [47, 49–52]. Indeed, DTA mice, again independent of NMDAR1-AB, showed an overall tendency of a PPI deficit, pointing to prefrontal cortical network dysfunction as a consequence of the induced pyramidal neuronal death (Fig. 2P).

To some surprise, our previously designed extensive cognitive, emotional, and social phenotyping of mice in an observer-independent setting, using IntelliCages [29], did not reveal any considerable differences, except for the above-delineated distinct hyperactivity. This is most likely explained by lower sensitivity or ceiling effects of this paradigm (requiring a higher level of damage to show impairment), and the just partial involvement of hippocampal functions that are apparently fully compensated (example of IntelliCage readouts in Fig. 2Q, R). Similarly, all other behavioral tests failed to show appreciable alterations. Few just marginally significant and sometimes rather counter intuitive results proved invalid upon multiple-testing correction (Table 1). In conclusion, behavioral testing uncovered the expected consequences of pyramidal neuronal degeneration, i.e., substantial hippocampal dysfunction (MWM), a strong tendency of gating deficits as prefrontal cortex measure (PPI), and lasting psychosis-like hyperactivity, with only the latter augmented by the presence of NMDAR1-AB.

**Table 1.** Detailed presentation of the results obtained with the behavioral test battery in the DTA immunization model.

| | Group 1 Control, OVA-AB | | Group 2 Control, GluN1-AB | | Comparison 1 vs. 2 | | Group 3 DTA, OVA-AB | | Group 4 DTA, GluN1-AB | | Comparison 3 vs. 4 | | Comparison 1 vs. 3 | | Comparison 2 vs. 4 | |
|---|---|---|---|---|---|---|---|---|---|---|---|---|---|---|---|---|
| | Mean ± SD | n | Mean ± SD | n | test | p value | Mean ± SD | n | Mean ± SD | n | test | p value | test | p value | test | p value |
| **Health status** | | | | | | | | | | | | | | | | |
| Body weight (g): pre tamoxifen | 19.1 ± 0.8 | 16 | 19.5 ± 1.0 | 16 | t | 0.3522 | 18.9 ± 0.9 | 16 | 19.0 ± 0.9 | 14 | t | 0.6899 | t | 0.3594 | t | 0.2221 |
| Body weight (g): 10d post tamoxifen | 21.4 ± 0.8 | 16 | 21.8 ± 0.7 | 16 | t | 0.1694 | 20.8 ± 0.8 | 16 | 21.2 ± 0.9 | 14 | t | 0.2066 | t | 0.0372 | t | 0.0489 |
| Body weight (g): 79d post tamoxifen | 23.6 ± 0.8 | 16 | 23.5 ± 0.8 | 16 | t | 0.6761 | 23.2 ± 1.0 | 16 | 23.2 ± 0.9 | 14 | t | 0.9760 | t | 0.1886 | t | 0.3524 |
| Food intake (g): pre tamoxifen | 10.9 ± 1.0 | 16 | 10.5 ± 1.3 | 16 | t | 0.3044 | 10.5 ± 1.0 | 16 | 10.8 ± 1.1 | 14 | t | 0.3649 | t | 0.2004 | t | 0.4688 |
| Food intake (g): post tamoxifen | 11.7 ± 1.1 | 16 | 12.5 ± 1.3 | 16 | t | 0.0659 | 12.1 ± 1.7 | 16 | 12.1 ± 1.4 | 14 | t | 0.9875 | t | 0.4654 | t | 0.3806 |
| Water intake (g): pre tamoxifen | 13.1 ± 2.3 | 16 | 12.8 ± 1.5 | 16 | U | 0.8744 | 12.3 ± 1.8 | 16 | 13.0 ± 1.7 | 14 | t | 0.2818 | U | 0.4962 | t | 0.7581 |
| Water intake (g): post tamoxifen | 12.1 ± 1.3 | 16 | 12.3 ± 1.3 | 16 | t | 0.6492 | 12.3 ± 1.6 | 16 | 11.7 ± 1.2 | 14 | t | 0.2722 | t | 0.7220 | t | 0.1966 |
| **Locomotor activity** | | | | | | | | | | | | | | | | |
| LABORAS (baseline): Time in locomotion (s) | 1798 ± 335 | 16 | 1804 ± 339 | 16 | t | 0.9598 | 1945 ± 392 | 16 | 1852 ± 712 | 14 | t | 0.6676 | t | 0.2613 | t | 0.8192 |
| LABORAS (post tam.): Time in locomotion (s) | 2092 ± 453 | 16 | 2096 ± 666 | 15 | t | 0.9836 | 3093 ± 872 | 16 | 3129 ± 909 | 14 | t | 0.9113 | t | **0.0005** | t | **0.0020** |
| Complex wheel running: Distance (m) | 1195 ± 729 | 6 | 1414 ± 556 | 6 | t | 0.5726 | 1841 ± 453 | 6 | 2045 ± 269 | 6 | t | 0.3691 | t | 0.1010 | t | 0.0400 |
| IC: Total corner visits (#) | 1420 ± 245 | 16 | 1506 ± 326 | 16 | t | 0.4071 | 1741 ± 288 | 16 | 2181 ± 321 | 14 | t | **0.0005** | t | **0.0020** | t | **<0.0001** |
| IC: Corner visits in dark phase (#) | 1076 ± 177 | 16 | 1136 ± 262 | 16 | t | 0.4547 | 1400 ± 270 | 16 | 1713 ± 264 | 14 | t | **0.0033** | t | **0.0005** | t | **<0.0001** |
| IC: Corner visits in light phase (#) | 344 ± 81 | 16 | 370 ± 81 | 16 | t | 0.3744 | 341 ± 85 | 16 | 468 ± 94 | 14 | t | **0.0006** | t | 0.9142 | t | **0.0052** |
| Dark vs. light phase | t-test | $p < 0.0001$ | t-test | $p < 0.0001$ | | | t-test | $p < 0.0001$ | t-test | $p < 0.0001$ | | | | | | |
| Number of circles (#) | 774 ± 248 | 16 | 772 ± 305 | 15 | t | 0.9813 | 874 ± 393 | 16 | 849 ± 283 | 14 | t | 0.6896 | U | 0.6689 | t | 0.4874 |
| **LABORAS phenotyping after tamoxifen-induction (activity)** | | | | | | | | | | | | | | | | |
| Time spent climbing (s) | 10274 ± 4243 | 16 | 10999 ± 6146 | 15 | t | 0.7075 | 9703 ± 3265 | 16 | 9336 ± 5312 | 14 | t | 0.8251 | t | 0.6726 | t | 0.4417 |
| Time spent rearing (s) | 1475 ± 373 | 16 | 1465 ± 322 | 15 | t | 0.9360 | 1668 ± 470 | 16 | 1532 ± 465 | 14 | t | 0.4352 | t | 0.2093 | t | 0.6570 |
| Time spent grooming (s) | 2907 ± 989 | 16 | 2768 ± 845 | 15 | t | 0.6780 | 2766 ± 820 | 16 | 2670 ± 1089 | 14 | t | 0.7899 | t | 0.6641 | t | 0.7887 |
| Time immobile (s) | 13124 ± 3843 | 16 | 12283 ± 6087 | 15 | t | 0.6522 | 11369 ± 3865 | 16 | 12320 ± 4191 | 14 | t | 0.5257 | t | 0.2075 | t | 0.9849 |
| **Exploration** | | | | | | | | | | | | | | | | |
| IC-Pheromone habituation: Time exploring (s) | 2531 ± 215 | 16 | 2518 ± 203 | 16 | t | 0.8636 | 2576 ± 186 | 16 | 2591 ± 236 | 14 | t | 0.8531 | t | 0.5272 | t | 0.3766 |
| Hole board: Visits (#) | 28.6 ± 9.1 | 16 | 29.8 ± 13.0 | 16 | t | 0.7553 | 25.6 ± 8.3 | 16 | 21.1 ± 9.3 | 14 | U | 0.1075 | t | 0.3393 | U | 0.0680 |
| **Marble test (stereotypy)** | | | | | | | | | | | | | | | | |
| Buried marbles (#) | 13.6 ± 4.4 | 16 | 13.6 ± 6.4 | 16 | t | >0.9999 | 12.1 ± 6.3 | 16 | 13.3 ± 7.8 | 14 | t | 0.6596 | t | 0.4401 | t | 0.8982 |
| **Bar test (catalepsy)** | | | | | | | | | | | | | | | | |
| Time immobile on bar (s) | 0.1 ± 0.1 | 16 | 0.1 ± 0.0 | 14 | U | 0.3139 | 0.1 ± 0.1 | 16 | 0.1 ± 0.1 | 13 | U | >0.9999 | U | 0.1579 | U | 0.0426 |
| **Hurdle test (executive function)** | | | | | | | | | | | | | | | | |
| Crossings (#) | 8.0 ± 2.9 | 16 | 8.8 ± 2.5 | 16 | U | 0.2352 | 8.9 ± 4.3 | 16 | 9.3 ± 3.2 | 14 | U | 0.4114 | U | 0.7702 | t | 0.6564 |
| Escape latency (s) | 35.3 ± 12.3 | 16 | 43.5 ± 23.0 | 16 | U | 0.5641 | 54.7 ± 33.4 | 16 | 44.3 ± 25.8 | 14 | U | 0.2751 | U | 0.0796 | U | 0.9510 |
| Ratio (Latency/(Crossings+1)) | 4.1 ± 1.4 | 16 | 4.5 ± 2.3 | 16 | U | 0.7240 | 6.3 ± 4.5 | 16 | 4.4 ± 2.7 | 14 | U | 0.1661 | U | 0.1188 | U | 0.6971 |
| **Startle** | | | | | | | | | | | | | | | | |
| Startle response at 120 db (AU) | 2.8 ± 2.0 | 16 | 2.3 ± 1.3 | 16 | U | 0.7450 | 2.0 ± 1.5 | 16 | 1.8 ± 0.8 | 14 | U | 0.5451 | U | 0.2203 | U | 0.3827 |

**Table 1** continued

| | Group 1 Control, OVA-AB Mean ± SD | n | Comparison 1 vs. 2 test | p value | Group 2 Control, GluN1-AB Mean ± SD | n | Group 3 DTA, OVA-AB Mean ± SD | n | Group 4 DTA, GluN1-AB Mean ± SD | n | Comparison 3 vs. 4 test | p value | Comparison 1 vs. 3 test | p value | Comparison 2 vs. 4 test | p value |
|---|---|---|---|---|---|---|---|---|---|---|---|---|---|---|---|---|
| **IC Pheromone preference** | | | | | | | | | | | | | | | | |
| Habituation: Time on target site (s) | 1111 ± 257 | 16 | t | 0.5116 | 1062 ± 141 | 16 | 1120 ± 190 | 16 | 1236 ± 227 | 14 | t | 0.1430 | t | 0.9121 | t | 0.0215 |
| Test phase: Time on target site (s) | 1548 ± 382 | 16 | t | 0.7674 | 1584 ± 288 | 16 | 1675 ± 211 | 16 | 1682 ± 375 | 14 | t | 0.9489 | t | 0.2581 | t | 0.4337 |
| Habituation vs. Test | t-test | **p < 0.0008** | | | t-test | **p < 0.0001** | t-test | **p < 0.0001** | t-test | **p < 0.00010** | | | | | | |
| **IC Sucrose preference (anhedonia)** | | | | | | | | | | | | | | | | |
| Preference to sucrose bottle (%) | 99.4 ± 0.7 | 16 | U | 0.3737 | 98.9 ± 1.1 | 16 | 99.8 ± 0.3 | 16 | 99.6 ± 0.6 | 14 | U | 0.5929 | U | **0.0112** | U | 0.0519 |
| **IC phenotyping (place & reversal learning)** | | | | | | | | | | | | | | | | |
| Place learning: Place error (%) | 69.5 ± 4.4 | 16 | t | 0.9623 | 69.4 ± 4.6 | 16 | 68.2 ± 5.3 | 16 | 71.8 ± 3.7 | 14 | t | 0.0345 | t | 0.4465 | t | 0.1241 |
| Reversal learning: Place error (%) | 66.8 ± 6.2 | 16 | t | 0.2599 | 69.0 ± 4.6 | 16 | 70.2 ± 5.8 | 16 | 71.7 ± 4.5 | 14 | U | 0.2572 | t | 0.1167 | t | 0.1204 |
| **IC phenotyping (What-Where-When memory): Preference to (former) sucrose corner (%)** | | | | | | | | | | | | | | | | |
| Acquisition | 27.0 ± 7.8 | 16 | t | 0.1605 | 30.5 ± 6.1 | 16 | 24.1 ± 10.2 | 16 | 30.1 ± 7.3 | 14 | t | 0.0728 | t | 0.3790 | t | 0.8637 |
| Retrieval | 37.8 ± 9.2 | 16 | t | 0.4805 | 40.2 ± 9.8 | 16 | 34.5 ± 13.9 | 16 | 43.0 ± 8.4 | 14 | t | 0.0505 | t | 0.4345 | t | 0.4092 |
| day1 vs day2 | t-test | **p < 0.0013** | | | t-test | **p < 0.0026** | t-test | **p < 0.0234** | t-test | **p < 0.0002** | | | | | | |

P values withstanding Bonferroni correction (α < 0.0125) are bolded.
IC intelliCage, t two-sided Welch's corrected t-test, U two-sided Mann–Whitney U-test.

## BBB integrity and measures of chronic inflammation in DTA and control groups with or without NMDAR1-AB

Using fluorescent tracers, as described in detail previously [28, 42], we addressed BBB leakiness in our DTA encephalitis model as a prerequisite for substantial NMDAR1-AB transfer to the brain and exertion of measurable effects. Tracer extravasation was enhanced for Evans blue and displayed a strong trend for fluorescein, confirming persistent BBB dysfunction. Brain water-content data showed remarkable scatters but were comparable in DTA and control mice at 3 months after encephalitis induction (Fig. 3A–D).

The chronic microglia and astrocyte response after tamoxifen-induced neuronal death in DTA mice was slightly milder as compared with the acute situation (see Fig. 1C, D), but still very obvious already from overview images (Fig. 3E, F). Histological quantification yielded distinct reductions of the areas of whole hippocampus, CA1 and CA3, whereas the dentate gyrus just revealed a similar tendency (Fig. 4A). Both Iba1 and GFAP quantifications followed the same pattern: strong microgliosis and astrogliosis in the whole hippocampus, CA1 and CA3, but only moderate in dentate gyrus of both DTA groups, with no significant differences in NMDAR1-AB carriers (Fig. 4B, C). NMDAR1-immunized control mice showed no signs of inflammation as reported previously [28]. Change of inhibition could be demonstrated by the relative increases in parvalbumin-positive interneurons upon DTA-induced encephalitis, sparing the dentate gyrus. Also regarding these interneurons, NMDAR1-AB presence did not modulate the ensuing picture (Fig. 4D, E). Hippocampal immune cell infiltration, determined by counting CD45 + cells, was modest but clear in DTA mice (Fig. 4F). Collectively, these data document persistent BBB disruption and distinct chronic inflammation in our DTA model but no obvious amplifying influence of NMDAR1-AB on any of these readouts. This additionally argues against any appreciable proinflammatory role of NMDAR1-AB of the IgG class.

## Failure to induce any signal of encephalitis by immunizing mice solely against the NMDAR1-N368/G369 region

During performance of the present work, a report claimed that immunizing mice against the NMDAR1-N368/G369 region alone induced an encephalopathy with remarkable B-cell response, provoking an autoimmune reaction against NMDAR, and encephalitis-like behavioral deficiencies [17]. We were first excited and wondered whether this model would finally help us to answer several burning questions of our own research, addressing for instance, the cellular–molecular mechanisms of NMDAR1-AB-mediated brain inflammation, which we had not been able to observe [28], or late consequences of an autoimmune encephalitis, or reasons for NMDAR1-AB titer fluctuations including the occurence and nature of late boosters [53]. Therefore, we started an extensive experiment, ultimately using two large independent cohorts of wild-type mice, and followed meticulously this report's protocol [17]. However, as detailed in Fig. 5 and Table 2, none of the described findings could be reproduced, although the adopted immunization protocol worked well. We found specific $GluN1_{359-378}$-AB of the IgG class in serum and no immune response using the non immunogenic control peptide $GluN1_{168-187}$ (Fig. 5A–D). There was no BBB disturbance (Fig. 5E), all behavioral tests were normal (Fig. 5F–I), histology did not show any abnormalities (Fig. 5J–L), and brain FACS results were physiological and did not reveal any differences between groups (Fig. 5M–R). Therefore, a second mouse cohort was employed to exclude potential by-chance failure of replication but, disappointingly, yielded the same overall negative results (data not shown).

Simultaneous with our anticlimactic replication failure, Ding et al. published a study, using a similar immunization strategy to investigate the pathogenicity of various GluN1 peptides (each also at a dose of 200 µg), including the $GluN1_{359-377}$. Yet, in contrast to the claims of Wagnon et al., the authors did not find $GluN1_{359-377}$-
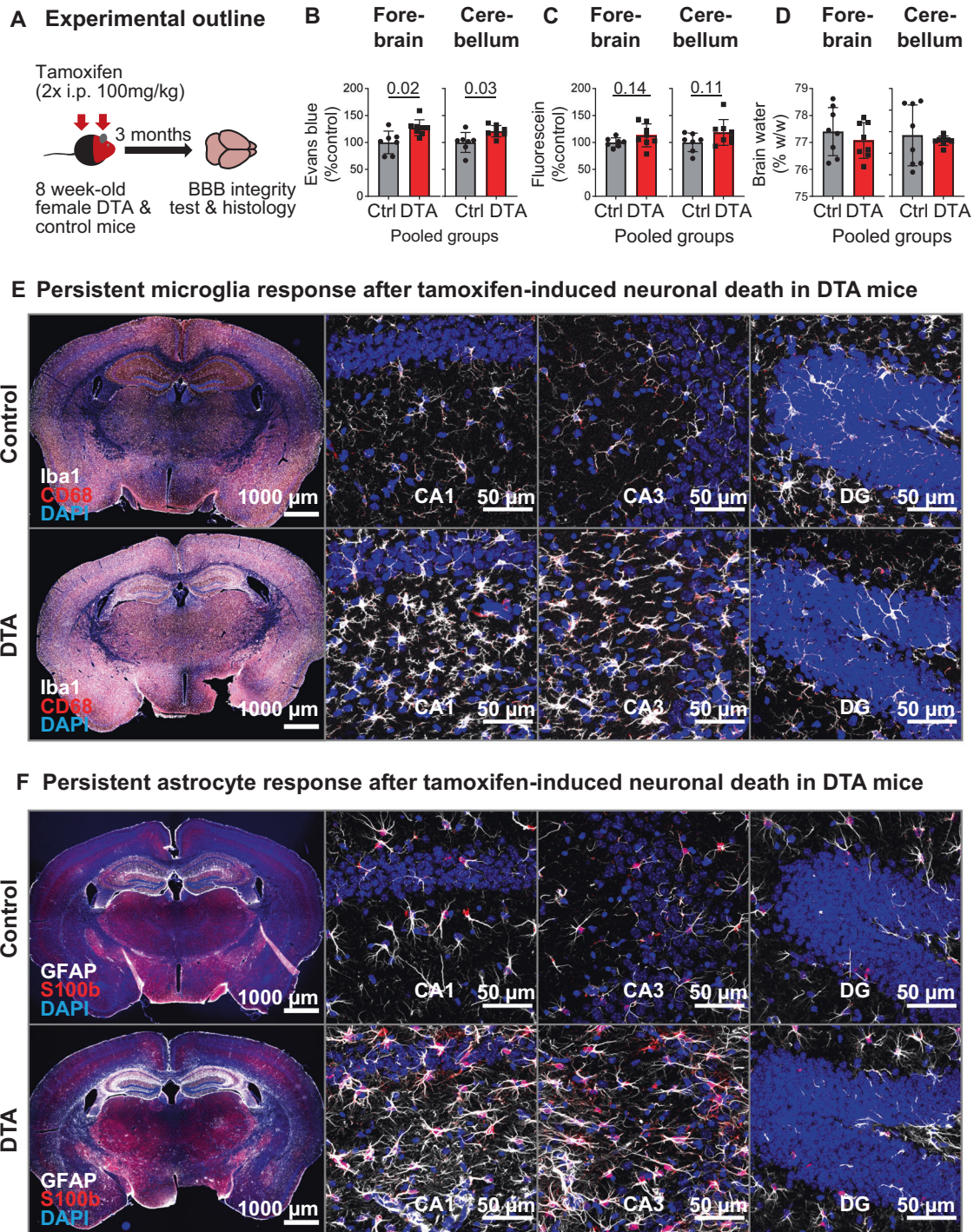
**Fig. 3 Long-lasting inflammatory response at 3 months after tamoxifen induction. A** Abbreviated experimental outline (detailed schematic in Fig. 2A). Blood–brain barrier (BBB) permeability, irrespective of NMDAR1-AB status, assessed by Evans blue (**B**) and fluorescein (**C**) extravasation, as well as brain-water content (**D**) in the forebrain and cerebellum of DTA and control mice. Data presented as mean ± SD. **E**, **F** Representative images demonstrating persistent inflammatory changes in the hippocampus of DTA mice, including increased microglia density and apparent changes in morphology (**E**, quantifications in Fig. 4B) and increased expression of glial fibrillary acidic protein, GFAP (**F**), quantified in Fig. 4C). High-resolution images of CA1, CA3, and dentate gyrus (DG) regions were acquired as 10 µm Z-stacks and displayed as maximum-intensity projections.

AB in the CSF of immunized mice [54]. In addition, these authors validated the functionality of GluN1$_{356-385}$-specific AB and assessed the in vivo consequences after triple immunization in combination with pertussis toxin, resulting in a behavioral phenotype (impaired social memory and novel object recognition, normal anxiety-, and depressive-like behavior), distinct from the one reported by Wagnon et al. (impaired spatial memory, abnormal anxiety-, and depressive-like behavior) [17, 54]. Unfortunately, Ding et al. did not investigate histopathological consequences of their immunization strategy, hence, it remains unclear whether they induced any features of an encephalitis. Another active immunization model, lately published as preprint, focused
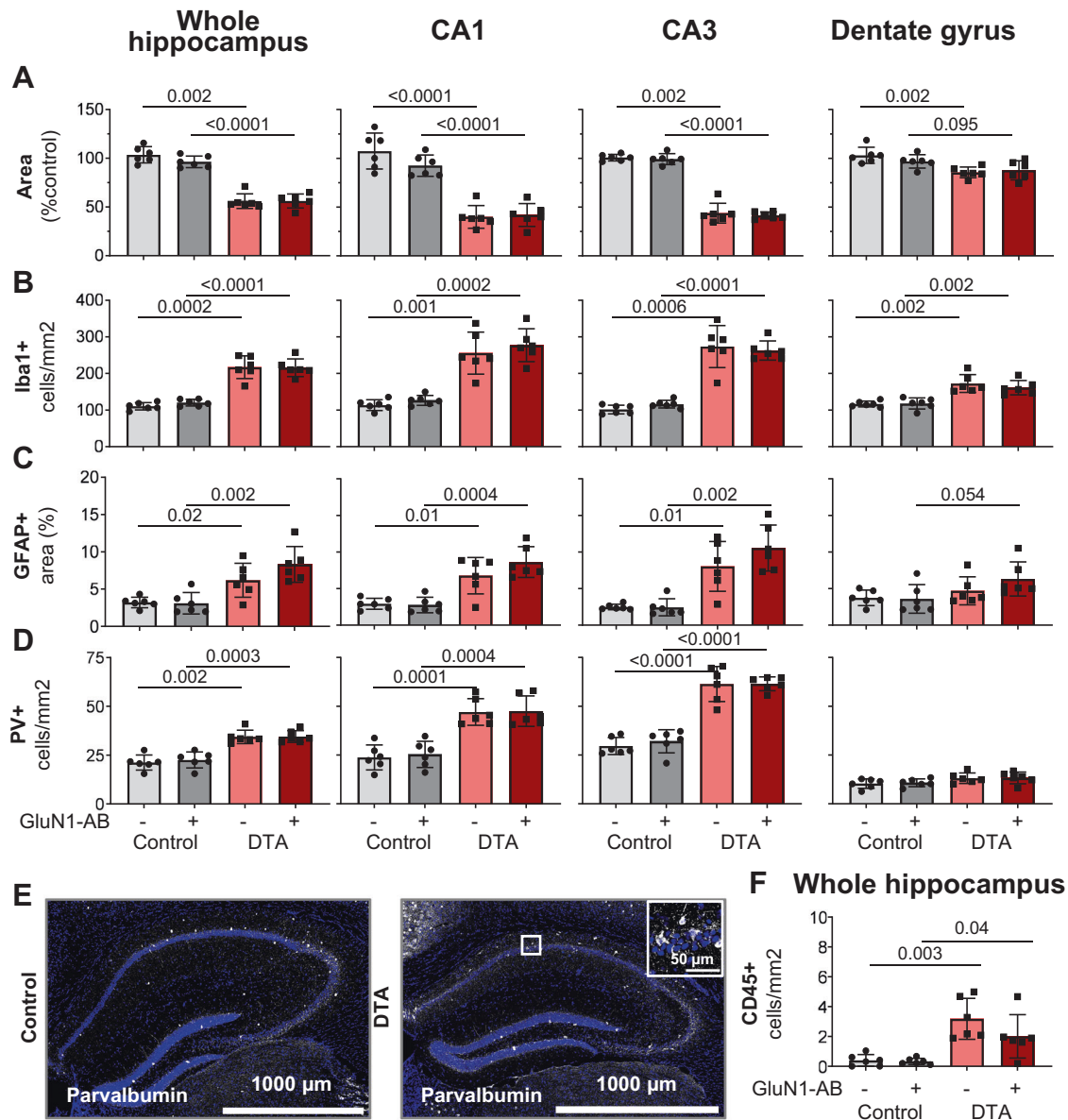
**Fig. 4 Histological quantification of typical encephalitis readouts in the hippocampus. A** For assessment of atrophy, the respective hippocampal areas were normalized to the mean of control mice. Normalized area shows the average of 6 sections per mouse (within Bregma −1.34 mm and −1.64 mm). **B** Number of Iba1+ cells (microglia). **C** GFAP+ area determined densitometrically upon uniform thresholding. **D** Density of parvalbumin (PV)-positive interneurons. **E** Representative images of parvalbumin stainings in control and DTA mice. **F** Leukocyte (CD45+ and Iba1− cells/mm²) infiltration into the hippocampal parenchyma. Data from 6 mice/group displayed as mean ± SD.

on the chronic effects of NMDAR1-AB upon immunization against GluN1$_{402-421}$ peptide. Similar to our experience with these immunizations, mice remained healthy and did not develop any encephalitic signs, despite the presence of persistent and functional NMDAR1-AB. The only behavioral alteration reliably observed in GluN1$_{402-421}$-immunized mice was impaired spatial memory and/or novelty recognition, assessed as spontaneous alternation in T-maze [55]. These findings are highly interesting since they underscore the possibility that chronic presence of circulating NMDAR1-AB can mildly modulate behavior, even in the absence of an appreciable BBB dysfunction. This is in line with a previous expert review [18] and our experimental observation that NMDAR1-AB can reach the brain to bind there at low titers even in healthy wild-type mice [26].

We are aware that—for comparison—in experimental auto-immune encephalitis (EAE), fluctuations can occur regarding the severity of the clinical/pathological picture [56–58]; however, the

absence of all claimed readouts as obtained in our replication approaches, is unheard of and quite surprising. This is more so, since the message of the report by Wagnon et al. will remain, if not questioned, and be taken for granted. This in turn can become an ethical issue, leading to (pre)clinical conclusions that are ultimately damaging for other scientists and unfortunately also for patients, as we observe on a regular basis.

**Conclusions from the NMDAR1-immunized DTA model: NMDAR1-AB modify rather than cause an encephalitis**
Using a well-standardizable, spatially and temporally defined mouse model of viral encephalitis by employing controlled DTA induction in pyramidal neurons, we find a multifaceted encephalitic phenotype, which persists over months. This phenotype involves pyramidal neurons and thus of course also their NMDAR, but is only marginally aggravated in NMDAR1-AB carriers versus non carriers. The aggravation essentially rests on hyperactivity as
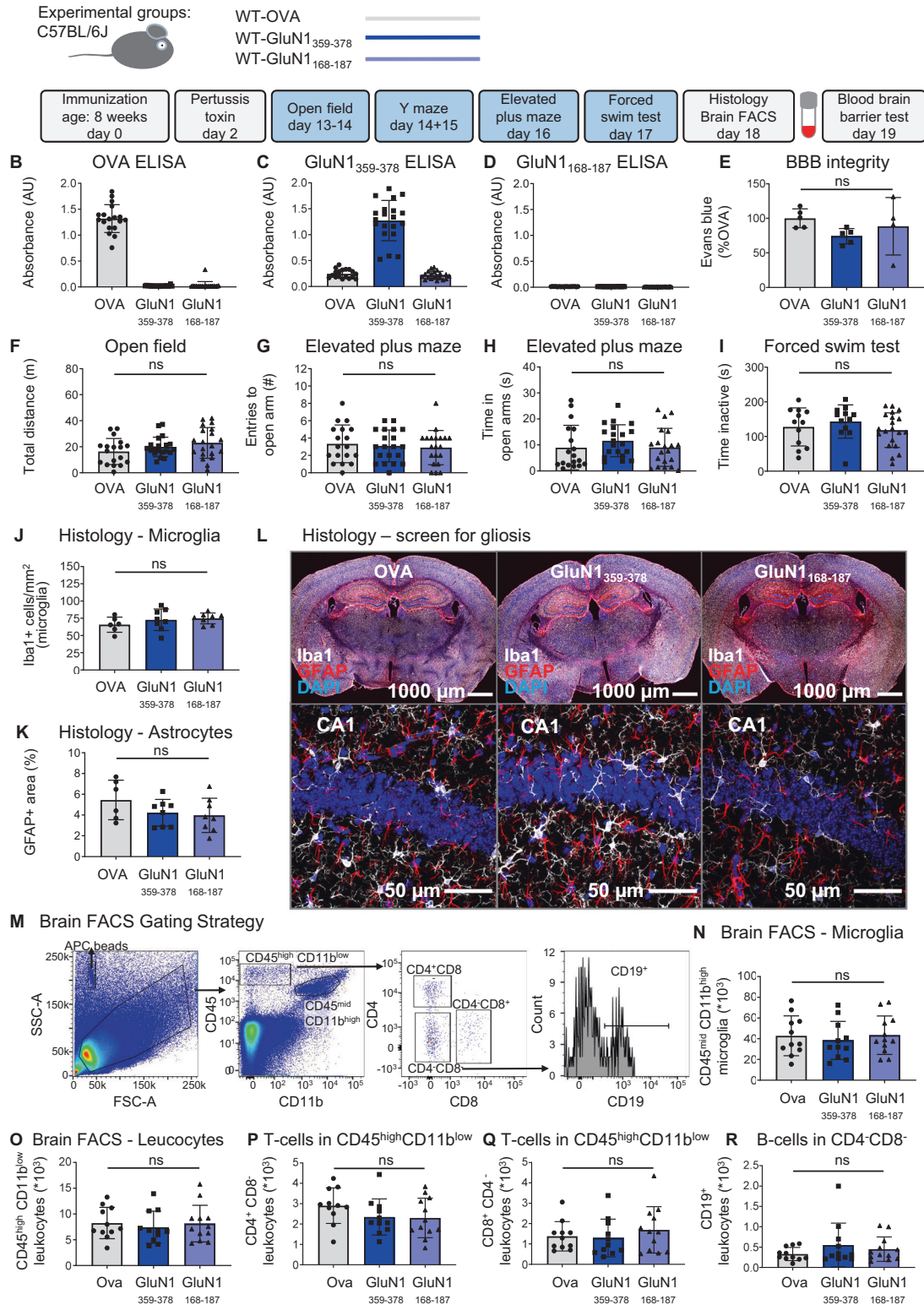
**Fig. 5 Summary of the results from the replication study. A** Experimental outline, following the protocol of Wagnon et al. [17]. **B–D** Experimental validation of immunization success using OVA-ELISA, GluN1$_{359-378}$-ELISA, and GluN1$_{168-187}$-ELISA. **E** Blood–brain-barrier (BBB) integrity assessed through Evans blue extravasation. **F–I** Results of behavioral phenotyping, showing locomotor activity in the open field, anxiety-related behavior in elevated plus maze, and depression-like behavior in the forced-swim test. **J–L** Histological quantification using 8 mice/immunization with focus on reactive gliosis, showing microglia numbers, GFAP+ area (densitometry), and representative images of quantified stainings. High-resolution images of CA1 were acquired as 10 µm Z-stacks and displayed as maximum-intensity projections. **M–R** Characterization of the brains' immune cell compartment by flow cytometry of 11–12 mice/group. **M** Gating strategy. Quantification of CD11b$^{high}$CD45$^{mid}$ cells (microglia). Quantification of CD11b$^{low}$CD45$^{high}$ leukocytes, CD4$^+$ T cells, CD8$^+$ T cells, and CD19$^+$ B cells. Data displayed as mean ±SD.

**Table 2.** Detailed presentation of behavior results obtained in replication study (protocol following Wagnon et al. [17]).

| | OVA | | GluN1$_{359-378}$ | | GluN1$_{168-187}$ | | ANOVA | |
|---|---|---|---|---|---|---|---|---|
| | Mean ± SD | n | Mean ± SD | n | Mean ± SD | n | test | p value |
| **Health status** | | | | | | | | |
| Pre immune: Body weight (g) | 24.2 ± 1.0 | 18 | 24.5 ± 0.9 | 20 | 24.6 ± 1.1 | 20 | 1way | 0.4515 |
| Post immune (+7d): Body weight (g) | 23.3 ± 1.2 | 18 | 23.0 ± 0.8 | 20 | 23.4 ± 1.0 | 20 | 1way | 0.3503 |
| **Depression-like behavior** | | | | | | | | |
| FST total time immobile (s) | 127.8 ± 54.9 | 12 | 143.4 ± 48.0 | 12 | 118.2 ± 49.8 | 20 | 1way | 0.4048 |
| **Locomotor activity** | | | | | | | | |
| Open field: Total distance (m) | 16.3 ± 10.0 | 18 | 19.8 ± 7.5 | 20 | 23.0 ± 11.8 | 20 | 1way | 0.1284 |
| **Activity** | | | | | | | | |
| Elevated plus maze: Total arm visits (#) | 11.4 ± 4.0 | 18 | 11.7 ± 4.7 | 20 | 10.5 ± 5.1 | 20 | KW | 0.8547 |
| Y maze (habituation): Total arm visits (#) | 10.0 ± 4.0 | 18 | 13.3 ± 5.8 | 19 | 13.9 ± 6.9 | 19 | 1way | 0.0956 |
| **Anxiety-related behavior** | | | | | | | | |
| Open field: Escape latency (s) | 56.1 ± 47.1 | 18 | 27.8 ± 16.0 | 20 | 40.3 ± 40.5 | 20 | KW | 0.1941 |
| Open field: Time in periphery (s) | 376.9 ± 31.9 | 18 | 383.2 ± 22.2 | 20 | 378.3 ± 23.8 | 20 | KW | 0.7324 |
| Open field: Time in intermediate zone (s) | 33.0 ± 26.7 | 18 | 27.7 ± 17.3 | 20 | 32.6 ± 18.7 | 20 | KW | 0.6139 |
| Open field: Time in center (s) | 9.5 ± 8.0 | 18 | 8.4 ± 9.1 | 20 | 8.3 ± 6.7 | 20 | KW | 0.6410 |
| Elevated plus maze: Visits to open arm (#) | 3.3 ± 2.2 | 18 | 3.1 ± 1.8 | 20 | 2.9 ± 2.0 | 20 | 1way | 0.7994 |
| Elevated plus maze: Time in open arm (s) | 9.0 ± 8.5 | 18 | 11.6 ± 6.1 | 20 | 9.1 ± 7.3 | 20 | KW | 0.2046 |
| **Y maze (habituation, 5 min)** | | | | | | | | |
| Y maze: Visits arm 1 (#) | 4.4 ± 2.4 | 18 | 6.4 ± 3.5 | 19 | 7.4 ± 4.5 | 19 | KW | 0.1004 |
| Y maze: Visits arm 2 (#) | 5.6 ± 2.5 | 18 | 6.9 ± 3.0 | 19 | 6.5 ± 2.9 | 19 | 1way | 0.3567 |
| arm1 vs. arm2 | U test | p = 0.1120 | t test | p = 0.5860 | t test | p = 0.4426 | | |
| **Y maze (test phase, 3 min)** | | | | | | | | |
| Y maze: Visits arm 1 (#) | 1.9 ± 1.6 | 18 | 2.5 ± 1.8 | 19 | 2.1 ± 2.1 | 19 | KW | 0.5813 |
| Y maze: Visits arm 2 (#) | 2.4 ± 2.6 | 18 | 2.6 ± 1.7 | 19 | 2.1 ± 1.2 | 19 | KW | 0.4752 |
| Y maze: Visits novel arm (#) | 2.8 ± 1.7 | 18 | 3.5 ± 2.2 | 19 | 3.3 ± 1.8 | 19 | KW | 0.5482 |
| 1way ANOVA | | p = 0.2367 | | p = 0.3093 | | **p = 0.0454** | | |
| novel vs. arm1 | U test | p = 0.1403 | U test | p = 0.1728 | U test | **p = 0.0364** | | |
| novel vs. arm2 | U test | p = 0.1479 | U test | p = 0.2151 | U test | **p = 0.0334** | | |

Significant p values (α < 0.05) in bold.
*FST* forced swim test, *1way* one-way ANOVA; *KW* Kruskal-Wallis test, *t* two-sided Welch's corrected *t*-test, *U* two-sided Mann–Whitney *U*-test.

psychosis-like behavioral readout but is not reflected in any histological quantification. Similarly, comparison of NMDAR1-AB-positive and -negative human encephalitis cases did not reveal appreciable differences, except for few NMDAR-antagonistic (ketamine-like) symptoms [14]. Most likely, human "NMDAR encephalitis" is simply not a separate condition, but rather marks an encephalitis where the highly prevalent NMDAR1-AB and/or the respective B cells happen to be present in the brain and shape the clinical picture. Therefore, it may be problematic, if the search for encephalitis causes stops after detection of NMDAR1-AB (of the IgG class). Reassuringly, "polypragmatic" treatment of any encephalitis of unknown origin (constituting the majority of cases) should anyhow include antibiotics, antivirals, and eventually corticosteroids/immunosuppressants on top of supporting measures.

The N-terminal domain containing the G7 epitope (N368/G369) was first deemed pathognomonic for "NMDAR encephalitis," and believed to be the target region of the pathological NMDAR1-AB of the IgG class seen responsible for this condition [59]. Therefore, the respective immunization model, leading to encephalitis as described by Wagnon and colleagues [17], seemed attractive at first view and worthwhile pursuing. Unfortunately, it was not reproducible in our hands, and is not supported by a similar recent paper [54]. Searching for an explanation by speculating about

possible reasons why Wagnon and colleagues found signs of an encephalitis that we did not see, interfering "iatrogenic" issues may be worthwhile considering, like e.g., undetected subclinical infections in their animal facility, leading to "occult" brain inflammation. Also, other factors, e.g., differences in the gut microbiota, which have the potential to modulate disease progression in EAE models [60], cannot be entirely excluded. However, it seems rather unlikely that the overall discrepancy, including BBB dysfunction, can be explained by such physiological factors.

Considering our own previous findings on epitopes recognized by the highly frequent NMDAR1-AB found in human serum, the negative outcome of the replication attempts is actually not too surprising. Epitope mapping using 7 different NMDAR1 constructs revealed recognition by NMDAR1-AB-positive sera of different epitopes, located in the extracellular ligand-binding and the N-terminal domain, as well as the intracellular C-terminal and the extended pore domain. NMDAR1-AB seropositivity was polyclonal/polyspecific in half of the investigated sera and likely mono- or oligoclonal/oligospecific (mainly IgG) in the other half. Overall, no particular disease-related pattern appeared. NMDAR1 epitopes were comparable across health and disease [61]. Also, the accentuated role of IgG in "NMDAR encephalitis" is still a matter of speculation, but likely related to inflammation-induced class

switch in the brain [62]. As mentioned in the Introduction, NMDAR1-AB are only one of many possible autoantibodies directed against brain epitopes [18–22]. The finally resulting phenotype would then depend on (i) the specific site(s) of brain inflammation, with either resident plasma cells producing AB or a local extent of BBB breach at that site (to allow sufficient AB transfer to the brain), and (ii) the specific circulating brain-reactive autoantibody profile of each individual.

To conclude, while NMDAR1-AB can contribute to the behavioral phenotype of an underlying encephalitis, there is no proof at present for induction of an encephalitis by NMDAR1-AB themselves. Thus, based on the results presented here, the answer to the question of whether or not NMDAR1-AB can, by themselves, induce encephalitis is probably no, with the caveat that perhaps it may be possible in extremely rare patients with an exceptionally high NMDAR1-AB titer. However, this would assume that a very high titer is somehow linked to brain inflammation (as cause or consequence) and/or local increases in BBB permeability, which is neither supported by the data from this nor from other studies.

## DATA AVAILABILITY
All data are available upon request.

## REFERENCES
1. Dalmau J, Gleichman AJ, Hughes EG, Rossi JE, Peng X, Lai M, et al. Anti-NMDA-receptor encephalitis: case series and analysis of the effects of antibodies. Lancet Neurol. 2008;7:1091–8.
2. Dalmau J, Tüzün E, Wu HY, Masjuan J, Rossi JE, Voloschin A, et al. Paraneoplastic anti-N-methyl-D-aspartate receptor encephalitis associated with ovarian teratoma. Ann Neurol. 2007;61:25–36.
3. Hughes EG, Peng X, Gleichman AJ, Lai M, Zhou L, Tsou R, et al. Cellular and synaptic mechanisms of anti-NMDA receptor encephalitis. J Neurosci. 2010;30:5866–75.
4. Manto M, Dalmau J, Didelot A, Rogemond V, Honnorat J. In vivo effects of antibodies from patients with anti-NMDA receptor encephalitis: further evidence of synaptic glutamatergic dysfunction. Orphanet J Rare Dis. 2010;5:1–12.
5. Mikasova L, De Rossi P, Bouchet D, Georges F, Rogemond V, Didelot A, et al. Disrupted surface cross-talk between NMDA and Ephrin-B2 receptors in anti-NMDA encephalitis. Brain 2012;135:1606–21.
6. Hammer C, Stepniak B, Schneider A, Papiol S, Tantra M, Begemann M, et al. Neuropsychiatric disease relevance of circulating anti-NMDA receptor autoantibodies depends on blood-brain barrier integrity. Mol Psychiatry. 2014;19:1143–9.
7. Wright S, Hashemi K, Stasiak L, Bartram J, Lang B, Vincent A, et al. Epileptogenic effects of NMDAR antibodies in a passive transfer mouse model. Brain 2015;138:3159–67.
8. Li Y, Tanaka K, Wang L, Ishigaki Y, Kato N. Induction of memory deficit in mice with chronic exposure to cerebrospinal fluid from patients with Anti-N-Methyl-D-Aspartate receptor encephalitis. Tohoku J Exp Med. 2015;237:329–38.
9. Würdemann T, Kersten M, Tokay T, Guli X, Kober M, Rohde M, et al. Stereotactic injection of cerebrospinal fluid from anti-NMDA receptor encephalitis into rat dentate gyrus impairs NMDA receptor function. Brain Res. 2016;1633:10–8.
10. Planagumà J, Leypoldt F, Mannara F, Gutiérrez-Cuesta J, Martín-García E, Aguilar E, et al. Human N-methyl D-aspartate receptor antibodies alter memory and behaviour in mice. Brain 2015;138:94–109.
11. Blome R, Bach W, Guli X, Porath K, Sellmann T, Bien CG, et al. Differentially altered NMDAR dependent and independent long-term potentiation in the CA3 subfield in a model of anti-NMDAR encephalitis. Front Synaptic Neurosci. 2018;10:1–13.
12. Kersten M, Rabbe T, Blome R, Porath K, Sellmann T, Bien CG, et al. Novel object recognition in rats with NMDAR dysfunction in CA1 after stereotactic injection of anti-NMDAR encephalitis cerebrospinal fluid. Front Neurol. 2019;10:1–11.
13. Taraschenko O, Fox HS, Pittock SJ, Zekeridou A, Gafurova M, Eldridge E, et al. A mouse model of seizures in anti-N-methyl-d-aspartate receptor encephalitis. Epilepsia. 2019;60:452–63.
14. Chen X, Li JM, Liu F, Wang Q, Zhou D, Lai X. Anti-N-methyl-D-aspartate receptor encephalitis: a common cause of encephalitis in the intensive care unit. Neurol Sci. 2016;37:1993–8.
15. Jones BE, Tovar KR, Goehring A, Jalali-Yazdi F, Okada NJ, Gouaux E, et al. Autoimmune receptor encephalitis in mice induced by active immunization

16. with conformationally stabilized holoreceptors. Sci Transl Med. 2019;11: eaaw0044.
16. Ehrenreich H, Pan H, Hollmann M. RE: Active immunization, autoimmunity and encephalitis: the missing links. Sci Transl Med. 2019. https://stm.sciencemag.org/content/11/500/eaaw0044/tab-e-letters.
17. Wagnon I, Hélie P, Bardou I, Regnauld C, Lesec L, Leprince J, et al. Autoimmune encephalitis mediated by B-cell response against N-methyl-d-aspartate receptor. Brain. 2020;143:2957–72.
18. Diamond B, Huerta PT, Mina-Osorio P, Kowal C, Volpe BT. Losing your nerves? Maybe it's the antibodies. Nat Rev Immunol. 2009;9:449–56.
19. Crisp SJ, Kullmann DM, Vincent A. Autoimmune synaptopathies. Nat Rev Neurosci. 2016;17:103–17.
20. Nagele EP, Han M, Acharya NK, DeMarshall C, Kosciuk MC, Nagele RG. Natural IgG autoantibodies are abundant and ubiquitous in human sera, and their number is influenced by age, gender, and disease. PLoS One. 2013;8:e60726.
21. Pollak TA, Lennox BR, Müller S, Benros ME, Prüss H, Tebartz van Elst L, et al. Autoimmune psychosis: an international consensus on an approach to the diagnosis and management of psychosis of suspected autoimmune origin. Lancet Psychiatry. 2020;7:93–108.
22. Cohen IR, Young DB. Autoimmunity, microbial immunity and the immunological homunculus. Immunol Today. 1991;12:105–10.
23. Prüss H, Finke C, Höltje M, Hofmann J, Klingbeil C, Probst C, et al. N-methyl-D-aspartate receptor antibodies in herpes simplex encephalitis. Ann Neurol. 2012;72:902–11.
24. Armangue T, Moris G, Cantarín-Extremera V, Conde CE, Rostasy K, Erro ME, et al. Autoimmune post-herpes simplex encephalitis of adults and teenagers. Neurology. 2015;85:1736–43.
25. Pan H, Steixner-Kumar AA, Seelbach A, Deutsch N, Ronnenberg A, Tapken D, et al. Multiple inducers and novel roles of autoantibodies against the obligatory NMDAR subunit NR1: a translational study from chronic life stress to brain injury. Mol Psychiatry. 2020. https://doi.org/10.1038/s41380-020-0672-1.
26. Castillo-Gomez E, Kästner A, Steiner J, Schneider A, Hettling B, Poggi G, et al. The brain as immunoprecipitator of serum autoantibodies against N-Methyl-D-aspartate receptor subunit NR1. Ann Neurol. 2016;79:144–51.
27. Dalmau J, Armangué T, Planagumà J, Radosevic M, Mannara F, Leypoldt F, et al. An update on anti-NMDA receptor encephalitis for neurologists and psychiatrists: mechanisms and models. Lancet Neurol. 2019;18:1045–57.
28. Pan H, Oliveira B, Saher G, Dere E, Tapken D, Mitjans M, et al. Uncoupling the widespread occurrence of anti-NMDAR1 autoantibodies from neuropsychiatric disease in a novel autoimmune model. Mol Psychiatry. 2019;24:1489–501.
29. Dere E, Ronnenberg A, Tampe B, Arinrad S, Schmidt M, Zeisberg E, et al. Cognitive, emotional and social phenotyping of mice in an observer-independent setting. Neurobiol Learn Mem. 2018;150:136–50.
30. Agarwal A, Dibaj P, Kassmann CM, Goebbels S, Nave KA, Schwab MH. In vivo imaging and noninvasive ablation of pyramidal neurons in adult NEX-CreERT2 mice. Cereb Cortex. 2012;22:1473–86.
31. Ivanova A, Signore M, Caro N, Greene ND, Copp AJ, Martinez-Barbera JP. In vivo genetic ablation by Cre-mediated expression of diphtheria toxin fragment A. Genes. 2005;43:129–35.
32. El-Kordi A, Winkler D, Hammerschmidt K, Kästner A, Krueger D, Ronnenberg A, et al. Development of an autism severity score for mice using Nlgn4 null mutants as a construct-valid model of heritable monogenic autism. Behav Brain Res. 2013;251:41–9.
33. Dere E, Dahm L, Lu D, Hammerschmidt K, Ju A, Tantra M, et al. Heterozygous ambra1 deficiency in mice: a genetic trait with autism-like behavior restricted to the female gender. Front Behav Neurosci. 2014;8:1–19.
34. Dere E, Winkler D, Ritter C, Ronnenberg A, Poggi G, Patzig J, et al. Gpm6b deficiency impairs sensorimotor gating and modulates the behavioral response to a 5-HT2A/C receptor agonist. Behav Brain Res. 2015;277:254–63.
35. Janova H, Arinrad S, Balmuth E, Mitjans M, Hertel J, Habes M, et al. Microglia ablation alleviates myelin-associated catatonic signs in mice. J Clin Invest. 2018;128:734–45.
36. Garcia-Agudo LF, Janova H, Sendler LE, Arinrad S, Steixner AA, Hassouna I, et al. Genetically induced brain inflammation by Cnp deletion transiently benefits from microglia depletion. FASEB J. 2019;33:8634–47.
37. Winkler D, Daher F, Wüstefeld L, Hammerschmidt K, Poggi G, Seelbach A, et al. Hypersocial behavior and biological redundancy in mice with reduced expression of PSD95 or PSD93. Behav Brain Res. 2018;352:35–45.
38. Netrakanti PR, Cooper BH, Dere E, Poggi G, Winkler D, Brose N, et al. Fast cerebellar reflex circuitry requires synaptic vesicle priming by munc13-3. Cerebellum. 2015;14:264–83.
39. Wakhloo D, Scharkowski F, Curto Y, Javed Butt U, Bansal V, Steixner-Kumar AA, et al. Functional hypoxia drives neuroplasticity and neurogenesis via brain erythropoietin. Nat Commun. 2020;11:1–12.

40. Liebetanz D, Baier PC, Paulus W, Meuer K, Bahr M, Weishaupt JH. A highly sensitive automated complex running wheel test to detect latent motor deficits in the mouse MPTP model of Parkinson's disease. Exp Neurol. 2007;205:207–13.

41. McKenzie IA, Ohayon D, Li H, de Faria JP, Emery B, Tohyama K, et al. Motor skill learning requires active central myelination. Science. 2014;346:318–22.

42. Berghoff SA, Duking T, Spieth L, Winchenbach J, Stumpf SK, Gerndt N, et al. Blood-brain barrier hyperpermeability precedes demyelination in the cuprizone model. Acta Neuropathol Commun. 2017;5:1–13.

43. Schindelin J, Arganda-Carreras I, Frise E, Kaynig V, Longair M, Pietzsch T, et al. Fiji: an open-source platform for biological-image analysis. Nat Methods. 2012;9:676–82.

44. R Development Core Team. R: A language and environment for statistical computing. Vienna, Austria: R Foundation for Statistical Computing; 2020.

45. Kassambara A. rstatix: pipe-friendly framework for basic statistical tests. 0.7.0 ed 2021.

46. Brockschnieder D, Lappe-Siefke C, Goebbels S, Boesl MR, Nave KA, Riethmacher D. Cell depletion due to diphtheria toxin fragment A after Cre-mediated recombination. Mol Cell Biol. 2004;24:7636–42.

47. Radyushkin K, El-Kordi A, Boretius S, Castaneda S, Ronnenberg A, Reim K, et al. Complexin2 null mutation requires a 'second hit' for induction of phenotypic changes relevant to schizophrenia. Genes Brain Behav. 2010;9:592–602.

48. Morris RGM. Spatial localization does not require the presence of local cues. Learn Motiv. 1981;12:239–60.

49. Braff D, Stone C, Callaway E, Geyer M, Glick I, Bali L. Prestimulus effects on human startle reflex in normals and schizophrenics. Psychophysiology. 1978;15:339–43.

50. Fendt M, Koch M. Translational value of startle modulations. Cell Tissue Res. 2013;354:287–95.

51. Kumari V, Das M, Zachariah E, Ettinger U, Sharma T. Reduced prepulse inhibition in unaffected siblings of schizophrenia patients. Psychophysiology. 2005;42: 588–94.

52. Poggi G, Boretius S, Möbius W, Moschny N, Baudewig J, Ruhwedel T, et al. Cortical network dysfunction caused by a subtle defect of myelination. Glia. 2016;64:2025–40.

53. Ehrenreich H, Wilke J, Steixner-Kumar AA. Spontaneous serum autoantibody fluctuations: To be or not to be. Mol Psychiatry. 2020. https://doi.org/10.1038/s41380-020-00883-4.

54. Ding Y, Zhou Z, Chen J, Peng Y, Wang H, Qiu W, et al. Anti-NMDAR encephalitis induced in mice by active immunization with a peptide from the amino-terminal domain of the GluN1 subunit. Journal of Neuroinflammation. 2021;18:1–10.

55. Yue W, Caldwell S, Risbrough V, Powell S, Zhou X. Chronic Presence of Blood Circulating Anti-NMDAR1 Autoantibodies Impairs Cognitive Function in Mice. bioRxiv. 2021. https://doi.org/10.1101/2021.04.22.440976.

56. Glatigny S, Bettelli E. Experimental autoimmune encephalomyelitis (EAE) as animal models of multiple sclerosis (MS). Cold Spring Harb Perspect Med. 2018;8:1–19.

57. Gold R, Linington C, Lassmann H. Understanding pathogenesis and therapy of multiple sclerosis via animal models: 70 years of merits and culprits in experimental autoimmune encephalomyelitis research. Brain 2006;129:1953–71.

58. Comabella M, Martin R. Genomics in multiple sclerosis—current state and future directions. J Neuroimmunol. 2007;187:1–8.

59. Gleichman AJ, Spruce LA, Dalmau J, Seeholzer SH, Lynch DR. Anti-NMDA receptor encephalitis antibody binding is dependent on amino acid identity of a small region within the GluN1 amino terminal domain. J Neurosci. 2012;32:11082–94.

60. Gandy KAO, Zhang J, Nagarkatti P, Nagarkatti M. The role of gut microbiota in shaping the relapse-remitting and chronic-progressive forms of multiple sclerosis in mouse models. Sci Rep. 2019;9:6923.

61. Castillo-Gómez E, Oliveira B, Tapken D, Bertrand S, Klein-Schmidt C, Pan H, et al. All naturally occurring autoantibodies against the NMDA receptor subunit NR1 have pathogenic potential irrespective of epitope and immunoglobulin class. Mol Psychiatry. 2017;22:1776–84.

62. Zhang J, Jacobi AM, Wang T, Berlin R, Volpe BT, Diamond B. Polyreactive autoantibodies in systemic lupus erythematosus have pathogenic potential. J Autoimmun. 2009;33:270–4.

## AUTHOR CONTRIBUTIONS
Concept, design, and supervision of the study: HE; data acquisition/analysis/interpretation: JBHW, MH, SAB, SZ, AR, SA, NB, AAS, SR, MH, WS, KAN, FL, and HE; drafting the paper: HE together with JBHW; Drafting display items: JBHW, SZ, together with HE; All authors read and approved the final version of the paper.

## FUNDING

## COMPETING INTERESTS
WS is a member of the board and holds stocks in Euroimmun AG. All other authors declare no competing financial or other interests.

## ADDITIONAL INFORMATION
**Correspondence** and requests for materials should be addressed to H.E.

**Reprints and permission information** is available at http://www.nature.com/reprints

**Publisher's note** Springer Nature remains neutral with regard to jurisdictional claims in published maps and institutional affiliations.

# 5 Project III: NMDAR1 autoantibodies amplify behavioral phenotypes of genetic white matter inflammation

## 5.1 Overview of Project III

Although NMDARE is predominantly associated with neuroinflammation in gray matter regions, inflammation of white matter and clinical evidence of demyelinating disorders have been repeatedly observed in a minority of NMDARE patients. As the association between NMDAR1-AB and white matter inflammation has been largely underinvestigated, a mouse model of progressive white matter encephalitis was used to investigate the impact of NMDAR1-AB on white matter pathology and behavioral features. Mice lacking the myelin protein 2′-3′-cyclic nucleotide 3′-phosphodiesterase (*Cnp* knockout; *Cnp*-KO) were immunized against a cocktail of GluN1-specific extracellular peptides ('NR1') or ovalbumin (OVA) and compared to NR1-immunized wildtype mice. Comparing NMDAR1-AB or OVA-AB carrying *Cnp*-KO and wildtype mice revealed distinct stair patterns of behavioral pathology in hippocampal learning and memory in the Morris-water maze as well as in tests of motor performance or motor coordination. In contrast, episodic-memory, analyzed in a what-where-when orientation task, was compromised in *Cnp*-KO mice but not affected by NMDAR1-AB. Similar to observations in gray matter inflammation, NMDAR1-AB had no add-on effect on microgliosis, astrogliosis, axonal degeneration or immune cell infiltration, which were prominent in the corpus callosum of *Cnp*-KO mice, and did not induce a 'spill-over' of inflammation into the hippocampus.

## 5.2 Original Publication

Arinrad S*, **Wilke JBH***, Seelbach A, Doeren J, Hindermann M, Butt UJ, Steixner-Kumar AA, Spieth L, Ronnenberg A, Pan H, Berghoff SA, Hollmann M, Lühder F, Nave KA, Bechter K and Ehrenreich H (2021). "NMDAR1 autoantibodies amplify behavioral phenotypes of genetic white matter inflammation: a mild encephalitis model with neuropsychiatric relevance." Mol Psychiatry: doi.org/10.1038/s41380-41021-01392-41388.

*shared first authorship

## Personal Contribution

I substantially contributed (data acquisition, analysis, and interpretation) to histology experiments as well as NMDAR1-AB assays, was involved in the data analysis and interpretation of flow cytometry data, and interpretation of behavioral experiments. Furthermore, I significantly contributed to drafting the manuscript and display items.

**ARTICLE**   OPEN

Check for updates

# NMDAR1 autoantibodies amplify behavioral phenotypes of genetic white matter inflammation: a mild encephalitis model with neuropsychiatric relevance

Sahab Arinrad[1,6], Justus B. H. Wilke [1,6], Anna Seelbach [1], José Doeren [1], Martin Hindermann[1], Umer Javed Butt [1], Agnes A. Steixner-Kumar [1], Lena Spieth[2], Anja Ronnenberg[1], Hong Pan[1], Stefan A. Berghoff[2], Michael Hollmann [3], Fred Lühder[4], Klaus-Armin Nave [2], Karl Bechter [5] and Hannelore Ehrenreich [1✉]

Encephalitis has an estimated prevalence of ≤0.01%. Even with extensive diagnostic work-up, an infectious etiology is identified or suspected in <50% of cases, suggesting a role for etiologically unclear, noninfectious processes. Mild encephalitis runs frequently unnoticed, despite slight neuroinflammation detectable postmortem in many neuropsychiatric illnesses. A widely unexplored field in humans, though clearly documented in rodents, is genetic brain inflammation, particularly that associated with myelin abnormalities, inducing primary white matter encephalitis. We hypothesized that "autoimmune encephalitides" may result from any brain inflammation concurring with the presence of brain antigen-directed autoantibodies, e.g., against N-methyl-D-aspartate-receptor NR1 (NMDAR1-AB), which are not causal of, but may considerably shape the encephalitis phenotype. We therefore immunized young female $Cnp^{-/-}$ mice lacking the structural myelin protein 2′-3′-cyclic nucleotide 3′-phosphodiesterase (Cnp) with a "cocktail" of NMDAR1 peptides. $Cnp^{-/-}$ mice exhibit early low-grade inflammation of white matter tracts and blood–brain barrier disruption. Our novel mental-time-travel test disclosed that $Cnp^{-/-}$ mice are compromised in what–where–when orientation, but this episodic memory readout was not further deteriorated by NMDAR1-AB. In contrast, comparing wild-type and $Cnp^{-/-}$ mice without/with NMDAR1-AB regarding hippocampal learning/memory and motor balance/coordination revealed distinct stair patterns of behavioral pathology. To elucidate a potential contribution of oligodendroglial NMDAR downregulation to NMDAR1-AB effects, we generated conditional NR1 knockout mice. These mice displayed normal Morris water maze and mental-time-travel, but beam balance performance was similar to immunized $Cnp^{-/-}$. Immunohistochemistry confirmed neuroinflammation/neurodegeneration in $Cnp^{-/-}$ mice, yet without add-on effect of NMDAR1-AB. To conclude, genetic brain inflammation may explain an encephalitic component underlying autoimmune conditions.

*Molecular Psychiatry*; https://doi.org/10.1038/s41380-021-01392-8

## INTRODUCTION

The discovery in 2007/2008 of autoantibodies directed against the NMDA receptor subunit NR1 (NMDAR1-AB = GluN1-AB) in the context of a paraneoplastic autoimmune disease, has stimulated extensive interest of clinicians and clinical researchers worldwide [1, 2]. As a consequence, diagnoses of autoimmune conditions underlying neuropsychiatric disorders of different severity and highly variable presentation began to boom [3–5]. Etiology and pathogenesis of "NMDAR encephalitis," however, are still as ambiguous as the role of NMDAR1-AB in this condition. In fact, NMDAR1-AB, reaching the brain from the circulation via a compromised blood–brain barrier (BBB), or being produced intrathecally, act as NMDAR antagonists, i.e., they produce ketamine-like phenotypical effects [6, 7]. This is mechanistically accomplished by internalization of the receptor, resulting (sub) acutely in lower surface expression of neuronal NMDAR upon

NMDAR1-AB binding [8–12]. Together with probably diverse local access to the brain [13], it matches well the broad spectrum and inconstant intensity of psychopathological and neurological symptoms, ranging from psychosis, cognitive decline and extra-pyramidal signs to motor dysfunction, autonomic dysregulation and epileptic seizures [1, 2]. At certainly lower amounts and dependent on the condition, NMDAR1-AB may also act as antidepressants [14] or in certain situations even behave like a double-edged sword, e.g., in ischemic stroke, where they can protect acutely from evolution of lesion size [15], but upon long-term exposure seem to contribute to poststroke dementia [16].

Notably, numerous brain-directed AB—apart from NMDAR1-AB —have been reported in serum of healthy humans and of various other mammalian species, likely constituting the preexisting physiological "autoimmune repertoire." These AB do have potential functionality and pathogenicity [3, 13, 17–19]. Regarding

[1]Clinical Neuroscience, Max Planck Institute of Experimental Medicine, Göttingen, Germany. [2]Department of Neurogenetics, Max Planck Institute of Experimental Medicine, Göttingen, Germany. [3]Department of Biochemistry I—Receptor Biochemistry, Ruhr University, Bochum, Germany. [4]Institute of Neuroimmunology and Multiple Sclerosis Research, University Medical Center, Göttingen, Germany. [5]Department of Psychiatry and Psychotherapy II, Ulm University, Günzburg, Germany. [6]These authors contributed equally: Sahab Arinrad, Justus B. H. Wilke. ✉email: ehrenreich@em.mpg.de

NMDAR1-AB, all immunoglobulin (Ig) classes are highly seroprevalent across mammals, with multiple possible inducers or boosters identified [2, 11, 14, 20–22]. But neither the "rules" of their induction nor the potentially different (patho)physiological significance of the various Ig classes has been elucidated yet, even though the class distribution of NMDAR1-AB is highly significantly predicted by the extracellular position of the antigen [23].

Importantly, a causal input of NMDAR1-AB themselves concerning encephalitis induction has not been convincingly demonstrated yet [24]. At least mild neuroinflammation [25, 26], if not obvious viral encephalitis caused by infections like herpes or influenza [11, 20–22], most likely prevail already during early stages of brain autoimmune disease. This might ultimately explain the encephalitic component of these conditions, and seamlessly supports Karl Bechter's mild encephalitis hypothesis of mental illness [25, 26]. Also the white matter damage described in "NMDAR encephalitis" patients with incomplete recovery blends into this view, highlighting the heterogeneity of underlying causes [27]. Overall, origins of encephalitides amount to 20–50% documented viral infections [28–30]. The remaining causes are to a large degree unknown, including the roots of mild encephalitis, running mostly undiagnosed. Of particular interest in this regard are genetic reasons of neuroinflammation, mainly those associated with myelin abnormalities leading to mild primary white matter encephalitis [31–33].

We note that already the normal aging process is associated with slightly increased brain inflammation, characterized by, e.g., enhanced levels of proinflammatory cytokines, higher microglial numbers and heightened reactivity [31, 34–36]. In major psychiatric disorders like schizophrenia and depression, low-grade inflammation constitutes a crucial mechanism in the final common disease pathway (reviewed in, e.g., [37, 38]), that has been linked to white matter abnormalities, as documented by postmortem studies. CNP (2′,3′-cyclic nucleotide 3′-phosphodiesterase) is among the oligodendrocyte/myelin-associated genes most robustly reduced on mRNA and protein level in these brains [39–41]. In fact, Cnp/CNP is a structural protein, present in noncompacted myelin and accounting for about 4% of total central nervous system myelin proteins [42]. Null mutant ($Cnp^{-/-}$) mice constitute a translationally interesting model of genetically induced, progressive brain inflammation [43]. Starting already at a few weeks of age, these animals develop behavioral abnormalities, low-grade white matter inflammation and progressive neurodegeneration [32, 44]. Analogously, in humans with a CNP loss-of-function allele (CNP single-nucleotide polymorphism, SNP: rs2070106-AA), diffusion tensor imaging points to axonal loss in the frontal corpus callosum [31], and white matter hyperintensities in rs2070106-AA carriers indicate mild signs of neuroinflammation and demyelination [32]. These findings suggest that CNP reduction (and the herewith associated inflammation) might be critical in a more general disease process and that the potential role of this protein is not restricted to a single neuropsychiatric diagnostic category but of global relevance for severe mental disorders.

Here, we immunized young female $Cnp^{-/-}$ mice with a cocktail of 4 NMDAR peptides [9, 24] to generate a novel autoimmune model based on preexisting white matter encephalitis. This cocktail includes a peptide covering the NMDAR1-N368/G369 region, claimed to be pathognomonic for NMDAR1-AB encephalitis [45], and most importantly, it induces functionally highly active NMDAR1-AB, leading to psychosis-like symptoms in mice with compromised BBB [9]. We report that NMDAR1-AB can substantially contribute to the behavioral abnormalities of an underlying white matter encephalitis, reflected by striking stair patterns of pathology. As indicated by additional behavioral phenotyping of conditional NR1 mutant mice, part of these behavioral NMDAR1-AB effects might be due to downregulation not only of neuronal, but also of oligodendroglial NMDAR.

## MATERIALS AND METHODS
### Mice
All animal experiments were conducted in accordance with the local authorities, i.e., the Animal Care and Use Committee (Niedersächsisches Landesamt für Verbraucherschutz und Lebensmittelsicherheit, LAVES). Sample sizes were based on previous experience under consideration of the RRR principle and adjusted to technical limitations (e.g., maximum of 16 mice per IntelliCage). All experiments were performed by investigators unaware of group assignment ("fully blinded"). Animals were kept under standard laboratory conditions (20–22 °C, 12 h light/dark cycle, lights off at 6 p.m.) in conventional type IV ($n = 13$–16 per cage) or type II cages ($n = 3$–5 per cage) (Tecniplast, Hohenpeißenberg, Germany) and maintained within ventilated cabinets (Scantainers, Scanbur Karlsunde, Denmark), separated by gender and with access to food (Sniff Spezialdiäten, Bad Sodenberg, Germany) and water ad libitum. Genotyping was carried out as previously described for Cnp [31, 43] and $NR1^{flox/flox}$ [46, 47].

### Experimental cohorts

(1) Immunization cohort: Female $Cnp^{-/-}$ (KO, $n = 26$) mice on a C57Bl/6 background along with their wild-type (WT, $n = 14$) littermates were immunized at age 8 weeks with either a cocktail of four GluN1 extracellular peptides (GluN1$_{35-53}$, GluN1$_{361-376}$, GluN1$_{385-399}$, and GluN1$_{660-811}$, coupled to keyhole limpet hemocyanin; Synaptic Systems, Göttingen, Germany) plus chicken ovalbumin (WT, $n = 14$, KO, $n = 13$) or ovalbumin only (KO, $n = 13$) ("OVA," A5503, Sigma-Aldrich, Taufkirchen, Germany) as previously described [9, 24].

(2) Oligodendroglial NR1 cKO cohorts: Female $CnpCre^{+/-}:NR1^{flox/flox}$ (cKO, $n = 16$) mice and their $NR1^{flox/flox}$ ($n = 16$) littermate controls were employed to elucidate the effect of NR1 deficiency on behavior between 3 and 11 months of age. A separate cohort of aged (12–14 months) female $CnpCre^{+/-}:NR1^{flox/flox}$ ($n = 10$) and $NR1^{flox/flox}$ controls ($n = 12$) was used to confirm findings.

(3) Cnp deficiency control cohorts: $Cnp^{+/-}$ ($n = 7$) and WT ($n = 9$) littermates were used at age 12 months as controls to separate Cnp heterozygosity effects from oligodendroglial NR1 cKO. For BBB integrity analysis, male WT ($n = 4$) and $Cnp^{-/-}$ ($n = 5$) mice, aged 18 weeks, were used.

### Transponder placement
Mice were anesthetized by intraperitoneal injections of 24 µL 2,2,2,-tribromoethanol (1.36%; T48402, Sigma) in ddH$_2$O/g body weight (Avertin). ISO standard transponders (8.5 mm length, 1.2 mm diameter, PM162-8) were implanted below the skin of the neck to enable experimenter-independent phenotyping of mice in IntelliCages® (TSE Systems, Bad Homburg, Germany). Mice were introduced to the IntelliCages on the following day.

### Behavioral characterization
For detailed information on order of testing in all cohorts, we refer to the respective figures.

IntelliCage-based behavioral phenotyping and mental-time-travel (MTT): The IntelliCage battery was carried out as detailed before [48], covering cognitive functions like place learning, reversal learning, and sucrose preference for assessment of potential anhedonia. Subsequently, higher-order cognition was tested over 9 days using our novel IntelliCage-based MTT paradigm. For this, mice receive tap water via a nose poke at first from all four corners. Starting with the second experimental day, access to drinking water is limited to a brief time window only during the active phase of the mice (6–8 p.m.). In one of the corners, mice receive a 1.5 bar air puff as negative reinforcement (day I). The individually assigned "punished" corner changes for each mouse on a daily basis following a distinct pattern, namely diametrically opposed to the first punished corner (day II), horizontally opposed (day III) and again diametrically opposed (day IV) (training cycle). This pattern is then repeated for a second round (days V–VIII) and the preference (% visits) to each corner on each day of the second round is used to assess MTT abilities (assessment cycle). Each corner on each day is considered either currently (=0 days after punishment), recently (=1 day after punishment), intermediately (=2 days after punishment) or longer ago punished (=3 days after punishment). The

average number of visits to each of these corners throughout the assessment cycle is calculated and used for statistical analyses. The steepness of the curve, best expressed as trend line, reflects the quality of MTT performance.

### Spatial memory and reversal learning
To assess hippocampus-dependent cognitive functions such as spatial learning and memory, we conducted the classical Morris water maze (MWM) as previously described [49–51]. Immunized mice were tested at 50–64 days post-immunization (DPI); cKO mice at the age of 3 months, including a subsequent reversal learning period followed by a second probe trial.

Motor performance, motor learning and coordination: Motor coordination was analyzed by beam balance as previously described [31, 50]. Motor performance and learning was tested using rotarod as previously described [31, 49]. Female cKO mice, having revealed a pathological rotarod phenotype, as well as $Cnp^{+/-}$ mice as controls were exposed to 4 h of voluntary running on complex running wheels (CRW) as previously described [52, 53] to further assess motor-cognitive performance.

### Blood sampling and NMDAR1-AB determination
Blood samples were collected from the retro-orbital sinus prior to immunization, before transponder placement (29 DPI) and before perfusion (~3 months post-immunization). EDTA plasma aliquots were stored at −80 °C. Specific antigen ELISA was performed as previously described [9, 24] using plasma diluted 1:1000 in phosphate buffered saline (PBS), to confirm successful immunization and persistence of NMDAR1-AB. To determine NMDAR1-AB IgG formation against full-length GluN1, a commercially available cell-based assay comprising Grin1-transfected and control-transfected HEK293 cells (FB 112d-1010-51, EUROIMMUN, Lübeck, Germany) was used as previously described [24]. Terminal plasma samples were diluted 1:100 in 0.2% Tween20/PBS and spiked with a commercial rabbit anti-GluN1 antibody directed against the intracellular C-terminal domain (1:1000, G8913, Sigma). Bound mouse and rabbit IgG were detected with Alexa Fluor 488-labeled anti-mouse-IgG (1:1000, A21202, Thermo Fisher Scientific, Darmstadt, Germany) and Alexa Fluor 647 labeled anti-rabbit IgG antibody (1:1000, A31573, Thermo). Nuclei were stained 10 min at RT with 1 µg/mL 4′,6-diamidino-2-phenylindole in PBS (DAPI, D9542, Sigma). Representative images were acquired on a confocal microscope (LSM 880, Zeiss, Oberkochen, Germany).

### Measurements assessing BBB integrity
BBB integrity was evaluated by quantifying extravasation of two distinct fluorescent tracers (Evans blue and fluorescein) as previously described [9, 54]. In addition, brain water content was determined by comparing wet and dry brain mass.

### Histology
Mice were anesthetized with Avertin and transcardially perfused with Ringer (B. Braun, Melsungen, Germany). Brains were collected and hemispheres separated. One hemisphere was snap-frozen and the other postfixed in 4% formaldehyde/PBS for 12 h, dehydrated in 30% sucrose/PBS for 48 h, embedded in optimal cutting medium (Tissue-Tek, #4583, Sakura, Umkirch, Germany) and frozen on dry ice. Fixed hemispheres were cut into 30 µm coronal sections on a cryostat (CM1950, Leica, Wetzlar, Germany) and stored at −20 °C in cryomedium (25% ethylene glycol/25% glycerol/PBS). Quantifications were performed as described previously [24, 51], using 3–5 regularly spaced sections per mouse (every 150 µm) between Bregma coordinates −1.34 and −2.24 mm. Free-floating frozen sections were blocked and permeabilized for 1 h at RT with 5% normal horse serum (NHS, 26050-088, Thermo) in 0.5% Triton X-100/PBS and incubated overnight at 4 °C with primary antibodies. Following primary antibodies were used: Mouse anti-GFAP (1:500, NCL-GFAP-GA5, Novocastra-Leica, Newcastle upon Tyne, UK), rabbit anti-Iba1 (1:1000, #019-19741, Wako, Neuss, Germany), guinea pig anti-parvalbumin (1:1000, #195004, Synaptic Systems), rat anti-CD3 (1:100, clone 17A2, BioLegend, Koblenz, Germany), rabbit anti-CD19 (1:500, clone D4V4B, Cell Signaling Technologies, Frankfurt am Main, Germany). Subsequently, sections were stained with corresponding fluorescently-labeled secondary antibodies for 2 h at RT. Secondary antibodies included: Alexa Fluor 555 anti-rabbit (1:1000, A21428, Thermo), Alexa Fluor 633 anti-guinea pig (1:1000, A21105, Thermo), Alexa Fluor 647 anti-mouse (1:1000, A31571, Thermo), and Alexa Fluor 647 anti-rat (1:1000, A21247, Thermo). Nuclei were stained for 10 min at RT with 0.2 µg/mL 4′,6-diamidino-2-phenylindole in PBS (DAPI, D9542,

Sigma). Sections were mounted on SuperFrost®-Plus slides (J1800AMNZ, Thermo) with Aqua-Poly/Mount (#18606, Polysciences, Warrington, PA, USA) and imaged on a confocal laser scanning microscope (LSM 880, Zeiss). For quantification of Iba1 and GFAP, 1 µm thick optical sections of hippocampi and corpora callosa were acquired as tile scans using a 40× oil objective (40×/1.4 NA Plan-APOCHROMAT, #420762-9900, Zeiss). Parvalbumin, CD3 and CD19 stainings were imaged using a 20× air objective (20×/0.8 Plan-APOCHROMAT, #420640-9903, Zeiss) with an optical thickness (Z-resolution) of 2 µm for parvalbumin and 5 µm for CD3 and CD19 stainings. Image acquisition parameters were kept constant within experiments. Quantifications and image processing were performed with FIJI-ImageJ software (Schindelin). Iba1+ cells (mostly microglia), parvalbumin+ cells (inhibitory neurons), CD3+ cells (T cells), and CD19+ cells (B cells) were manually counted. GFAP+ area was quantified densitometrically upon uniform thresholding. Cell counts and GFAP+ area were normalized to quantified areas. Data from 3–5 hippocampi/mouse was averaged. Fluorojade C staining of dying neurons was performed as previously described [51]. Neuronal death was qualitatively evaluated in hippocampus and corpus callosum by a blinded investigator using two sections per mouse. Representative images were acquired as tile scans on a confocal laser scanning microscope (LSM 880, Zeiss). DAB-based APP staining and quantification of APP+ axonal swellings was carried out in corpus callosum and hippocampus (three sections per mouse) as described previously [32], using a monoclonal anti-APP antibody (1:850, MAB348, Merck KGaA, Darmstadt, Germany) in 3% NHS/0.5% Triton X-100 in PBS for 48 h at 4 °C. Biotinylated horse anti-mouse secondary antibody (1:200, Vector Laboratories, Burlingame, CA, USA) in 3% NHS/0.5% Triton X-100 in PBS followed by Vectastain Elite ABC Kit (Vector Laboratories) were applied according to manufacturer's instructions. Mayer's hemalum (Merck KGaA, Darmstadt, Germany) served as counterstain of nuclei. Quantifications were conducted with Stereoinvestigator 6.55 software (MicroBrightfield Inc.), using a light microscope (Olympus BX-50, Olympus, Hamburg, Germany), attached to a computer-driven motorized stage and a microfire video camera. Representative images were obtained on a light microscope (Zeiss Imager Z1) with a 40×/NA 1.30 oil objective lens.

### Blood flow cytometry
Per mouse, 50 µL EDTA blood was diluted in 50 µL PBS and overlaid on 100 µL lymphocyte separation medium (1077, PromoCell). After centrifugation, cells were isolated from the interphase, washed and stained for 15 min at 4 °C with the following antibodies: PECy5 anti-CD4 (1:1000, clone H129.19, BioLegend), PECy7 anti-CD8 (1:500, clone 53-6.7, BioLegend), BV510 anti-B220 (1:333, clone RA3-6B2, BioLegend), PerCpCy5.5 anti-CD11b (1:1000, clone M1/70, BioLegend), PE anti-Gr1 (1:1000, clone RB6-8C5, BioLegend), and FITC anti-F4/80 (1:1000, BM8, BioLegend). After staining, cells were washed, suspended in 250 µL PBS containing 2% bovine serum albumin (#8076.3, Roth), and filtered through 40 µm cell strainers. Samples were measured on a FACSAria Sorp (BD). Total cell numbers were determined using forward and side scatter. Frequency of helper T cells (CD4+, CD8−), cytotoxic T cells (CD8+, CD4−), B cells (B220+), macrophages (CD11b+, F4/80+) and neutrophils/monocytes (CD11b+, Gr1+) were determined as percentage of total lymphocytes.

### Statistical analysis
Statistical analyses were performed using Prism software (GraphPad Software, version 9) or R 4.0.5. Data normality was assessed using the Shapiro–Wilk test with an alpha error of 0.05. Dependent on data distribution, two-tailed unpaired Welch's corrected $t$-test or Mann–Whitney $U$ tests were used to compare groups of 2. Similarly, groups of three were compared by Welch's ANOVA or Kruskal–Wallis test. Linear trends were tested via Jonckheere–Terpstra trend tests. Repeated measure data was analyzed using mixed-model ANOVA. Linear regression analyses of MTT datasets were performed in Prism 9 using least squares regression, a straight line model, and extra sum of squares $F$ test to compare slopes. Results are presented as mean ± SEM; $p$ values < 0.05 were considered statistically significant.

## RESULTS AND DISCUSSION
### Immunization of $Cnp^{-/-}$ mice, a genetic model of mild primary white matter encephalitis, against NMDAR1
Young female $Cnp^{-/-}$ mice lacking the structural myelin protein 2′-3′-cyclic nucleotide 3′-phosphodiesterase (Cnp), which is causal
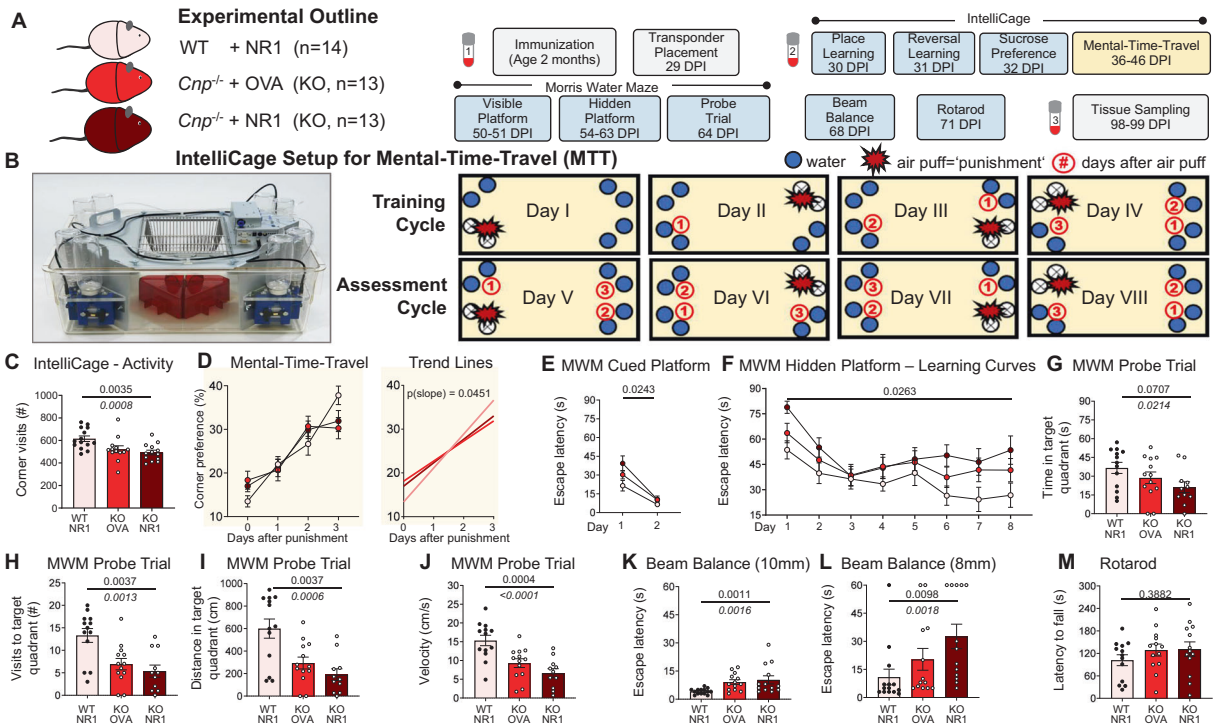
S. Arinrad et al.



**Fig. 1** **Amplification of pathological behavior in white matter inflammation by high levels of circulating NMDAR1-AB (=GluN1-AB), giving rise to remarkable behavioral stair patterns. A** Experimental outline of the immunization study using female C57Bl/6 WT ($n = 14$) and $Cnp^{-/-}$ (KO, $n = 2 \times 13$) mice. Numbered vials (1–3; compare Fig. 2) represent time points of blood sampling. DPI, days post-immunization; NR1 cocktail of four GluN1 extracellular peptides (GluN1$_{35-53}$, GluN1$_{361-376}$, GluN1$_{385-399}$, and GluN1$_{660-811}$), OVA, ovalbumin. **B** Schematic depiction of the novel IntelliCage-based experimental paradigm of mental-time-travel (MTT): Illustrating photograph of the IntelliCage kindly provided by TSE Systems (Berlin, Germany); top row (days 1–4) represents the training cycle, bottom row (days 5–8) the assessment cycle, used for statistical analysis; blue circles denote water bottles (two per corner) placed in the corners of the cage; red star-shaped symbol indicates the currently punished (1.5 bar air puff) corner of the cage on the respective experimental day; red encircled numbers refer to the conditioned corners following experienced punishment over test days. **C** Overall activity during IntelliCage-based testing battery assessed by sum of total visits to all corners (#) in 72 h, including place learning, reversal learning, sucrose preference. **D** MTT of WT versus KO expressed as preference to corners (visits in %) that were either currently (0 days after punishment), recently (1 day), intermediately (2 days), or longer ago (3 days) punished. Both KO groups ($n = 13$ each), irrespective of immunization, exhibit reduced MTT abilities compared to WT ($n = 14$), as demonstrated by the trend lines (right), calculated by linear regression (GraphPad Prism 9 Software, San Diego, CA, USA), delineating the different slopes. All slopes were nonzero ($p < 0.001$), showing successful execution and MTT learning. (**E–J**) Impaired spatial memory in the Morris water maze (MWM) test shown during cued (**E**) and hidden (**F**) platform training as well as during the probe trial (**G–J**). Immunized KO mice exhibit the poorest performance during the probe trial regarding time spent in (**G**), number of visits to (**H**) and distance swum in the target quadrant (**I**), as well as on average velocity (**J**). A total of 13 immunized WT and ovalbumin-treated KO mice were compared to 11 immunized KO mice. (**K–M**) Beam balance (motor coordination) testing reveals again stair patterns of performance on 10 mm (**K**) and 8 mm (**L**) diameter beams, while motor performance on the rotarod (**M**) appears unaffected; results of group effects of repeated measure mixed-models ANOVA, Welch's ANOVA, or Kruskal–Wallis test on top, of Jonckheere–Terpstra trend test in italics underneath; mean ± SEM presented.

of progressive, genetically induced white matter inflammation [43], were immunized at the age of 8 weeks with a cocktail of four GluN1 extracellular peptides (GluN1$_{35-53}$, GluN1$_{361-376}$, GluN1$_{385-399}$, and GluN1$_{660-811}$) [9, 24], including a peptide in the N-terminal domain containing the G7 epitope (N368/G369) [45], versus ovalbumin as control immunization. We used females to account for the 4:1 female/male ratio in human "NMDAR encephalitis" [55]. WT mice receiving the identical cocktail of four GluN1 extracellular peptides served as controls (all same C57BL/6 background, age and gender as $Cnp^{-/-}$ mice). Transponders were implanted 4 weeks later and mice went through a series of tests as detailed in Fig. 1A.

**Modeling autoimmune encephalitis: NMDAR1-AB aggravate behavioral consequences of white matter inflammation**

Mouse behavior testing was started in an observer-independent setting, namely our previously designed, extensive cognitive, emotional and social phenotyping, using IntelliCages (Fig. 1B; [48]). This setting did not reveal notable differences between groups (Table 1), except for a reduction in the total number of corner visits (assessed over the first three IntelliCage paradigms),

resulting in a stair pattern from WT to $Cnp^{-/-}$ without and with NMDAR1-AB (Fig. 1C). This paucity of differences in the IntelliCage setup is most likely explained by a relatively low sensitivity or ceiling effects of this paradigm, requiring prominent brain damage to show changes [24]. However, in an attempt to provide more challenging tasks for testing of higher brain functions, including executive performance, we established a novel test, described here for the first time, which measures episodic-like memory in the IntelliCage setup (Fig. 1B). Mice have to show their ability of what–where–when discrimination [56–58]. Indeed, $Cnp^{-/-}$ mice with their progressing white matter inflammation reveal compromised MTT capacity. In this task, the presence of NMDAR1-AB had no add-on effect. These results are clearly visualized by the trend lines showing the steepest curve (best MTT performance) in WT controls (Fig. 1D).

Similar to the corner visits in the IntelliCage (Fig. 1C), nearly all subsequently conducted conventional tests, including MWM readouts of hippocampal learning and memory, presented with line and bar graphs (Fig. 1 E–J), as well as beam balance performance (Fig. 1K, L) revealed highly significant stair patterns. Just the final test, rotarod, did not show differences between

**Table 1.** IntelliCage-based cognitive and emotional testing.

**(A) Mice immunized with GluN1 extracellular peptides (NR1) or ovalbumin (OVA)**

| | Group 1 | | Group 2 | | Group 3 | | Comparison | |
|---|---|---|---|---|---|---|---|---|
| | WT + NR1 | | $Cnp^{-/-}$ + OVA | | $Cnp^{-/-}$ + NR1 | | Across groups | |
| | Mean ± SEM | n | Mean ± SEM | n | Mean ± SEM | n | Test | p value |
| IntelliCage-based behavioral test battery | | | | | | | | |
| Place learning − place errors [% of corner visits] | 67.89 ± 1.6 | 14 | 70.98 ± 1.1 | 13 | 71.49 ± 1.1 | 13 | Welch's ANOVA | 0.207 |
| Reversal learning − place errors [% of corner visits] | 66.25 ± 1.7 | 14 | 70.01 ± 1.7 | 13 | 71.18 ± 1.1 | 13 | Kruskal–Wallis | 0.087 |
| Sucrose preference − delta [sucrose − water] | 15.68 ± 3.5 | 14 | 15.38 ± 2.8 | 13 | 14.45 ± 2.7 | 13 | Kruskal–Wallis | 0.673 |

**(B) Mice with oligodendrocyte-specific deletion of NR1**

| | Group 1 | | Group 2 | | Comparison | |
|---|---|---|---|---|---|---|
| | $NR1^{flox/flox}$ | | $CnpCre^{+/-}*NR1^{flox/flox}$ | | Group 1 versus Group 2 | |
| | Mean ± SEM | n | Mean ± SEM | n | Test | p value |
| IntelliCage-based behavioral test battery | | | | | | |
| Place learning − place errors [% of corner visits] | 68.37 ± 1.2 | 15 | 69.70 ± 1.3 | 14 | t | 0.463 |
| Reversal learning − place errors [% of corner visits] | 62.21 ± 1.7 | 15 | 68.94 ± 1.7 | 14 | t | 0.011 |
| Sucrose preference − delta [sucrose − water] | 15.03 ± 4.4 | 15 | 10.29 ± 2.7 | 14 | t | 0.373 |
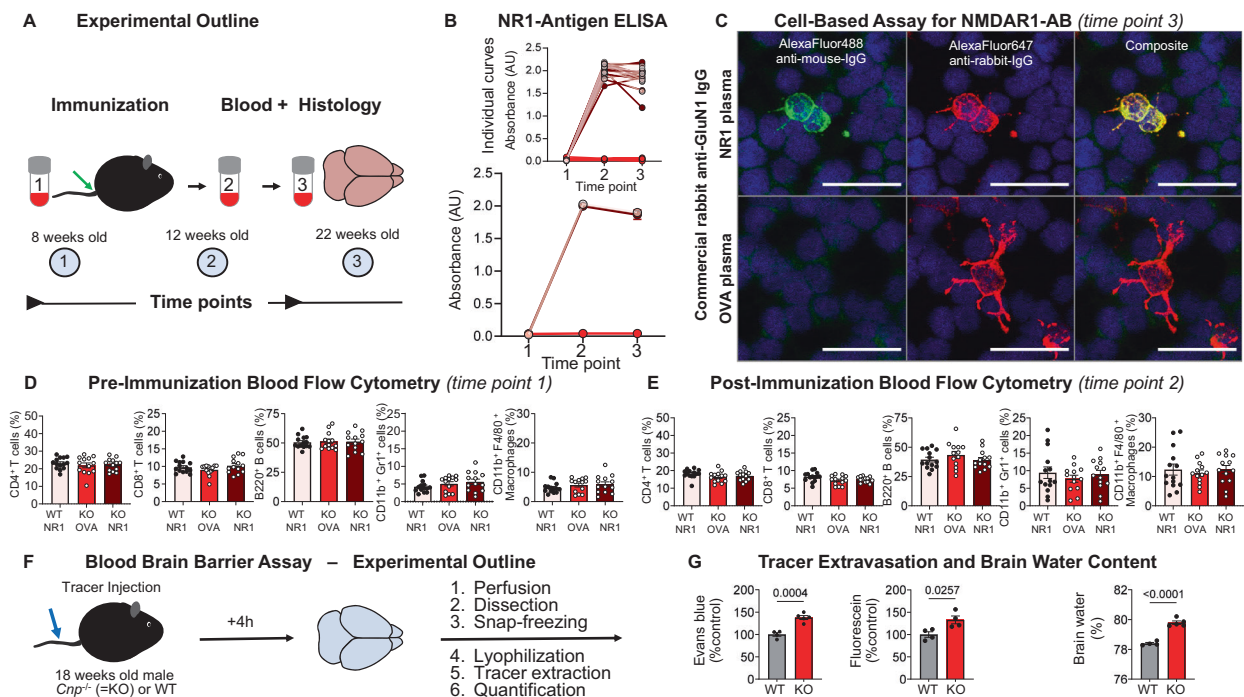


**Fig. 2 Validation of immunization, analysis of main peripheral immune cell distribution, and assessment of BBB functionality in $Cnp^{-/-}$ (KO) and WT mice. A** Experimental outline depicting time points of blood sampling, immunization, and tissue processing. **B** NR1-antigen ELISA, showing substantial NMDAR1-AB formation at the start of behavioral testing and NMDAR1-AB persistence throughout the experimental period (~3 months); data of 13–14 mice/group; mean ± SEM. **C** Immunocytochemical co-localization of NR1-immunized mouse plasma (1:100, green) with a commercial rabbit GluN1-AB (red) in a cell-based (HEK293T) clinical standard assay for NMDAR1-AB (Euroimmun); plasma (1:100) of OVA-immunized mice did not show specific staining for NMDAR1; GluN1/NR1, glutamate ionotropic receptor NMDA type subunit 1; OVA, ovalbumin. (**D**, **E**) Flow cytometric analysis of peripheral blood immune cells before (**D**) and 1 month after immunization (**E**). Note the physiological peripheral immune cell subsets in all groups, despite white matter inflammation in $Cnp^{-/-}$ mice; data of 13–14 mice/ group mean ± SEM. **F** Experimental outline for the assessment of blood–brain barrier (BBB) function in 18-week-old male $Cnp^{-/-}$ and WT mice. **G** Extravasation of Evans blue and fluorescein into CNS tissue as well as increased brain water content in $Cnp^{-/-}$ mice; data of 4–5 mice/group; two-tailed unpaired Welch's corrected $t$-test or Mann–Whitney $U$ tests; mean ± SEM.
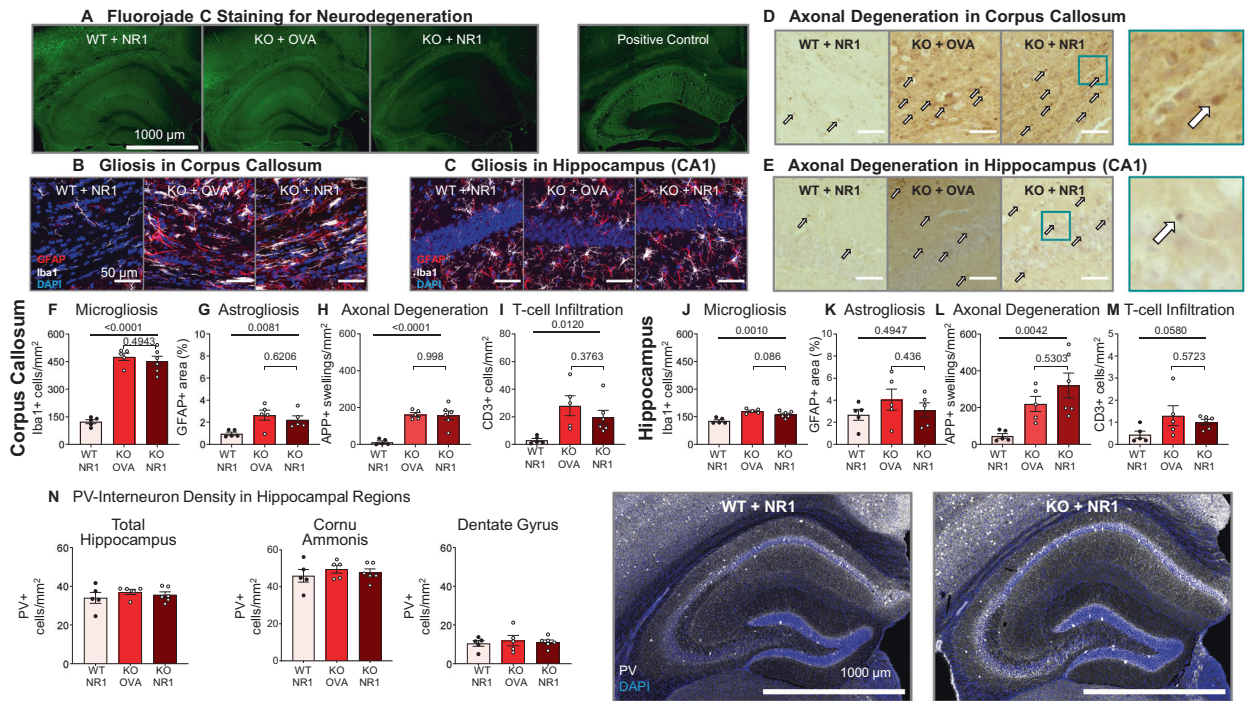
Fig. 3 Histological examination of neuroinflammation and neurodegeneration in immunized $Cnp^{-/-}$ (KO) and WT mice. A Fluorojade C staining as sensitive marker of dying neurons shows absence of neuronal death in all three groups; representative images provided; as positive control image, a section of a mouse after induced pyramidal neuronal death is given [51]. (B, C) Representative images of microglia and astrocytes in corpus callosum (B) and hippocampal CA1 region (C), depicting prominent reactive gliosis in corpus callosum of $Cnp^{-/-}$ mice, and virtually normal astrocytes and ramified microglia in the hippocampus; images acquired as 10 μm Z-stacks, displayed as maximum-intensity projections. (D, E) Representative images of amyloid precursor protein (APP)+ axonal swellings as neurodegeneration readout in corpus callosum (D) and hippocampal CA1 (E), illustrating axonal degeneration in $Cnp^{-/-}$ mice. (F–M) Quantification of neuroinflammation (microgliosis, astrogliosis), axonal degeneration, and T cell infiltration in corpus callosum (F–I) and hippocampus (J–M) of $Cnp^{-/-}$ mice with/ without NR1-immunization versus NR1-immunized WT. Note the absence of any measurable influence of NMDAR1-AB. N Quantification of parvalbumin (PV)+ interneurons did not show differences between groups in hippocampus or hippocampal subregions; data from 5–6 mice/ group; Welch's ANOVA or Kruskal–Wallis test; two-tailed unpaired Welch's corrected $t$-test or Mann–Whitney $U$ tests; mean ± SEM presented.

groups, pointing to a widely normal motor performance. In conclusion, these data indicate that in many behavioral paradigms, the presence of NMDAR1-AB aggravated the measured pathology, consistent with a significant autoimmune shaping of the encephalitis phenotype. These findings in white matter inflammation are in interesting contrast to previously modeled gray matter inflammation—where only marginal shaping of the phenotype by NMDAR1-AB was observed [24]. We note, however, that in the gray matter model, pyramidal neurons were induced to express diphtheria toxin, leading to a substantially reduced excitatory neuron number. Therefore, NMDAR were already highly diminished and their downregulation by NMDAR1-AB did not further exacerbate the resulting pathological picture [24].

### Comparable formation and persistence of circulating NMDAR1-AB in all immunized mice
Testing the immunization efficiency of our cocktail of four GluN1 extracellular peptides with a respective NR1-antigen ELISA confirmed the presence of high circulating NMDAR1-AB levels in all immunized mice that persisted up to the end of the experiment at age 22 weeks (Fig. 2A, B). Moreover, a cell-based assay using NR1-transfected cells revealed the presence of specific NMDAR1-AB, additionally validated by double-labeling with a commercial rabbit anti-GluN1 IgG (Fig. 2C).

### Peripheral immune cells in post-immunization flow cytometry remain unremarkable despite BBB disruption in $Cnp^{-/-}$ mice
Blood flow cytometry at 12 weeks of age, i.e. 4 weeks after immunization, did not show any abnormalities of $Cnp^{-/-}$ mice with or without NMDAR1-AB in number and distribution of

circulating immune cells compared to WT or pre-immunization state (Fig. 2D, E). In contrast, determination of BBB integrity [9, 24, 54] showed distinctly enhanced tracer extravasation and brain water content (Fig. 2F, G), consistent with a clear BBB disruption, allowing NMDAR1-AB to readily reach the brain. Similar to the observations in gray matter encephalitis after diphtheria toxin-induction [51], the complete lack of peripheral changes in a situation of substantial white matter inflammation, including BBB breakdown and inflammatory degeneration, is intriguing. At the same time it is alarming for clinicians who are not infrequently confronted with the necessity to diagnose or exclude an encephalitis in vivo, particularly upon suddenly occurring behavioral abnormalities in neuropsychiatric practice [51].

### Histological analysis of basic brain inflammation readouts fails to reveal any add-on effect of NMDAR1-AB
When employing MWM, we found clear behavioral changes in classical hippocampal tasks, magnified by the presence of NMDAR1-AB. Thus, we first checked whether Fluorojade staining would reveal neurodegeneration in the hippocampus. Using this method, however, we saw overall intact hippocampal structures and cells (Fig. 3A). Overview images of gliosis (both micro- and astrogliosis) uncovered clear respective signals in corpus callosum of $Cnp^{-/-}$ mice with or without NMDAR1-AB, but only weak signals in the hippocampus, consistent with the predominant white matter inflammation (Fig. 3B, C). Axonal degeneration, estimated by APP+ axonal swellings, was prominent both in callosal white matter tracts and hippocampus (Fig. 3D, E). The impressions gained by the overview images were subsequently confirmed by quantifications which additionally revealed T cell
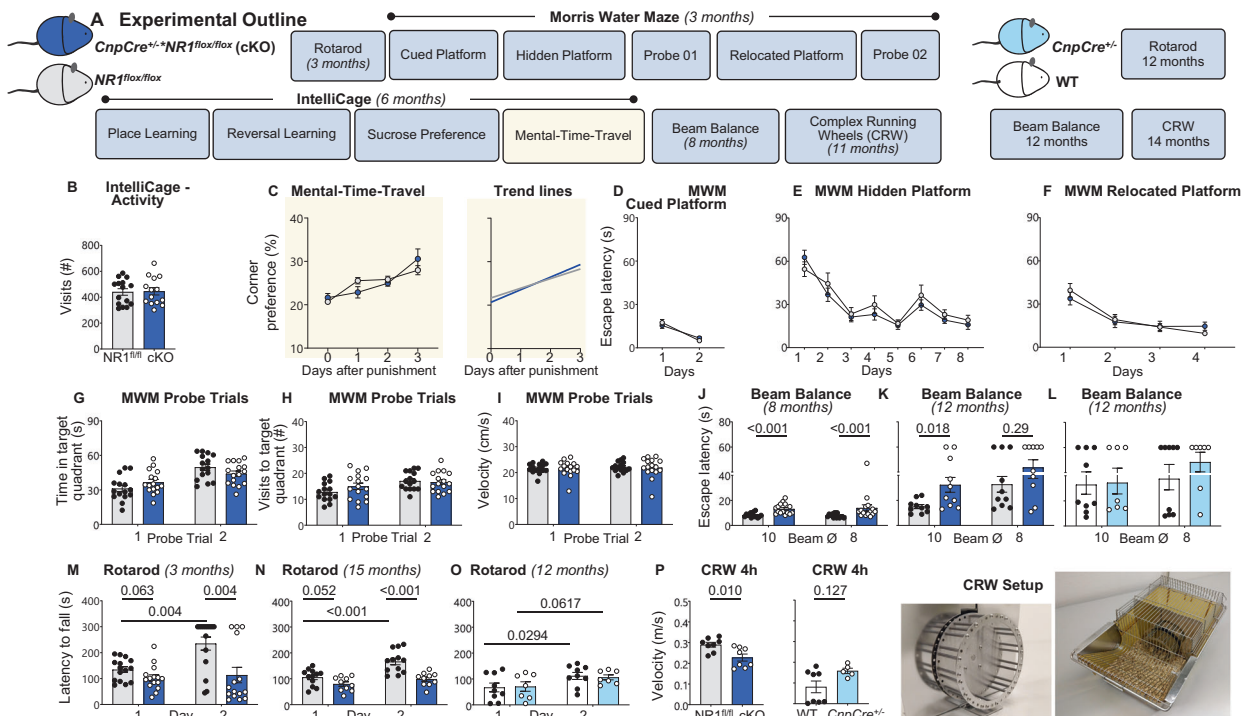
**Fig. 4 Behavioral characterization of mice lacking NR1 in oligodendrocytes suggests participation of oligodendroglial NMDAR in NMDAR1-AB effects. A** Experimental outline of the study on female C57Bl/6 $CnpCre^{+/-}:NR1^{flox/flox}$ (cKO) mice and their $NR1^{flox/flox}$ littermate controls ($n = 16$ each). Note that distinct behavioral paradigms were additionally tested in WT ($n = 9$) and $CnpCre^{+/-}$ ($n = 7$) mice, to separate a potential impact of heterozygous $Cnp$ deficiency from loss of oligodendroglial NR1. **B** Overall activity in IntelliCage paradigms and **C** MTT performance of cKO ($n = 13-14$) does not differ from $NR1^{flox/flox}$ controls ($n = 15$), as demonstrated by trend lines (right), calculated by linear regression (GraphPad Prism 9 Software, San Diego, CA, USA). All slopes were non-zero ($p < 0.001$), documenting successful execution and MTT learning; similar MTT capabilities in cKO and control mice, p(slope)=0.345 (compare Fig. 1C, D). **D–I** Unaffected spatial memory and reversal learning in Morris water maze (MWM) during cued, hidden, and relocated platform training as well as during first and second probe trials. No differences were observed regarding the time spent in (**G**) or the number of visits to (**H**) the target quadrant. Overall locomotion was unaffected in cKO mice (**I**); $n = 15$ controls; $n = 16$ cKO; repeated measure mixed-model ANOVA revealed successful learning of the task, irrespective of genotype, with a significant main effect of time at all stages ($p < 0.001$). No significant time × genotype interaction was observed during the cued ($p = 0.235$), hidden ($p = 0.654$), or relocated ($p = 0.211$) platform training. **J** Motor coordination during beam balance is impaired in female cKO mice at the age of 8 months ($n = 15$) versus controls ($n = 15$); as well as **K** in a separate cohort of older females (12 months; $n = 10$ per genotype). **L** $CnpCre^{+/-}$ mice are not affected ($n = 9$ and 7 for WT and $CnpCre^{+/-}$, respectively). **M** Motor performance and learning in the rotarod is impaired in female cKO mice at the age of 3 months ($n = 16$ and 15 for control and cKO, respectively) as well as **N** in a separate cohort of aged females ($n = 12$ and 10, respectively). **O** Motor learning is unaffected in $CnpCre^{+/-}$ mice; one-sided Welch's corrected $t$-test. **P** Motor-cognitive abilities during 4 h of CRW (complex running wheel) performance is impaired in cKO mice but normal in $CnpCre^{+/-}$; $n = 8$ per genotype; photographs of the CRW setup show omitted bars of CRW, demanding mice to adapt to irregular wheel pattern, i.e., requesting motor-cognitive performance; two-tailed unpaired Welch's corrected $t$-test or Mann–Whitney $U$ tests; mean ± SEM.

infiltration in $Cnp^{-/-}$ mice, regardless of NMDAR1-AB presence (Fig. 3F–M). B cell numbers were very low and not different between groups (not shown). Interestingly, in contrast to the diphtheria toxin-induced gray matter encephalitis [24], parvalbumin+ interneurons in total hippocampus or its subregions, cornu ammonis and dentate gyrus, were not quantitatively changed in any of the conditions compared to WT (Fig. 3N), likely explained by the morphologically intact pyramidal layer (Fig. 3A). Together, these histological data emphasize once more the predominant white matter inflammation in the $Cnp^{-/-}$ model with just moderate spreading of the inflammatory process to the hippocampus or other gray matter areas [32, 44]. The degenerative process, however, evaluated by APP+ axon counts, was clearly present in both compartments. Moreover, histological quantifications attest that NMDAR1-AB do not enhance the preexisting (before immunization) and progressing inflammatory condition. This obviously implies that the observed stair patterns of behavioral changes, with NMDAR1-AB playing an amplifier role, are due to an additional NMDAR1 dysfunction or downregulation by NMDAR1-AB rather than an exaggerated underlying

encephalitis. Thus, NMDAR1-AB not only fail to induce an encephalitis on their own [9, 24, 59–63], but also to augment an underlying gray [24] or white matter inflammation as shown here. However, they can considerably shape the resulting behavioral phenotype. Of course, brain regions, other than those examined here, may well be involved in the behavioral NMDAR1-AB effects, too. Also, our findings with NMDAR1-AB, suggesting lack of any proinflammatory potential of these autoantibodies, may not necessarily be translatable to other conditions, e.g. systemic lupus erythematosus, where more toxic "autoantibody cousins," targeting the NR2A and B subunits, may be at work [64–66].

## Genetic elimination of oligodendroglial NMDAR uncovers a potential contribution of these receptors to behavioral consequences of NMDAR1-AB

NMDA receptors are not only expressed by excitatory neurons but also by other cell types, like oligodendrocytes [67–69]. These in turn play a key role in regulating glucose uptake in response to axonal glutamate release upon neuronal activity, thus mediating metabolic support of axons on demand. Targeted inactivation of

oligodendroglial NMDA receptors impairs axonal energy metabolism [47, 70]. So far, consequences of NMDAR downregulation by NMDAR1-AB in oligodendrocytes have only been addressed in vitro, showing robust downregulation of the glucose transporter GLUT1 and diminished $Ca^{2+}$ responses upon NMDAR agonist application after NMDAR1-AB exposure [71]. Since in vivo aftereffects have remained unexplored, we wondered whether some of the impaired behavioral features, amplified by NMDAR1-AB in our model, might perhaps overlap with respective readouts measurable in mice with genetic elimination of oligodendroglial NMDAR. In other words, would such findings provide first hints of an involvement of oligodendroglial NMDAR in the overall consequences of NMDAR downregulation by NMDAR1-AB?

Thus, female conditional oligodendroglial NMDAR KO mice ($CnpCre^{+/-}*NR1^{flox/flox}$) went through an analogous test battery and were compared to $NR1^{flox/flox}$ controls (Fig. 4A). These mice did not show any abnormalities in IntelliCage, including MTT, and MWM (Fig. 4B–I; Table 1). Interestingly, beam balance at 8 and 12 months of age, i.e. walking on 10 mm versus 8 mm diameter beams, revealed inferior escape latency in cKO females as compared to controls. Rotarod performance and, in particular, motor learning, defined as improvement from day 1 to day 2, was clearly compromised, as was the average velocity on CRW. Collectively, these data disclose a predominant motor/coordination inferiority of oligodendroglial NMDAR cKO mice. Reassuringly, these phenotypes were not observed in an extra control group of $CnpCre^{+/-}$ and WT mice, employed to exclude effects of $Cnp$ heterozygosity alone (Fig. 4J–P). Based on these observations, we speculate that the amplified MWM pathology in immunized $Cnp^{-/-}$ mice (compare Fig. 1E–J) is explained mainly through downregulation by NMDAR1-AB of neuronal NMDAR, whereas their beam balance phenotype (compare Fig. 1K, L) may be contributed by the downregulation of oligodendroglial NMDAR. Even though this postulation is just indirect at this point, it may stimulate further research on a multicellular input to NMDAR1-AB mediated phenotypes.

## CONCLUSIONS AND OUTLOOK

The present mild encephalitis model tested the hypothesis that high-level circulating NMDAR1-AB can shape the behavioral consequences of an underlying white matter inflammation in $Cnp^{-/-}$ mice with confirmed BBB dysfunction. Whereas in the previously tested gray matter model [24], the magnitude of phenotype shaping was slight, it is relatively strong in the genetically induced, mild white matter encephalitis employed here, resulting in an intriguing stair pattern of behavioral pathology. However, also in white matter inflammation, NMDAR1-AB failed to further expand any histological readouts of inflammation. Together, these data indicate that the nature, location and degree of an underlying encephalitic process ultimately determine the clinical picture upon NMDAR1-AB exposure. This may also well be the case in the mild encephalitis forms typically diagnosed only postmortem in various neuropsychiatric conditions. At the same time, they explain the highly variable presenting symptoms as well as the different courses of "NMDAR encephalitis."

## DATA AVAILABILITY
All data are available upon request.

## REFERENCES
1. Dalmau J, Tuzun E, Wu HY, Masjuan J, Rossi JE, Voloschin A, et al. Paraneoplastic anti-N-methyl-D-aspartate receptor encephalitis associated with ovarian teratoma. Ann Neurol. 2007;61:25–36.
2. Dalmau J, Gleichman AJ, Hughes EG, Rossi JE, Peng X, Lai M, et al. Anti-NMDA-receptor encephalitis: case series and analysis of the effects of antibodies. Lancet Neurol. 2008;7:1091–8.
3. Pollak TA, Lennox BR, Muller S, Benros ME, Pruss H, Tebartz van Elst L, et al. Autoimmune psychosis: an international consensus on an approach to the diagnosis and management of psychosis of suspected autoimmune origin. Lancet Psychiatry. 2020;7:93–108.
4. Mane-Damas M, Hoffmann C, Zong S, Tan A, Molenaar PC, Losen M, et al. Autoimmunity in psychotic disorders. Where we stand, challenges and opportunities. Autoimmun Rev. 2019;18:1–14.
5. Endres D, Maier V, Leypoldt F, Wandinger KP, Lennox B, Pollak TA, et al. Autoantibody-associated psychiatric syndromes: a systematic literature review resulting in 145 cases. Psychol Med. 2020;1–12. https://doi.org/10.1017/S0033291720002895.
6. Ehrenreich H. Autoantibodies against the N-Methyl-d-aspartate receptor subunit NR1: untangling apparent inconsistencies for clinical practice. Front Immunol. 2017;8:1–7.
7. Ehrenreich H. Autoantibodies against N-methyl-d-aspartate receptor 1 in health and disease. Curr Opin Neurol. 2018;31:306–12.
8. Hughes EG, Peng X, Gleichman AJ, Lai M, Zhou L, Tsou R, et al. Cellular and synaptic mechanisms of anti-NMDA receptor encephalitis. J Neurosci. 2010;30:5866–75.
9. Pan H, Oliveira B, Saher G, Dere E, Tapken D, Mitjans M, et al. Uncoupling the widespread occurrence of anti-NMDAR1 autoantibodies from neuropsychiatric disease in a novel autoimmune model. Mol Psychiatry. 2019;24:1489–501.
10. Castillo-Gomez E, Oliveira B, Tapken D, Bertrand S, Klein-Schmidt C, Pan H, et al. All naturally occurring autoantibodies against the NMDA receptor subunit NR1 have pathogenic potential irrespective of epitope and immunoglobulin class. Mol Psychiatry. 2017;22:1776–84.
11. Hammer C, Stepniak B, Schneider A, Papiol S, Tantra M, Begemann M, et al. Neuropsychiatric disease relevance of circulating anti-NMDA receptor autoantibodies depends on blood-brain barrier integrity. Mol Psychiatry. 2014;19:1143–9.
12. Hammer C, Zerche M, Schneider A, Begemann M, Nave KA, Ehrenreich H. Apolipoprotein E4 carrier status plus circulating anti-NMDAR1 autoantibodies: association with schizoaffective disorder. Mol Psychiatry. 2014;19:1054–6.
13. Diamond B, Huerta PT, Mina-Osorio P, Kowal C, Volpe BT. Losing your nerves? Maybe it's the antibodies. Nat Rev Immunol. 2009;9:449–56.
14. Pan H, Steixner-Kumar AA, Seelbach A, Deutsch N, Ronnenberg A, Tapken D, et al. Multiple inducers and novel roles of autoantibodies against the obligatory NMDAR subunit NR1: a translational study from chronic life stress to brain injury. Mol Psychiatry. 2021;26:2471–82.
15. Zerche M, Weissenborn K, Ott C, Dere E, Asif AR, Worthmann H, et al. Preexisting serum autoantibodies against the NMDAR subunit NR1 modulate evolution of lesion size in acute ischemic stroke. Stroke. 2015;46:1180–6.
16. Deutsch NR, Worthmann H, Steixner-Kumar AA, Schuppner R, Grosse GM, Pan H, et al. Autoantibodies against the NMDAR subunit NR1 are associated with neuropsychiatric outcome after ischemic stroke. Brain Behav Immun. 2021;96:73–9.
17. Crisp SJ, Kullmann DM, Vincent A. Autoimmune synaptopathies. Nat Rev Neurosci. 2016;17:103–17.
18. Nagele EP, Han M, Acharya NK, DeMarshall C, Kosciuk MC, Nagele RG. Natural IgG autoantibodies are abundant and ubiquitous in human sera, and their number is influenced by age, gender, and disease. PLoS ONE. 2013;8:e60726.
19. Cohen IR, Young DB. Autoimmunity, microbial immunity and the immunological homunculus. Immunol Today. 1991;12:105–10.
20. Pruss H, Finke C, Holtje M, Hofmann J, Klingbeil C, Probst C, et al. N-methyl-D-aspartate receptor antibodies in herpes simplex encephalitis. Ann Neurol. 2012;72:902–11.
21. Armangue T, Moris G, Cantarin-Extremera V, Conde CE, Rostasy K, Erro ME, et al. Autoimmune post-herpes simplex encephalitis of adults and teenagers. Neurology. 2015;85:1736–43.
22. Castillo-Gomez E, Kastner A, Steiner J, Schneider A, Hettling B, Poggi G, et al. The brain as immunoprecipitator of serum autoantibodies against N-Methyl-D-aspartate receptor subunit NR1. Ann Neurol. 2016;79:144–51.
23. Dahm L, Ott C, Steiner J, Stepniak B, Teegen B, Saschenbrecker S, et al. Seroprevalence of autoantibodies against brain antigens in health and disease. Ann Neurol. 2014;76:82–94.
24. Wilke JBH, Hindermann M, Berghoff SA, Zihsler S, Arinrad S, Ronnenberg A, et al. Autoantibodies against NMDA receptor 1 modify rather than cause encephalitis. Mol Psychiatry. 2021. https://doi.org/10.1038/s41380-021-01238-3.
25. Bechter K. Encephalitis, mild encephalitis, neuroprogression, or encephalopathy—not merely a question of terminology. Front Psychiatry. 2019;9:1–8.
26. Bechter K. Updating the mild encephalitis hypothesis of schizophrenia. Prog Neuropsychopharmacol Biol Psychiatry. 2013;42:71–91.

27. Phillips OR, Joshi SH, Narr KL, Shattuck DW, Singh M, Di Paola M, et al. Superficial white matter damage in anti-NMDA receptor encephalitis. J Neurol Neurosurg Psychiatry. 2018;89:518–25.

28. Messacar K, Fischer M, Dominguez SR, Tyler KL, Abzug MJ. Encephalitis in US Children. Infect Dis Clin North Am. 2018;32:145–62.

29. Sejvar JJ, Kohl KS, Bilynsky R, Blumberg D, Cvetkovich T, Galama J, et al. Encephalitis, myelitis, and acute disseminated encephalomyelitis (ADEM): case definitions and guidelines for collection, analysis, and presentation of immunization safety data. Vaccine. 2007;25:5771–92.

30. Venkatesan A, Tunkel AR, Bloch KC, Lauring AS, Sejvar J, Bitnun A, et al. Case definitions, diagnostic algorithms, and priorities in encephalitis: consensus statement of the international encephalitis consortium. Clin Infect Dis. 2013;57:1114–28.

31. Hagemeyer N, Goebbels S, Papiol S, Kastner A, Hofer S, Begemann M, et al. A myelin gene causative of a catatonia-depression syndrome upon aging. EMBO Mol Med. 2012;4:528–39.

32. Janova H, Arinrad S, Balmuth E, Mitjans M, Hertel J, Habes M, et al. Microglia ablation alleviates myelin-associated catatonic signs in mice. J Clin Investig. 2018;128:734–45.

33. Poggi G, Boretius S, Mobius W, Moschny N, Baudewig J, Ruhwedel T, et al. Cortical network dysfunction caused by a subtle defect of myelination. Glia. 2016;64:2025–40.

34. Miller KR, Streit WJ. The effects of aging, injury and disease on microglial function: a case for cellular senescence. Neuron Glia Biol. 2007;3:245–53.

35. Sparkman NL, Johnson RW. Neuroinflammation associated with aging sensitizes the brain to the effects of infection or stress. Neuroimmunomodulation. 2008;15:323–30.

36. Streit WJ. Microglial senescence: does the brain's immune system have an expiration date? Trends Neurosci. 2006;29:506–10.

37. Monji A, Kato T, Kanba S. Cytokines and schizophrenia: microglia hypothesis of schizophrenia. Psychiatry Clin Neurosci. 2009;63:257–65.

38. Weissleder C, North HF, Shannon, Weickert C. Important unanswered questions about adult neurogenesis in schizophrenia. Curr Opin Psychiatr. 2019;32:170–8.

39. Aston C, Jiang L, Sokolov BP. Transcriptional profiling reveals evidence for signaling and oligodendroglial abnormalities in the temporal cortex from patients with major depressive disorder. Mol Psychiatry. 2005;10:309–22.

40. Mitkus SN, Hyde TM, Vakkalanka R, Kolachana B, Weinberger DR, Kleinman JE, et al. Expression of oligodendrocyte-associated genes in dorsolateral prefrontal cortex of patients with schizophrenia. Schizophr Res. 2008;98:129–38.

41. Tkachev D, Mimmack ML, Ryan MM, Wayland M, Freeman T, Jones PB, et al. Oligodendrocyte dysfunction in schizophrenia and bipolar disorder. Lancet. 2003;362:798–805.

42. Jahn O, Tenzer S, Werner HB. Myelin proteomics: molecular anatomy of an insulating sheath. Mol Neurobiol. 2009;40:55–72.

43. Lappe-Siefke C, Goebbels S, Gravel M, Nicksch E, Lee J, Braun PE, et al. Disruption of Cnp1 uncouples oligodendroglial functions in axonal support and myelination. Nat Genet. 2003;33:366–74.

44. Garcia-Agudo LF, Janova H, Sendler LE, Arinrad S, Steixner AA, Hassouna I, et al. Genetically induced brain inflammation by Cnp deletion transiently benefits from microglia depletion. FASEB J. 2019;33:8634–47.

45. Gleichman AJ, Spruce LA, Dalmau J, Seeholzer SH, Lynch DR. Anti-NMDA receptor encephalitis antibody binding is dependent on amino acid identity of a small region within the GluN1 amino terminal domain. J Neurosci. 2012;32:11082–94.

46. Tsien JZ, Huerta PT, Tonegawa S. The essential role of hippocampal CA1 NMDA receptor-dependent synaptic plasticity in spatial memory. Cell. 1996;87:1327–38.

47. Saab AS, Tzvetavona ID, Trevisiol A, Baltan S, Dibaj P, Kusch K, et al. Oligodendroglial NMDA Receptors regulate glucose import and axonal energy metabolism. Neuron. 2016;91:119–32.

48. Dere E, Ronnenberg A, Tampe B, Arinrad S, Schmidt M, Zeisberg E, et al. Cognitive, emotional and social phenotyping of mice in an observer-independent setting. Neurobiol Learn Mem. 2018;150:136–50.

49. Dere E, Dahm L, Lu D, Hammerschmidt K, Ju A, Tantra M, et al. Heterozygous ambra1 deficiency in mice: a genetic trait with autism-like behavior restricted to the female gender. Front Behav Neurosci. 2014;8:1–19.

50. Netrakanti PR, Cooper BH, Dere E, Poggi G, Winkler D, Brose N, et al. Fast cerebellar reflex circuitry requires synaptic vesicle priming by munc13-3. Cerebellum. 2015;14:264–83.

51. Wilke JBH, Hindermann M, Moussavi A, Butt UJ, Dadarwal R, Berghoff SA, et al. Inducing sterile pyramidal neuronal death in mice to model distinct aspects of gray matter encephalitis. Acta Neuropathol Commun. 2021;9:121.

52. Wakhloo D, Scharkowski F, Curto Y, Javed Butt U, Bansal V, Steixner-Kumar AA, et al. Functional hypoxia drives neuroplasticity and neurogenesis via brain erythropoietin. Nat Commun. 2020;11:1313.

53. Butt UJ, Steixner-Kumar AA, Depp C, Sun T, Hassouna I, Wustefeld L, et al. Hippocampal neurons respond to brain activity with functional hypoxia. Mol Psychiatry. 2021;26:1790–807.

54. Berghoff SA, Duking T, Spieth L, Winchenbach J, Stumpf SK, Gerndt N, et al. Blood-brain barrier hyperpermeability precedes demyelination in the cuprizone model. Acta Neuropathol Commun. 2017;5:94.

55. Dalmau J, Armangue T, Planaguma J, Radosevic M, Mannara F, Leypoldt F, et al. An update on anti-NMDA receptor encephalitis for neurologists and psychiatrists: mechanisms and models. Lancet Neurol. 2019;18:1045–57.

56. Pause BM, Zlomuzica A, Kinugawa K, Mariani J, Pietrowsky R, Dere E. Perspectives on episodic-like and episodic memory. Front Behav Neurosci. 2013;7:1–12.

57. Dere D, Zlomuzica A, Dere E. Fellow travellers in cognitive evolution: co-evolution of working memory and mental-time-travel? Neurosci Biobehav Rev. 2019;105:94–105.

58. Chao OY, de Souza Silva MA, Yang YM, Huston JP. The medial prefrontal cortex—hippocampus circuit that integrates information of object, place and time to construct episodic memory in rodents: behavioral, anatomical and neurochemical properties. Neurosci Biobehav Rev. 2020;113:373–407.

59. During MJ, Symes CW, Lawlor PA, Lin J, Dunning J, Fitzsimons HL, et al. An oral vaccine against NMDAR1 with efficacy in experimental stroke and epilepsy. Science. 2000;287:1453–60.

60. Li Y, Tanaka K, Wang L, Ishigaki Y, Kato N. Induction of memory deficit in mice with chronic exposure to cerebrospinal fluid from patients with anti-N-methyl-D-aspartate receptor encephalitis. Tohoku J Exp Med. 2015;237:329–38.

61. Planaguma J, Leypoldt F, Mannara F, Gutierrez-Cuesta J, Martin-Garcia E, Aguilar E, et al. Human N-methyl D-aspartate receptor antibodies alter memory and behaviour in mice. Brain. 2015;138:94–109.

62. Taraschenko O, Fox HS, Pittock SJ, Zekeridou A, Gafurova M, Eldridge E, et al. A mouse model of seizures in anti-N-methyl-d-aspartate receptor encephalitis. Epilepsia. 2019;60:452–63.

63. Yue W, Caldwell S, Risbrough V, Powell S, Zhou X. Chronic presence of blood circulating anti-NMDAR1 autoantibodies impairs cognitive function in mice. PLoS ONE. 2021;16:e0256972.

64. Faust TW, Chang EH, Kowal C, Berlin R, Gazaryan IG, Bertini E, et al. Neurotoxic lupus autoantibodies alter brain function through two distinct mechanisms. Proc Natl Acad Sci USA. 2010;107:18569–74.

65. Chan K, Nestor J, Huerta TS, Certain N, Moody G, Kowal C, et al. Lupus autoantibodies act as positive allosteric modulators at GluN2A-containing NMDA receptors and impair spatial memory. Nat Commun. 2020;11:1–11.

66. Mackay M, Vo A, Tang CC, Small M, Anderson EW, Ploran EJ, et al. Metabolic and microstructural alterations in the SLE brain correlate with cognitive impairment. JCI Insight. 2019;4:1–18.

67. Salter MG, Fern R. NMDA receptors are expressed in developing oligodendrocyte processes and mediate injury. Nature. 2005;438:1167–71.

68. Karadottir R, Cavelier P, Bergersen LH, Attwell D. NMDA receptors are expressed in oligodendrocytes and activated in ischaemia. Nature. 2005;438:1162–6.

69. Micu I, Jiang Q, Coderre E, Ridsdale A, Zhang L, Woulfe J, et al. NMDA receptors mediate calcium accumulation in myelin during chemical ischaemia. Nature. 2006;439:988–92.

70. Krasnow AM, Attwell D. NMDA receptors: power switches for oligodendrocytes. Neuron. 2016;91:3–5.

71. Matute C, Palma A, Serrano-Regal MP, Maudes E, Barman S, Sanchez-Gomez MV, et al. N-methyl-D-aspartate receptor antibodies in autoimmune encephalopathy alter oligodendrocyte function. Ann Neurol. 2020;87:670–6.

## ACKNOWLEDGEMENTS

## AUTHOR CONTRIBUTIONS

Concept, design, and supervision of the study: HE. Data acquisition/analysis/interpretation: SA, JBHW, AS, MH, JD, UJB, AAS-K, LS, AR, HP, SAB, MH, FL, K-AN, KB, and HE. Drafting manuscript and drafting display items: HE together with SA and JBHW. All authors read and approved the final version of the manuscript.

## FUNDING

## COMPETING INTERESTS

The authors declare no competing interests.

## ADDITIONAL INFORMATION

**Correspondence** and requests for materials should be addressed to Hannelore Ehrenreich.

**Reprints and permission information** is available at http://www.nature.com/reprints

**Publisher's note** Springer Nature remains neutral with regard to jurisdictional claims in published maps and institutional affiliations.

# 6 Summary and Conclusion

For the development and evaluation of valid animal models a good understanding of the disease of interest is of utmost importance. Reviewing the current literature on the anti-NMDAR encephalitis revealed a number of key aspects, namely (1) a complex, heterogeneous, and severe neuropsychiatric phenotype with relatively acute onset, (2) characteristic features of neuroinflammation, (3) heterogeneity with respect to affected brain regions, often non-exclusively including the hippocampus, (4) the presence of NMDAR1-AB that have the potential to induce NMDAR hypofunction (5) a strong dependency on NMDAR1-AB assays in differential diagnosis, due to substantial phenotypic overlap with other encephalitides, and (6) an insufficient representation of the neuroinflammatory component of NMDARE in currently available animal models. Most strikingly, however, is the lack of knowledge about the etiology and pathogenesis of NMDARE. Hence, the question arises if the anti-NMDAR encephalitis is a distinct disease entity, caused by an autoimmune response against NMDAR as originally proposed by Dalmau and colleagues but not yet proven (for simplicity referred to as 'type I'), or rather a collection/spectrum of encephalitides classified as NMDARE (hereafter referred to as 'type II') based on the presence of NMDAR1-AB in patient CSF, which may be preexisting or secondary to the underlying pathology. Considering the present literature, both types likely exist, however, their relative frequency may only be evaluated after substantial research on the encephalitogenesis and identification of factors initiating neuroinflammation in type I NMDARE. A scheme that summarizes the three main strategies on how to model distinct aspects of the anti-NMDAR encephalitis is provided in Figure 3. Importantly, the potential of NMDAR1-AB to bind NMDAR and trigger internalization and ultimately NMDAR hypofunction, should be similar across NMDARE models but may differ in magnitude depending on the amount of intrathecal NMDAR1-AB.

At the start of this thesis, no animal model for either type I or type II NMDARE existed and studies were limited to passive transfer models or active immunization models lacking the neuroinflammatory component of NMDARE (During et al. 2000, Hughes et al. 2010, Manto et al. 2010, 2011, Mikasova et al. 2012, Hammer et al. 2014a, Lin et al. 2014, Li et al. 2015, Planaguma et al. 2015, Wright et al. 2015, Planaguma et al. 2016, Wurdemann et al. 2016, Malviya et al. 2017, Blome et al. 2018, Pan et al. 2018). To systematically disentangle the relative contribution of NMDAR1-AB and neuroinflammation in encephalitides, which might not be feasible in type I NMDARE models due to the lack of a relevant NMDAR1-AB negative encephalitis comparator, core features of type II NMDARE were modeled in mice and compared to a well-characterized and standardized encephalitis mouse model lacking NMDAR1-AB as well as NMDAR1-AB positive and negative healthy littermate controls (Wilke et al. 2021a). This was achieved by combining a previously published gray matter inflammation mouse model (Agarwal et al. 2012), which was extensively characterized as part of this thesis (Wilke et al. 2021b), with an immunization strategy that induces high titers of functional NMDAR1-AB or control immunization against the ovalbumin (Pan et al. 2018). In addition, *Cnp* knockout mice were immunized to investigate the impact of NMDAR1-AB during white matter inflammation (Arinrad et al. 2021). Lastly, a replication study was conducted with the aim to investigate the pathogenesis of type I NMDARE and to complement a previously published report (Wagnon et al. 2020, Wilke et al. 2021a).
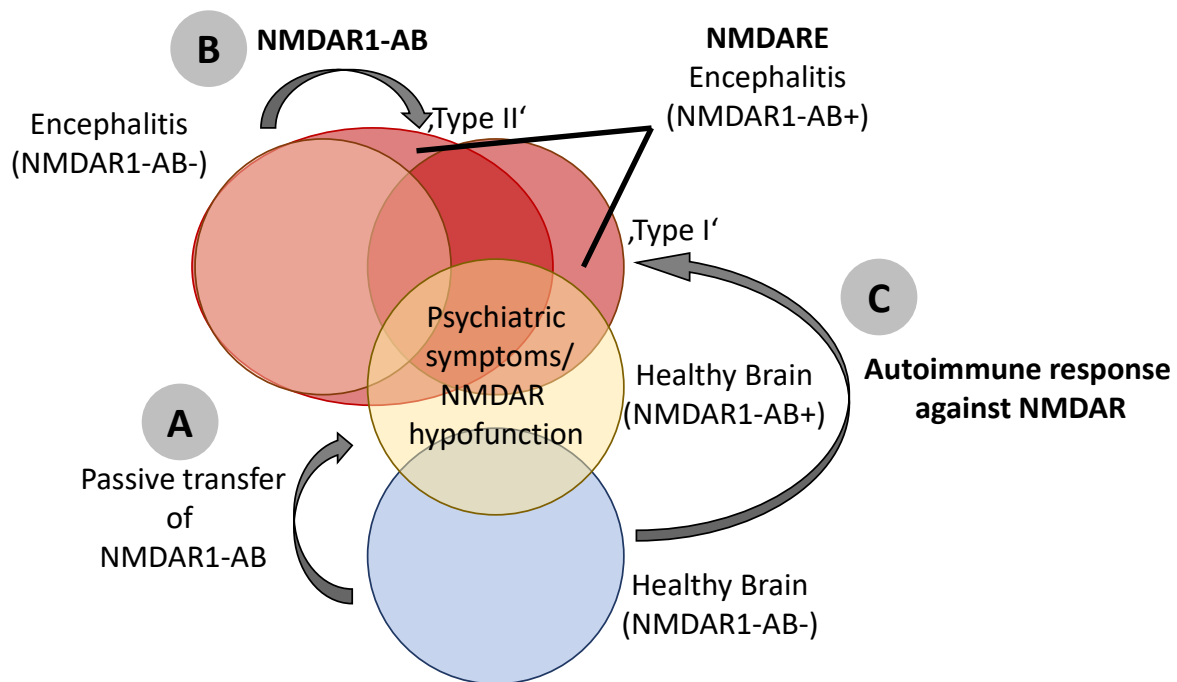
**Figure 3:** Modeling anti-NMDAR encephalitis. **A**, a variety of passive transfer models have confirmed the pathophysiological potential of NMDAR1-AB in vivo. NMDAR1-AB transferred into the CNS of healthy rodents, either by intrathecal injections or via 'spill-over' from the periphery in models with an impaired blood-brain barrier, cause a reversible state of NMDAR hypofunction via receptor internalization resulting in symptoms reminiscent of NMDAR antagonism, including psychosis-like hyperlocomotion and memory impairments. However, these models lack the neuroinflammatory component of NMDARE (see 1.8). **B**, first indications that NMDAR1-AB shape the clinical manifestation of encephalitis were obtained by comparisons of human NMDAR1-AB positive and negative encephalitis cases that revealed a higher frequency of psychiatric symptoms in NMDAR1-AB positive patients, whereas other neuropsychiatric symptoms such as seizures, memory deficits or cognitive dysfunction, decreased level of consciousness were common and independent of NMDAR1-AB (see 1.1). The high seroprevalence of NMDAR1-AB in mammals, NMDARE induction in response to viral encephalitides, the heterogeneous clinical manifestation of NMDARE, frequency of concomitant pathologies, and often unidentified causes suggest that NMDARE reflects a spectrum of encephalitides, in which the presence of NMDAR1-AB shapes the clinical phenotype ('type II'). **C**, 'type I' NMDARE reflects the pathomechanism originally proposed by Dalmau and colleagues, in which an autoimmune response against NMDAR results in encephalitis with concomitant NMDAR1-AB that contribute to the encephalitic phenotype. The observation of ectopic NMDAR expression and presence of NMDAR1-specific B cells in NMDARE-associated ovarian teratomas as well as the recent development of an active immunization model against NMDAR-proteoliposomes that induces fulminant encephalitis provide strong evidence for the existence of type I NMDARE (see 1.6 and 1.9). However, as NMDAR1-AB and neuroinflammation are inherently linked by the underlying autoimmune process in this type I NMDARE model, it lacks the required comparator to formally establish the relevance of NMDAR1-AB during neuroinflammation. For this reason, this thesis modeled type II NMDARE and systematically disentangled the role of NMDAR1-AB from neuroinflammation in two distinct encephalitis models.

**Modeling acute gray matter inflammation in mice**

Originally, ablation of Nex1 (Neurod6) positive pyramidal neurons by tamoxifen-inducible diphtheria toxin fragment A expression was first described by Agarwal and colleagues to initiate a substantial neuroinflammatory response within three weeks, which was characterized by strong reactive gliosis and T cell infiltration in the hippocampus and some other gray matter regions (Agarwal et al. 2012). The authors further identified that the degree of CreERT2-mediated recombination is dose-dependent and that daily injections of tamoxifen for ten days ablates about half the neurons in the CA1 hippocampal subfield (Agarwal et al. 2012).

To elaborate the downstream consequences of pyramidal cell death and spatiotemporally defined sterile gray matter inflammation, homozygous Neurod6[tm2.1(cre/ERT2)Kan] ('NexCreERT2') mice (Agarwal et al. 2012) were crossbred to heterozygous Gt(ROSA)26Sor[tm1(DTA)Jpmb] mice (Ivanova et al. 2005) generating double heterozygous tamoxifen-inducible 'DTA' mice and littermate controls lacking the DTA allele (Wilke et al. 2021b). All animals were heterozygous for NexCreERT2 to avoid confounding effects of Cre expression or potential Nex1 haploinsufficiency, although Nex1 (Neurod6) seems to be dispensable as no obvious histopathological or phenotypic alterations were found in Nex1 knockout mice (Schwab et al. 1998, Goebbels et al. 2006). Following 3x or 5x tamoxifen administration, pyramidal cell death was present within one week in DTA but not in control mice and triggered a prominent neuroinflammatory response in the hippocampus, characterized by an increased expression of GFAP, which is a typical feature of reactive astrogliosis (Sofroniew 2009, Sofroniew 2014), increased microglia numbers, confirmed by brain flow cytometry and histology, as well as increased CD4+ and CD8+ T cell infiltration into the CNS (Wilke et al. 2021b). The strong and persistent neuroinflammatory response after DTA-mediated neuronal death is consistent with a similar mouse model in which DTA expression was coupled to Camk2a regulatory elements (Yamasaki et al. 2007, Rice et al. 2017, Wilke et al. 2021b). Consistent with the expression pattern of Nex1 in the adult rodent brain (Bartholoma and Nave 1994), volumetric analyses of distinct brain regions via magnetic resonance imaging revealed prominent atrophy of the hippocampus and significant but less pronounced atrophy in cortical regions and the cerebellum in DTA compared to control mice. Substantial hippocampal atrophy was additionally confirmed in both 3x and 5x tamoxifen treated DTA mice by histology (Wilke et al. 2021b). Furthermore, in vivo injections of fluorescent tracers and quantification of tracer extravasation into the CNS (Berghoff et al. 2017) revealed a long lasting impairment of the blood-brain barrier in DTA mice (Wilke et al. 2021b).

In summary, DTA mice displayed key features of encephalitides involving the limbic system, namely (I) acute onset, (2) neuroinflammation in gray matter regions prominently but not exclusively affecting the hippocampus, and (3) long-lasting blood-brain barrier impairment that likely facilitates CNS extravasation of peripheral autoantibodies.

**Modeling type II NMDARE in mice**

In order to model 'type II' NMDARE and to systematically disentangle the relative contribution of NMDAR1-AB and neuroinflammation, the DTA mouse model was utilized and combined with a previously established immunization protocol (Pan et al. 2018) to generate encephalitis mice that carry either NMDAR1-AB or anti-ovalbumin antibodies, as well as NMDAR1-AB positive and negative control mice without neuroinflammation (Wilke et al. 2021a). Previous work has shown that functional NMDAR1-AB of the IgG subclass are expressed within ten days after immunization and persist for at least one month (Pan et al. 2018). Here, persistence of NMDAR1-AB (IgG) was shown for at least four months after immunization and NMDAR1-AB titers were determined in a slightly modified version (to detect mouse instead of human autoantibodies) of a commercial cell-based assay that is routinely used in clinics for the diagnosis of NMDARE (FB 112d-1010-51, Euroimmun). Four months after immunization, median NMDAR1-AB titers were 1:100 and ranged up to 1:3200 (Wilke et al. 2021a), which is within the range of serum titers in human NMDARE cases, although slightly lower on average (Bastiaansen et al. 2022). To account for the predominance of young females amongst NMDARE patients (Dalmau et al. 2019, Nosadini et al. 2021, Bastiaansen et al. 2022, Nissen et al. 2022), young female mice were chosen to model type II NMDARE.

After onset of pyramidal cell death and neuroinflammation in DTA mice, multifaceted behavioral phenotyping was conducted and revealed (a) absence of cataleptic signs, (b) normal executive functioning, (c) normal exploratory behavior, (d) normal stereotypic behavior such as circling, climbing, rearing, and marble burying, (e) normal task-learning in a visible platform task of the Morris water maze, as well as (f) normal sucrose and pheromone preferences, indicating absence of anhedonia, in all mice independent of DTA or NMDAR1-AB induction. Independent of NMDAR1-AB status, DTA compared to control mice displayed pronounced deficits in spatial learning and memory function assessed in the classical Morris water maze, which are common in hippocampal lesion models (Morris et al. 1982, Broadbent et al. 2004, Rice et al. 2017) and likely related to the decrease of pyramidal neurons. The reduction in hippocampal pyramidal neuronal numbers, which densely express NMDAR (Monaghan and Cotman 1985, Moriyoshi et al. 1991, Kutsuwada et al. 1992, Meguro et al. 1992, Monyer et al. 1992, Monyer et al. 1994, Traynelis et al. 2010, Paoletti et al. 2013), may also explain why NMDAR1-AB had no add-on effect on the spatial learning/memory impairments, which would be expected from NMDAR hypofunction (Morris et al. 1986, Morris 1989). In contrast, similar to the NMDAR antagonist MK-801, NMDAR1-AB exacerbated hyperlocomotion in DTA mice (van den Buuse 2010, Pan et al. 2018, Wilke et al. 2021a). The observation of exacerbated hyperlocomotion without increased deficits in spatial learning and memory may be explained by differential effects of NMDAR hypofunction in pyramidal cells and interneurons and/or the imbalance of pyramidal- and interneurons in the hippocampus of DTA mice (Hudson et al. 2020, Wilke et al. 2021a). Although hyperlocomotion is a relatively unspecific behavioral abnormality in mice, in the context of NMDAR hypofunction, which is induced by NMDAR1-AB upon access to the CNS (see 1.8 and 1.9), hyperlocomotion is considered a surrogate marker for psychosis (Willetts et al. 1990, Jentsch and Roth 1999, Bygrave et al. 2016). In this regard, the findings of persistently exacerbated hyperlocomotion in NMDAR1-AB positive compared to NMDAR1-AB negative DTA or

healthy control mice, is consistent with studies comparing NMDAR1-AB positive and negative encephalitis patients that show higher frequency of psychosis in NMDAR1-AB carriers (Gable et al. 2009, Chen et al. 2016, Seifert-Held et al. 2021)

Importantly, NMDAR1-AB did not induce aberrant behavior in control mice with an intact blood-brain barrier (Wilke et al. 2021a), which extends previous findings of normal MK-801 responses in healthy NMDAR1-AB positive mice (Pan et al. 2018). Consistent with previous findings, immunization against a cocktail of GluN1-peptides did not cause neuroinflammation (Pan et al. 2018, Wilke et al. 2021a). Furthermore, NMDAR1-AB did not alter the neuroinflammatory response or neurodegeneration in DTA mice, which was characterized by long-lasting hippocampal atrophy, increased microglia density, increased GFAP density, and CD45+ immune cell infiltration. Lasting blood-brain barrier impairment, which likely facilitates NMDAR1-AB extravasation into the CNS, was present in DTA mice independent of NMDAR1-AB (Wilke et al. 2021a) and is in line with about one third of human NMDARE cases that likewise display BBB-dysfunction (Malter et al. 2013, Durr et al. 2021, Yu et al. 2021).

In contrast to herpes simplex encephalitis or Japanese encephalitis, which have been associated with the induction of NMDAR1-AB (Armangue et al. 2014, Hacohen et al. 2014, Mohammad et al. 2014, Armangue et al. 2015, Sutcu et al. 2016, Westman et al. 2016, Ma et al. 2017, Nosadini et al. 2017, Pruss 2017, Armangue et al. 2018, Ma et al. 2020, Liu et al. 2021), non-immunized DTA mice did not develop NMDAR1-AB of the IgG subclass (cut-off titer 1:100 in cell-based assay; unpublished observation) in response to neuroinflammation, and NMDAR1-AB titers of GluN1-immunized mice were comparable between DTA and control groups (Wilke et al. 2021a), indicating that the induction of pyramidal cell death and subsequent neuroinflammatory response did not boost NMDAR1-AB production. This could be explained by an insufficient peripheral immune activation in DTA mice or by a lack of neuronal-autoantigen shedding, perhaps due to rapid phagocytosis of activated microglia. Indeed, flow cytometric analysis of white blood cell subsets and quantification of the alarmin HMGB1 via ELISA revealed a physiological immune cell composition in blood and normal HMGB1 plasma levels in DTA mice two weeks after encephalitis induction (Wilke et al. 2021b). Furthermore, histopathological studies of ovarian teratomas have shown that ectopic expression of GluN1/NMDAR is not sufficient to induce NMDAR1-AB or NMDARE (Tuzun et al. 2009, Tabata et al. 2014, Iemura et al. 2018, Chefdeville et al. 2019). Ultimately, the type of antigen presentation and immune stimulation may not only determine NMDAR1-AB induction but also the encephalitogenic potential of immunization strategies against GluN1 and/or NMDAR (see 1.9).

Considering the reduction of NMDAR expressing pyramidal neurons in DTA mice, and slightly lower average titers of peripheral NMDAR1-AB in mice as compared to NMDARE patients, it cannot be excluded that the effect of NMDAR1-AB was underrepresented in the here established mouse model. Nevertheless, it has been shown that NMDAR1-AB can contribute to the behavioral phenotype of an underlying encephalitis by exacerbating hyperlocomotion similar to NMDAR antagonists, without majorly affecting neuroinflammation. Furthermore, confirming and extending previous findings of Pan and colleagues, immunization against GluN1 did not cause neuroinflammation and NMDAR1-AB had no major impact on the behavior of mice with an intact blood-brain barrier.

**NMDAR1 autoantibodies and white matter inflammation**

Although NMDARE is mostly associated with neuroinflammation in gray matter regions and in particular the hippocampus, several case reports describe NMDARE in patients with features of inflammatory demyelinating disorders, including relapsing remitting multiple sclerosis (Fleischmann et al. 2015, Gulec et al. 2020, Huang et al. 2020), acute disseminated encephalomyelitis (Lekoubou et al. 2012), optic neuritis (Uzawa et al. 2012), or myelitis (Pennington et al. 2012). Furthermore, white matter lesions as well as white matter inflammation have been associated with intrathecal NMDAR1-AB (Takeda et al. 2014, Mariotto et al. 2019) and MRI abnormalities in white matter regions have been repeatedly reported in a number of case series (Irani et al. 2010, Finke et al. 2012, Finke et al. 2013, Titulaer et al. 2014, Phillips et al. 2018). According to two observational cohort studies, features of demyelinating disorders occur in about 5% of NMDARE cases (Titulaer et al. 2014, Nissen et al. 2022). In approximately half these cases, NMDARE and demyelination coincide, whereas the other half displays sequential episodes (Titulaer et al. 2014). In addition to demyelinating disorders, changes in the superficial white matter have been observed by diffusion tensor imaging in a substantial number of non-recovered NMDARE patients, in contrast to recovered patients or neurologically normal controls (Phillips et al. 2018). The association between NMDAR1-AB and white matter abnormalities was further substantiated by an in vitro study showing that NMDAR1-AB are able to reduce NMDAR-dependent oligodendrocyte function, such as NMDAR-mediated $Ca^{2+}$ currents and NMDAR activity dependent upregulation of Glut1 (Matute et al. 2020).

To investigate the pathophysiological relevance of NMDAR1-AB in white matter inflammation, 2'-3'-cylcic nucleotide 3'-phosphodiesterase (CNP) knockout mice (*Cnp* KO) were immunized against GluN1-specific peptides and/or ovalbumin (Arinrad et al. 2021) as previously described (Pan et al. 2018). Mice lacking CNP are characterized by axonal degeneration and neuroinflammation that is present already in eight weeks old mice, progresses with age, and predominates in white matter regions, such as the corpus callosum (Lappe-Siefke et al. 2003, Hagemeyer et al. 2012, Janova et al. 2018, Garcia-Agudo et al. 2019). Furthermore, a blood-brain barrier dysfunction is already present in young *Cnp* KO mice (Arinrad et al. 2021) thereby facilitating extravasation of peripheral NMDAR1-AB into the CNS. Wildtype mice were only immunized against GluN1-specific peptides (Pan 2018), as mice with an intact blood-brain barrier are phenotypically unremarkable after 'GluN1-cocktail' immunization (Pan et al. 2018, Wilke et al. 2021a).

Comparing NMDAR1-AB or OVA-AB carrying *Cnp* KO and NMDAR1-AB positive wildtype mice revealed distinct stair patterns of behavioral pathology in hippocampal learning and memory in the Morris water maze as well as in tests of motor performance or motor coordination mice. In contrast, episodic-memory, analyzed in a what-where-when orientation task, was compromised in *Cnp* KO mice but not affected by NMDAR1-AB (Arinrad et al. 2021). Similar to observations in gray matter inflammation (Wilke et al. 2021a), NMDAR1-AB had no add-on effect on microgliosis, astrogliosis, axonal degeneration or immune cell infiltration, which were prominent in the corpus callosum of *Cnp* KO mice, and did not enhance inflammation in the hippocampus, which was mildly affected in *Cnp* KO compared to control mice (Arinrad et al. 2021).

In conclusion, NMDAR1-AB alter the behavioral phenotype of mice with a genetically induced progressive genetic white matter inflammation without major effects on inflammation itself, suggesting that the observed effects result from NMDAR1-AB mediated reversible NMDAR internalization and induction of NMDAR hypofunction.

## Modeling type I NMDARE in mice

Considering the lack of knowledge about the etiology and pathogenesis of NMDARE, reliable and construct valid animal models of 'type I' NMDARE are of utmost importance. While conducting this thesis, two at first view promising mouse models were published, both claiming encephalitis induction and NMDAR1-AB formation upon active immunization against either NMDAR holoreceptors reconstituted into proteoliposomes (Jones et al. 2019) or a $GluN1_{359-378}$-peptide (Wagnon et al. 2020). While Jones and colleagues convincingly confirmed fulminant neuroinflammation by histological examinations, Wagnon and colleagues did not report on reactive astrogliosis or microgliosis, which are core features of neuroinflammation (Sofroniew 2009, Glass et al. 2010, Saijo and Glass 2011, Sofroniew 2014) and NMDARE (Tuzun et al. 2009, Bien et al. 2012, Filatenkov et al. 2017, Nauen 2017, Hirano et al. 2019, Zrzavy et al. 2021b). Furthermore, $GluN1_{359-378}$-immunized mice lacked parenchymal and perivascular T cell infiltration (Wagnon et al. 2020), which is common in human NMDARE cases (Tuzun et al. 2009, Martinez-Hernandez et al. 2011, Bien et al. 2012, Filatenkov et al. 2017, Nauen 2017, Zrzavy et al. 2021b). For this reason, two cohorts were designed to replicate and complement the study of Wagnon and colleagues by investigating the acute neuroinflammatory response, long-term outcome, and mortality in addition to previously published behavior tests, assessment of BBB-integrity, and flow cytometric analysis of the brain immune compartment acutely after immunization. However, after exact replication of the published immunization protocol and following their study outline, mice neither developed neuroinflammation nor did their behavior differ from control immunized mice despite induction of NMDAR1-AB in $GluN1_{359-378}$-immunized mice. As the acute cohort did not reproduce published findings, the cohort planned for long-term investigations was used for a second independent replication and confirmed the non-reproducibility (Wilke et al. 2021a). In addition to potential iatrogenic issues or effects of the gut microbiome (Wilke et al. 2021a), unintentional or unpublished modifications of the peptide may explain the non-reproducibility. $GluN1_{359-378}$ contains residues (KLV**Q**VGIY**NG**THVIP**N**DRK) prone to side reactions, such as deamination of glutamine (Q) and deamination or deamidation of asparagine (N). To test the stability of $GluN1_{359-378}$, a frozen aliquot, stored at -80°C, was measured by high-performance liquid chromatography coupled with mass spectrometry immediately after thawing as well as after one week at room temperature. The resulting chromatograms and molecular masses matched the original peptide sequence (personal communication with Lars Van Werven, Neuroproteomics, Max Planck Institute for Multidisciplinary Sciences) thereby excluding peptide side reactions as potential confounds.

To conclude, the immunization protocol published by Wagnon et al. does not reliably induce NMDARE-like pathology in mice despite the induction of NMDAR1-AB directed against $GluN1_{359-378}$. Therefore, the pathomechanism(s) initiating neuroinflammation in NMDARE remain unknown.

# References

1.  Aan Het Rot M, Zarate CA, Jr., Charney DS, Mathew SJ. Ketamine for depression: where do we go from here? Biological psychiatry. 2012;72(7):537-47.

2.  Abboud H, Probasco JC, Irani S, Ances B, Benavides DR, Bradshaw M, et al. Autoimmune encephalitis: proposed best practice recommendations for diagnosis and acute management. J Neurol Neurosurg Psychiatry. 2021;92(7):757-68.

3.  Agarwal A, Dibaj P, Kassmann CM, Goebbels S, Nave KA, Schwab MH. In vivo imaging and noninvasive ablation of pyramidal neurons in adult NEX-CreERT2 mice. Cereb Cortex. 2012;22(7):1473-86.

4.  Ai P, Zhang X, Xie Z, Liu G, Liu X, Pan S, et al. The HMGB1 is increased in CSF of patients with an Anti-NMDAR encephalitis. Acta Neurol Scand. 2018;137(2):277-82.

5.  Al-Diwani A, Handel A, Townsend L, Pollak T, Leite MI, Harrison PJ, et al. The psychopathology of NMDAR-antibody encephalitis in adults: a systematic review and phenotypic analysis of individual patient data. Lancet Psychiatry. 2019;6(3):235-46.

6.  Arinrad S, Wilke JBH, Seelbach A, Doeren J, Hindermann M, Butt UJ, et al. NMDAR1 autoantibodies amplify behavioral phenotypes of genetic white matter inflammation: a mild encephalitis model with neuropsychiatric relevance. Mol Psychiatry. 2021:https://doi.org/10.1038/s41380-021-01392-8.

7.  Armangue T, Leypoldt F, Malaga I, Raspall-Chaure M, Marti I, Nichter C, et al. Herpes simplex virus encephalitis is a trigger of brain autoimmunity. Ann Neurol. 2014;75(2):317-23.

8.  Armangue T, Moris G, Cantarin-Extremera V, Conde CE, Rostasy K, Erro ME, et al. Autoimmune post-herpes simplex encephalitis of adults and teenagers. Neurology. 2015;85(20):1736-43.

9.  Armangue T, Spatola M, Vlagea A, Mattozzi S, Carceles-Cordon M, Martinez-Heras E, et al. Frequency, symptoms, risk factors, and outcomes of autoimmune encephalitis after herpes simplex encephalitis: a prospective observational study and retrospective analysis. Lancet Neurol. 2018;17(9):760-72.

10. Ashraf U, Ding Z, Deng S, Ye J, Cao S, Chen Z. Pathogenicity and virulence of Japanese encephalitis virus: Neuroinflammation and neuronal cell damage. Virulence. 2021;12(1):968-80.

11. Avery DT, Kalled SL, Ellyard JI, Ambrose C, Bixler SA, Thien M, et al. BAFF selectively enhances the survival of plasmablasts generated from human memory B cells. J Clin Invest. 2003;112(2):286-97.

12. Baizabal-Carvallo JF, Stocco A, Muscal E, Jankovic J. The spectrum of movement disorders in children with anti-NMDA receptor encephalitis. Mov Disord. 2013;28(4):543-7.

13. Ballard TM, Pauly-Evers M, Higgins GA, Ouagazzal AM, Mutel V, Borroni E, et al. Severe impairment of NMDA receptor function in mice carrying targeted point mutations in the glycine binding site results in drug-resistant nonhabituating hyperactivity. J Neurosci. 2002;22(15):6713-23.

14. Balu DT. The NMDA Receptor and Schizophrenia: From Pathophysiology to Treatment. Adv Pharmacol. 2016;76:351-82.

15. Balu R, McCracken L, Lancaster E, Graus F, Dalmau J, Titulaer MJ. A score that predicts 1-year functional status in patients with anti-NMDA receptor encephalitis. Neurology. 2019;92(3):e244-e52.

16. Bartholoma A, Nave KA. NEX-1: a novel brain-specific helix-loop-helix protein with autoregulation and sustained expression in mature cortical neurons. Mech Dev. 1994;48(3):217-28.

17. Bastiaansen AEM, de Bruijn M, Schuller SL, Martinez-Hernandez E, Brenner J, Paunovic M, et al. Anti-NMDAR Encephalitis in the Netherlands, Focusing on Late-Onset Patients and Antibody Test Accuracy. Neurol Neuroimmunol Neuroinflamm. 2022;9(2):e1127.

18. Belnoue E, Pihlgren M, McGaha TL, Tougne C, Rochat AF, Bossen C, et al. APRIL is critical for plasmablast survival in the bone marrow and poorly expressed by early-life bone marrow stromal cells. Blood. 2008;111(5):2755-64.

19. Benson MJ, Dillon SR, Castigli E, Geha RS, Xu S, Lam KP, et al. Cutting edge: the dependence of plasma cells and independence of memory B cells on BAFF and APRIL. J Immunol. 2008;180(6):3655-9.

20. Berghoff SA, Gerndt N, Winchenbach J, Stumpf SK, Hosang L, Odoardi F, et al. Dietary cholesterol promotes repair of demyelinated lesions in the adult brain. Nat Commun. 2017;8(4):14241.

21. Bickel S, Lipp H-P, Umbricht D. Early Auditory Sensory Processing Deficits in Mouse Mutants with Reduced NMDA Receptor Function. Neuropsychopharmacology. 2008;33(7):1680-9.

22. Bien CG, Vincent A, Barnett MH, Becker AJ, Blumcke I, Graus F, et al. Immunopathology of autoantibody-associated encephalitides: clues for pathogenesis. Brain. 2012;135(Pt 5):1622-38.

23. Blinder T, Lewerenz J. Cerebrospinal Fluid Findings in Patients With Autoimmune Encephalitis-A Systematic Analysis. Front Neurol. 2019;10(804):804.

24. Blome R, Bach W, Guli X, Porath K, Sellmann T, Bien CG, et al. Differentially Altered NMDAR Dependent and Independent Long-Term Potentiation in the CA3 Subfield in a Model of Anti-NMDAR Encephalitis. Front Synaptic Neurosci. 2018;10(26):26.

25. Bost C, Chanson E, Picard G, Meyronet D, Mayeur ME, Ducray F, et al. Malignant tumors in autoimmune encephalitis with anti-NMDA receptor antibodies. J Neurol. 2018;265(10):2190-200.

26. Broadbent NJ, Squire LR, Clark RE. Spatial memory, recognition memory, and the hippocampus. Proc Natl Acad Sci U S A. 2004;101(40):14515-20.

27. Broadley J, Seneviratne U, Beech P, Buzzard K, Butzkueven H, O'Brien T, et al. Prognosticating autoimmune encephalitis: A systematic review. J Autoimmun. 2019;96:24-34.

28. Broadley J, Wesselingh R, Seneviratne U, Kyndt C, Beech P, Buzzard K, et al. Prognostic value of acute cerebrospinal fluid abnormalities in antibody-positive autoimmune encephalitis. J Neuroimmunol. 2021;353:577508.

29. Brown GC, Neher JJ. Microglial phagocytosis of live neurons. Nat Rev Neurosci. 2014;15(4):209-16.

30. Bygrave AM, Masiulis S, Nicholson E, Berkemann M, Barkus C, Sprengel R, et al. Knockout of NMDA-receptors from parvalbumin interneurons sensitizes to schizophrenia-related deficits induced by MK-801. Transl Psychiatry. 2016;6(4):e778.

31. Byun JI, Lee ST, Moon J, Jung KH, Sunwoo JS, Lim JA, et al. Distinct intrathecal interleukin-17/interleukin-6 activation in anti-N-methyl-d-aspartate receptor encephalitis. J Neuroimmunol. 2016;297:141-7.

32. Camdessanche JP, Streichenberger N, Cavillon G, Rogemond V, Jousserand G, Honnorat J, et al. Brain immunohistopathological study in a patient with anti-NMDAR encephalitis. Eur J Neurol. 2011;18(6):929-31.

33. Carboni E, Carta AR, Carboni E, Novelli A. Repurposing Ketamine in Depression and Related Disorders: Can This Enigmatic Drug Achieve Success? Frontiers in Neuroscience. 2021;15.

34. Castillo-Gomez E, Kastner A, Steiner J, Schneider A, Hettling B, Poggi G, et al. The brain as immunoprecipitator of serum autoantibodies against N-Methyl-D-aspartate receptor subunit NR1. Ann Neurol. 2016;79(1):144-51.

35. Castillo-Gomez E, Oliveira B, Tapken D, Bertrand S, Klein-Schmidt C, Pan H, et al. All naturally occurring autoantibodies against the NMDA receptor subunit NR1 have pathogenic potential irrespective of epitope and immunoglobulin class. Mol Psychiatry. 2017;22(12):1776-84.

36. Chefdeville A, Treilleux I, Mayeur ME, Couillault C, Picard G, Bost C, et al. Immunopathological characterization of ovarian teratomas associated with anti-N-methyl-D-aspartate receptor encephalitis. Acta Neuropathol Commun. 2019;7(1):38.

37. Chen J, Ding Y, Zheng D, Wang Z, Pan S, Ji T, et al. Elevation of YKL-40 in the CSF of Anti-NMDAR Encephalitis Patients Is Associated With Poor Prognosis. Front Neurol. 2018;9:727.

38. Chen X, Li JM, Liu F, Wang Q, Zhou D, Lai X. Anti-N-methyl-D-aspartate receptor encephalitis: a common cause of encephalitis in the intensive care unit. Neurol Sci. 2016;37(12):1993-8.

39. Coyle JT, Tsai G, Goff D. Converging evidence of NMDA receptor hypofunction in the

pathophysiology of schizophrenia. Ann N Y Acad Sci. 2003;1003(1):318-27.

40. Cui Z, Wang H, Tan Y, Zaia KA, Zhang S, Tsien JZ. Inducible and reversible NR1 knockout reveals crucial role of the NMDA receptor in preserving remote memories in the brain. Neuron. 2004;41(5):781-93.

41. Dabner M, McCluggage WG, Bundell C, Carr A, Leung Y, Sharma R, et al. Ovarian teratoma associated with anti-N-methyl D-aspartate receptor encephalitis: a report of 5 cases documenting prominent intratumoral lymphoid infiltrates. Int J Gynecol Pathol. 2012;31(5):429-37.

42. Dahm L, Ott C, Steiner J, Stepniak B, Teegen B, Saschenbrecker S, et al. Seroprevalence of autoantibodies against brain antigens in health and disease. Ann Neurol. 2014;76(1):82-94.

43. Dale RC, Pillai S, Brilot F. Cerebrospinal fluid CD19(+) B-cell expansion in N-methyl-D-aspartate receptor encephalitis. Dev Med Child Neurol. 2013;55(2):191-3.

44. Dalmau J, Tuzun E, Wu HY, Masjuan J, Rossi JE, Voloschin A, et al. Paraneoplastic anti-N-methyl-D-aspartate receptor encephalitis associated with ovarian teratoma. Ann Neurol. 2007;61(1):25-36.

45. Dalmau J, Gleichman AJ, Hughes EG, Rossi JE, Peng X, Lai M, et al. Anti-NMDA-receptor encephalitis: case series and analysis of the effects of antibodies. Lancet Neurol. 2008;7(12):1091-8.

46. Dalmau J, Lancaster E, Martinez-Hernandez E, Rosenfeld MR, Balice-Gordon R. Clinical experience and laboratory investigations in patients with anti-NMDAR encephalitis. Lancet Neurol. 2011;10(1):63-74.

47. Dalmau J, Armangue T, Planaguma J, Radosevic M, Mannara F, Leypoldt F, et al. An update on anti-NMDA receptor encephalitis for neurologists and psychiatrists: mechanisms and models. Lancet Neurol. 2019;18(11):1045-57.

48. Dang MT, Yokoi F, Yin HH, Lovinger DM, Wang Y, Li Y. Disrupted motor learning and long-term synaptic plasticity in mice lacking NMDAR1 in the striatum. Proc Natl Acad Sci U S A. 2006;103(41):15254-9.

49. Dantzer R, O'Connor JC, Freund GG, Johnson RW, Kelley KW. From inflammation to sickness and depression: when the immune system subjugates the brain. Nat Rev Neurosci. 2008;9(1):46-56.

50. Day GS, Laiq S, Tang-Wai DF, Munoz DG. Abnormal neurons in teratomas in NMDAR encephalitis. JAMA Neurol. 2014;71(6):717-24.

51. Day GS, Yarbrough MY, Kortvelyessy P, Pruss H, Bucelli RC, Fritzler MJ, et al. Prospective Quantification of CSF Biomarkers in Antibody-Mediated Encephalitis. Neurology. 2021;96(20):e2546-e57.

52. de Bruijn M, Aarsen FK, van Oosterhout MP, van der Knoop MM, Catsman-Berrevoets CE, Schreurs MWJ, et al. Long-term neuropsychological outcome following pediatric anti-NMDAR encephalitis. Neurology. 2018;90(22):e1997-e2005.

53. de Bruijn M, van Sonderen A, van Coevorden-Hameete MH, Bastiaansen AEM, Schreurs MWJ, Rouhl RPW, et al. Evaluation of seizure treatment in anti-LGI1, anti-NMDAR, and anti-GABABR encephalitis. Neurology. 2019;92(19):e2185-e96.

54. de Juan-Sanz J, Zafra F, López-Corcuera B, Aragón C. Endocytosis of the Neuronal Glycine Transporter GLYT2: Role of Membrane Rafts and Protein Kinase C-Dependent Ubiquitination. Traffic. 2011;12(12):1850-67.

55. de Montmollin E, Demeret S, Brule N, Conrad M, Dailler F, Lerolle N, et al. Anti-N-Methyl-d-Aspartate Receptor Encephalitis in Adult Patients Requiring Intensive Care. Am J Respir Crit Care Med. 2017;195(4):491-9.

56. Deng B, Liu XN, Li X, Zhang X, Quan C, Chen XJ. Raised cerebrospinal fluid BAFF and APRIL levels in anti-N-methyl-d-aspartate receptor encephalitis: Correlation with clinical outcome. J Neuroimmunol. 2017;305:84-91.

57. Desestret V, Chefdeville A, Viaccoz A, Bost C, Ducray F, Picard G, et al. CSF IgA NMDAR antibodies are potential biomarkers for teratomas in anti-NMDAR encephalitis. Neurol Neuroimmunol Neuroinflamm. 2015;2(6):e166.

58.	Diamond B, Huerta PT, Mina-Osorio P, Kowal C, Volpe BT. Losing your nerves? Maybe it's the antibodies. Nat Rev Immunol. 2009;9(6):449-56.

59.	Ding Y, Zhou Z, Chen J, Peng Y, Wang H, Qiu W, et al. Anti-NMDAR encephalitis induced in mice by active immunization with a peptide from the amino-terminal domain of the GluN1 subunit. J Neuroinflammation. 2021;18(1):53.

60.	Dinoto A, Cheli M, Bratina A, Sartori A, Manganotti P. Bortezomib in anti-N-Methyl-d-Aspartate-Receptor (NMDA-R) encephalitis: A systematic review. J Neuroimmunol. 2021;356:577586.

61.	During MJ, Symes CW, Lawlor PA, Lin J, Dunning J, Fitzsimons HL, et al. An oral vaccine against NMDAR1 with efficacy in experimental stroke and epilepsy. Science. 2000;287(5457):1453-60.

62.	Durr M, Nissen G, Suhs KW, Schwenkenbecher P, Geis C, Ringelstein M, et al. CSF Findings in Acute NMDAR and LGI1 Antibody-Associated Autoimmune Encephalitis. Neurol Neuroimmunol Neuroinflamm. 2021;8(6):e1086.

63.	Ehrenreich H. Autoantibodies against the N-Methyl-d-Aspartate Receptor Subunit NR1: Untangling Apparent Inconsistencies for Clinical Practice. Front Immunol. 2017;8(181):181.

64.	Ehrenreich H. Autoantibodies against N-methyl-d-aspartate receptor 1 in health and disease. Curr Opin Neurol. 2018;31(3):306-12.

65.	Ehrenreich H, Pan H, Hollmann M. Active immunization, autoimmunity and encephalitis: The missing links [E-letter]. Science Translational Medicine2019 [updated Jul 10PMC6729143]. 2019/07/12:[https://stm.sciencemag.org/content/11/500/eaaw0044/tab-e-letters]. Available from: https://www.ncbi.nlm.nih.gov/pubmed/31292262.

66.	Ehrenreich H, Wilke J, Steixner-Kumar AA. Spontaneous serum autoantibody fluctuations: To be or not to be. Mol Psychiatry. 2021;26(6):1723-5.

67.	Feng J, Yang M, Cui D, Huang Z, Ji T, Lian Y. Recurrence of Anti-N-Methyl-D-Aspartate Receptor Encephalitis: A Cohort Study in Central China. Frontiers in Neurology. 2022;13.

68.	Filatenkov A, Richardson TE, Daoud E, Johnson-Welch SF, Ramirez DM, Torrealba J, et al. Persistence of parenchymal and perivascular T-cells in treatment-refractory anti-N-methyl-D-aspartate receptor encephalitis. Neuroreport. 2017;28(14):890-5.

69.	Finke C, Kopp UA, Pruss H, Dalmau J, Wandinger KP, Ploner CJ. Cognitive deficits following anti-NMDA receptor encephalitis. J Neurol Neurosurg Psychiatry. 2012;83(2):195-8.

70.	Finke C, Kopp UA, Scheel M, Pech LM, Soemmer C, Schlichting J, et al. Functional and structural brain changes in anti-N-methyl-D-aspartate receptor encephalitis. Ann Neurol. 2013;74(2):284-96.

71.	Finke C, Kopp UA, Pajkert A, Behrens JR, Leypoldt F, Wuerfel JT, et al. Structural Hippocampal Damage Following Anti-N-Methyl-D-Aspartate Receptor Encephalitis. Biol Psychiatry. 2016;79(9):727-34.

72.	Finke C, Bartels F, Lutt A, Pruss H, Harms L. High prevalence of neuronal surface autoantibodies associated with cognitive deficits in cancer patients. J Neurol. 2017;264(9):1968-77.

73.	Fleischmann R, Pruss H, Rosche B, Bahnemann M, Gelderblom H, Deuschle K, et al. Severe cognitive impairment associated with intrathecal antibodies to the NR1 subunit of the N-methyl-D-aspartate receptor in a patient with multiple sclerosis. JAMA Neurol. 2015;72(1):96-9.

74.	Florance NR, Davis RL, Lam C, Szperka C, Zhou L, Ahmad S, et al. Anti-N-methyl-D-aspartate receptor (NMDAR) encephalitis in children and adolescents. Ann Neurol. 2009;66(1):11-8.

75.	Forrest D, Yuzaki M, Soares HD, Ng L, Luk DC, Sheng M, et al. Targeted disruption of NMDA receptor 1 gene abolishes NMDA response and results in neonatal death. Neuron. 1994;13(2):325-38.

76.	Fradley RL, O'Meara GF, Newman RJ, Andrieux A, Job D, Reynolds DS. STOP knockout and NMDA NR1 hypomorphic mice exhibit deficits in sensorimotor gating. Behav Brain Res. 2005;163(2):257-64.

77.	Gable MS, Gavali S, Radner A, Tilley DH, Lee B, Dyner L, et al. Anti-NMDA receptor encephalitis: report of ten cases and comparison with viral encephalitis. Eur J Clin Microbiol Infect Dis. 2009;28(12):1421-9.

78. Galovic M, Al-Diwani A, Vivekananda U, Torrealdea F, Erlandsson K, Fryer TD, et al. In vivo NMDA receptor function in people with NMDA receptor antibody encephalitis. medRxiv. 2021:2021.12.04.21267226.

79. Garcia-Agudo LF, Janova H, Sendler LE, Arinrad S, Steixner AA, Hassouna I, et al. Genetically induced brain inflammation by Cnp deletion transiently benefits from microglia depletion. FASEB J. 2019;33(7):8634-47.

80. Garcia-Serra A, Radosevic M, Rios J, Aguilar E, Maudes E, Landa J, et al. Blocking Placental Class G Immunoglobulin Transfer Prevents NMDA Receptor Antibody Effects in Newborn Mice. Neurol Neuroimmunol Neuroinflamm. 2021;8(6):e1061.

81. Geoffroy C, Paoletti P, Mony L. Positive allosteric modulation of NMDA receptors: mechanisms, physiological impact and therapeutic potential. J Physiol. 2022;600(2):233-59.

82. Gibson LL, Pollak TA, Blackman G, Thornton M, Moran N, David AS. The Psychiatric Phenotype of Anti-NMDA Receptor Encephalitis. J Neuropsychiatry Clin Neurosci. 2019;31(1):70-9.

83. Gibson LL, McKeever A, Coutinho E, Finke C, Pollak TA. Cognitive impact of neuronal antibodies: encephalitis and beyond. Transl Psychiatry. 2020;10(1):304.

84. Glass CK, Saijo K, Winner B, Marchetto MC, Gage FH. Mechanisms Underlying Inflammation in Neurodegeneration. Cell. 2010;140(6):918-34.

85. Gleichman AJ, Spruce LA, Dalmau J, Seeholzer SH, Lynch DR. Anti-NMDA receptor encephalitis antibody binding is dependent on amino acid identity of a small region within the GluN1 amino terminal domain. J Neurosci. 2012;32(32):11082-94.

86. Goebbels S, Bormuth I, Bode U, Hermanson O, Schwab MH, Nave KA. Genetic targeting of principal neurons in neocortex and hippocampus of NEX-Cre mice. Genesis. 2006;44(12):611-21.

87. Gomez-Figueroa E, Garcia-Estrada C, Paredes-Aragon E, Salado-Burbano J, Cortes-Enriquez F, Marrufo-Melendez O, et al. Brain MRI volumetric changes in the follow-up of patients with anti-NMDAr encephalitis. Clin Neurol Neurosurg. 2021;209:106908.

88. Graus F, Titulaer MJ, Balu R, Benseler S, Bien CG, Cellucci T, et al. A clinical approach to diagnosis of autoimmune encephalitis. Lancet Neurol. 2016;15(4):391-404.

89. Gresa-Arribas N, Titulaer MJ, Torrents A, Aguilar E, McCracken L, Leypoldt F, et al. Antibody titres at diagnosis and during follow-up of anti-NMDA receptor encephalitis: a retrospective study. The Lancet Neurology. 2014;13(2):167-77.

90. Gu J, Jin T, Li Z, Chen H, Xia H, Xu X, et al. Exosomes expressing neuronal autoantigens induced immune response in antibody-positive autoimmune encephalitis. Mol Immunol. 2021;131:164-70.

91. Guasp M, Martín-Aguilar L, Sabater L, Bioque M, Armangué T, Martínez-Hernández E, et al. Neurofilament Light Chain Levels in Anti-NMDAR Encephalitis and Primary Psychiatric Psychosis. Neurology. 2022;98(14):e1489.

92. Gulec B, Kurucu H, Bozbay S, Dikmen Y, Sayman H, Tuzun E, et al. Co-existence of multiple sclerosis and anti-NMDA receptor encephalitis: A case report and review of literature. Mult Scler Relat Disord. 2020;42:102075.

93. Guo Y, Lv X, Wei Q, Wu Y, Chen Y, Ji Y, et al. Impaired neurovascular coupling and cognitive deficits in anti-N-methyl-D-aspartate receptor encephalitis. Brain Imaging Behav. 2021.

94. Hacohen Y, Deiva K, Pettingill P, Waters P, Siddiqui A, Chretien P, et al. N-methyl-D-aspartate receptor antibodies in post-herpes simplex virus encephalitis neurological relapse. Mov Disord. 2014;29(1):90-6.

95. Hagemeyer N, Goebbels S, Papiol S, Kastner A, Hofer S, Begemann M, et al. A myelin gene causative of a catatonia-depression syndrome upon aging. EMBO Mol Med. 2012;4(6):528-39.

96. Hammer C, Stepniak B, Schneider A, Papiol S, Tantra M, Begemann M, et al. Neuropsychiatric disease relevance of circulating anti-NMDA receptor autoantibodies depends on blood-brain barrier integrity. Mol Psychiatry. 2014a;19(10):1143-9.

97. Hammer C, Zerche M, Schneider A, Begemann M, Nave KA, Ehrenreich H. Apolipoprotein E4 carrier status plus circulating anti-NMDAR1 autoantibodies: association with schizoaffective disorder. Mol Psychiatry. 2014b;19(10):1054-6.

98. Hansen HC, Klingbeil C, Dalmau J, Li W, Weissbrich B, Wandinger KP. Persistent intrathecal antibody synthesis 15 years after recovering from anti-N-methyl-D-aspartate receptor encephalitis. JAMA Neurol. 2013;70(1):117-9.

99. Heine J, Pruss H, Bartsch T, Ploner CJ, Paul F, Finke C. Imaging of autoimmune encephalitis--Relevance for clinical practice and hippocampal function. Neuroscience. 2015;309:68-83.

100. Heine J, Kopp UA, Klag J, Ploner CJ, Pruss H, Finke C. Long-Term Cognitive Outcome in Anti-N-Methyl-D-Aspartate Receptor Encephalitis. Ann Neurol. 2021;90(6):949-61.

101. Hirano M, Itoh T, Fujimura H, Inoue K, Samukawa M, Nose K, et al. Pathological Findings in Male Patients With Anti-N-methyl-d-Aspartate Receptor Encephalitis. J Neuropathol Exp Neurol. 2019;78(8):735-41.

102. Huang Y, Wang Q, Zeng S, Zhang Y, Zou L, Fu X, et al. Case Report: Overlapping Multiple Sclerosis With Anti-N-Methyl-D-Aspartate Receptor Encephalitis: A Case Report and Review of Literature. Front Immunol. 2020;11:595417.

103. Huber AK, Irani DN. Targeting CXCL13 During Neuroinflammation. Adv Neuroimmune Biol. 2015;6(1):1-8.

104. Hudson MR, Sokolenko E, O'Brien TJ, Jones NC. NMDA receptors on parvalbumin-positive interneurons and pyramidal neurons both contribute to MK-801 induced gamma oscillatory disturbances: Complex relationships with behaviour. Neurobiology of Disease. 2020;134:104625.

105. Hughes EG, Peng X, Gleichman AJ, Lai M, Zhou L, Tsou R, et al. Cellular and synaptic mechanisms of anti-NMDA receptor encephalitis. J Neurosci. 2010;30(17):5866-75.

106. Iemura Y, Yamada Y, Hirata M, Kataoka TR, Minamiguchi S, Haga H. Histopathological characterization of the neuroglial tissue in ovarian teratoma associated with anti-N-methyl-D-aspartate (NMDA) receptor encephalitis. Pathol Int. 2018;68(12):677-84.

107. Irani SR, Bera K, Waters P, Zuliani L, Maxwell S, Zandi MS, et al. N-methyl-D-aspartate antibody encephalitis: temporal progression of clinical and paraclinical observations in a predominantly non-paraneoplastic disorder of both sexes. Brain. 2010;133(Pt 6):1655-67.

108. Ivanova A, Signore M, Caro N, Greene ND, Copp AJ, Martinez-Barbera JP. In vivo genetic ablation by Cre-mediated expression of diphtheria toxin fragment A. Genesis. 2005;43(3):129-35.

109. Janova H, Arinrad S, Balmuth E, Mitjans M, Hertel J, Habes M, et al. Microglia ablation alleviates myelin-associated catatonic signs in mice. J Clin Invest. 2018;128(2):734-45.

110. Jentsch JD, Roth RH. The neuropsychopharmacology of phencyclidine: from NMDA receptor hypofunction to the dopamine hypothesis of schizophrenia. Neuropsychopharmacology. 1999;20(3):201-25.

111. Jones BE, Tovar KR, Goehring A, Okada NJ, Gouaux E, Westbrook GL. Anti-NMDA receptor encephalitis in mice induced by active immunization with conformationally-stabilized holoreceptors. bioRxiv. 2018:467902-.

112. Jones BE, Tovar KR, Goehring A, Jalali-Yazdi F, Okada NJ, Gouaux E, et al. Autoimmune receptor encephalitis in mice induced by active immunization with conformationally stabilized holoreceptors. Sci Transl Med. 2019;11(500).

113. Jurek B, Chayka M, Kreye J, Lang K, Kraus L, Fidzinski P, et al. Human gestational N-methyl-d-aspartate receptor autoantibodies impair neonatal murine brain function. Ann Neurol. 2019;86(5):656-70.

114. Kamei S, Sekizawa T, Shiota H, Mizutani T, Itoyama Y, Takasu T, et al. Evaluation of combination therapy using aciclovir and corticosteroid in adult patients with herpes simplex virus encephalitis. J Neurol Neurosurg Psychiatry. 2005;76(11):1544-9.

115. Kayser MS, Titulaer MJ, Gresa-Arribas N, Dalmau J. Frequency and characteristics of isolated psychiatric episodes in anti-N-methyl-d-aspartate receptor encephalitis. JAMA Neurol. 2013;70(9):1133-9.

116. Kennedy PG, Chaudhuri A. Herpes simplex encephalitis. J Neurol Neurosurg Psychiatry. 2002;73(3):237-8.

117. Kersten M, Rabbe T, Blome R, Porath K, Sellmann T, Bien CG, et al. Novel Object Recognition in Rats With NMDAR Dysfunction in CA1 After Stereotactic Injection of Anti-NMDAR Encephalitis

Cerebrospinal Fluid. Front Neurol. 2019;10(586):586.

118. Kew JN, Koester A, Moreau JL, Jenck F, Ouagazzal AM, Mutel V, et al. Functional consequences of reduction in NMDA receptor glycine affinity in mice carrying targeted point mutations in the glycine binding site. J Neurosci. 2000;20(11):4037-49.

119. Kornfeld R, Kornfeld S. Assembly of asparagine-linked oligosaccharides. Annu Rev Biochem. 1985;54:631-64.

120. Kostakis E, Smith C, Jang MK, Martin SC, Richards KG, Russek SJ, et al. The neuroactive steroid pregnenolone sulfate stimulates trafficking of functional N-methyl D-aspartate receptors to the cell surface via a noncanonical, G protein, and Ca2+-dependent mechanism. Mol Pharmacol. 2013;84(2):261-74.

121. Kothur K, Wienholt L, Brilot F, Dale RC. CSF cytokines/chemokines as biomarkers in neuroinflammatory CNS disorders: A systematic review. Cytokine. 2016a;77:227-37.

122. Kothur K, Wienholt L, Mohammad SS, Tantsis EM, Pillai S, Britton PN, et al. Utility of CSF Cytokine/Chemokines as Markers of Active Intrathecal Inflammation: Comparison of Demyelinating, Anti-NMDAR and Enteroviral Encephalitis. PLoS One. 2016b;11(8):e0161656.

123. Kowarik MC, Cepok S, Sellner J, Grummel V, Weber MS, Korn T, et al. CXCL13 is the major determinant for B cell recruitment to the CSF during neuroinflammation. J Neuroinflammation. 2012;9(1):93.

124. Kowarik MC, Grummel V, Wemlinger S, Buck D, Weber MS, Berthele A, et al. Immune cell subtyping in the cerebrospinal fluid of patients with neurological diseases. J Neurol. 2014;261(1):130-43.

125. Kreye J, Wenke NK, Chayka M, Leubner J, Murugan R, Maier N, et al. Human cerebrospinal fluid monoclonal N-methyl-D-aspartate receptor autoantibodies are sufficient for encephalitis pathogenesis. Brain. 2016;139(Pt 10):2641-52.

126. Kruer MC, Koch TK, Bourdette DN, Chabas D, Waubant E, Mueller S, et al. NMDA receptor encephalitis mimicking seronegative neuromyelitis optica. Neurology. 2010;74(18):1473-5.

127. Krumbholz M, Theil D, Derfuss T, Rosenwald A, Schrader F, Monoranu CM, et al. BAFF is produced by astrocytes and up-regulated in multiple sclerosis lesions and primary central nervous system lymphoma. J Exp Med. 2005;201(2):195-200.

128. Krystal JH, Karper LP, Seibyl JP, Freeman GK, Delaney R, Bremner JD, et al. Subanesthetic Effects of the Noncompetitive NMDA Antagonist, Ketamine, in Humans: Psychotomimetic, Perceptual, Cognitive, and Neuroendocrine Responses. Archives of General Psychiatry. 1994;51(3):199-214.

129. Krystal JH, Abdallah CG, Sanacora G, Charney DS, Duman RS. Ketamine: A Paradigm Shift for Depression Research and Treatment. Neuron. 2019;101(5):774-8.

130. Kuchling J, Jurek B, Kents M, Kreye J, Geis C, Wickel J, et al. Impaired functional connectivity of the hippocampus in murine models of NMDA-receptor antibody associated pathology. bioRxiv. 2022:2022.01.12.476037.

131. Kutsuwada T, Kashiwabuchi N, Mori H, Sakimura K, Kushiya E, Araki K, et al. Molecular diversity of the NMDA receptor channel. Nature. 1992;358(6381):36-41.

132. Ladepeche L, Planaguma J, Thakur S, Suarez I, Hara M, Borbely JS, et al. NMDA Receptor Autoantibodies in Autoimmune Encephalitis Cause a Subunit-Specific Nanoscale Redistribution of NMDA Receptors. Cell Rep. 2018;23(13):3759-68.

133. Lappe-Siefke C, Goebbels S, Gravel M, Nicksch E, Lee J, Braun PE, et al. Disruption of Cnp1 uncouples oligodendroglial functions in axonal support and myelination. Nat Genet. 2003;33(3):366-74.

134. Lee CH, Lu W, Michel JC, Goehring A, Du J, Song X, et al. NMDA receptor structures reveal subunit arrangement and pore architecture. Nature. 2014;511(7508):191-7.

135. Lekoubou A, Viaccoz A, Didelot A, Anastasi A, Marignier R, Ducray F, et al. Anti-N-methyl-D-aspartate receptor encephalitis with acute disseminated encephalomyelitis-like MRI features. Eur J Neurol. 2012;19(2):e16-7.

136. Leng F, Edison P. Neuroinflammation and microglial activation in Alzheimer disease: where do

we go from here? Nat Rev Neurol. 2021;17(3):157-72.

137. Lepennetier G, Hracsko Z, Unger M, Van Griensven M, Grummel V, Krumbholz M, et al. Cytokine and immune cell profiling in the cerebrospinal fluid of patients with neuro-inflammatory diseases. J Neuroinflammation. 2019;16(1):219.

138. Leypoldt F, Hoftberger R, Titulaer MJ, Armangue T, Gresa-Arribas N, Jahn H, et al. Investigations on CXCL13 in anti-N-methyl-D-aspartate receptor encephalitis: a potential biomarker of treatment response. JAMA Neurol. 2015;72(2):180-6.

139. Li Q, Chen J, Yin M, Zhao J, Lu F, Wang Z, et al. High Level of Soluble CD146 In Cerebrospinal Fluid Might be a Biomarker of Severity of Anti-N-Methyl-D-Aspartate Receptor Encephalitis. Frontiers in Immunology. 2021;12:2263.

140. Li Y, Tanaka K, Wang L, Ishigaki Y, Kato N. Induction of Memory Deficit in Mice with Chronic Exposure to Cerebrospinal Fluid from Patients with Anti-N-Methyl-D-Aspartate Receptor Encephalitis. Tohoku J Exp Med. 2015;237(4):329-38.

141. Li Y, Gu J, Mao Y, Wang X, Li Z, Xu X, et al. Cerebrospinal Fluid Extracellular Vesicles with Distinct Properties in Autoimmune Encephalitis and Herpes Simplex Encephalitis. Mol Neurobiol. 2022.

142. Liba Z, Kayserova J, Elisak M, Marusic P, Nohejlova H, Hanzalova J, et al. Anti-N-methyl-D-aspartate receptor encephalitis: the clinical course in light of the chemokine and cytokine levels in cerebrospinal fluid. J Neuroinflammation. 2016;13(1):55.

143. Lin EJ, Symes CW, Townsend-Nicholson A, Klugmann M, Klugmann CB, Lehnert K, et al. An Immunological Approach to Increase the Brain's Resilience to Insults. ISRN Neurosci. 2014;2014:103213.

144. Linnoila JJ, Binnicker MJ, Majed M, Klein CJ, McKeon A. CSF herpes virus and autoantibody profiles in the evaluation of encephalitis. Neurol Neuroimmunol Neuroinflamm. 2016;3(4):e245.

145. Liu B, Ai P, Zheng D, Jiang Y, Liu X, Pan S, et al. Cerebrospinal fluid pentraxin 3 and CD40 ligand in anti-N-menthyl-d-aspartate receptor encephalitis. J Neuroimmunol. 2018a;315:40-4.

146. Liu B, Xie Z, Liu G, Gu Y, Pan S, Wang H. Elevated neuron-specific enolase and S100 calcium-binding protein B concentrations in cerebrospinal fluid of patients with anti-N-methyl-d-aspartate receptor encephalitis. Clin Chim Acta. 2018b;480:79-83.

147. Liu B, Liu J, Sun H, Xie M, Yang C, Pan Y, et al. Autoimmune encephalitis after Japanese encephalitis in children: A prospective study. J Neurol Sci. 2021;424:117394.

148. Liu J, Liu L, Kang W, Peng G, Yu D, Ma Q, et al. Cytokines/Chemokines: Potential Biomarkers for Non-paraneoplastic Anti-N-Methyl-D-Aspartate Receptor Encephalitis. Front Neurol. 2020;11(1707):582296.

149. Loerinc LB, Blackwell L, Howarth R, Gombolay G. Evaluation of the Anti-N-Methyl-D-Aspartate Receptor Encephalitis One-Year Functional Status Score in Predicting Functional Outcomes in Pediatric Patients with Anti-N-Methyl-D-Aspartate Receptor Encephalitis. Pediatr Neurol. 2021;124:21-3.

150. Lu W, Du J, Goehring A, Gouaux E. Cryo-EM structures of the triheteromeric NMDA receptor and its allosteric modulation. Science. 2017;355(6331):eaal3729-eaal.

151. Ma J, Zhang T, Jiang L. Japanese encephalitis can trigger anti-N-methyl-D-aspartate receptor encephalitis. J Neurol. 2017;264(6):1127-31.

152. Ma J, Han W, Jiang L. Japanese encephalitis-induced anti-N-methyl-d-aspartate receptor encephalitis: A hospital-based prospective study. Brain Dev. 2020;42(2):179-84.

153. Ma X, Lu Y, Peng F, Wang Y, Sun X, Luo W, et al. Serum NfL associated with anti-NMDA receptor encephalitis. Neurol Sci. 2022.

154. Machado-Santos J, Saji E, Troscher AR, Paunovic M, Liblau R, Gabriely G, et al. The compartmentalized inflammatory response in the multiple sclerosis brain is composed of tissue-resident CD8+ T lymphocytes and B cells. Brain. 2018;141(7):2066-82.

155. Magliozzi R, Columba-Cabezas S, Serafini B, Aloisi F. Intracerebral expression of CXCL13 and BAFF is accompanied by formation of lymphoid follicle-like structures in the meninges of mice with relapsing experimental autoimmune encephalomyelitis. J Neuroimmunol. 2004;148(1-2):11-

23.

156. Makuch M, Wilson R, Al-Diwani A, Varley J, Kienzler AK, Taylor J, et al. N-methyl-D-aspartate receptor antibody production from germinal center reactions: Therapeutic implications. Ann Neurol. 2018;83(3):553-61.

157. Malter MP, Elger CE, Surges R. Diagnostic value of CSF findings in antibody-associated limbic and anti-NMDAR-encephalitis. Seizure. 2013;22(2):136-40.

158. Malviya M, Barman S, Golombeck KS, Planaguma J, Mannara F, Strutz-Seebohm N, et al. NMDAR encephalitis: passive transfer from man to mouse by a recombinant antibody. Ann Clin Transl Neurol. 2017;4(11):768-83.

159. Mannara F, Radosevic M, Planaguma J, Soto D, Aguilar E, Garcia-Serra A, et al. Allosteric modulation of NMDA receptors prevents the antibody effects of patients with anti-NMDAR encephalitis. Brain. 2020;143(9):2709-20.

160. Manto M, Dalmau J, Didelot A, Rogemond V, Honnorat J. In vivo effects of antibodies from patients with anti-NMDA receptor encephalitis: further evidence of synaptic glutamatergic dysfunction. Orphanet J Rare Dis. 2010;5(31):31.

161. Manto M, Dalmau J, Didelot A, Rogemond V, Honnorat J. Afferent facilitation of corticomotor responses is increased by IgGs of patients with NMDA-receptor antibodies. J Neurol. 2011;258(1):27-33.

162. Mariotto S, Zamo A, Franchini E, Bonetti B, Parisi A, Hoftberger R, et al. Lymphomatosis cerebri and anti-NMDAR antibodies: A unique constellation. J Neurol Sci. 2019;398:19-21.

163. Martinez-Hernandez E, Horvath J, Shiloh-Malawsky Y, Sangha N, Martinez-Lage M, Dalmau J. Analysis of complement and plasma cells in the brain of patients with anti-NMDAR encephalitis. Neurology. 2011;77(6):589-93.

164. Matricardi S, Patrini M, Freri E, Ragona F, Zibordi F, Andreetta F, et al. Cognitive and neuropsychological evolution in children with anti-NMDAR encephalitis. J Neurol. 2016;263(4):765-71.

165. Matute C. Oligodendrocyte NMDA receptors: a novel therapeutic target. Trends Mol Med. 2006;12(7):289-92.

166. Matute C, Palma A, Serrano-Regal MP, Maudes E, Barman S, Sanchez-Gomez MV, et al. N-Methyl-D-Aspartate Receptor Antibodies in Autoimmune Encephalopathy Alter Oligodendrocyte Function. Ann Neurol. 2020;87(5):670-6.

167. McKeon GL, Scott JG, Spooner DM, Ryan AE, Blum S, Gillis D, et al. Cognitive and Social Functioning Deficits after Anti-N-Methyl-D-Aspartate Receptor Encephalitis: An Exploratory Case Series. J Int Neuropsychol Soc. 2016;22(8):828-38.

168. McKeon GL, Robinson GA, Ryan AE, Blum S, Gillis D, Finke C, et al. Cognitive outcomes following anti-N-methyl-D-aspartate receptor encephalitis: A systematic review. J Clin Exp Neuropsychol. 2018;40(3):234-52.

169. Meguro H, Mori H, Araki K, Kushiya E, Kutsuwada T, Yamazaki M, et al. Functional characterization of a heteromeric NMDA receptor channel expressed from cloned cDNAs. Nature. 1992;357(6373):70-4.

170. Meinl E, Krumbholz M, Derfuss T, Junker A, Hohlfeld R. Compartmentalization of inflammation in the CNS: a major mechanism driving progressive multiple sclerosis. J Neurol Sci. 2008;274(1-2):42-4.

171. Mellquist JL, Kasturi L, Spitalnik SL, Shakin-Eshleman SH. The amino acid following an asn-X-Ser/Thr sequon is an important determinant of N-linked core glycosylation efficiency. Biochemistry. 1998;37(19):6833-7.

172. Meyding-Lamade UK, Oberlinner C, Rau PR, Seyfer S, Heiland S, Sellner J, et al. Experimental herpes simplex virus encephalitis: a combination therapy of acyclovir and glucocorticoids reduces long-term magnetic resonance imaging abnormalities. J Neurovirol. 2003;9(1):118-25.

173. Mikasova L, De Rossi P, Bouchet D, Georges F, Rogemond V, Didelot A, et al. Disrupted surface cross-talk between NMDA and Ephrin-B2 receptors in anti-NMDA encephalitis. Brain. 2012;135(Pt 5):1606-21.

174. Moghaddam B, Javitt D. From Revolution to Evolution: The Glutamate Hypothesis of Schizophrenia and its Implication for Treatment. Neuropsychopharmacology. 2012;37(1):4-15.

175. Mohammad SS, Sinclair K, Pillai S, Merheb V, Aumann TD, Gill D, et al. Herpes simplex encephalitis relapse with chorea is associated with autoantibodies to N-Methyl-D-aspartate receptor or dopamine-2 receptor. Mov Disord. 2014;29(1):117-22.

176. Mohammad SS, Jones H, Hong M, Nosadini M, Sharpe C, Pillai SC, et al. Symptomatic treatment of children with anti-NMDAR encephalitis. Dev Med Child Neurol. 2016;58(4):376-84.

177. Mohn AR, Gainetdinov RR, Caron MG, Koller BH. Mice with reduced NMDA receptor expression display behaviors related to schizophrenia. Cell. 1999;98(4):427-36.

178. Monaghan D, Cotman C. Distribution of N-methyl-D-aspartate-sensitive L-[3H]glutamate-binding sites in rat brain. The Journal of Neuroscience. 1985;5(11):2909-19.

179. Monyer H, Sprengel R, Schoepfer R, Herb A, Higuchi M, Lomeli H, et al. Heteromeric NMDA receptors: molecular and functional distinction of subtypes. Science. 1992;256(5060):1217-21.

180. Monyer H, Burnashev N, Laurie DJ, Sakmann B, Seeburg PH. Developmental and regional expression in the rat brain and functional properties of four NMDA receptors. Neuron. 1994;12(3):529-40.

181. Moriyoshi K, Masu M, Ishii T, Shigemoto R, Mizuno N, Nakanishi S. Molecular cloning and characterization of the rat NMDA receptor. Nature. 1991;354(6348):31-7.

182. Morris RG, Garrud P, Rawlins JN, O'Keefe J. Place navigation impaired in rats with hippocampal lesions. Nature. 1982;297(5868):681-3.

183. Morris RG. Synaptic plasticity and learning: selective impairment of learning rats and blockade of long-term potentiation in vivo by the N-methyl-D- aspartate receptor antagonist AP5. The Journal of Neuroscience. 1989;9(9):3040.

184. Morris RGM, Anderson E, Lynch GS, Baudry M. Selective impairment of learning and blockade of long-term potentiation by an N-methyl-D-aspartate receptor antagonist, AP5. Nature. 1986;319(6056):774-6.

185. Moscato EH, Peng X, Jain A, Parsons TD, Dalmau J, Balice-Gordon RJ. Acute mechanisms underlying antibody effects in anti-N-methyl-D-aspartate receptor encephalitis. Ann Neurol. 2014;76(1):108-19.

186. Nauen DW. Extra-central nervous system target for assessment and treatment in refractory anti-N-methyl-d-aspartate receptor encephalitis. J Crit Care. 2017;37:234-6.

187. Newcomer JW, Farber NB, Jevtovic-Todorovic V, Selke G, Melson AK, Hershey T, et al. Ketamine-induced NMDA receptor hypofunction as a model of memory impairment and psychosis. Neuropsychopharmacology. 1999;20(2):106-18.

188. Newcomer JW, Krystal JH. NMDA receptor regulation of memory and behavior in humans. Hippocampus. 2001;11(5):529-42.

189. Nissen MS, Orvik MS, Nilsson AC, Ryding M, Lydolph M, Blaabjerg M. NMDA-receptor encephalitis in Denmark from 2009 to 2019: a national cohort study. J Neurol. 2022;269(3):1618-30.

190. Nosadini M, Mohammad SS, Corazza F, Ruga EM, Kothur K, Perilongo G, et al. Herpes simplex virus-induced anti-N-methyl-d-aspartate receptor encephalitis: a systematic literature review with analysis of 43 cases. Dev Med Child Neurol. 2017;59(8):796-805.

191. Nosadini M, Eyre M, Molteni E, Thomas T, Irani SR, Dalmau J, et al. Use and Safety of Immunotherapeutic Management of N-Methyl-d-Aspartate Receptor Antibody Encephalitis: A Meta-analysis. JAMA Neurol. 2021;78(11):1333-44.

192. Nutt SL, Hodgkin PD, Tarlinton DM, Corcoran LM. The generation of antibody-secreting plasma cells. Nat Rev Immunol. 2015;15(3):160-71.

193. Oliveira B, Ehrenreich H. Pursuing functional connectivity in NMDAR1 autoantibody carriers. Lancet Psychiatry. 2018;5(1):21-2.

194. Olney JW, Newcomer JW, Farber NB. NMDA receptor hypofunction model of schizophrenia. J Psychiatr Res. 1999;33(6):523-33.

195. Pan H, Oliveira B, Saher G, Dere E, Tapken D, Mitjans M, et al. Uncoupling the widespread occurrence of anti-NMDAR1 autoantibodies from neuropsychiatric disease in a novel autoimmune model. Mol Psychiatry. 2018;24(10):1489-501.

196. Pan H, Steixner-Kumar AA, Seelbach A, Deutsch N, Ronnenberg A, Tapken D, et al. Multiple inducers and novel roles of autoantibodies against the obligatory NMDAR subunit NR1: a translational study from chronic life stress to brain injury. Mol Psychiatry. 2021;26(6):2471-82.

197. Paoletti P, Bellone C, Zhou Q. NMDA receptor subunit diversity: impact on receptor properties, synaptic plasticity and disease. Nat Rev Neurosci. 2013;14(6):383-400.

198. Pape K, Tamouza R, Leboyer M, Zipp F. Immunoneuropsychiatry - novel perspectives on brain disorders. Nat Rev Neurol. 2019;15(6):317-28.

199. Paul SM, Doherty JJ, Robichaud AJ, Belfort GM, Chow BY, Hammond RS, et al. The major brain cholesterol metabolite 24(S)-hydroxycholesterol is a potent allosteric modulator of N-methyl-D-aspartate receptors. J Neurosci. 2013;33(44):17290-300.

200. Peer M, Pruss H, Ben-Dayan I, Paul F, Arzy S, Finke C. Functional connectivity of large-scale brain networks in patients with anti-NMDA receptor encephalitis: an observational study. Lancet Psychiatry. 2017;4(10):768-74.

201. Peng Y, Liu B, Pei S, Zheng D, Wang Z, Ji T, et al. Higher CSF Levels of NLRP3 Inflammasome Is Associated With Poor Prognosis of Anti-N-methyl-D-Aspartate Receptor Encephalitis. Front Immunol. 2019;10:905.

202. Peng Y, Dai F, Liu L, Chen W, Yan H, Liu A, et al. Validation of the NEOS score in Chinese patients with anti-NMDAR encephalitis. Neurol Neuroimmunol Neuroinflamm. 2020;7(5):e860.

203. Pennington C, Livingstone S, Santosh C, Razvi S. N-methyl D-aspartate receptor antibody encephalitis associated with myelitis. J Neurol Sci. 2012;317(1-2):151-3.

204. Peperzak V, Vikstrom I, Walker J, Glaser SP, LePage M, Coquery CM, et al. Mcl-1 is essential for the survival of plasma cells. Nat Immunol. 2013;14(3):290-7.

205. Phillips OR, Joshi SH, Narr KL, Shattuck DW, Singh M, Di Paola M, et al. Superficial white matter damage in anti-NMDA receptor encephalitis. J Neurol Neurosurg Psychiatry. 2018;89(5):518-25.

206. Planaguma J, Leypoldt F, Mannara F, Gutierrez-Cuesta J, Martin-Garcia E, Aguilar E, et al. Human N-methyl D-aspartate receptor antibodies alter memory and behaviour in mice. Brain. 2015;138(Pt 1):94-109.

207. Planaguma J, Haselmann H, Mannara F, Petit-Pedrol M, Grunewald B, Aguilar E, et al. Ephrin-B2 prevents N-methyl-D-aspartate receptor antibody effects on memory and neuroplasticity. Ann Neurol. 2016;80(3):388-400.

208. Pruss H, Finke C, Holtje M, Hofmann J, Klingbeil C, Probst C, et al. N-methyl-D-aspartate receptor antibodies in herpes simplex encephalitis. Ann Neurol. 2012;72(6):902-11.

209. Pruss H. Postviral autoimmune encephalitis: manifestations in children and adults. Curr Opin Neurol. 2017;30(3):327-33.

210. Radosevic M, Planaguma J, Mannara F, Mellado A, Aguilar E, Sabater L, et al. Allosteric Modulation of NMDARs Reverses Patients' Autoantibody Effects in Mice. Neurol Neuroimmunol Neuroinflamm. 2022;9(1):e1122.

211. Reiber H, Peter JB. Cerebrospinal fluid analysis: disease-related data patterns and evaluation programs. Journal of the Neurological Sciences. 2001;184(2):101-22.

212. Rice RA, Pham J, Lee RJ, Najafi AR, West BL, Green KN. Microglial repopulation resolves inflammation and promotes brain recovery after injury. Glia. 2017;65(6):931-44.

213. Rosch RE, Wright S, Cooray G, Papadopoulou M, Goyal S, Lim M, et al. NMDA-receptor antibodies alter cortical microcircuit dynamics. Proc Natl Acad Sci U S A. 2018;115(42):E9916-E25.

214. Sabatino JJ, Jr., Probstel AK, Zamvil SS. B cells in autoimmune and neurodegenerative central nervous system diseases. Nat Rev Neurosci. 2019;20(12):728-45.

215. Saijo K, Glass CK. Microglial cell origin and phenotypes in health and disease. Nat Rev Immunol. 2011;11(11):775-87.

216. Salvador AF, de Lima KA, Kipnis J. Neuromodulation by the immune system: a focus on cytokines. Nat Rev Immunol. 2021.

217. Sarkis RA, Coffey MJ, Cooper JJ, Hassan I, Lennox B. Anti-N-Methyl-D-Aspartate Receptor Encephalitis: A Review of Psychiatric Phenotypes and Management Considerations: A Report of the American Neuropsychiatric Association Committee on Research. J Neuropsychiatry Clin Neurosci. 2019;31(2):137-42.

218. Schneider A, Rajendran L, Honsho M, Gralle M, Donnert G, Wouters F, et al. Flotillin-Dependent Clustering of the Amyloid Precursor Protein Regulates Its Endocytosis and Amyloidogenic Processing in Neurons. The Journal of Neuroscience. 2008;28(11):2874.

219. Schneider P. The role of APRIL and BAFF in lymphocyte activation. Curr Opin Immunol. 2005;17(3):282-9.

220. Schwab MH, Druffel-Augustin S, Gass P, Jung M, Klugmann M, Bartholomae A, et al. Neuronal basic helix-loop-helix proteins (NEX, neuroD, NDRF): spatiotemporal expression and targeted disruption of the NEX gene in transgenic mice. J Neurosci. 1998;18(4):1408-18.

221. Seifert-Held T, Eberhard K, Lechner C, Macher S, Hegen H, Moser T, et al. Functional Recovery in Autoimmune Encephalitis: A Prospective Observational Study. Front Immunol. 2021;12(1916):641106.

222. Serafini B, Rosicarelli B, Magliozzi R, Stigliano E, Aloisi F. Detection of ectopic B-cell follicles with germinal centers in the meninges of patients with secondary progressive multiple sclerosis. Brain Pathol. 2004;14(2):164-74.

223. Sharma R, Al-Saleem FH, Panzer J, Lee J, Puligedda RD, Felicori LF, et al. Monoclonal antibodies from a patient with anti-NMDA receptor encephalitis. Ann Clin Transl Neurol. 2018;5(8):935-51.

224. Sofroniew MV. Molecular dissection of reactive astrogliosis and glial scar formation. 2009. p. 638-47.

225. Sofroniew MV. Astrogliosis. Cold Spring Harb Perspect Biol. 2014;7(2):a020420.

226. Sutcu M, Akturk H, Somer A, Tatli B, Torun SH, Yildiz EP, et al. Role of Autoantibodies to N-Methyl-d-Aspartate (NMDA) Receptor in Relapsing Herpes Simplex Encephalitis: A Retrospective, One-Center Experience. J Child Neurol. 2016;31(3):345-50.

227. Tabata E, Masuda M, Eriguchi M, Yokoyama M, Takahashi Y, Tanaka K, et al. Immunopathological significance of ovarian teratoma in patients with anti-N-methyl-d-aspartate receptor encephalitis. Eur Neurol. 2014;71(1-2):42-8.

228. Tajima N, Karakas E, Grant T, Simorowski N, Diaz-Avalos R, Grigorieff N, et al. Activation of NMDA receptors and the mechanism of inhibition by ifenprodil. Nature. 2016;534(7605):63-8.

229. Takeda A, Shimada H, Tamura A, Yasui M, Yamamoto K, Itoh K, et al. A case of anti-N-methyl-d-aspartate receptor encephalitis with multiple sclerosis-like demyelinated lesions. Mult Scler Relat Disord. 2014;3(3):391-7.

230. Taraschenko O, Fox HS, Pittock SJ, Zekeridou A, Gafurova M, Eldridge E, et al. A mouse model of seizures in anti-N-methyl-d-aspartate receptor encephalitis. Epilepsia. 2019;60(3):452-63.

231. Taraschenko O, Fox HS, Zekeridou A, Pittock SJ, Eldridge E, Farukhuddin F, et al. Seizures and memory impairment induced by patient-derived anti-N-methyl-D-aspartate receptor antibodies in mice are attenuated by anakinra, an interleukin-1 receptor antagonist. Epilepsia. 2021;62(3):671-82.

232. Terrando N, Rei Fidalgo A, Vizcaychipi M, Cibelli M, Ma D, Monaco C, et al. The impact of IL-1 modulation on the development of lipopolysaccharide-induced cognitive dysfunction. Crit Care. 2010;14(3):R88.

233. Thaler FS, Zimmermann L, Kammermeier S, Strippel C, Ringelstein M, Kraft A, et al. Rituximab Treatment and Long-term Outcome of Patients With Autoimmune Encephalitis: Real-world Evidence From the GENERATE Registry. Neurol Neuroimmunol Neuroinflamm. 2021;8(6):e1088.

234. Thompson KA, Blessing WW, Wesselingh SL. Herpes simplex replication and dissemination is not increased by corticosteroid treatment in a rat model of focal Herpes encephalitis. J Neurovirol. 2000;6(1):25-32.

235. Titulaer MJ, McCracken L, Gabilondo I, Armangue T, Glaser C, Iizuka T, et al. Treatment and prognostic factors for long-term outcome in patients with anti-NMDA receptor encephalitis: an observational cohort study. Lancet Neurol. 2013;12(2):157-65.

236. Titulaer MJ, Hoftberger R, Iizuka T, Leypoldt F, McCracken L, Cellucci T, et al. Overlapping demyelinating syndromes and anti-N-methyl-D-aspartate receptor encephalitis. Ann Neurol. 2014;75(3):411-28.

237. Traynelis SF, Wollmuth LP, McBain CJ, Menniti FS, Vance KM, Ogden KK, et al. Glutamate receptor ion channels: structure, regulation, and function. Pharmacol Rev. 2010;62(3):405-96.

238. Tsien JZ, Huerta PT, Tonegawa S. The essential role of hippocampal CA1 NMDA receptor-dependent synaptic plasticity in spatial memory. Cell. 1996;87(7):1327-38.

239. Tuzun E, Zhou L, Baehring JM, Bannykh S, Rosenfeld MR, Dalmau J. Evidence for antibody-mediated pathogenesis in anti-NMDAR encephalitis associated with ovarian teratoma. Acta Neuropathol. 2009;118(6):737-43.

240. Uzawa A, Mori M, Takahashi Y, Ogawa Y, Uchiyama T, Kuwabara S. Anti-N-methyl D-aspartate-type glutamate receptor antibody-positive limbic encephalitis in a patient with multiple sclerosis. Clin Neurol Neurosurg. 2012;114(4):402-4.

241. van den Buuse M. Modeling the Positive Symptoms of Schizophrenia in Genetically Modified Mice: Pharmacology and Methodology Aspects. Schizophrenia Bulletin. 2010;36(2):246-70.

242. van Swieten JC, Koudstaal PJ, Visser MC, Schouten HJ, van Gijn J. Interobserver agreement for the assessment of handicap in stroke patients. Stroke. 1988;19(5):604-7.

243. Varley JA, Webb AJS, Balint B, Fung VSC, Sethi KD, Tijssen MAJ, et al. The Movement disorder associated with NMDAR antibody-encephalitis is complex and characteristic: an expert video-rating study. J Neurol Neurosurg Psychiatry. 2019;90(6):724-6.

244. Venkatesan A, Tunkel AR, Bloch KC, Lauring AS, Sejvar J, Bitnun A, et al. Case definitions, diagnostic algorithms, and priorities in encephalitis: consensus statement of the international encephalitis consortium. Clin Infect Dis. 2013;57(8):1114-28.

245. Wagner F, Goertzen A, Kiraly O, Laube G, Kreye J, Witte OW, et al. Detailed morphological analysis of rat hippocampi treated with CSF autoantibodies from patients with anti-NMDAR encephalitis discloses two distinct types of immunostaining patterns. Brain Res. 2020;1747:147033.

246. Wagnon I, Helie P, Bardou I, Regnauld C, Lesec L, Leprince J, et al. Autoimmune encephalitis mediated by B-cell response against N-methyl-d-aspartate receptor. Brain. 2020;143(10):2957-72.

247. Wang X, Ma C, Liu CY, Li GJ, Zhao D, Han DF. Neuronal NMDAR Currents of the Hippocampus and Learning Performance in Autoimmune Anti-NMDAR Encephalitis and Involvement of TNF-alpha and IL-6. Front Neurol. 2019;10:684.

248. Wang Y, Miao A, Shi Y, Ge J, Wang L, Yu C, et al. Influencing electroclinical features and prognostic factors in patients with anti-NMDAR encephalitis: a cohort follow-up study in Chinese patients. Sci Rep. 2020;10(1):10753.

249. Wang Y, Li X, He P, Yin J, Dong R, Fu Y, et al. Characteristics and outcome-related factors of seizure at the first onset of autoimmune encephalitis: A retrospective study. CNS Neurosci Ther. 2021;27(6):694-701.

250. Warikoo N, Brunwasser SJ, Benz A, Shu HJ, Paul SM, Lewis M, et al. Positive Allosteric Modulation as a Potential Therapeutic Strategy in Anti-NMDA Receptor Encephalitis. J Neurosci. 2018;38(13):3218-29.

251. Warren N, Siskind D, O'Gorman C. Refining the psychiatric syndrome of anti-N-methyl-d-aspartate receptor encephalitis. Acta Psychiatr Scand. 2018;138(5):401-8.

252. Wenke NK, Kreye J, Andrzejak E, van Casteren A, Leubner J, Murgueitio MS, et al. N-methyl-D-aspartate receptor dysfunction by unmutated human antibodies against the NR1 subunit. Ann Neurol. 2019;85(5):771-6.

253. Westman G, Studahl M, Ahlm C, Eriksson BM, Persson B, Ronnelid J, et al. N-methyl-d-aspartate receptor autoimmunity affects cognitive performance in herpes simplex encephalitis. Clin

Microbiol Infect. 2016;22(11):934-40.

254. Whitley RJ. Herpes simplex encephalitis: Adolescents and adults. Antiviral Research. 2006;71(2):141-8.

255. Wilke JBH, Ehrenreich H, Hollmann M. Autoantibodies Against NMDA Receptors – Janus-Faced Molecules? Neuroforum. 2019;25(2):89-98.

256. Wilke JBH, Hindermann M, Berghoff SA, Zihsler S, Arinrad S, Ronnenberg A, et al. Autoantibodies against NMDA receptor 1 modify rather than cause encephalitis. Mol Psychiatry. 2021a;26(12):7746-59.

257. Wilke JBH, Hindermann M, Moussavi A, Butt UJ, Dadarwal R, Berghoff SA, et al. Inducing sterile pyramidal neuronal death in mice to model distinct aspects of gray matter encephalitis. Acta Neuropathol Commun. 2021b;9(121):https://doi.org/10.1186/s40478-021-01214-6.

258. Willetts J, Balster RL, Leander JD. The behavioral pharmacology of NMDA receptor antagonists. Trends in Pharmacological Sciences. 1990;11(10):423-8.

259. Wilson CJ, Finch CE, Cohen HJ. Cytokines and cognition--the case for a head-to-toe inflammatory paradigm. J Am Geriatr Soc. 2002;50(12):2041-56.

260. Wright S, Hashemi K, Stasiak L, Bartram J, Lang B, Vincent A, et al. Epileptogenic effects of NMDAR antibodies in a passive transfer mouse model. Brain. 2015;138(Pt 11):3159-67.

261. Wright SK, Rosch RE, Wilson MA, Upadhya MA, Dhangar DR, Clarke-Bland C, et al. Multimodal electrophysiological analyses reveal that reduced synaptic excitatory neurotransmission underlies seizures in a model of NMDAR antibody-mediated encephalitis. Commun Biol. 2021;4(1):1106.

262. Wu P, Pang X, Liang X, Wei W, Li X, Zhao J, et al. Correlation analysis between regional homogeneity and executive dysfunction in anti-N-methyl-D-aspartate receptor encephalitis patients. Eur J Neurol. 2022;29(1):277-85.

263. Wurdemann T, Kersten M, Tokay T, Guli X, Kober M, Rohde M, et al. Stereotactic injection of cerebrospinal fluid from anti-NMDA receptor encephalitis into rat dentate gyrus impairs NMDA receptor function. Brain Res. 2016;1633:10-8.

264. Xu X, Lu Q, Huang Y, Fan S, Zhou L, Yuan J, et al. Anti-NMDAR encephalitis: A single-center, longitudinal study in China. Neurol Neuroimmunol Neuroinflamm. 2020;7(1):e633.

265. Yamasaki TR, Blurton-Jones M, Morrissette DA, Kitazawa M, Oddo S, LaFerla FM. Neural stem cells improve memory in an inducible mouse model of neuronal loss. J Neurosci. 2007;27(44):11925-33.

266. Yang R, Ge F, Jiang J, Wang Y, Wan M, Zhang W. Temporal rank of clinical characteristics and prognosis of anti-N-methyl-d-aspartate receptor encephalitis. Brain Behav. 2021;11(8):e2277.

267. Yeshokumar AK, Coughlin A, Fastman J, Psaila K, Harmon M, Randell T, et al. Seizures in autoimmune encephalitis-A systematic review and quantitative synthesis. Epilepsia. 2021;62(2):397-407.

268. Yu Y, Wu Y, Cao X, Li J, Liao X, Wei J, et al. The Clinical Features and Prognosis of Anti-NMDAR Encephalitis Depends on Blood Brain Barrier Integrity. Mult Scler Relat Disord. 2021;47:102604.

269. Yue W, Caldwell S, Risbrough V, Powell S, Zhou X. Chronic presence of blood circulating anti-NMDAR1 autoantibodies impairs cognitive function in mice. PLoS One. 2021;16(9):e0256972.

270. Zhang L, Lu Y, Xu L, Liu L, Wu X, Zhang Y, et al. Anti-N-methyl-D-aspartate receptor encephalitis with accompanying ovarian teratoma in female patients from East China: Clinical features, treatment, and prognostic outcomes. Seizure. 2020;75:55-62.

271. Zhang Q, Tanaka K, Sun P, Nakata M, Yamamoto R, Sakimura K, et al. Suppression of synaptic plasticity by cerebrospinal fluid from anti-NMDA receptor encephalitis patients. Neurobiol Dis. 2012;45(1):610-5.

272. Zhang Y, Ye F, Zhang T, Lv S, Zhou L, Du D, et al. Structural basis of ketamine action on human NMDA receptors. Nature. 2021;596(7871):301-5.

273. Zhong R, Chen Q, Zhang X, Zhang H, Lin W. Risk Factors for Mortality in Anti-NMDAR, Anti-LGI1, and Anti-GABABR Encephalitis. Frontiers in Immunology. 2022;13.

274. Zhu S, Stein RA, Yoshioka C, Lee CH, Goehring A, McHaourab HS, et al. Mechanism of NMDA

Receptor Inhibition and Activation. Cell. 2016;165(3):704-14.

275. Zografou C, Vakrakou AG, Stathopoulos P. Short- and Long-Lived Autoantibody-Secreting Cells in Autoimmune Neurological Disorders. Front Immunol. 2021;12:686466.

276. Zou C, Pei S, Yan W, Lu Q, Zhong X, Chen Q, et al. Cerebrospinal Fluid Osteopontin and Inflammation-Associated Cytokines in Patients With Anti-N-Methyl-D-Aspartate Receptor Encephalitis. Front Neurol. 2020;11:519692.

277. Zrzavy T, Endmayr V, Bauer J, Macher S, Mossaheb N, Schwaiger C, et al. Neuropathological Variability within a Spectrum of NMDAR-Encephalitis. Ann Neurol. 2021a;90(5):725-37.

278. Zrzavy T, Hoftberger R, Wimmer I, Berger T, Rommer P, Macher S. Longitudinal CSF Findings in Autoimmune Encephalitis-A Monocentric Cohort Study. Front Immunol. 2021b;12(741):646940.

**Declaration**

I hereby declare that the thesis "Modeling anti-NMDAR encephalitis" has been written independently and with no other sources and aids than quoted.

Justus Wilke                                     Göttingen, 11.05.2022

# Appendix

## List of Publications

*shared first authorship

**Wilke JBH**, Ehrenreich H and Hollmann M (2019). "Autoantibodies Against NMDA Receptors – Janus-Faced Molecules?" Neuroforum 25(2): 89-98.

Ehrenreich H, **Wilke JBH** and Steixner-Kumar AA (2021). "Spontaneous serum autoantibody fluctuations: To be or not to be." Mol Psychiatry 26(6): 1723-1725.

**Wilke JBH\***, Hindermann M\*, Moussavi A, Butt UJ, Dadarwal R, Berghoff SA, Sarcheshmeh AK, Ronnenberg A, Zihsler S, Arinrad S, Hardeland R, Seidel J, Lühder F, Nave KA, Boretius S and Ehrenreich H (2021). "Inducing sterile pyramidal neuronal death in mice to model distinct aspects of gray matter encephalitis." Acta Neuropathol Commun 9(121): https://doi.org/10.1186/s40478-40021-01214-40476.

**Wilke JBH**, Hindermann M, Berghoff SA, Zihsler S, Arinrad S, Ronnenberg A, Barnkothe N, Steixner-Kumar AA, Röglin S, Stöcker W, Hollmann M, Nave KA, Lühder F and Ehrenreich H (2021). "Autoantibodies against NMDA receptor 1 modify rather than cause encephalitis." Mol Psychiatry 26(12): 7746-7759.

Arinrad S\*, **Wilke JBH\***, Seelbach A, Doeren J, Hindermann M, Butt UJ, Steixner-Kumar AA, Spieth L, Ronnenberg A, Pan H, Berghoff SA, Hollmann M, Lühder F, Nave KA, Bechter K and Ehrenreich H (2021). "NMDAR1 autoantibodies amplify behavioral phenotypes of genetic white matter inflammation: a mild encephalitis model with neuropsychiatric relevance." Mol Psychiatry: https://doi.org/10.1038/s41380-41021-01392-41388.

Ehrenreich H, Garcia-Agudo LF, Steixner-Kumar AA, **Wilke JBH** and Butt UJ (2022) "Introducing the brain erythropoietin circle to explain adaptive brain hardware upgrade and improved performance" Mol Psychiatry: https://doi.org/10.1038/s41380-022-01551-5

Teller J\*, Jung C\*, **Wilke JBH\***, Schimmelpfennig S, Hindermann M, Hinken L, Gabriel MM, Fegbeutel C, Schäfer A, Laser H, Lichtinghagen R, Worthmann H, Weissenborn K and Ehrenreich H (in review). „Circulating autoantibodies against the NMDAR subunit NR1 disappear from blood upon general anesthesia"

# Curriculum Vitae

**Academic career**

09/2019 – present        PhD student
Clinical Neuroscience
Supervisor: Prof. Dr. Dr. Hannelore Ehrenreich
Max Planck Institute for Multidisciplinary Sciences
(until 12/2021: Max Planck Institute of Experimental Medicine)

11/2018 – 09/2019        Research Associate
Clinical Neuroscience
Supervisor: Prof. Dr. Dr. Hannelore Ehrenreich
Max Planck Institute of Experimental Medicine

10/2016 – 09/2018        Master of Science in Biochemistry (Grade 1.0)
Master Thesis (Grade 1.0)
Supervisor: Prof. Dr. Michael Hollmann
Department of Biochemistry I
Ruhr University Bochum

12/2016 – 02/2017        Student Assistant – Tutor of a physical chemistry seminar
Department of Physical Chemistry II
Ruhr University Bochum, Germany

09/2016 -11/2016        Student Assistant - Supervision of students in a chemistry practical course
Department of Organic Chemistry I
Ruhr University Bochum, Germany

10/2013 – 09/2016        Bachelor of Science in Biochemistry (Grade 1.2)
Bachelor Thesis (Grade 1.0)
Supervisor: Prof. Dr. Michael Hollmann
Department of Biochemistry I
Ruhr University Bochum

**Awards and Stipends:**

| | |
|---|---|
| 12/2018 | Price of the VFCh for the best M.Sc. Biochemistry Graduation in 2018 |
| | Ruhr University Bochum, Germany |
| 10/2017 – 09/2018 | Deutschlandstipendium |
| 12/2016 | Price of the VFCh for the best B.Sc. Biochemistry Graduation in 2016 |
| | Ruhr University Bochum, Germany |
| 10/2016 – 09/2017 | Deutschlandstipendium |

**Additional Qualifications:**

| | |
|---|---|
| 12/2020 | Advanced Training Course in Accordance with §15 GenTSV |
| | for Project Managers and Assigned Persons for Biological Security |
| | Max Planck Institute of Biochemistry, Martinsried, Germany |
| 03/2019 | Animal Handling Course |
| | Max Planck Institute of Experimental Medicine, Göttingen, Germany |
| 04/2018 | Animal Handling Course |
| | Bayer AG, Wuppertal, Germany |
| | Ruhr University Bochum, Germany |
| 03/2017 | Radiation Safety Course (Fachkundegruppe S4.1) |
| | RUBION, Ruhr University Bochum, Germany |